PB83-159400

REPORT NO.
UCB/EERC-82/13
AUGUST 1982

EARTHQUAKE ENGINEERING RESEARCH CENTER

PRELIMINARY REPORT ON THE SMART 1 STRONG MOTION ARRAY IN TAIWAN

by

B. A. BOLT
C. H. LOH
J. PENZIEN
Y. B. TSAI
Y. T. YEH

Report to the National Science Foundation

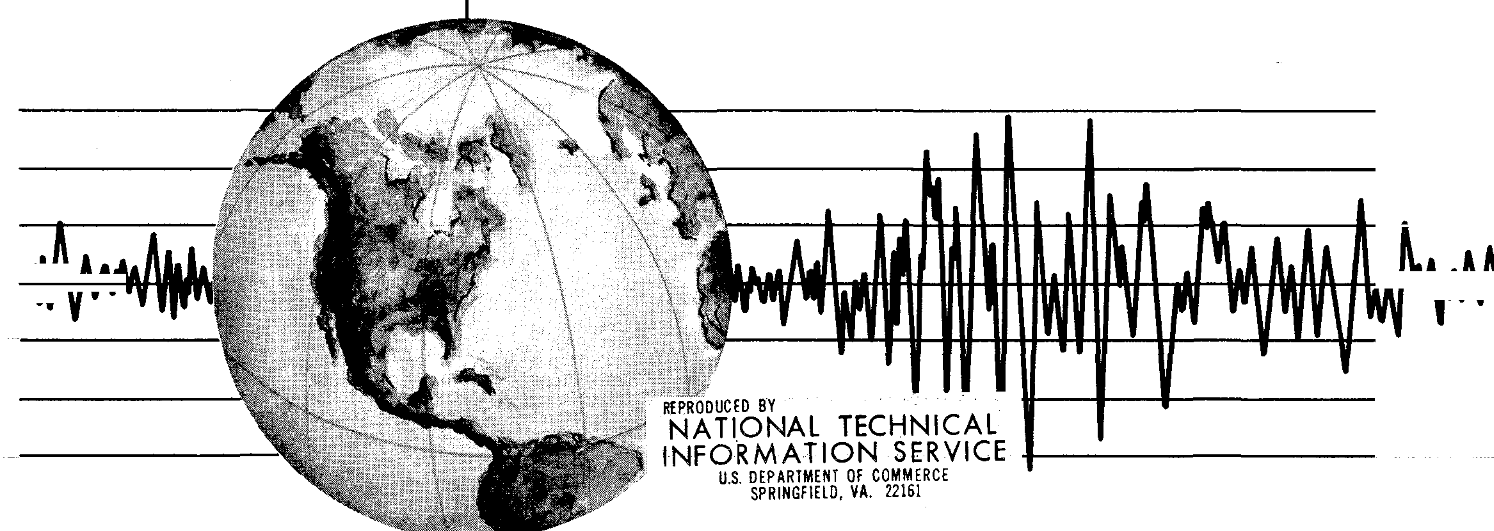

COLLEGE OF ENGINEERING
UNIVERSITY OF CALIFORNIA · Berkeley, California

For sale by the National Technical Information Service, U.S. Department of Commerce, Springfield, Virginia 22161.

See back of report for up to date listing of EERC reports.

DISCLAIMER

REPORT DOCUMENTATION PAGE

1. REPORT NO. NSF/CEE-82065

2.

3. Recipient's Accession No. PB83 159400

4. Title and Subtitle
Preliminary Report on the SMART 1 Strong Motion Array in Taiwan

5. Report Date August 1982

6.

7. Author(s)
B. A. Bolt, C. H. Loh, J. Penzien, Y. B. Tsai, Y. T. Yeh

8. Performing Organization Rept. No. UCB/EERC-82/13

9. Performing Organization Name and Address

Earthquake Engineering Research Center
University of California, Berkeley
47th Street & Hoffman Blvd.
Richmond, Calif. 94804

10. Project/Task/Work Unit No.

11. Contract(C) or Grant(G) No.
(C)
(G) CEE-7908982

12. Sponsoring Organization Name and Address
National Science Foundation
1800 G Street, N.W.
Washington, D.C. 20550

13. Type of Report & Period Covered

14.

15. Supplementary Notes

16. Abstract (Limit: 200 words)

The first large digital array, called SMART 1 (with radius 2 km and 37 accelerometers), to record substantial ground motion (up to 0.24g horizontal acceleration) became operational in September 1980 in a highly seismic region of Taiwan. During the first year of operation, SMART 1 recorded fifteen earthquakes with local magnitudes ranging from 3.4 to 6.9.

Installational and operational details and likely errors in the data processing are presented.

For this major preliminary study, recorded wave forms across the array were analyzed for two earthquakes. The correlation coefficient between the acceleration wave forms of the same component recorded at any two array sites was studied. Representative measurements were made of seismic wave coherency, Fourier wave number, and response spectra. Comparisons of power spectra as a function of wave number, frequency, azimuth of propagation, and wave type were made.

The engineering analysis included (1) transformations to principal axes, (2) development of generalized response spectrum ratios for characterizing multi-support excitations, and (3) moving window analysis in the time and frequency domains for studying spectral variations of recorded ground motions. The dynamic properties of site conditions and spatial correlations of earthquake motions were studied. A technique using the principal variance ratio was developed to identify the wave direction and type of waves.

17. Document Analysis a. Descriptors

b. Identifiers/Open-Ended Terms

c. COSATI Field/Group

18. Availability Statement:
Release Unlimited

19. Security Class (This Report)

20. Security Class (This Page)

21. No. of Pages 213

22. Price

NOTICE

PRELIMINARY REPORT ON THE SMART 1
STRONG MOTION ARRAY IN TAIWAN

by

B. A. Bolt
C. H. Loh

Seismographic Station
University of California, Berkeley

J. Penzien

Earthquake Engineering Research Center
University of California, Berkeley

Y. B. Tsai
Y. T. Yeh

Institute of Earth Sciences
Academia Sinica, Taipei

Report to the National Science Foundation

Report No. UCB/EERC-82/13
Earthquake Engineering Research Center
University of California
Berkeley, California

August 1982

ABSTRACT

Specially designed arrays of strong-motion seismographs near to the earthquake source are required for seismological and engineering studies of the generation and near-field properties of seismic waves. The first such large digital array, called SMART 1 (with radius 2 km and 37 accelerometers), to record substantial ground motion (up to 0.24g horizontal acceleration) became operational in September 1980 in a highly seismic region of Taiwan. During the first year of operation, SMART 1 recorded fifteen earthquakes with local magnitudes (M_L) ranging from 3.4 to 6.9. Three were located directly below the array at focal depths of 59 to 76 km. The remaining twelve had shallow depths with epicentral distances from 1.8 to 76 km. Digital records from 27 three-component accelerographs were obtained from a magnitude 6.9 (M_L) local earthquake on January 29, 1981.

The digital accelerographs were tested on the shaking table at U.C. Berkeley before they were sent to the field. Calculated instrumental transfer functions show that the calibration up to 20 Hz is known sufficiently well for normal wave analysis. Installational and operational details and likely errors in the data processing are also presented.

For the major preliminary study, recorded wave forms across the array were analyzed for the January 29, 1981 and November 14, 1980 earthquakes. The correlation coefficient between the acceleration wave forms of the same component recorded at any two array sites was studied. Representative measurements were made of seismic wave coherency, Fourier wave number, and response spectra. Comparisons of power spectra as a function of wave number, frequency, azimuth of propagation, and wave type show that wave forms and local magnitude varied significantly across the array for each event. On average, peak accelerations of horizontal components were about three

times that of the vertical component. Relative spectral changes from earthquake to earthquake were large.

The preliminary engineering analysis included (1) transformations to principal axes, (2) development of generalized response spectrum ratios for characterizing multi-support excitations, and (3) moving window analysis in the time and frequency domains for studying the spectral variations of recorded ground motions. The dynamic properties of site conditions and, following ideas of Newmark, spatial correlations of earthquake motions were also studied. A technique using the principal variance ratio was developed to identify the wave direction and type of waves.

ACKNOWLEDGMENTS

Operation of SMART 1 is a joint effort between the University of California, Berkeley, and the Academia Sinica, Taiwan, R.O.C. Financial support is provided by the National Science Foundation under the grant No. CEE-7908982 and by the National Science Council under the grant No. 70-0202-M0001-03.

The authors wish to express their appreciation to Norman Abrahamson, Russell Sell, M. K. Hsu, C. C. Liu and J. Marrone for essential contributions.

Requests for digital tape copies of the SMART 1 records in standard ASCII format should be made to the first author.

Preceding page blank

TABLE OF CONTENTS

LIST OF TABLES

Preceding page blank

LIST OF FIGURES

1. GENERAL INTRODUCTION

1.1 Objectives

Installation of specially designed arrays of strong-motion seismographs in highly seismic areas of the world was recommended at an international workshop[1] in Hawaii in 1978. Since that time, a number of large-scale arrays have been designed for siting in California, Japan, Assam (India), Mexico, People's Republic of China, Turkey, and in Taiwan, R.O.C., among other places. In addition, an International Strong-Motion Array Council (ISMAC) has been formed and has held two meetings to assist development and recommend future international meetings, data standardization and dissemination, instrumental comparisons, and so on.

Array measurements of seismic waves near to the source of a great earthquake are needed for two main reasons: first, such data provide a fuller understanding of both the generation of seismic waves from the moving dislocation along the causative fault and the effect of the intervening geology on the wave propagation. Secondly, such data supply essential knowledge about the spatio-temporal variations of seismic ground motions for engineering design of structures with large base dimensions, such as dams and bridges. With these objectives, the International Workshop on Strong Motion in Hawaii in May, 1978, recognized the need for groups of broadband accelerometers within a specified seismic area and with a specified site geometry and common time base. The first such digital array to become operational is located at the town of Lotung in the northeast corner of Taiwan, a particularly seismic area.[2]

For engineering purposes, the prediction of strong ground motion and of the response of engineered structures in earthquakes[3] depends upon measurements of the spatial variability of earthquake intensities. Pioneering work of this kind for small ground motions was first carried out in Japan[4] using a small array of seismographs and correlational analysis. In this report, we describe more extensive measurements of seismic waves from strong earthquakes near to their sources, from a dense multiple-element array of digital strong-motion seismographs, and summarize the basic strong-motion data recorded by the array in its first 12 months of operation. An indication of preliminary research with some of the data is also given.

The SMART 1 research project is conducted jointly by the Seismographic Station, University of California, Berkeley, and the Institute of Earth Sciences, Academia Sinica, Taipei.

1.2 Strong Motion Array Configuration and Site Conditions

The strong-motion array, called SMART 1, installed at Lotung in Taiwan, is a two-dimensional surface array and consists of a center element C00 and three concentric circles (inner I, middle M, and outer O), each with 12 strong-motion seismographs having a common time base, and radii of 200 meters, 1 km, and 2 km, respectively (see Figs. 1.1 and 1.2). The inner ring controls the spatial aliasing since, for a wave velocity of 1 km/sec and element spacing of 100 m, say, the aliasing frequency is 5 Hz. Only one instrument in the I-ring is located more than 10 m from the position of perfect symmetry. The coordinates of SMART 1 are shown in Table 1.1. Details of the Lotung area and the soil conditions are shown in Figs. 1.3 and 1.4; for the upper 500 meters depth, the P wave velocity is about 0.5 to 1.0 km/sec.

Installation began in September, 1980, and by January, 1981, 27 instruments were in place. By September, 1981, 15 earthquakes of local magnitude $3.4 \le M_L \le 6.9$ had triggered array elements (see Table 1.2).

The largest, on January 29, 1981, was a strong earthquake centered 30 km from the center of the array and felt all over Taiwan. Its focal depth was approximately 11 km. The (Richter) magnitude calculated locally by the Institute of Earth Sciences (Taipei) was 6.9. The world-wide average m_b magnitude (NEIS) was 5.6. In this case, the seismic waves triggered all the 27 operational digital accelerometers, thereby providing the largest comprehensive multi-dimensional recording of strong ground motion near a significant fault rupture yet obtained. This set of accelerograms can now be compared with important strong motions measured with other arrays such as in the 1979 Imperial Valley earthquake[5] and the 1975 Oroville aftershocks.[6] In the 1981 Taiwan earthquake, the maximum horizontal and vertical accelerations recorded were 0.24g and 0.09g, respectively. (A number of strong-motion accelerometers of conventional analog type also triggered in the vicinity of SMART 1, allowing crucial comparison between the two types of measurements[7]; see Figs. 3.4a and 3.4b.)

Large aperture seismic arrays (linear dimension of order 100 km) have been used for over 15 years to discriminate between underground nuclear explosions and earthquakes by enhancing the signal-to-noise ratio.[8, 9] In contrast, a strong-motion array of aperture 2 km is not designed to enhance small signals, but rather to determine wave speed, direction of propagation, type of wave component, and spatial variations and phase relations. As in an array of radio telescopes, a seismic array, like SMART 1, allows wave correlations for consecutive time and frequency intervals. Also, a computer algorithm can be used to insert appropriate time lags in the signals at each element, thereby steering the array response towards a known azimuth. One seismological objective is to follow the seismic dislocation as it moves along the rupturing fault. On the engineering side, the measurements are designed to address such key questions as how the intensity of seismic waves varies over short distances, what is the contribution of seismic surface waves to shaking at a given site and, in particular, to provide information on out-of-phase wave components over distances comparable to the base dimensions of large engineered structures. Accelerograms from individual strong-motion seismographs cannot, in general, provide the resolution needed to resolve such questions.

1.3 References

1. Iwan, W.D. (Editor), Proc. Int. Workshop Strong Motion Earthquake Instrument Arrays, Hawaii, 103 (1978).

2. Wu, F.T., "Focal Mechanisms and Tectonics in the Vicinity of Taiwan," Bull. Seism. Soc. Am., 60, 2045-2056 (1970).

3. Housner, G.W., "Behavior of Structures During Earthquakes," J. Eng. Mech. Div., ASCE, 85, 109-129 (1959).

4. Aki, I. and M. Tsujiura, "Correlational Study of Near Earthquake Waves," Bull. E.R.I. Tokyo, 37, 207-232 (1959).

5. Rojahn, C. (Editor), "Selected Papers on the Imperial Valley, California Earthquake of October 15, 1979," U.S. Geol. Surv. Open-File Report, 80-1094 (1981).

6. Fletcher, J.B., A.G. Brady, and T.C. Hanks, "Strong-Motion Accelerograms of the Oroville, California Aftershocks of August 6, 1975," Bull. Seism. Soc. Am., 70, 243-268 (1980).

7. Hudson, D.E., Reading and Interpreting Strong Motion Records, Earthquake Engineering Research Institute, Berkeley, California (1979).

8. Birtill, J.W. and F.E. Whiteway, "The Application of Phased Arrays to the Analysis of Seismic Body Waves," Phil. Trans. Roy. Soc. Lon., A 258, 421-493 (1965).

9. Capon, J., in Methods in Computational Physics, Vol. 13 (Editor Bolt, B.A.) Academic Press, New York (1973).

TABLE 1.1

SMART 1 Site Coordinates (from June 1, 1982)

Site	X (meters)	Y (meters)	Longitude (E) deg.	Longitude (E) min.	Longitude (E) sec.	Latitude (N) deg.	Latitude (N) min.	Latitude (N) sec.	R (meters)	Azimuth (degrees)	Level (meters)
C00	0.0	0.0	121	45	53.23	24	40	25.55			6.1
I01	30.5	190.9	121	45	54.33	24	40	31.76	193.3	9.07	5.9
I02	132.5	141.6	121	45	57.93	24	40	30.15	193.9	43.10	5.5
I03	193.6	65.1	121	46	00.09	24	40	27.67	204.2	71.41	6.1
I04	202.2	-43.2	121	46	00.40	24	40	24.15	206.8	102.05	6.1
I05	150.9	-134.0	121	45	58.58	24	40	21.20	201.8	131.60	6.3
I06	45.5	-188.2	121	45	54.84	24	40	18.46	193.6	166.42	6.6
I07	-51.8	-193.8	121	45	51.39	24	40	19.22	200.6	194.98	6.3
I08	-122.3	-142.4	121	45	48.89	24	40	20.92	187.7	220.65	6.2
I09	-196.7	-64.2	121	45	46.25	24	40	23.46	206.9	251.93	7.0
I10	-196.3	36.5	121	45	46.30	24	40	26.74	199.7	280.53	7.0
I11	-136.1	120.3	121	45	48.40	24	40	29.46	181.6	311.46	6.8
I12	-59.2	192.5	121	45	51.13	24	40	31.81	201.4	342.90	6.4
M01*	186.6	938.6	121	45	59.87	24	40	56.05	956.9	11.24	5.0
M02**	696.9	850.9	121	46	18.00	24	40	53.21	1099.9	39.32	4.4
M03	879.6	348.4	121	46	24.45	24	40	36.87	946.1	68.39	4.0
M04	988.3	-219.9	121	46	28.26	24	40	18.40	1012.5	102.55	4.5
* From 10/18/80 to 5/30/81:											
M01	193.3	972.9	121	46	00.12	24	40	57.05	991.5	11.24	5.5
** From 10/18/80 to 1/1/81:											
M02	696.6	850.6	121	46	18.05	24	40	53.09	1099.4	39.31	4.4

TABLE 1.1

(Continued)

Site	X (meters)	Y (meters)	Longitude (E)			Latitude (N)			R (meters)	Azimuth (degrees)	Level (meters)
			deg.	min.	sec.	deg.	min.	sec.			
M05	743.0	-608.1	121	46	19.54	24	40	05.79	960.1	129.30	3.9
M06	307.4	-954.5	121	46	3.72	24	39	54.45	1002.7	162.15	4.3
M07	-265.0	-987.9	121	45	43.84	24	39	53.44	1002.9	195.01	5.2
M08	-639.2	-747.8	121	45	30.58	24	40	01.25	983.7	220.52	7.4
M09	-961.9	-379.0	121	45	19.13	24	40	13.23	1033.9	248.49	10.8
M10	-913.0	135.7	121	45	20.84	24	40	29.96	923.0	278.46	7.6
M11	-740.0	675.1	121	45	26.93	24	40	47.49	1002.0	312.36	7.1
M12	-294.6	959.2	121	45	42.77	24	40	56.73	1003.5	342.93	5.8
O01	389.9	1988.5	121	46	07.14	24	41	30.18	2026.4	11.09	5.3
O02	1348.7	1487.8	121	46	41.23	24	41	13.91	2008.2	42.19	4.9
O03	1948.0	608.0	121	47	02.42	24	40	45.31	2040.7	72.67	3.4
O04	1949.3	-370.7	121	47	02.31	24	40	13.50	1984.3	100.77	2.4
O05	1538.4	-1276.5	121	46	47.63	24	39	43.06	1999.0	129.68	3.8
O06	627.4	-1909.8	121	45	15.37	24	39	23.48	2010.2	161.81	4.8
O07	-381.1	-1964.1	121	45	39.74	24	39	21.71	2000.8	190.98	7.2
O08	-1298.8	-1594.3	121	45	07.30	24	39	33.73	2056.4	219.17	18.1
O09	-1921.0	-702.0	121	44	45.19	24	40	02.73	2045.2	249.92	9.6
O10	-1953.5	442.3	121	44	43.58	24	40	31.93	2002.9	282.76	13.4
O11	-1440.8	1312.3	121	45	01.99	24	41	08.20	1948.8	312.33	9.1
O12	-599.5	1904.2	121	45	31.90	24	41	27.44	1996.4	342.53	6.5

TABLE 1.2

Earthquakes Recorded by the SMART 1 Array from October 1980 to October 1981.

Event No.	Origin Time (GMT)		Epicenter Longitude (E)		Epicenter Latitude (N)		Depth (km)	Mag.	Azim. (deg.)	Δ (km)	T/I*	Max. Acc. (gal)		
			deg.	min.	deg.	min.						V	EW	NS
1	1980.10.18	00:08:22.9	121	52	24	17	8	5.8	166.5	45.0	16/21	14.8	21.1	23.7
2	1980.11.14	13:37: 4.0	121	47	24	35	62	5.9	164.2	10.0	16/21	29.7	69.7	78.7
3	1980.11.14	13:38:15.8	121	49	24	34	59	5.6	152.1	12.5	13/21	10.7	22.9	24.6
4	1981. 1.24	14:10:31.7	121	44	23	53	43	5.8	181.7	87.5	2/27	2.4	8.1	9.0
5	1981. 1.29	04:51:36.0	121	53	24	26	11	6.9	153.8	30.0	27/27	64.5	158.2	244.1
6	1981. 2.27	02:27:33.9	121	52	24	33	76	5.8	140.4	17.2	10/27	4.4	13.6	12.2
7	1981. 3. 2	12:13:46.5	121	25	22	57	9	6.9	190.6	192.6	3/27	2.7	6.4	10.5
8	1981. 3.10	08:24:51.2	121	47	24	44	7	4.4	15.4	7.0	19/27	16.0	23.5	34.5
9	1981. 3.22	21:25:32.5	121	49	24	45	11	3.8	30.9	9.7	12/28	13.1	22.8	19.1
10	1981. 5. 3	19:19:51.3	121	59	24	42	68	5.3	82.4	21.5	10/28	16.6	21.0	18.3
11	1981. 6. 1	11:53:44.2	121	50	24	23	2	5.3	165.5	32.5	8/28	10.1	13.2	15.0
12	1981. 8.20	19:03:28.1	121	45	24	41	0.1	4.7	286.7	1.8	18/36	22.9	23.3	35.5
13	1981. 8.20	20:55: 6.6	121	46	24	43	0.3	3.9	23.1	4.3	14/36	13.4	25.8	35.5
14	1981. 8.30	18:54:53.6	121	45	24	28	0.2	5.0	180.0	23.0	31/36	17.7	31.6	43.5
15	1981.10. 5	13:24:30.5	121	45	24	39	3.6	3.4	219.2	2.7	29/37	40.5	95.5	55.7

Azim: Array to epicenter azimuth; *T: Number of stations triggered

Δ: Distance; I: Number of stations installed in the field

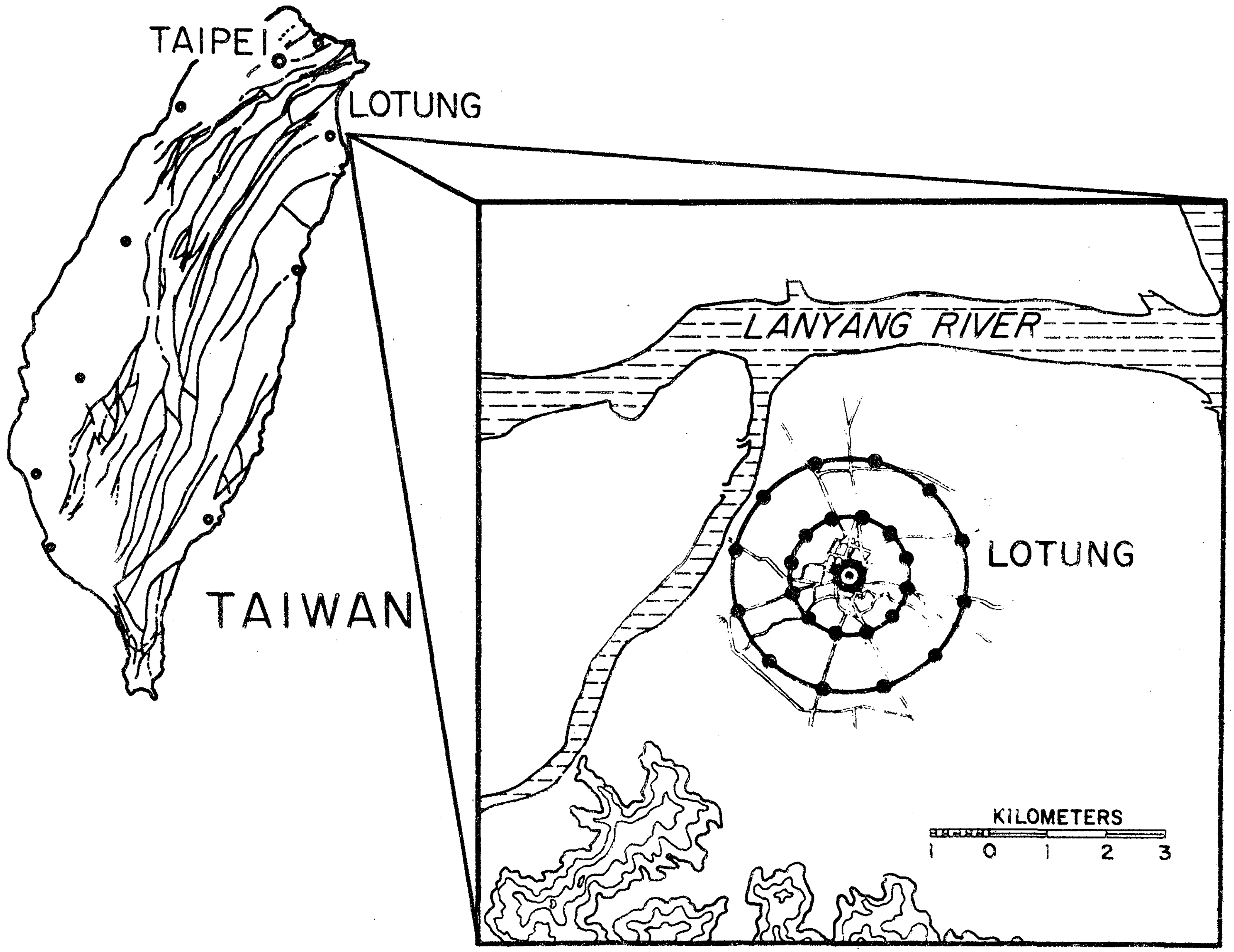

Fig. 1.1 Location of SMART 1

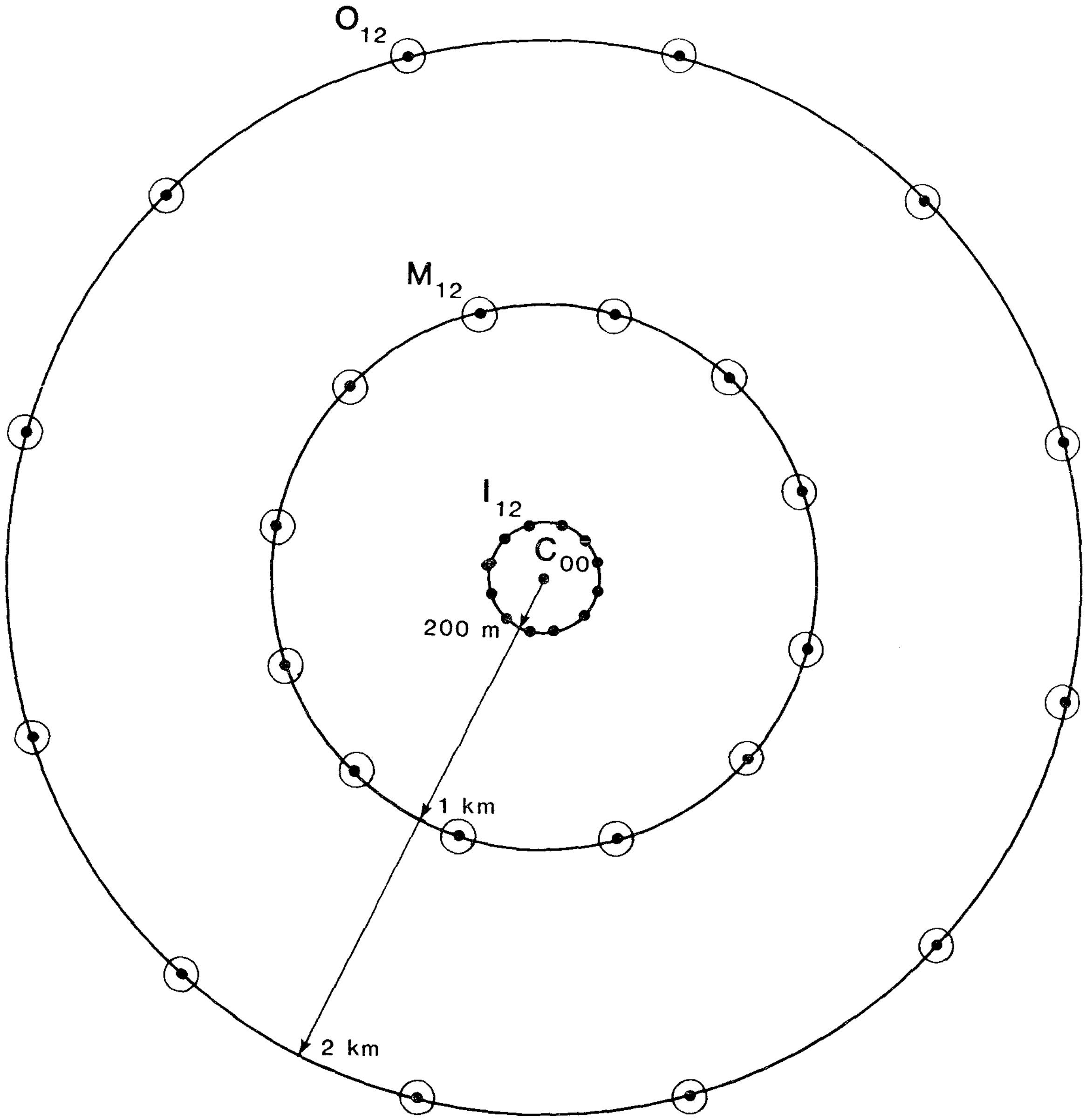

Fig. 1.2 The SMART 1 array

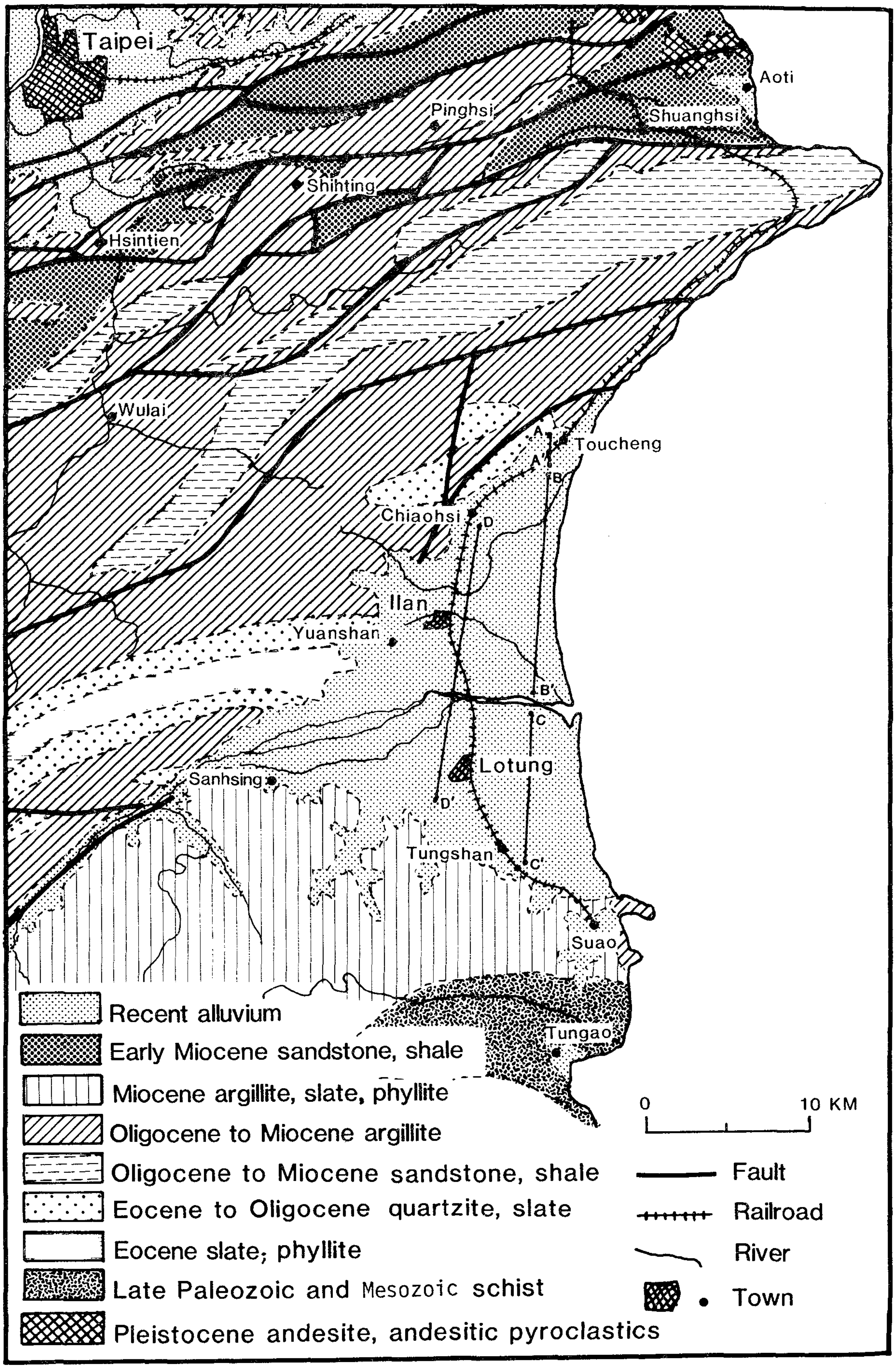

Fig. 1.3 Geological map of Lotung area

Subsurface geology along profile A-C' (see Fig. 1.3)

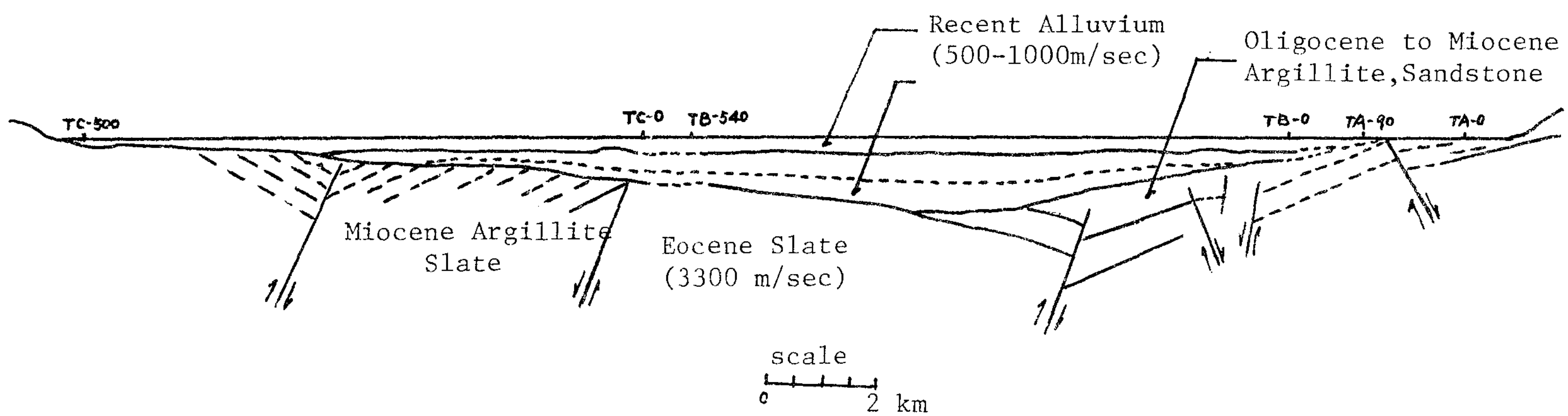

Subsurface geology along profile D-D'

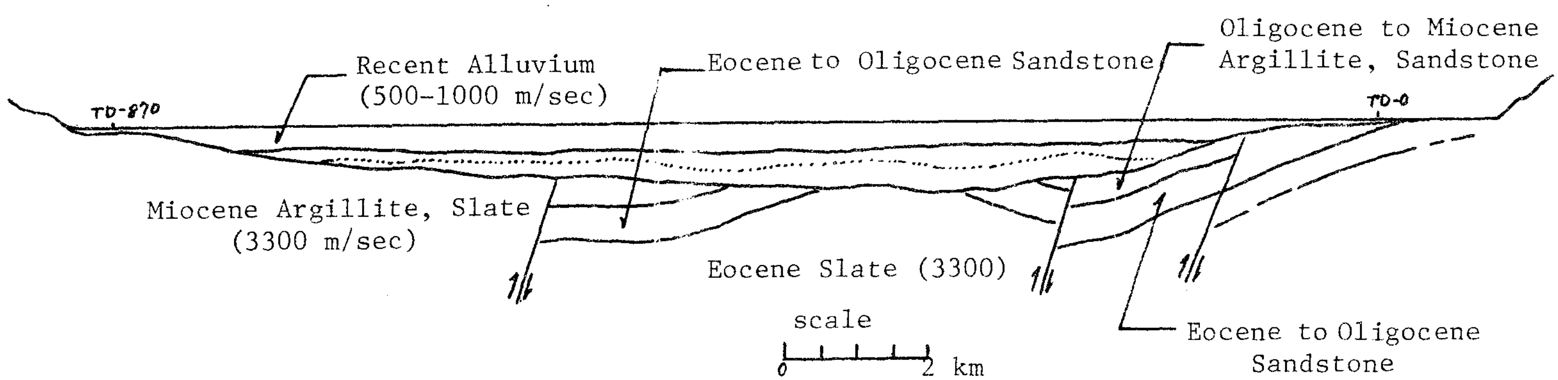

Fig. 1.4 Profile of array site

2. INSTRUMENTATION

2.1 Introduction

All the instruments selected for the SMART 1 array were extensively tested at the University of California, Berkeley, before they were shipped to Taiwan where they were again checked before final installation. Installation of the SMART 1 instruments in the field in Taiwan began in September 1980 by engineers from the Institute of Earth Sciences, Taiwan, initially jointly with the staff of the Seismographic Station of the University of California at Berkeley. By October 1980, twenty-one elements of the array were operational and the remaining elements were added in the following months (Table 1.1). All thirty-seven elements were installed by September 1981. A second-order traverse was made in January 1981 to determine the exact location of each element. The coordinates are given in Table 1.1. The deviations of the actual site locations from the planned configuration are listed in Table 2.1.

By June 1981, eleven earthquakes had been recorded by SMART 1, with excellent performance in that most instruments triggered and the digital records were of high quality.

In this section some of the technical insights gained from the installation and operation of SMART 1 during its first year are presented.

2.2 Instrument Specification

The array elements at the field stations are triaxial strong-motion accelerographs which include digital cassette recorders with precision timing capability. A detailed description of the instrumental components is given below.

(i) Accelerographs

There are 37 self-contained digital accelerographs having low power dissipation. Tie-down bolts anchor the unit to a surface pad. The three-component accelerometers (SA-3000) are self-triggering when the vertical acceleration exceeds 0.01g (adjustable). The accelerometer is connected to a Sprengnether DR 100 recorder (shown in Fig. 2.1) in which data are filtered to prevent aliasing. The signal sampling at 100 sps per channel is converted to 12 bit binary. The digital delay memory has a capacity of 2.5 seconds. Digital data are recorded on magnetic tape cassettes which have a high signal-to-noise ratio. An automatic time-code generator records on tape such time information as day of year, hour, minute, second. The accelerograph also is capable of recording externally generated reference time signals on the cassette tape.

The sensitivity of the SA-3000 is 3.75 V/g with $\pm$ 2.0g full scale; its resolution is 0.001 percent of full scale or 2.0×10^{-3} g. Arrows on the case of the sensor indicate the positive directions of the motions as shown in Fig. 4.8. The SA-3000 consists of three force-balanced accelerometers oriented so that their sensitive axes are orthogonal. Their full-scale output is $\pm$ 7.5 V. A bubble is provided in the lid of the SA-3000 to ensure level installation of the sensor. Calibration data for level output voltage are provided with each unit so that an absolute level can be achieved for the horizontal sensors to approximately +3 minutes of arc. The AC/DC converter, calibration, circuit, and three-channel, five-pole Butterworth low-pass anti-aliasing filter are incorporated within the unit. The calibration input injects current into each sensor so as to provide approximately a 1g bias of the sensor. Specifications of the SA-3000 are shown in Table 2.2.

(ii) Power Units

Each of the 37 elements of the array is powered by lead-acid batteries, charged regularly from the local electricity supply.

(iii) Portable Comparator

A portable field clock and comparator unit that can be taken from station to station is used to compute and display accumulated time corrections for the internal station clock to an accuracy of 1 millisecond. A comparator reference clock is also displayed. Manual adjustments of the comparator clock to GMT from radio time-signals are necessary.

(iv) Portable Playback Unit

The portable playback unit has the capacity to play the accelerograph digital tape cassettes onto strip charts with variable gain. The analog signals are displayed in parallel with the coded time data.

(v) Laboratory Playback System

The laboratory playback system selected was the Sprengnether DP-200 (shown in Fig. 4.1) which has the capability to play cassette tapes into a recorder that displays the signals on three-channel paper with time annotation. The system can also transfer the digital data from cassettes to nine-track tape (10-1/2 inch reels) in ASCII-coded 800 bpi records with character representation. The length of the record is 5120 characters.

During the initial testing, if any malfunction was noted in an instrument, all other instruments were checked particularly with regard to this function. Most difficulties occurred with individual accelerometers which are easily damaged by rough handling since they are of the pivot and jewel type. One symptom of damage was variation of the base line, called DC drift or DC offset. In all, 24 of the 111 SA-3000 accelerometers were returned to the manufacturer, Columbia Research Laboratories, Inc., for repairs.

Some available strong motion instrumentation was rejected for a variety of reasons. For example, some nine-track tape recorders were not acceptable since they used binary format, not ASCII. The latter code was selected because it was decided that the system must be independent of a particular computer from the outset; the project is an international one and could not be tied to a specific data processing system.

In particular, the instruments selected have the following features: the crystal oscillator specifications of the clock-comparator are very precise; the anti-aliasing filter for the seismic data has sharp attenuation; the annotation on the paper recorder playout is quite complete, and includes a simultaneous time information unit, serial number, and accurate reference time. Furthermore, the cassette playback system is convenient in that it displays time of event and event number while the tape is read, and the tape automatically stops between events. It would be even more satisfactory, however, if the start-up time were slightly faster and the tape recording time longer.

2.3 Shaking Table Test

Finally, before they were shipped to Taiwan, all accelerometers and digital recorders were tested on the earthquake simulator (shaking table) at the Earthquake Engineering Research Center of the University of California, Berkeley (Fig. 2.2). Recorded strong ground motions from California earthquakes scaled to various acceleration levels were used to drive the shaking table to which both the accelerometers and recorders were rigidly attached.

This laboratory test for defects in the instrumentation also provided an opportunity to check the specified responses of the accelerometers against the known response of the shaking table. A time-history of the shaking table input and the corresponding response of one of the instruments is shown in Fig. 2.3. The response of the shaking table is measured by an accelerometer placed at the center of the table. Tests were also done at low acceleration levels to test the trigger circuitry.

On subsequent evaluation, the shaking table tests proved to be of great value. Undoubtedly, malfunctions in the field in Taiwan were minimized by this procedure.

The following shaking table inputs based on accelerograms recorded at El Centro, Taft, and Pacoima Dam during the earthquakes of May 1940, June 1952, and February 1971, respectively, were used.

(1)	El Centro	vertical
(2)	El Centro	NS horizontal - max. accel. 0.33g
(3)	(1) and (2) combined	
(4)	Pacoima	horizontal and vertical combined
(5)	Taft	horizontal S69E (max. accel. 0.18g) and vertical combined, with amplitude increased to maximum possible for the table.

A comparison of El Centro (2) with the response of one of the instruments in Fig. 2.3 shows no significant differences in the time domain. The relation between the driving force and the transfer functions of the shaking table and instrument are illustrated in Fig. 2.4. When all the systems are assumed to be linear, the instrument transfer function is defined as

$$H(\omega) = \frac{Y(\omega)}{F(\omega)}$$

where $Y(\omega)$ and $F(\omega)$ are the Fourier transforms of the responses of the instrument, $y(t)$, and shaking table, $f(t)$, respectively.

Figures 2.5 and 2.6 show the transfer functions of instruments 290 and 300, for the different driving forces, El Centro (1) and (2). The curves show that at frequencies below 16 Hz, $|H(\omega)|$ is approximately equal to one. This means that below 16 Hz the signal recorded by the instrument is essentially the same as the movement of the shaking table. Comparison of the recorded response of the instrument with the input motion indicates close agreement.

2.4 Field Adjustments

A typical field installation is shown in Fig. 2.7. The elements of the array are routinely checked every 2 to 3 days in accordance with the following directions to the local operator:

1. Before visiting station, observe clock error of TS-500 on scope. Adjust clock to zero error once every two weeks.
2. On entry to station, take a general look at the system. The "clock" lamp on DR-100 should flash once per second. Turn on "display" switch to make sure that the clock works in normal conditions.
3. Read event number and record it on operational log.
4. Check the time error between TS-500 and DR-100. Enter the time and time error on this operational log. On giving a "step" calibration

or writing a time error from the TS-500, make a note on the operational log and observe the tape movement. Adjust DR-100 clock to zero error once every two weeks (after TS-500 adjustment).

5. Use a digital voltage meter to check external battery voltage and record on operational log.
6. Replace external battery at each station once a week.
7. Measure output signal of each channel of the SA-3000 accelerometer and record on the operational log.
8. Do not change sample rate and time duration switch.
9. If a change in trigger level is made or the tape is replaced, make a note on the operational log.
10. Before leaving the station, observe event number again and turn display off.
11. Immediately following an earthquake, each station should be visited. Write time error on the tape and operational log, then replace the tape. Send data back to the Institute as soon as possible.

TABLE 2.1

Deviation of Actual Site Locations from the Planned Configuration

Station	Distance Error (meters)	Azimuth Error (degrees)	Station	Distance Error (meters)	Azimuth Error (degrees)
I01	- 6.7	-3.29	M07	+22.9	+2.65
I02	- 6.1	+0.74	M08	-16.3	-1.84
I03	+ 4.2	-0.95	M09	+33.9	-3.87
I04	+ 6.8	-0.31	M10	-77.0	-3.9
I05	+ 1.8	-0.76	M11	+ 2.0	0 *
I06	- 6.4	+4.06	M12	+ 3.5	+0.57
I07	+ 0.6	+2.62	001	+26.4	-1.27
I08	-12.3	-1.71	002	+ 8.2	-0.17
I09	+ 6.9	-0.43	003	+40.7	+0.31
I10	- 0.3	-1.83	004	-15.7	-1.59
I11	-18.4	-0.90	005	- 1.0	-2.68
I12	+ 1.4	+0.54	006	+10.2	-0.55
M01	- 8.1	-1.12	007	+ 0.8	-1.38
M02	+99.9	-3.04	008	+56.4	-3.19
M03	-53.9	-3.97	009	+45.2	-2.44
M04	+12.5	+0.19	010	+ 2.9	+0.40
M05	-39.9	-3.06	011	-51.2	-0.03
M06	+ 2.7	-0.21	012	- 3.6	+0.17

* Reference Station

TABLE 2.2

Specifications of the SA-3000 Accelerometer

RANGE: ± 2.0g

SCALE FACTOR: 3.75 v/g

INPUT POWER: + 12 vdc @ 165 ma

RESOLUTION: 0.001% of full scale

NON-LINEARITY: Less than 0.2% of full scale

HYSTERESIS: Less than 0.05% of full scale

CROSS-AXIS SENSITIVITY: Less than 1%

TEMPERATURE SENSITIVITY: Less than 0.01% per degree F

NATURAL FREQUENCY: > 50 Hz

DAMPING RATIO: 0.7 ± 0.2

ZERO OUTPUT: Less than 0.50%

TEMPERATURE RANGE:

65° F to 200° F	storage
0° F to 150° F	operation

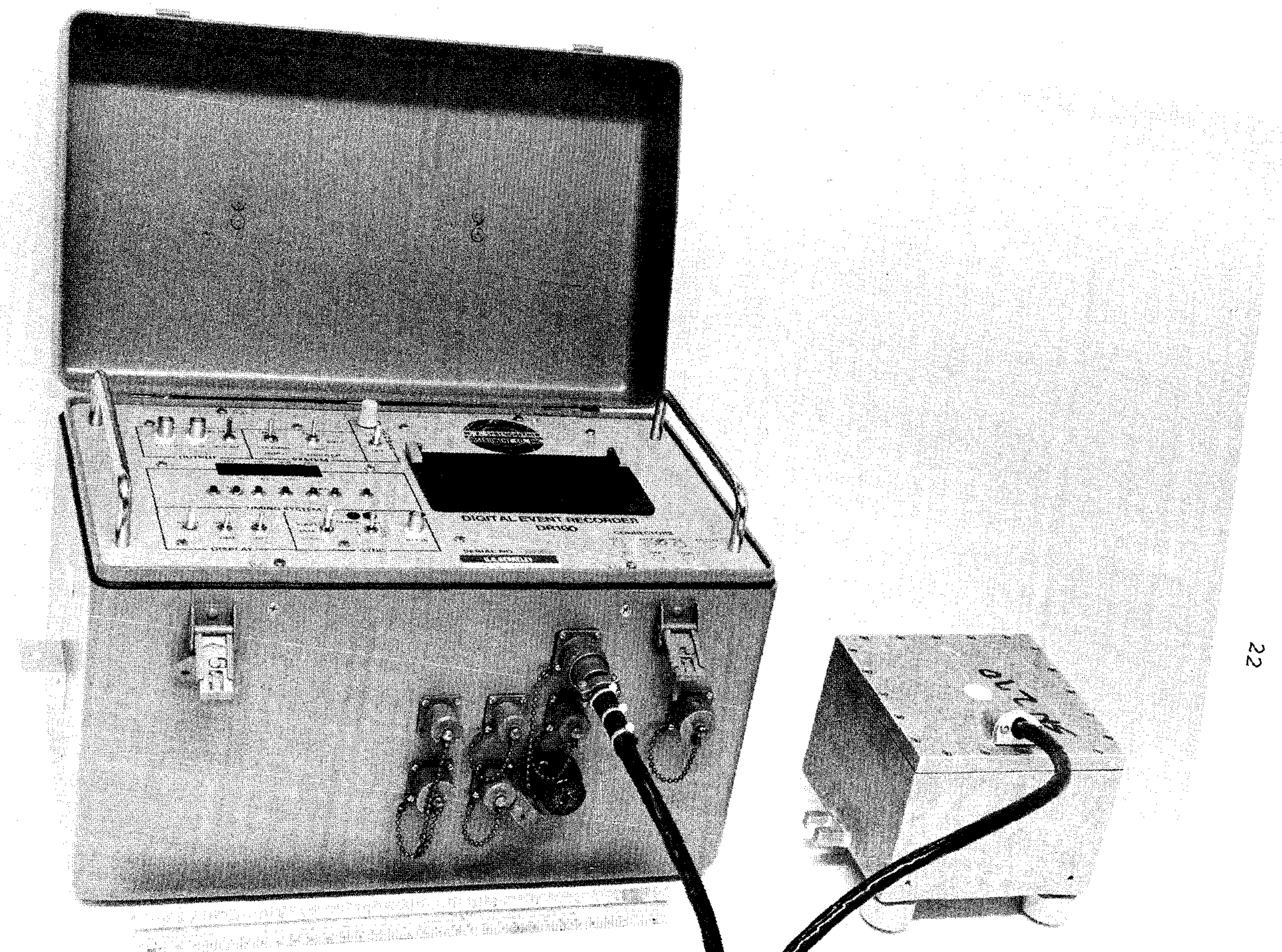

Fig. 2.1 Digital cassette recorder

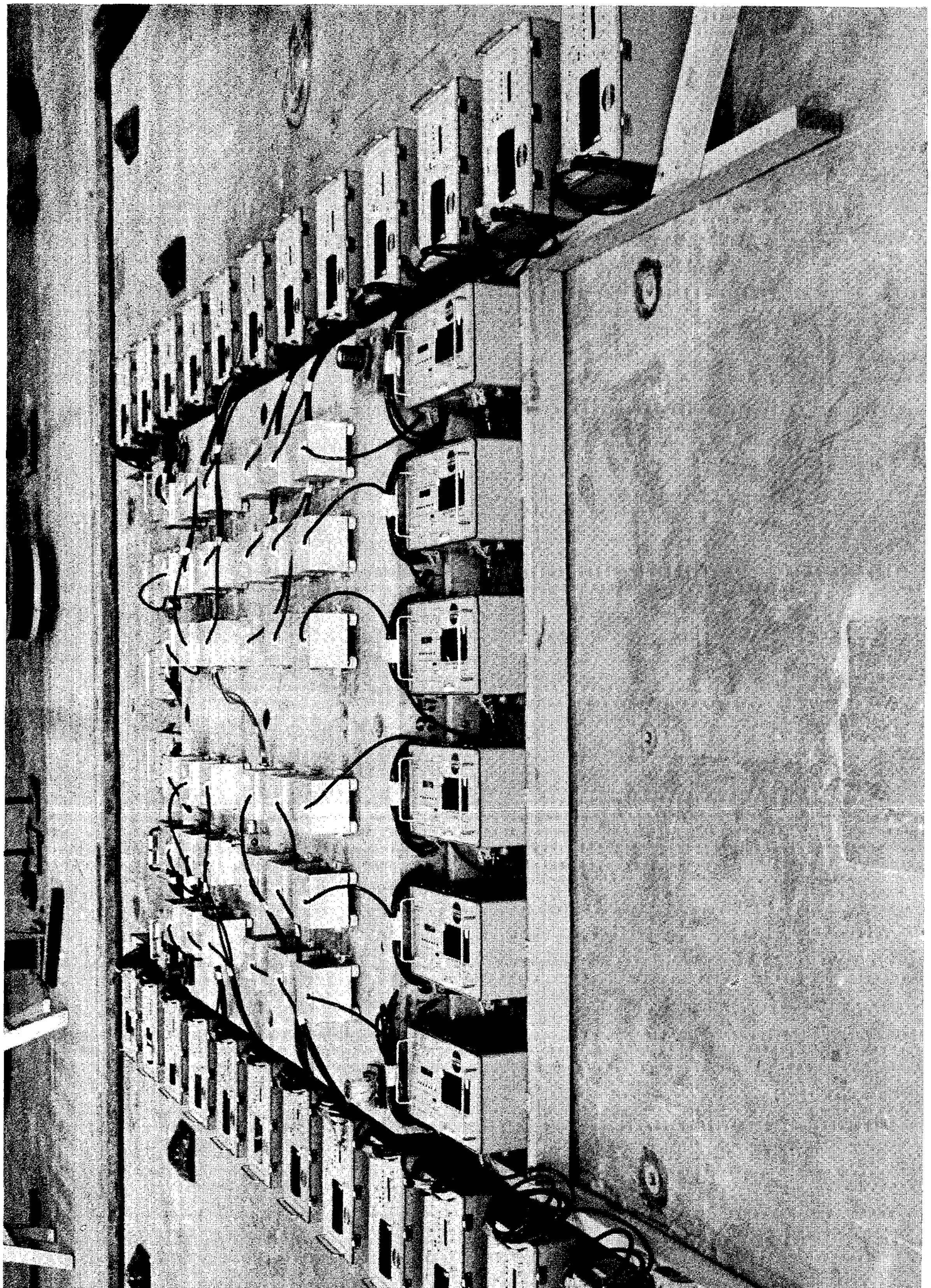

Fig. 2.2 Shaking table test of digital seismographs

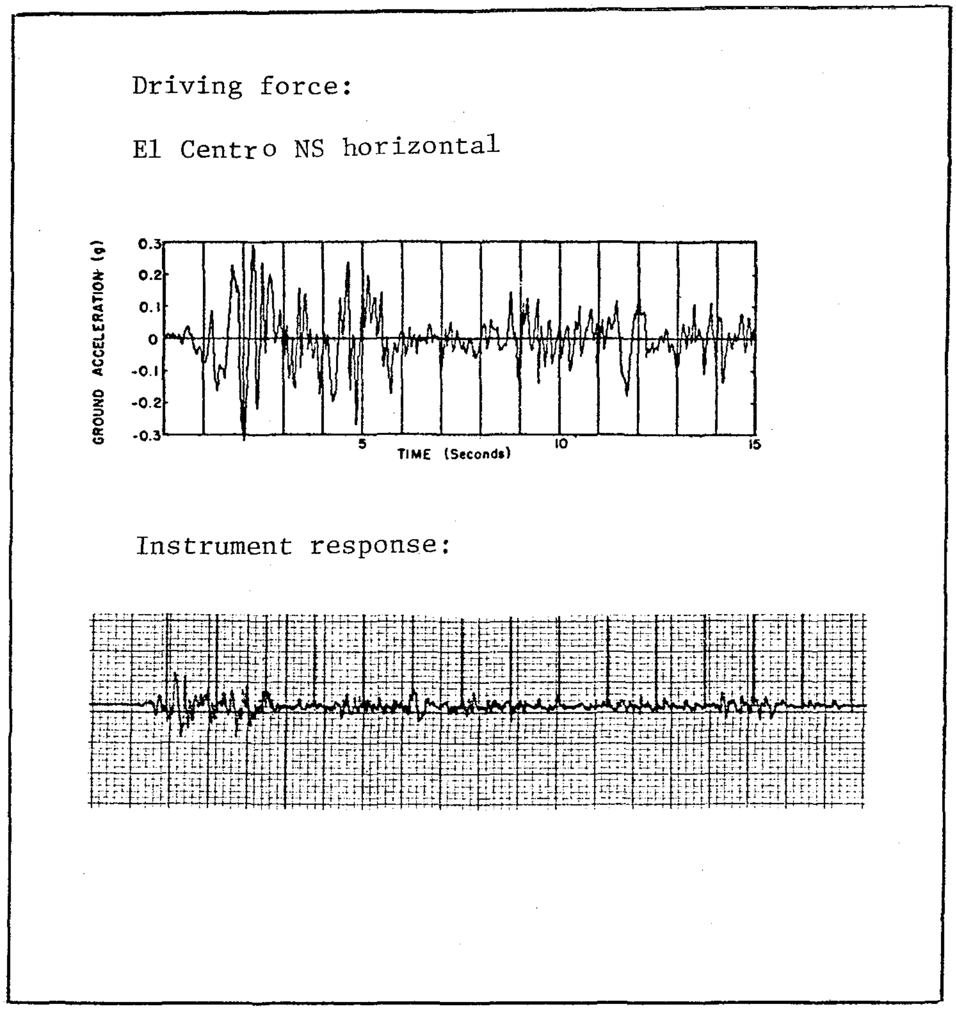

Fig. 2.3 Comparison between input acceleration and instrument response from shaking table test

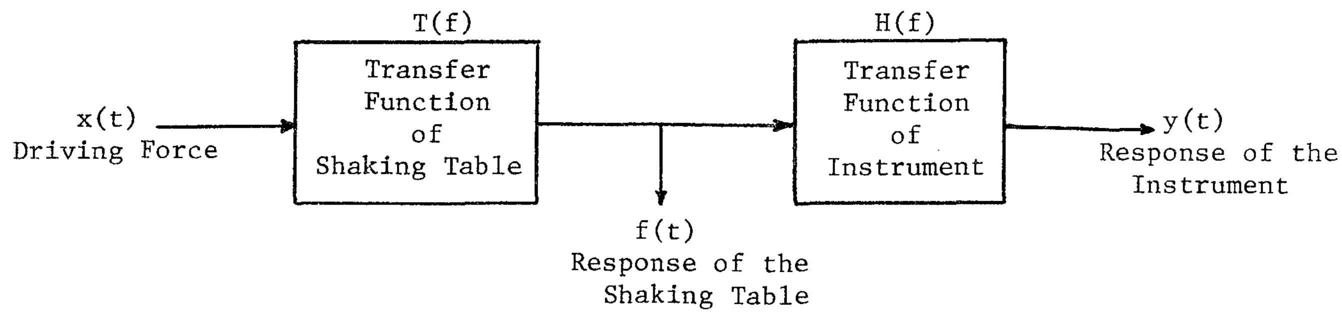

Fig. 2.4 Diagrammatic representation of shaking table test

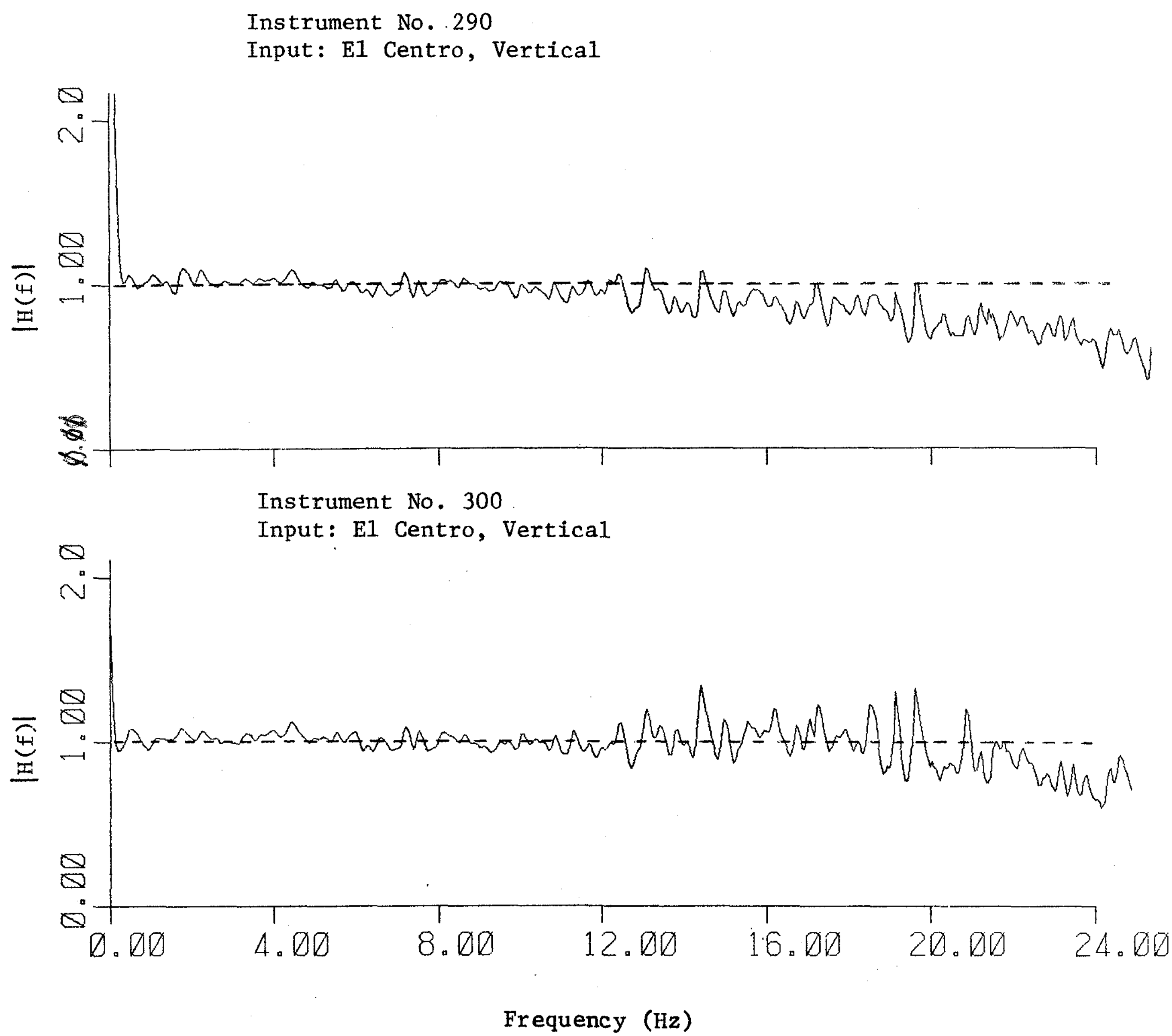

Fig. 2.5 Instrument transfer function for El Centro vertical input

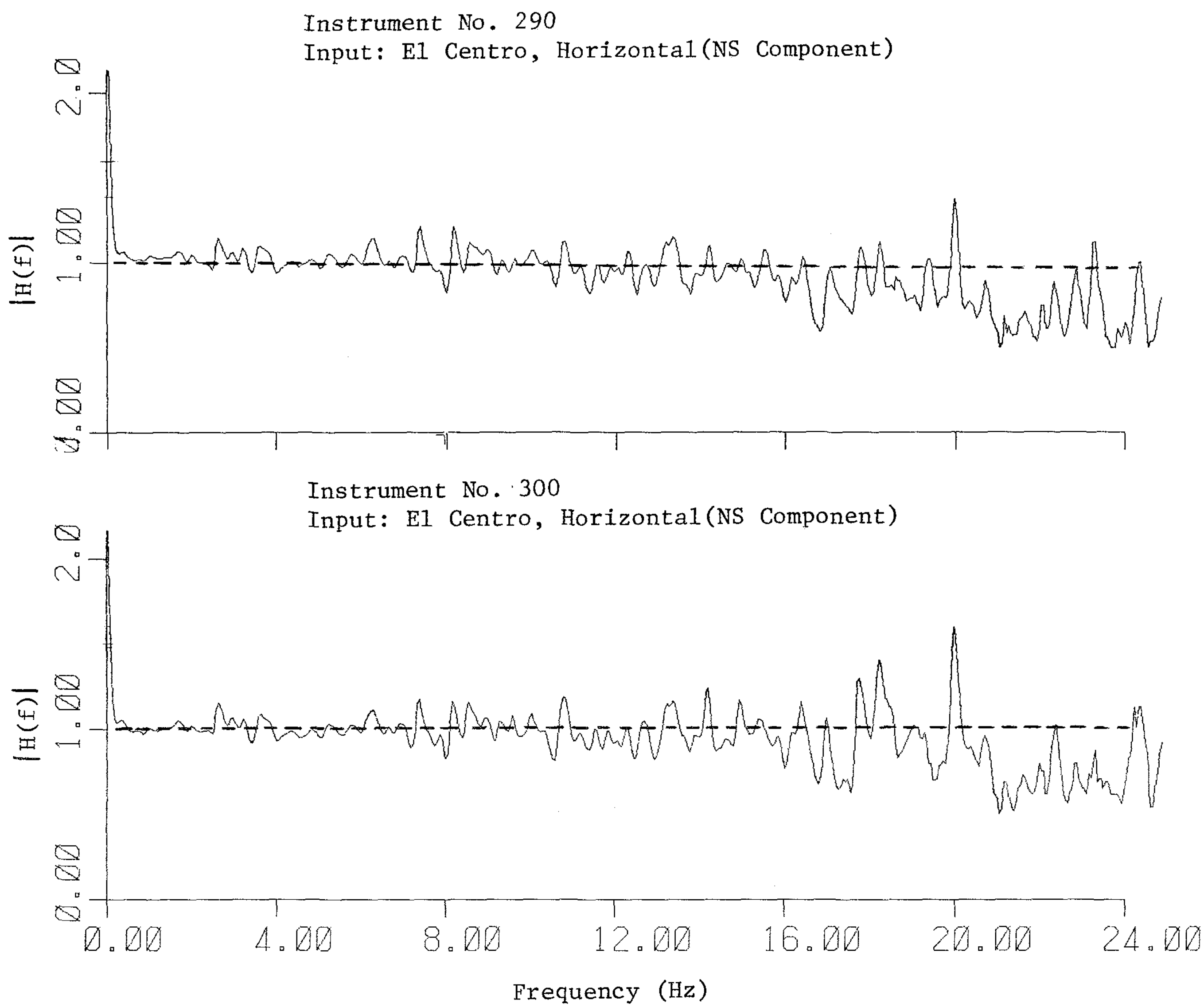

Fig. 2.6 Instrument transfer function for El Centro horizontal input

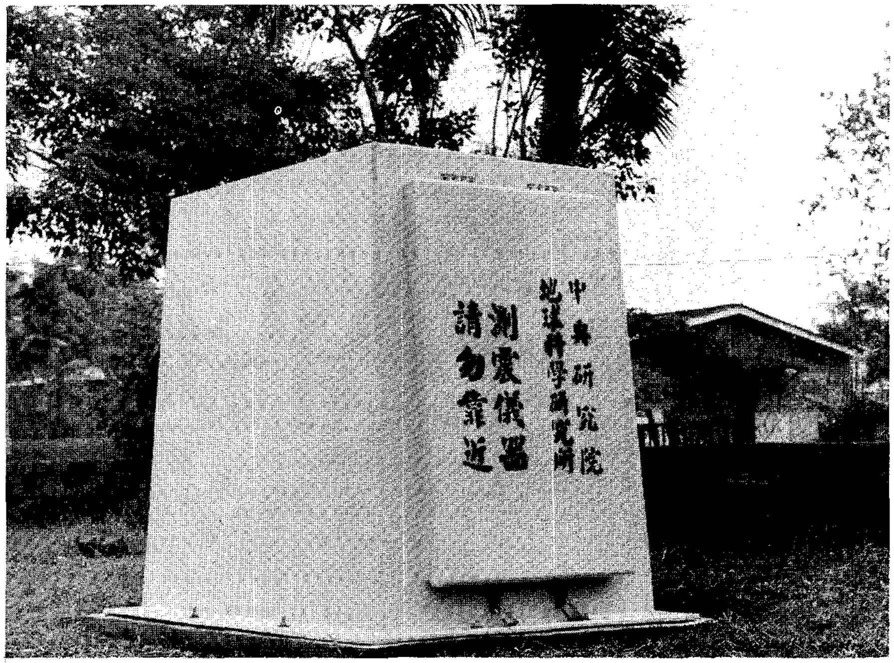

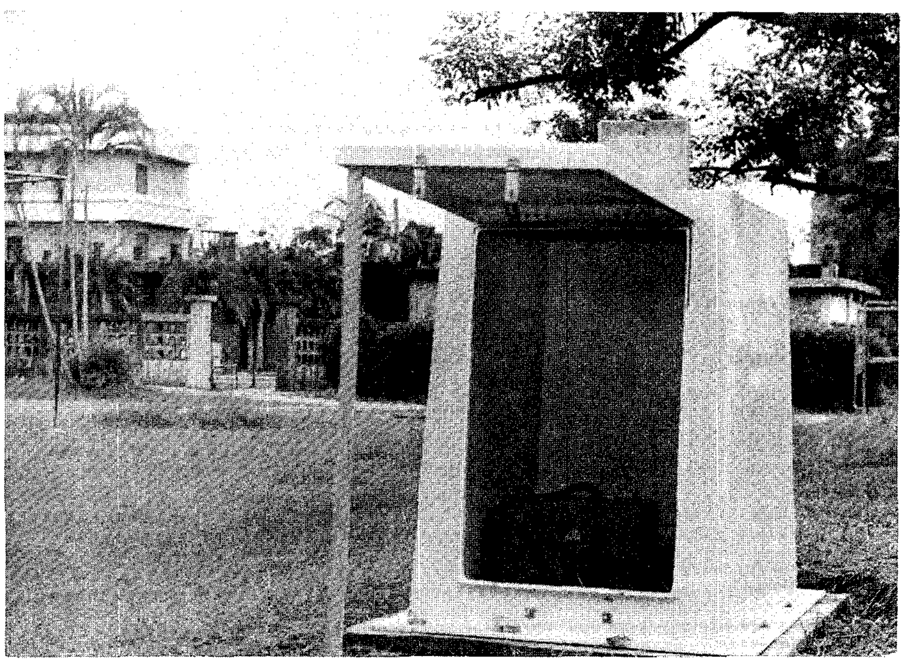

Fig. 2.7 Typical field installation

3. A PRELIMINARY STUDY OF THE TAIWAN STRONG MOTION ARRAY DATA

3.1 Description of Available SMART 1 Data

During the first six-month period of operation, from October 1980 to March 1981, SMART 1 was triggered partially or wholly by nine earthquakes. Most analysis to date has been given to this early data set. The parameters of these earthquakes are listed in Table 1.2, together with preliminary results for six subsequent earthquakes up till October 1981. The earthquakes in the total set are referred to as Event 1 through Event 15. The recorded maximum peak accelerations of the vertical, EW, and NS components of each earthquake are also included in Table 1.2. The epicenters of the first nine earthquakes are shown in Fig. 3.1. Table 1.2 and Fig. 3.1 show that three earthquakes with M_L in the range 5.6-5.9 were located almost directly below SMART 1 at depths ranging from 59 to 76 km. The remaining six earthquakes with M_L in the range 3.8 to 6.9 were all shallow, with depths ranging from 7 to 43 km. The epicentral distance ranges from 7 to 193 km. The ratio of triggered instruments to operational instruments ranges from 2/27 to 27/27 for the first nine earthquakes. With only few exceptions, failure to trigger was simply because actual ground accelerations did not reach the preset trigger levels of 10-15 gals. The highest acceleration recorded during the initial twelve-month period was 244 gals.

Following each event, the triggered tape cassettes were retrieved from the field and returned to the Institute of Earth Sciences, Taipei, where their contents were transferred onto a regular 9-track magnetic tape (see Section 2.2). The data on this regular tape were then read into a computer for decoding, checking, editing and correction for DC offsets before they were stored onto a data tape for further processing. Time corrections of individual records were included in the event header.

Figures 3.2a, b, and c show recorded waveforms of the vertical, EW and NS components, respectively, for Event 2, the M_L = 5.9 earthquake of November 14, 1980. This earthquake at 62 km depth was only 10 km from SMART 1, so that it was located almost right under the array; 16 out of the 21 operating instruments were triggered. Both P and S waves were recorded, showing an S-P time of about 9 sec. A small delay of P waves as well as of S waves across the array was observed, consistent with the near-vertical incidence of these waves. The signal levels of the vertical component (primarily P waves) were significantly lower than those of both the EW component (primarily SH waves) and the NS component (primarily SV waves). The two horizontal components had about the same strength. The waveforms of individual components varied considerably across the array. Figures 3.3a, b and c show recorded waveforms for Event 5.

Tables 3.1 and 3.2 list the peak accelerations of the vertical, EW and NS components and their occurrence times recorded by SMART 1 for Events 2 and 5, respectively. The values range from 9.3 to 29.7 gal, 19.9 to 69.7 gal and 29.0 to 78.7 gal for the vertical, EW and NS components, respectively, so that the peak accelerations vary by a factor of 2 to 4 across the array. The following two observations can be made from these results. First, variations in both vertical and horizontal peak accelerations by a factor of 2 to 3 were not uncommon over a circular area having a radius of only 2 km. Secondly, the peak accelerations of the horizontal components were about 3 times greater than those of the vertical component.

A comparison between the free-field motion and the motion recorded by an analog-recording SMA-1 instrument at the Lotung Town Hall in the SMART 1 area can be seen from Figs. 3.4a and b.

3.2 Correlation Coefficients of Acceleration Waveforms Across SMART 1

An important consideration in the design of a long-base structure concerns the coherency of input acceleration functions at different points of its base. The SMART 1 data provide valuable information for this problem. The correlation coefficients ρ_{ij} (see Chapter 7) between the acceleration waveforms of the same component recorded at two array sites were computed. The results are plotted as a function of site separation for the largest intermediate-depth earthquake, Event 2, whose waves arrive at the array in a nearly vertical direction, and for the largest shallow earthquake, Event 5, whose waves arrive at the array in a more horizontal direction.

Figure 3.5 shows the correlation coefficient ρ_{ij} for the vertical, EW, and NS components for Event 5 to be about 0.5, 0.6, and 0.7, respectively, at site separation about 0.2 km. For larger site separations, ρ_{ij} drops to within ±0.2 , ±0.3, and ±0.4 for the vertical, EW, and NS components, respectively. Thus, the waveforms are better correlated for the NS component than for the EW component. The vertical component has the poorest correlation.

TABLE 3.1

Maximum Acceleration: Event 2

EARTHQUAKE OF NOV. 14, 1980, 13H, 37M, 4.00S (GMT)

EPICENTER: 121-47.49E 24-35.14N
DEPTH : 62.06 (KM)
MAGNITUDE: 5.90

STATION CODE	V COMPONENT		EW COMPONENT		NS COMPONENT	
	gal	second	gal	second	gal	second
C00	19.8	24.342	56.8	23.522	49.7	25.732
I03	23.4	22.626	34.4	23.946	45.0	24.606
I06	19.5	23.578	31.0	23.508	29.0	25.688
M02	29.7	15.297	60.3	25.387	78.7	23.377
M03	14.9	22.637	19.9	27.557	40.1	24.547
M04	14.4	15.037	37.0	25.597	39.2	24.017
M05	21.4	15.402	49.2	23.182	36.7	25.392
M06	24.2	24.709	28.3	22.999	40.6	24.709
M08	17.0	22.936	67.8	23.486	35.1	23.746
M09	11.5	15.442	27.7	23.472	29.8	24.672
M10	17.9	23.936	61.5	24.866	60.9	24.616
M12	21.5	25.506	34.3	24.616	36.2	23.546
O03	20.4	15.023	37.0	24.013	68.6	24.853
O06	27.9	23.841	69.7	24.031	72.8	23.931
O09	20.8	23.428	42.4	24.478	38.9	23.748
O12	9.3	22.647	51.9	24.277	33.2	24.067

TABLE 3.2

Maximum Acceleration: Event 5

EARTHQUAKE OF JAN. 29, 1981, 4H, 51M, 36.06S (GMT)

EPICENTER: 121-53.78E 24-25.75N
DEPTH : 11.05 (KM)
MAGNITUDE: 6.9

STATION CODE	V COMPONENT		EW COMPONENT		NS COMPONENT	
	gal	second	gal	second	gal	second
C00	42.5	44.456	97.2	48.356	112.0	48.316
I03	44.1	44.945	76.4	48.355	86.4	48.155
I06	31.5	44.423	89.5	48.633	76.4	48.323
I09	64.5	48.703	89.0	48.343	127.6	48.583
I12	57.5	44.203	136.0	48.313	110.2	48.433
M01	91.5	47.560	80.1	48.660	173.9	48.420
M02	47.5	48.211	120.4	48.781	118.8	48.351
M03	28.5	44.506	60.8	48.276	118.9	48.466
M04	31.1	47.150	158.2	48.130	129.8	48.510
M05	42.6	47.340	112.8	48.200	100.3	48.740
M06	53.4	48.748	62.9	48.758	96.4	48.758
M07	47.7	48.560	110.4	48.460	106.4	49.040
M08	35.6	48.521	96.4	48.231	102.6	47.861
M09	32.5	47.250	68.7	48.340	73.4	49.330
M10	40.3	44.519	127.3	48.379	121.0	48.449
M11	55.3	48.455			115.7	48.385
M12	44.5	49.184	93.6	48.474	150.3	48.394
O01	30.6	44.600	87.2	49.190	113.0	48.600
O02	39.0	47.334	139.4	48.574	244.1	48.544
O03	29.2	48.549	156.1	48.309	132.1	48.259
O04	27.5	46.987	123.0	48.147	111.3	48.677

TABLE 3.2 (continued)

STATION CODE	V COMPONENT		EW COMPONENT		NS COMPONENT	
	gal	second	gal	second	gal	second
005	23.4	43.560	97.7	47.790	115.4	48.330
006	39.8	47.183	117.8	48.653	102.7	48.343
007	27.4	47.240	84.5	48.130	79.3	48.060
009	34.7	47.310	116.2	48.220	92.7	49.200
010	40.9	48.478	90.1	48.458	112.3	48.508
012	26.8	47.822	87.0	48.622	161.5	48.682

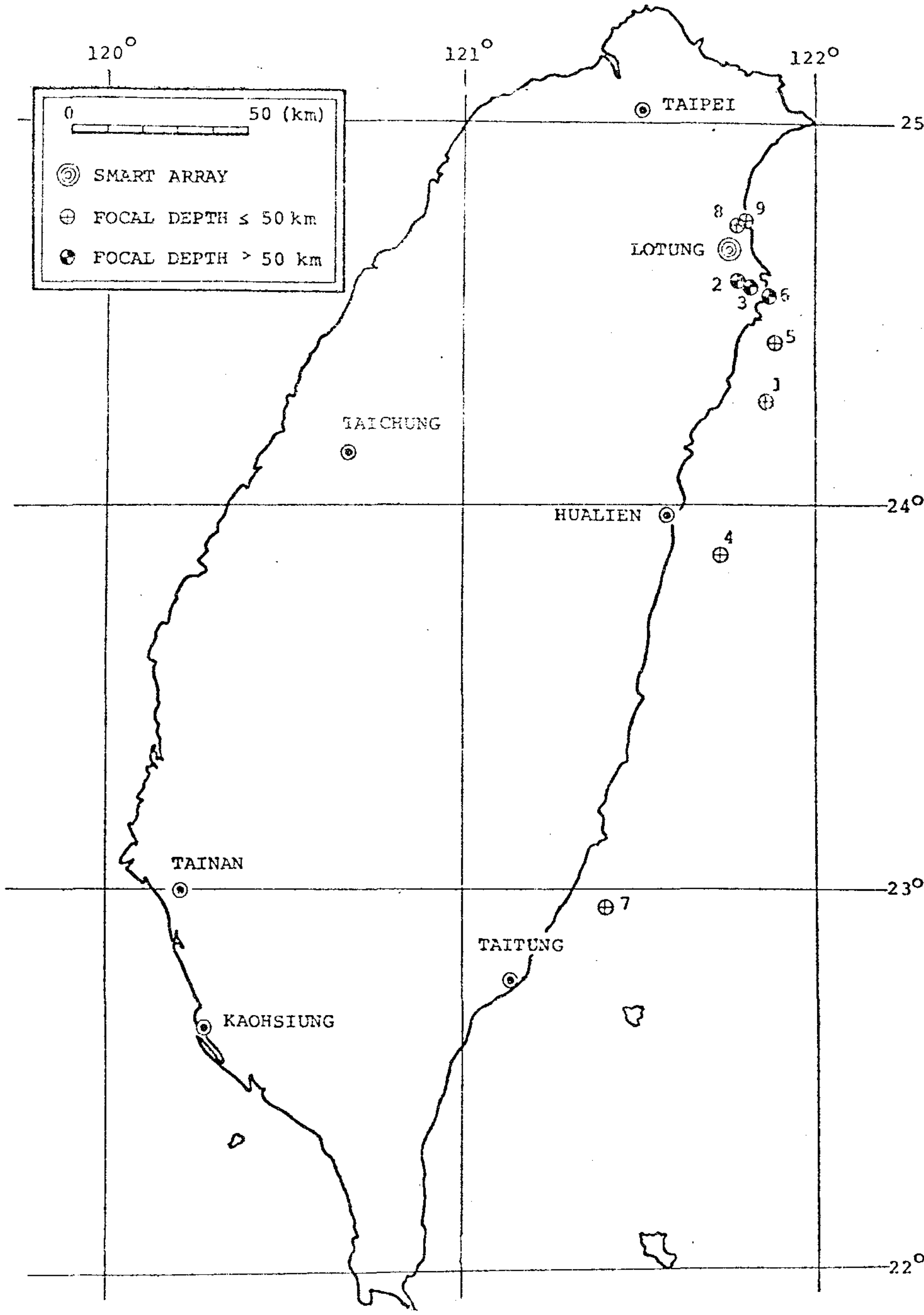

Fig. 3.1 Location of SMART 1 and epicenters of earthquakes recorded during the first six months of operation

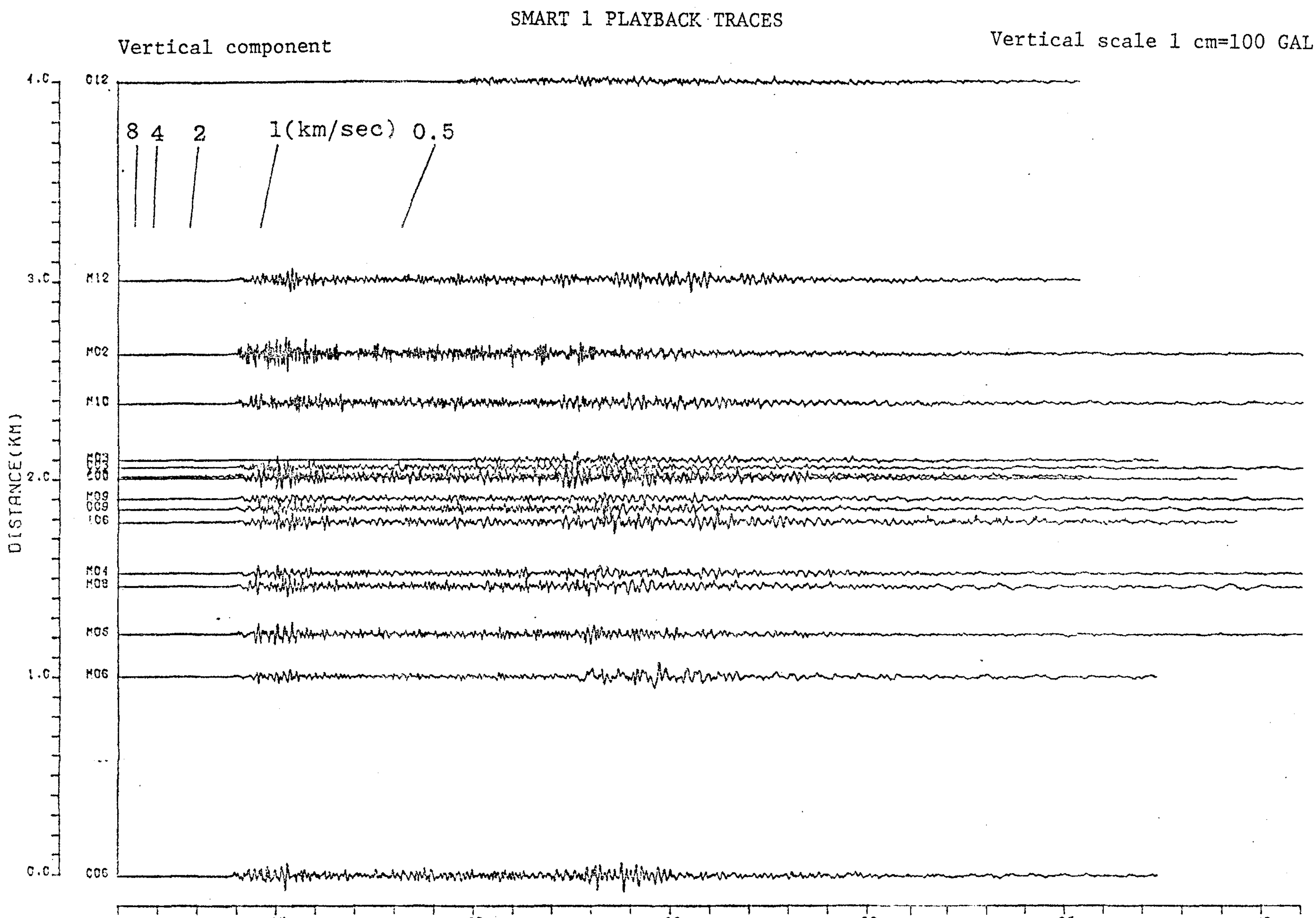

Fig. 3.2a Acceleration waveforms of the vertical component of Event 2

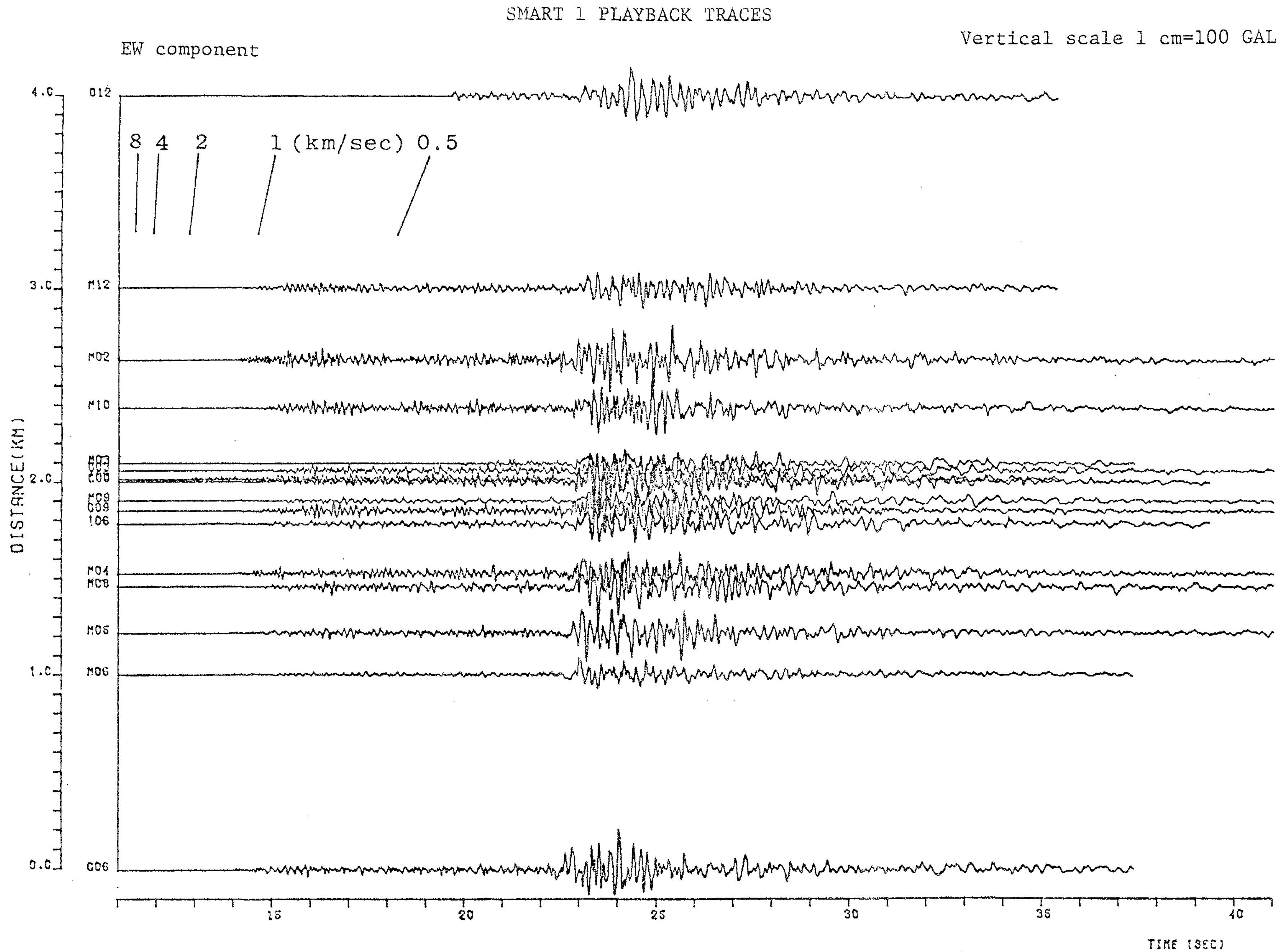

Fig. 3.2b Acceleration waveforms of the EW component of Event 2

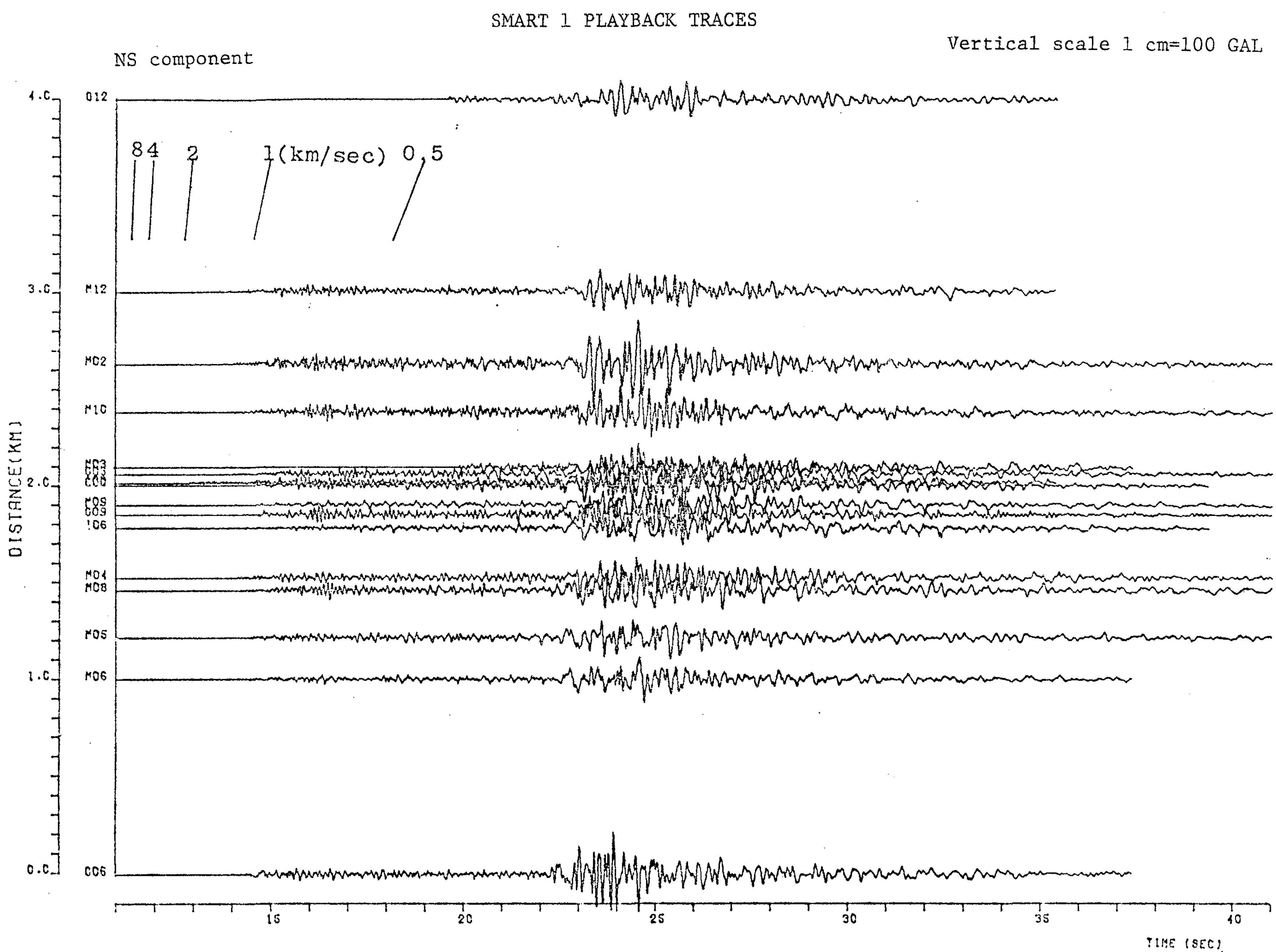

Fig. 3.2c Acceleration waveforms of the NS component of Event 2

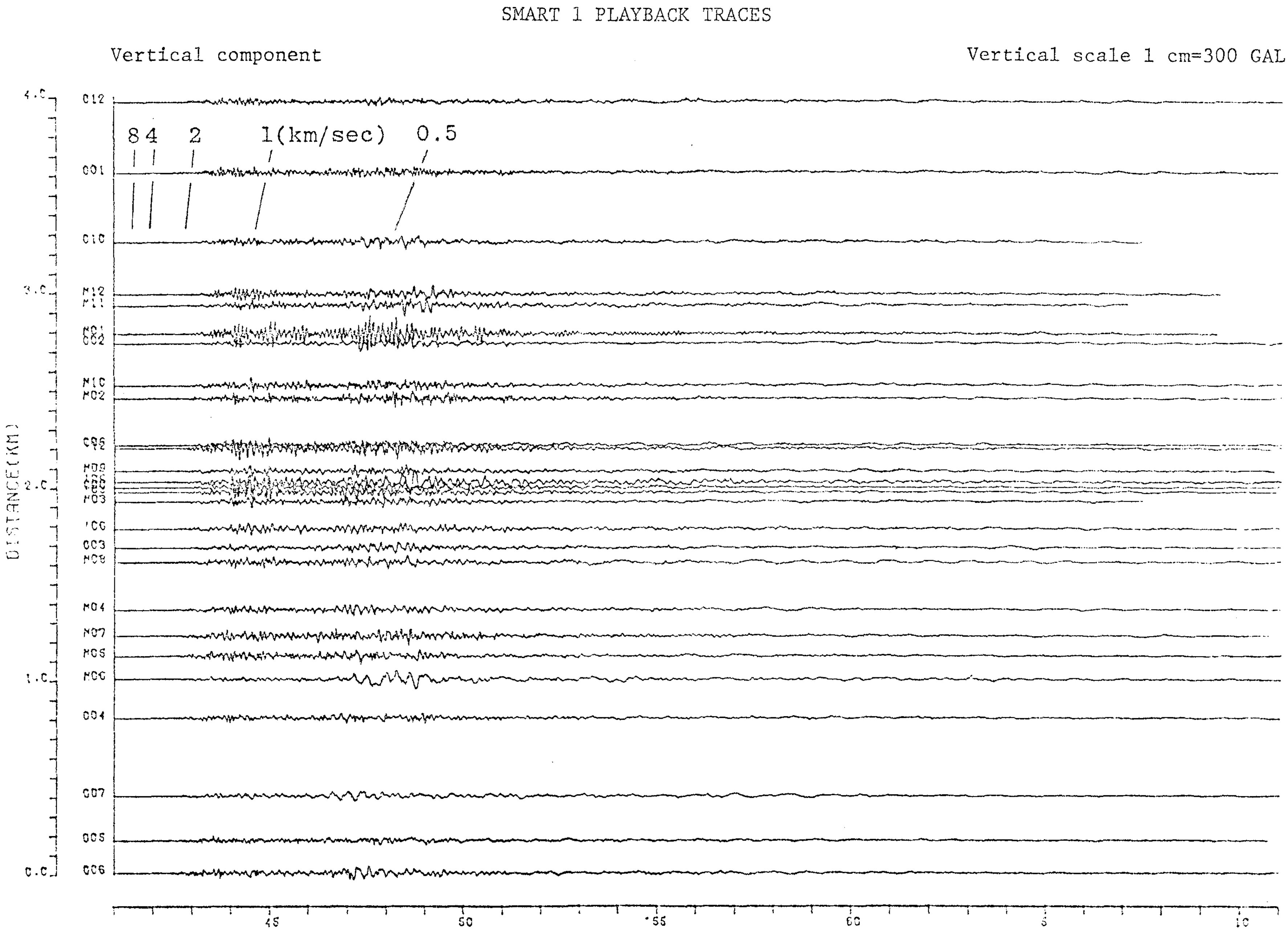

Fig. 3.3a Acceleration waveforms of the vertical component of Event 5

SMART 1 PLAYBACK TRACES

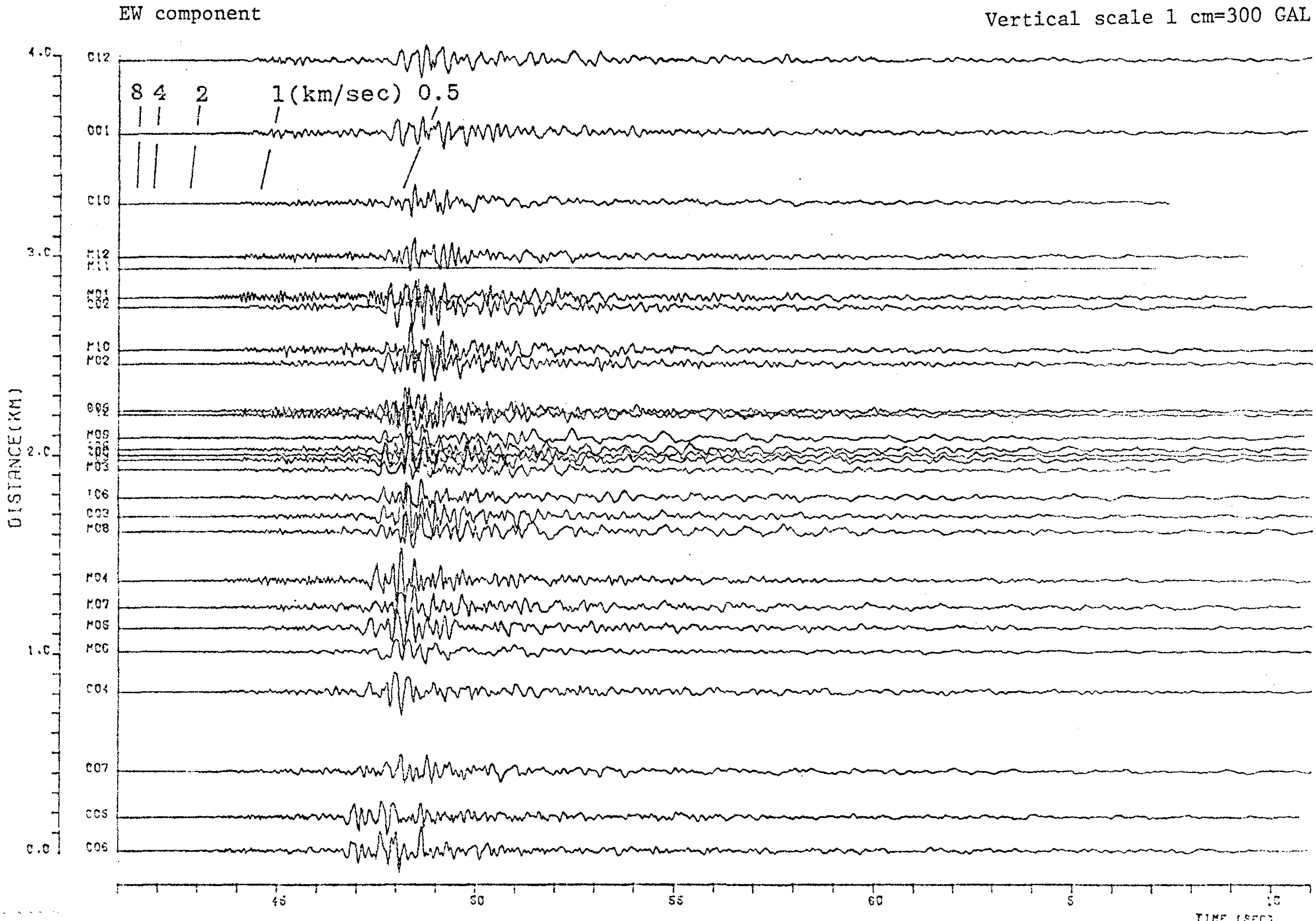

Fig. 3.3b Acceleration waveforms of the EW component of Event 5

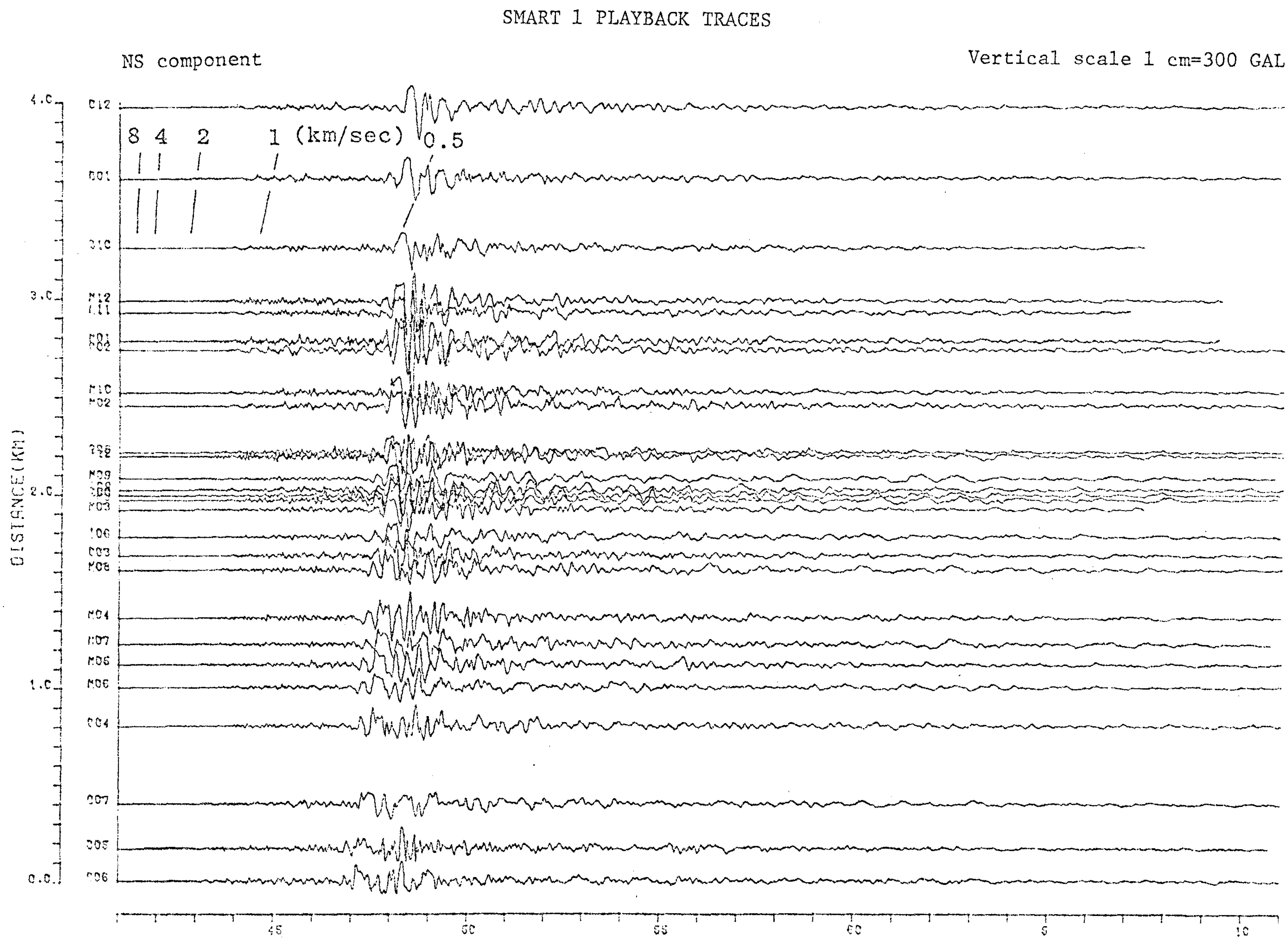

Fig. 3.3c Acceleration waveforms of the NS component of Event 5

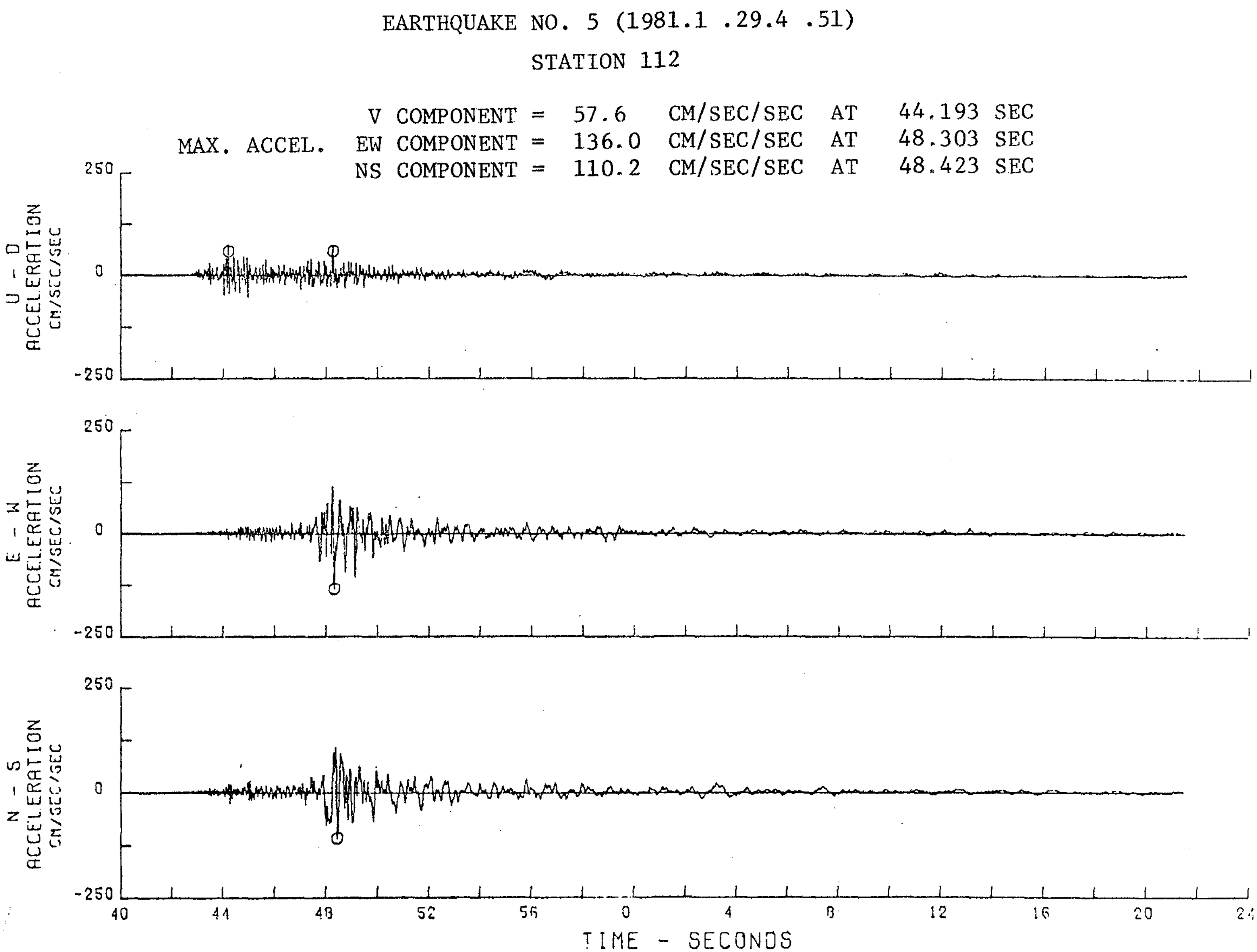

Fig. 3.4a Comparison accelerograms recorded by the digital instruments at array station I12 for Event 5

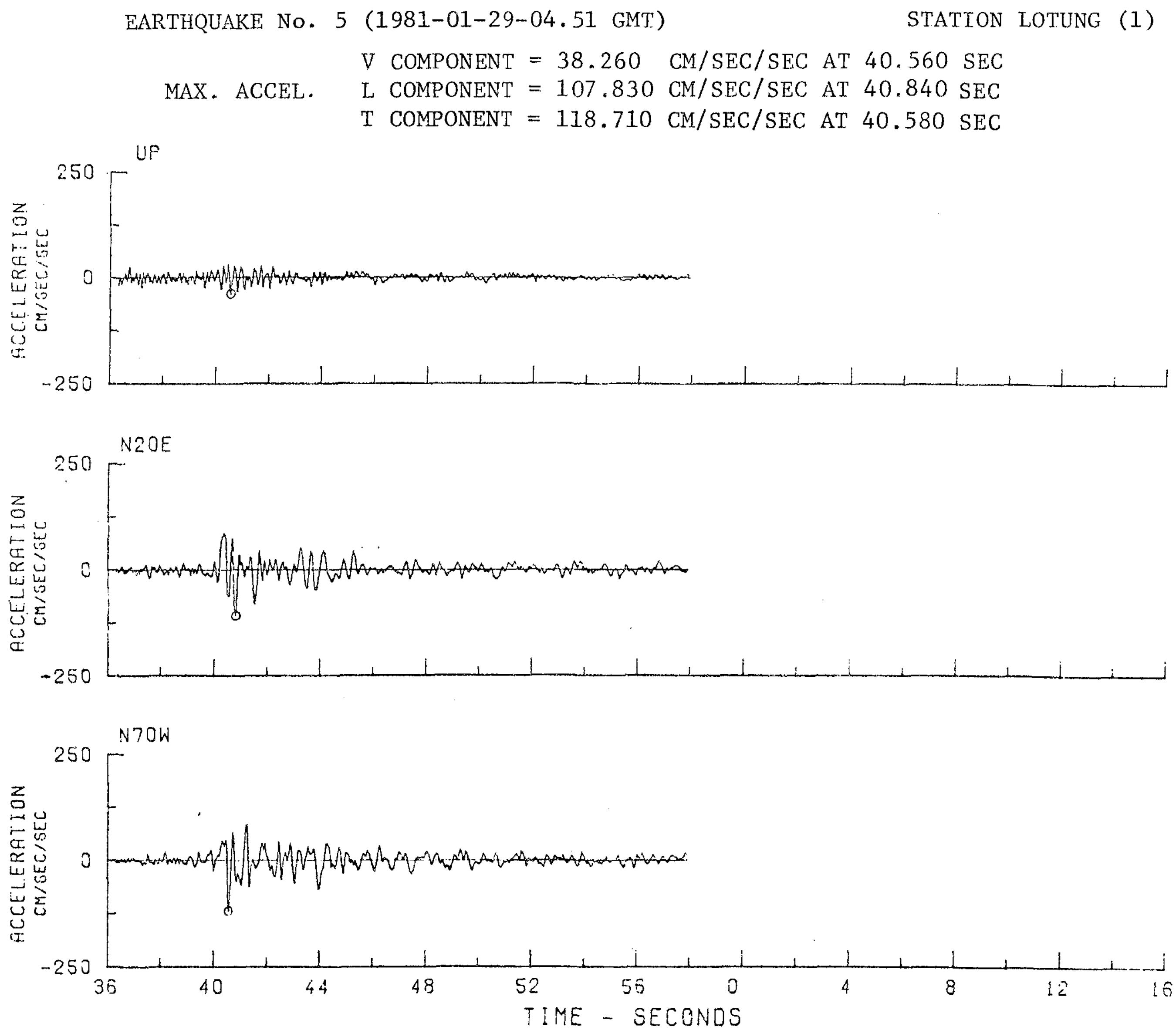

Fig. 3.4b Acceleration waveforms of the vertical and two horizontal components of Event 5 at Lotung Town Hall recorded by an SMA-1 instrument

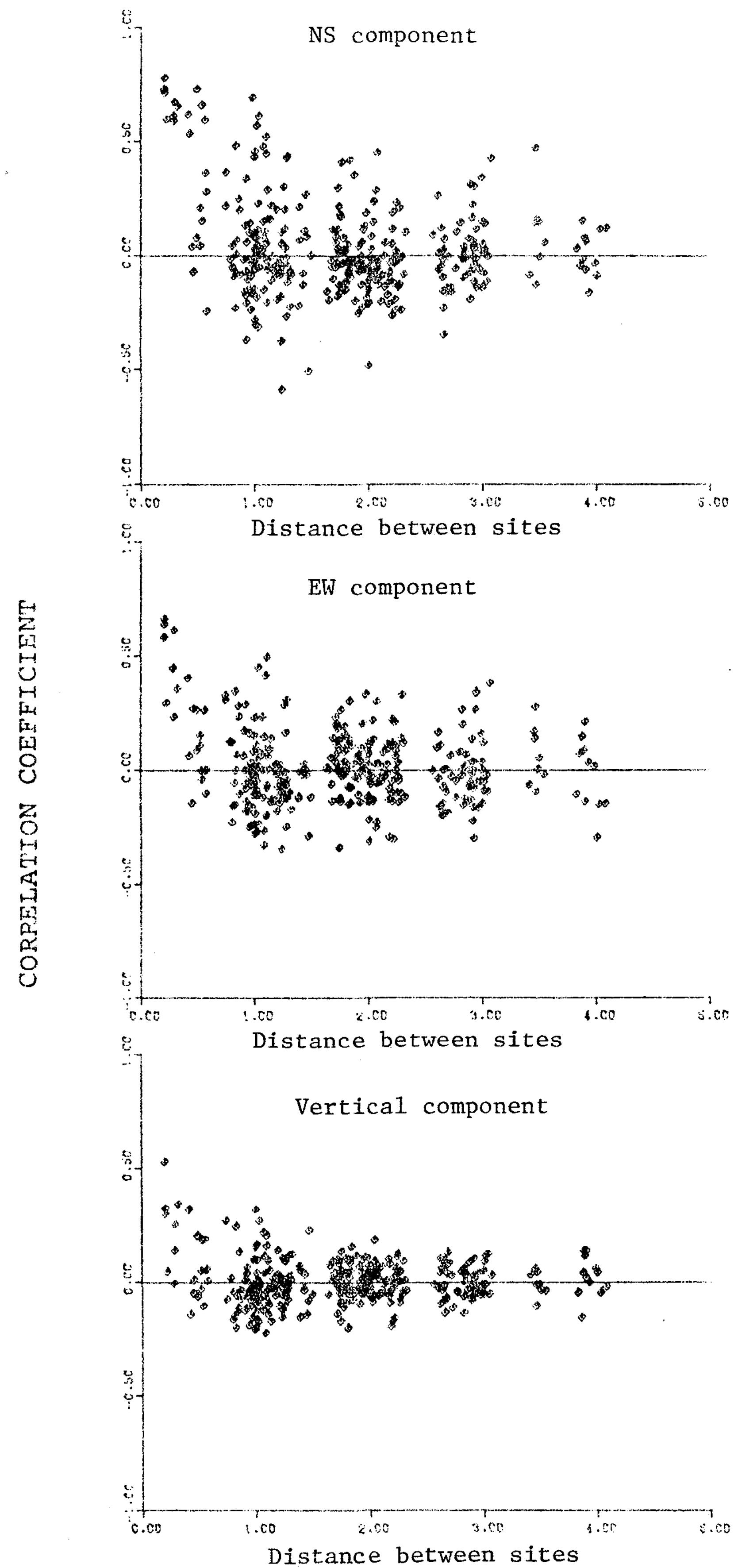

Fig. 3.5a Correlation coefficients of the whole waveform between paired sites for Event 5

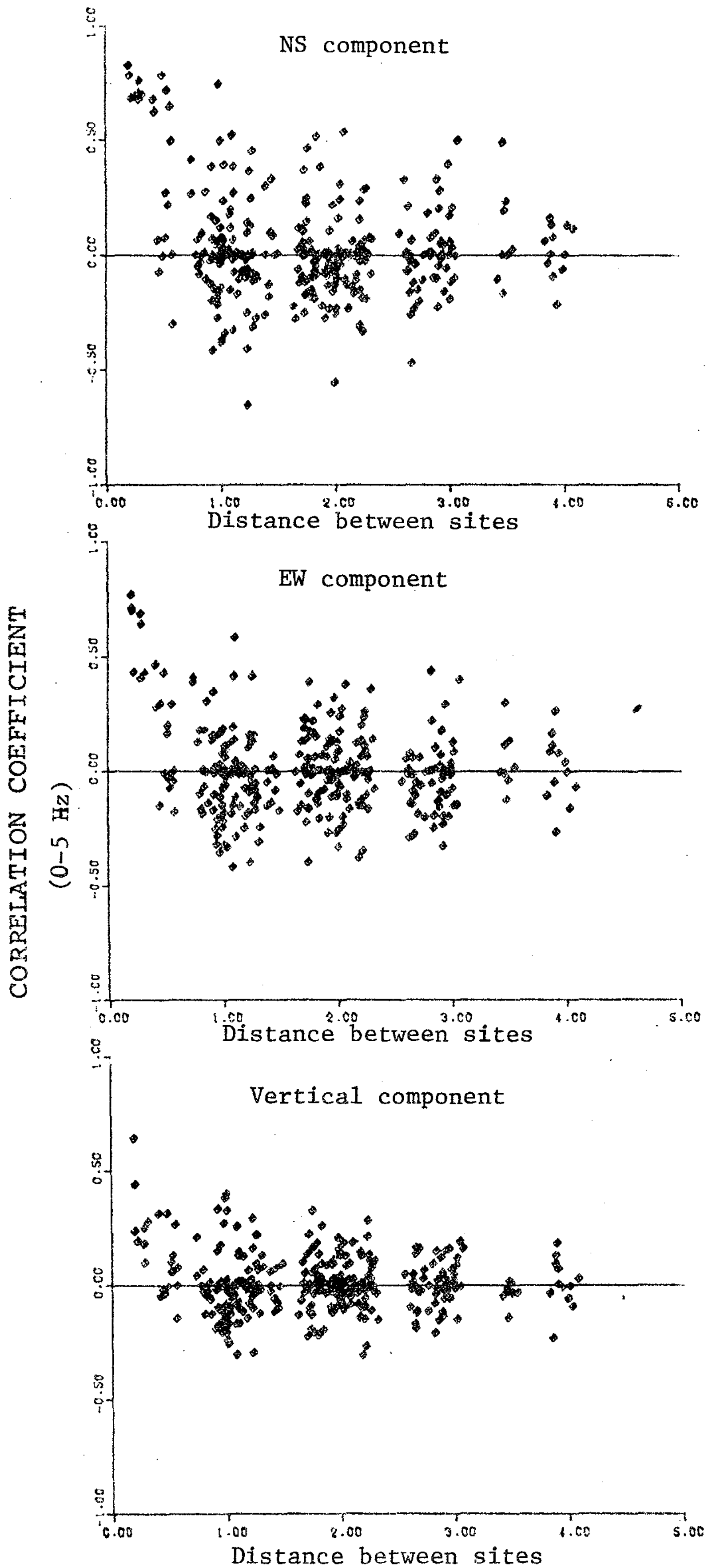

Fig. 3.5b. Correlation coefficients of the waveform for the low-frequency band between paired sites for Event 5

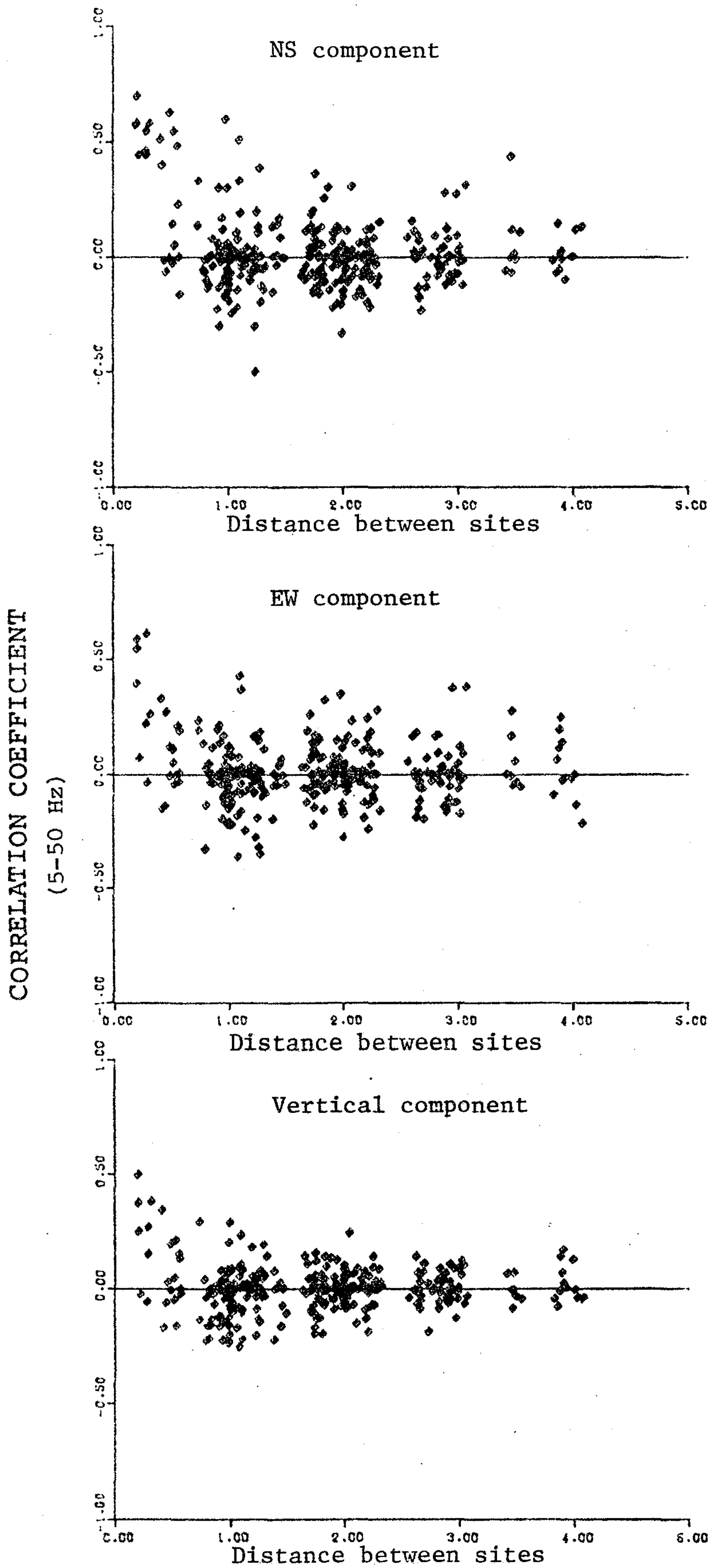

Fig. 3.5c. Correlation coefficients of the waveform for the high-frequency band between paired sites for Event 5

4. DATA PROCESSING

4.1 Timing

SMART 1 is designed so that individual elements trigger when seismic waves having peak accelerations above 0.01g propagate across the Lotung area. Complete wave trains are obtained because of the 2.5 second memory associated with each element. Universal time, correct to at least 0.01 sec, is marked on each tape at the time of the first earthquake that triggers the element. Timing of aftershocks is given by the relative interoccurrence times specified by the internal crystal clock. Immediately after a significant earthquake is recorded, technicians check the internal clock of each element with the portable comparator. This final check of the internal clock is made no later than two or three hours after the recording of the main shock so that inter-element time corrections are less than 0.01 sec. In this section, some basic processing of recorded data from SMART 1 is discussed.

4.2 Digital Processing

The cassettes obtained in the field at the array elements are taken to the digital playback system (shown in Fig. 4.1) at the Institute of Earth Sciences in Taipei, where they are converted to computer-compatible digital stacks and filed on magnetic tape by the laboratory playback system.

When the recorded cassette tapes are sent back to the laboratory, they are played back on paper for visual inspection. Valid records are picked out and transformed from the cassette tapes to a regular 9-track magnetic tape. The raw data tape is then read into a computer for decoding and editing. The edited records with related header information are written onto a user's data tape for further processing.

The traces of the V, EW, and NS components of acceleration recorded by each element are plotted for easy visual inspection by potential users of the

SMART 1 data. The digital format of recording makes it possible to perform fast data processing on an extensive scale. The following six steps summarize the decoding and editing involved in the processing of the SMART 1 data.

a) The recorded cassette tapes are played back on paper. On these playback traces, the number of stations that recorded during the earthquake are marked as well as the event number and the maximum ground acceleration (see Figs. 3.2 and 3.3).

b) The recorded cassette tapes are transformed to 9-track magnetic tape.

c) Decode: The seismic event is recorded as a file consisting of 5120 character records for header, data and trailer. The number of records per file depends on the event duration. The file organization is shown in Tables 4.1 to 4.4.

d) The record is printed out and errors corrected. Both the original record and the transformed record (decode) are printed out. The error corrections are needed for missing data, adjustments for time mark errors, glitches and D.C. shifts. Examples of possible errors are given in Figs. 4.2 to 4.4.

e) The time correction, hypocentral location, and magnitude are all inserted in the data. The time correction is shown in Fig. 4.5.

f) The corrected data are transferred to regular 9-track magnetic tape.

After data processing, the basic instrument correction and base-line correction developed by Trifunac[1] and Hudson[2] are applied. Then the Fourier amplitude spectrum, response spectrum, correlation coefficient and the velocity and displacement are calculated from the corrected data. The data processing procedure is shown graphically in Fig. 4.6.

The natural frequency of the SMART 1 instrument is >50 Hz and the damping ratio is 0.7 ±0.2 critical damping; however, the cutoff-frequency of the 3-channel, anti-aliasing filter (5-pole low-pass Butterworth) is set to 25 Hz. The filter response curve for the test input which is shown in Fig. 4.7 indicates that the recorded accelerogram is quite close to the ground acceleration. Hence, no instrument correction was applied to the SMART 1 data. The positive direction of the recording is shown in Fig. 4.8.

4.3 References

1. Trifunac, M.D., "A Note on Correction of Strong Motion Accelerograms for Instrument Response," Bull. Seisn. Soc. Am., 62, No. 1, 401-409 (1972).

2. Hudson, E.C., Reading and Interpreting Strong Motion Records, Earthquake Engineering Research Institute, Berkeley, California (1979).

TABLE 4.1

File Organization

A file consists of records as follows:

Record	Data
1	Header Data
2	Digital Data
"	"
"	"
"	"
N	Digital Data
N+1	Trailer Data
File Mark	

TABLE 4.2

Header Record

The header record is a 5120 character record consisting of ASCII coded BCD for DAYS, HRS, MINS, SEC, SERIAL NUMBER of recorder, EVENT COUNT, and SYSTEM (16 characters). The remaining characters in the record are ASCII spaces (Hex 20). A header record is therefore:

Char.#	Data
1	Days MSD (N*100)
2	Days MSD (N*10)
3	Days LSD (N*1)
4	Hours MSD (N*10)
5	Hours LSD (N*1)
6	Mins MSD (N*10)
7	Mins LSD (N*1)
8	Secs MSD (N*10)
9	Secs LSD (N*1)
10	S/N MSD (N*100)
11	S/N MSD (N*10)
12	S/N LSD (N*1)
13	EV MSD (N*10)
14	EV LSD (N*1)
15	SYS MSD (N*10)
16	SYS LSD (N*1)
17	ASCII Spaces
"	"
5120	

TABLE 4.3

Data Record

The data samples are formatted into 6 ASCII characters per sample, as follows:

Char.#		
1	ID#	ASCII 0,1, or 2 (V, EW, NS)
2	SIGN	ASCII + or -
3	MSD	ASCII BCD (N*1000)
4	"	" " (N*100)
5	"	" " (N*10)
6	LSD	" " (N*1)

The above pattern repeats for 853 samples (284 samples/channel), a total of 5118 characters. The remaining 2 characters are ASCII spaces.

TABLE 4.4

Trailer Record

The trailer record is a 5120 character record consisting of 16 ASCII coded BCD characters and 5104 ASCII nulls (Hex 00). A trailer record is as follows:

Char.#	Data
1	Days MSD (N*100)
2	Days MSD (N*10)
3	Days LSD (N*1)
4	Hours MSC (N*10)
5	Hours LSD (N*1)
6	Mins MSD (N*10)
7	Mins LSD (N*1)
8	Secs. MSD (N*10)
9	Secs LSD (N*1)
10	S/N MSD (N*100)
11	S/N " (N*10)
12	S/N LSD (N*1)
13	EV MSD (N*10)
14	EV LSD (N*1)
15	SYS MSD (N*10)
16	SYS LSD (N*1)
17	ASCII Nulls
"	"
5120	

Fig. 4.1 Digital playback system DP-200

0+0000	1-0004	2+0006	0+0000	1-0004	2+0006	0+0000
0+0000	1-0002	2+0002	0-0001	1-0002	2+0002	0+0000
0+0000	1-0002	2+0002	0+0000	1+0000	2+0000	0+0000
0+0000	1+0000	2+0002	0+0000	1+0000	2+0002	0+0000
0-0002	1-0002	2+0003	0-0002	1+0000	2+0004	0-0002
0+0000	1-0002	2+0003	0+0000	1-0002	2+0002	0+0000
0-0002	1-0002	2+0002	0-0002	1-0002	2+0002	0+0000
0+0000	1-0002	2+0002	0+0000	1+0000	2+0003	0+0000
0+0000	1+0000	2+0003	0+0000	1+0000	2+0003	0+0000
0+0000	1-0002	2+0002	0-0001	1-0002	2+0002	0+0000
0+0000	1+0000	2+0002	0+0000	1+0000	2+0002	0-0002
0-0002	1+0000	2+0002	0-0002	1+0000	2+0002	0-0002
0+0000	1+0000	2+0003	0+0000	1+0000	2+0003	0+0000
0+0000	1+0000	2+0003	0+0000	1+0000	2+0003	0+0000
0+0000	1+0000	2+0002	0+0000	1+0000	2+0002	0+0000
0+0000	1-0002	2+0003	0+0000	1-0002	2+0003	0-0002
0+0000	1-0002	2+0002	0+0000	1-0002	2+0002	0+0000
0+0000	1-0002	2+0003	0+0000	1-0002	2+0003	0+0000
0-0002	1-0002	2+0003	0-0002	1+00		

Fig. 4.2 Data missing at end of file

2+0002	0-0013	1-0005	2+0003	0-0013	1-0006	2+0005	0-0013
2+0005	0-0013	1-0006	2+0003	0-0013	1-0006	2+0003	0-0013
2+0004	0-0011	1-0008	2+0005	0-0011	1-0009	2+0006	0-0012
2+0005	0-0013	1-0012	2+0005	0-0013	1-0012	2+0006	0-0014
2+0005	0-0014	1-0008	2+0005	0-0014	1-0008	2+0004	0-0014
2+0000	0-0015	1-0007	2+0001	0-0015	1-0009	2+0001	0-0015
2+0002	0-0010	1-0011	2+0003	0-0010	1-0010	2+0003	0-0011
2+0002	0-0013	1-0011	2+0001	0-0013	1-0011	2+0000	0-0013
2-0003	0+2047	1+2047	2+2047	0+2047	1+2047	2+2047	0-0011
2+0002	0-0013	1-0005	2+0001	0-0013	1-0004	2+0001	0-0014
2+0007	0-0013	1-0007	2+0008	0-0013	1-0007	2+0010	0-0011
2+0007	0-0013	1-0009	2+0003	0-0013	1-0010	2+0000	0-0014
2+0001	0-0013	1-0012	2+0002	0-0013	1-0012	2+0003	0-0012
2+0005	0-0013	1-0009	2+0003	0-0013	1-0009	2+0002	0-0013
2+0001	0-0013	1-0007	2+0002	0-0013	1-0008	2+0002	0-0013
2+0005	0-0013	1-0011	2+0005	0-0013	1-0011	2+0004	0-0013
2+0001	0-0013	1-0011	2+0000	0-0013	1-0009	2+0000	0-0013

Fig. 4.3 Repeated time mark occurring in the middle of the data file

FILE 5 3191337252890132

2-0683	0-0684	1-1878	0-0683	1+0514	0-0683	1+0680	2-1707	0-0763
1+0680	2-1707	0-0763	1+0682	0-0684	1-1878	0-0683	1+0642	0-0683
0-0683	1+0642	0-0683	1+0682	2-1707	2-1023	0+0003	1+0002	2+0000
0+0000	1+0000	2-0006	0+0000	1+0000	2-0009	0+0000	1+0000	2-0010
0+0000	1+0003	2-0002	0-0002	1+0003	2-0002	0-0003	1+0003	2-0002
0+0003	1+0002	2-0005	0+0005	1+0000	2-0006	0+0004	1-0001	2-0009
0+0001	1+0000	2-0006	0+0000	1+0000	2-0004	0-0002	1+0000	2-0002
0-0003	1+0000	2-0002	0-0002	1-0002	2-0002	0+0000	1+0000	2-0004
0+0003	1+0003	2-0004	0+0003	1+0002	2-0002	0+0003	1+0000	2-0002
0+0004	1+0000	2+0002	0+0002	1+0002	2+0002	0+0000	1+0002	2+0002
0-0003	1+0002	2-0002	0+0000	1+0002	2-0004	0+0000	1+0000	2-0006
0+0000	1+0000	2-0004	0+0002	1+0000	2-0002	0+0002	1+0000	2-0002
0+0000	1+0000	2-0006	0-0002	1+0000	2-0006	0-0003	1+0000	2-0006
0+0002	1+0000	2+0000	0+0002	1+0000	2+0002	0+0003	1+0000	2+0000
0+0003	1+0002	2-0006	0+0002	1+0002	2-0006	0+0000	1+0002	2-0010
0+0000	1+0000	2-0014	0+0002	1+0002	2-0013	0+0005	1+0003	2-0010
0+0003	1+0002	2-0004	0+0002	1+0002	2-0002	0+0000	1+0000	2-0002

Fig. 4.4a Glitch in the data at beginning of the data file

2+0006	0+0002	1+0004	2+0006	0+0002	1+0003	2+0005	0+0002	1+0003
2+0006	0+0002	1+0003	2+0005	0+0002	1+0003	2+0005	0+0002	1+0004
2+0006	0+0002	1+0003	2+0005	0+0003	1+0003	2+0006	0+0002	1+0002
2+0006	0+0002	1+0003	2+0006	0+0003	1+0003	2+0005	0+0002	1+0003
2+0006	0+0001	1+0004	2+0004	0+0000	1+0003	2+0005	0+0001	1+0003
2+0006	0+0005	1+0003	2+0005	0+0004	1+0004	2+0006	0+0002	1+0003
2+0006	0+0008	1+0003	2+0005	0+0005	1+0003	2+0005	0+0000	1+0004
2+0006	0+0004	1-2040	2-2038	0+0010	1+0003	2+0006	0+0004	1+0002
2+0006	0+0004	1+0003	2+0006	0+0012	1+0004	2+0005	0+0010	1+0003
2+0005	0--0003	1+0004	2+0004	0+0000	1+0004	2+0006	0+0004	1+0004
2+0005	0-0002	1+0002	2+0004	0-0003	1+0004	2+0006	0+0001	1+0004
2+0005	0+0004	1+0002	2+0004	0+0004	1+0002	2+0005	0+0004	1+0003
2+0006	0+0004	1+0003	2+0004	0+0006	1+0002	2+0004	0+0005	1+0002
2+0008	0+0000	1+0003	2+0005	0+0000	1+0003	2+0005	0+0004	1+0002
2+0006	0+0001	1+0004	2+0004	0+0001	1+0004	2+0004	0+0004	1+0004

Fig. 4.4b Glitch in the data at the middle of the data file

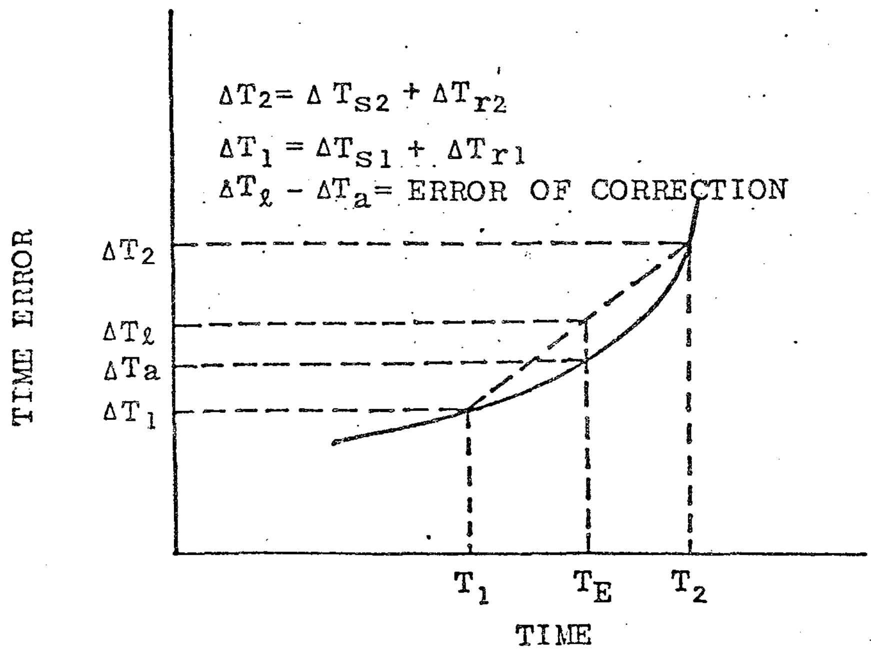

T_1: Time of the time-error checking before event

T_2: Time of the time-error checking after event

T_E: Time of event

ΔT_s: Time-error of TS-500 time comparator (checked by standard time receiver and scope

ΔT_r: Time-error between TS-500 and DR-100 digital event recorder

ΔT_a: Actual time-error used for correction

ΔT_ℓ: Estimated time-error (by using linear interpolation)

$\Delta T_\ell - \Delta T_a$: Error of time correction (should be < 10 millisec.)

Fig. 4.5 Time correction

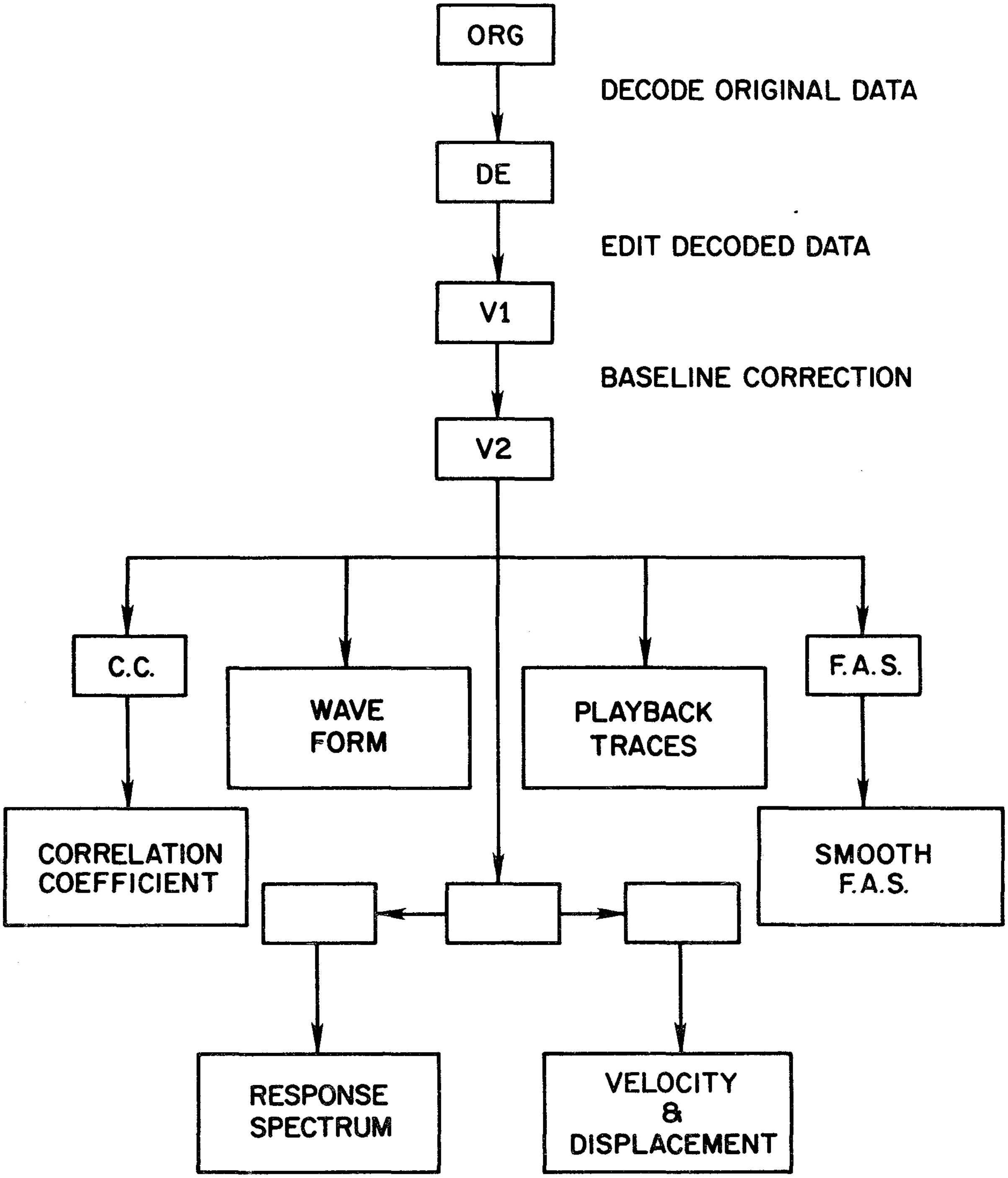

Fig. 4.6 Data processing procedure

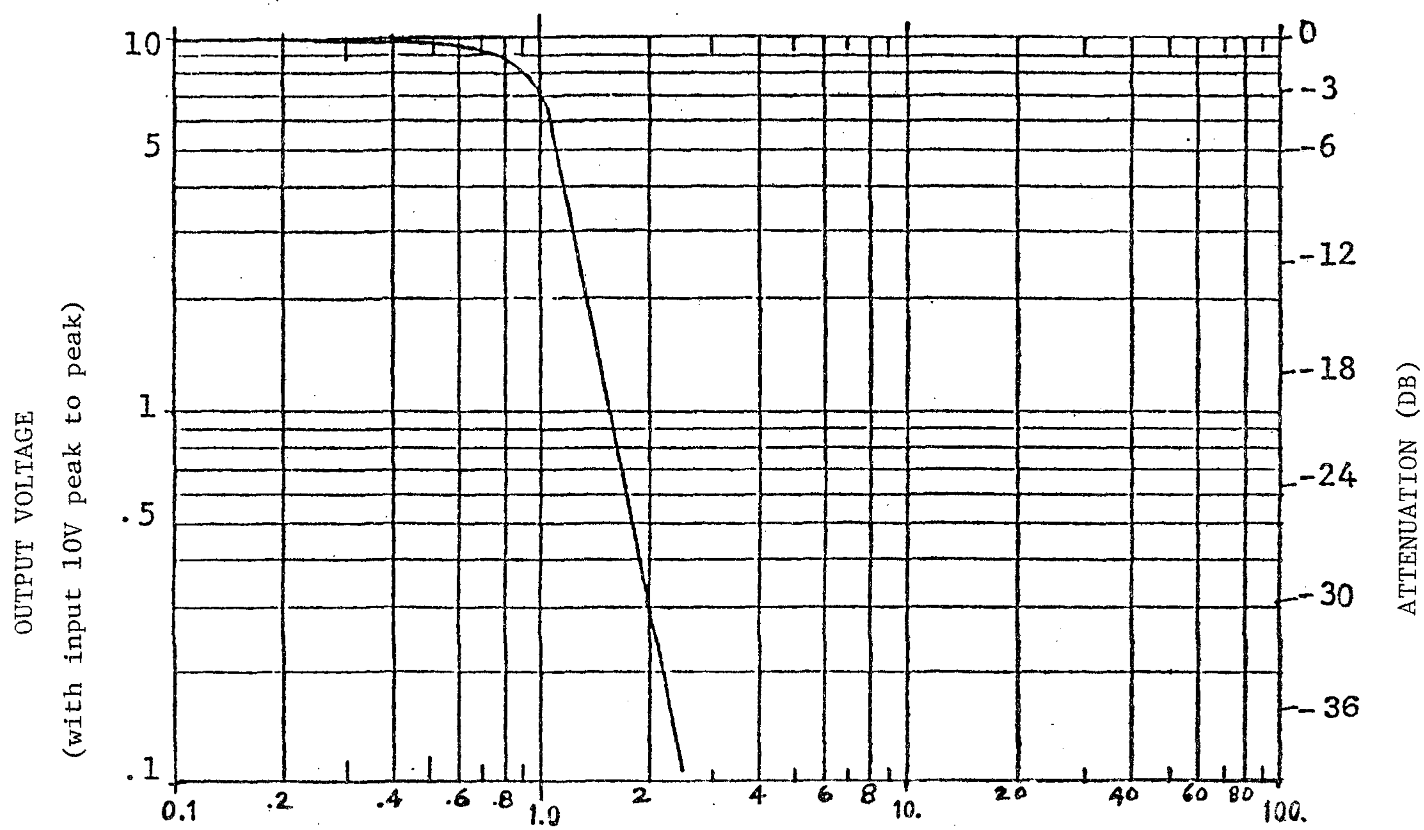

Fig. 4.7 Filter response curve for test input

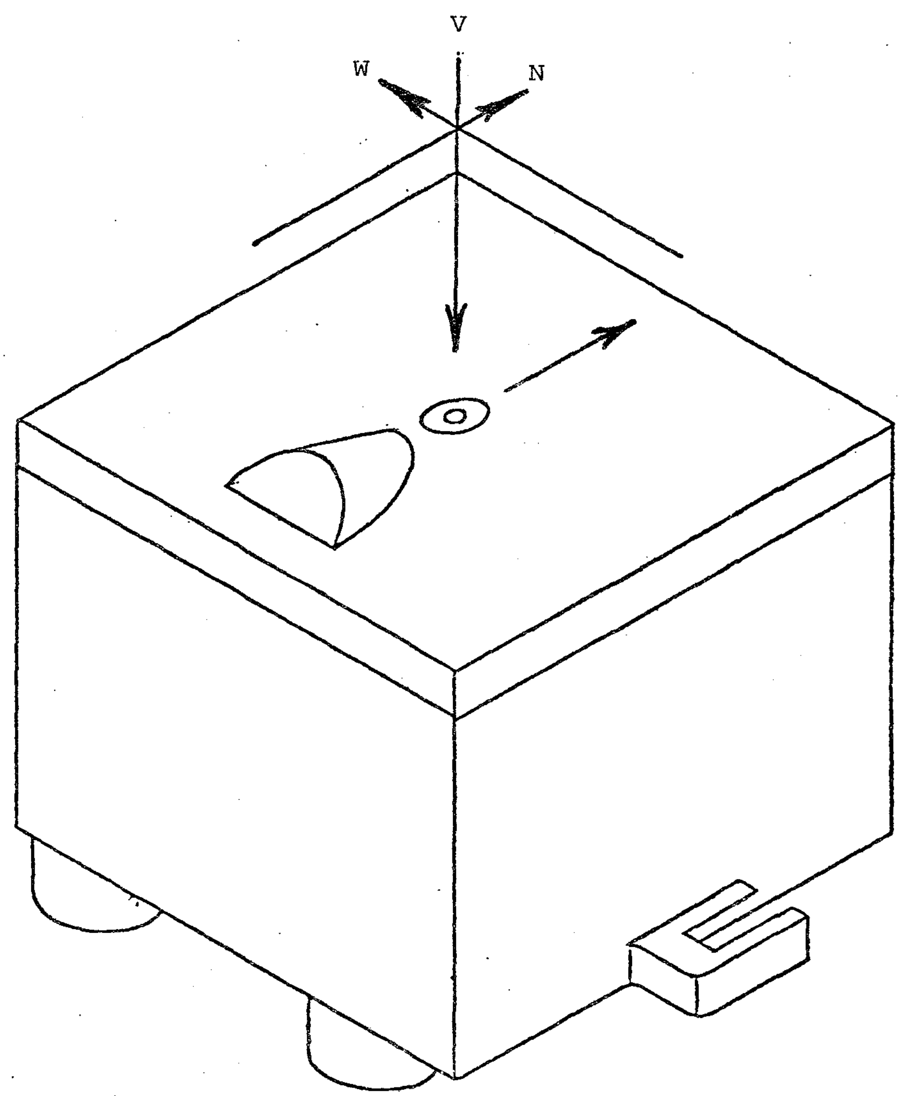

POSITIVE OUTPUT FROM THE SENSORS RESULTS FROM ACCELERATIONS WHICH CAUSE GROUND MOTION AS SHOWN

Fig. 4.8 Positive direction of sensor

5. SPECTRAL ANALYSIS OF THE ACCELEROGRAMS

5.1 Introduction

The format of SMART 1 records makes processing by computer relatively fast and easy. For instance, the Fourier spectra of the considerable number of records obtained in the first six months were calculated in one pass. This speed is difficult to match with conventional film accelerograms. Because absolute time is available, the records can be correlated against epicentral distance in real time.

The high P wave signal strength for the January 29, 1981 earthquake (Event 5) resulted in both P and S waves being recorded by all 27 operating instruments. The signal amplitudes are different for the three components, with the vertical and north-south components being the weakest and strongest, respectively.

5.2 Fourier Spectra and Response Spectra

Figure 5.1 shows the smoothed Fourier spectra of the acceleration waveforms of the vertical, EW and NS components at the Site C00, at the center of the array, for Event 2, the November 14, 1980 earthquake of M_L = 5.9. It should be noted that the vertical scales in each figure are not always the same for the three components. Variations in the Fourier spectra of the vertical components are greater than those of the horizontal components across SMART 1.

The SMART 1 records also permit the ready calculation of the response spectra. The group of records for the first six months was processed together to generate individual response spectra and produce mean response spectra. A goal of the project is, eventually, to separate the effects of site and source conditions on the response spectra by appropriate group analysis. Figures 5.2a, b, and c show the response spectra of the vertical, EW and NS components, respectively, of the C00 records for Event 5, the January 29, 1981 earthquake of magnitude $M_L = 6.9$. These curves are representative of the response curves of most sites for Event 5. They show that the NS component has more energy than the EW component for periods greater than 0.5 sec, and that the vertical component has significantly lower spectral levels and a flatter shape than the horizontal components.

Figures 5.3a, b, and c show the response spectra of the vertical, EW and NS components, respectively, of the C00 records for Event 2. For this earthquake, the EW and NS components have about the same spectral level and, as for Event 5, the vertical component has correspondingly lower levels than the horizontal components. In comparison with Event 5, this event has relatively less energy for periods greater than one second than for shorter periods, especially in the case of the NS component.

In general, the shapes of the response spectra differ between vertical and horizontal components as well as between different earthquakes.

5.3 Frequency-Wave Number Spectral Analysis

Figure 5.4 shows the three components of ground motion measured at two array elements (stations 001 and 002) during Event 5. Wave trains of what are assumed *a priori* to be predominantly P, S and surface waves can be seen lasting about 20 sec. Each record is aligned vertically according to Universal Time. The records demonstrate significant spatial variability (confirmed separately by the frequency spectrum analysis described in Section 5.2) between array elements about 1 km apart. This aspect of the variability of strong ground motion will be discussed at length in a later study.

Consider next the phased correlations of a specified portion of such records for a given component at all array elements so that not only the average power in the seismic signal may be estimated, but also the speed and direction of any coherently propagating seismic wave. A convenient method is to plot the power spectrum for a particular time window as a function of wave number k (cycles per km) and azimuth. An outline of the algorithm is given in Appendix E. If the plot is made at a particular frequency f, the distance from the center is inversely proportional to the apparent wave speed c (where kc = f).

As an illustration of the method, wave-number spectral plots are shown in Figs. 5.5 and 5.6, computed using a high resolution algorithm[1] from 26 SMART 1 vertical and north-south component accelerograms, respectively. (Digital data from one triggered element were not included in the analysis.) The two time windows chosen are marked 1 and 4, respectively, at the bottom of Fig. 5.4. Similar spectra of each ground motion component were computed for frequencies of 8, 6, 4, 2, 1, 0.5, 0.25, and 0.125 Hz for each sequential time window, 1 through 5 in Fig. 5.4, from the beginning to the end of the record. Preliminary analysis of these 120 spectral plots have been made but for the sake of brevity only Figs. 5.5 and 5.6 are reproduced here.

The spectra show that the wave trains in the first and second windows (each 4 sec long) correspond principally to P waves crossing the array. In Fig. 5.5, the main power (marked A) is at 1 to 2 Hz and arrives at an apparent velocity of about 8.3 km/sec (appropriate for P waves) from an azimuth of E 58° S. (The azimuth of the earthquake focus is E 64° S.) In the third window, the predominant maximum power (not shown here) is very coherent at 1 to 2 Hz, but propagates from E 68° S at about 3 km/sec. This motion (see Fig. 5.4) corresponds mainly to Rayleigh and S waves crossing the array. The spectral plots show also that during this time interval a large amount of the energy being produced by the rupturing dislocation was being scattered away from the direct path between source and array. This scattering may be associated with structural irregularities in the crust and the superficial soil layers.

The spectrum shown in Fig. 5.6 for a window of 10 sec length in the coda of strong ground motion has a maximum peak energy (A) appropriate to waves moving with an apparent speed of $\sim$1.0 km/sec across the array from E 75° S. The interpretation, supported by the orbital motion measured by the three components of acceleration, is that at this time the NS component of wave motion is predominantly of Rayleigh type. A summary of the estimated average apparent velocities and directions of approach of the seismic waves in each of the five time windows is given in Fig. 5.7. The diagram indicates that the preliminary body wave arrivals (P and S waves) are from a direction to the east of the epicenter, while the later arrivals (surface coda waves) arrive successively from directions more and more westerly of the epicenter. This change in azimuth may be due to lateral refraction in the crustal structure or it may arise from the propagation of the seismic dislocation on the rupturing fault. A separate determination of the fault plane parameters is now under way.

5.4 Wave Coherency and Type

The above examples demonstrate that arrays like SMART 1 may have the capability, for the first time in seismology, of following the elastic dislocation as it moves along the fault. There is also the ability to determine whether, in a given time, the predominant seismic motion is of P wave, S wave or surface wave type. The lack of such identification has previously hindered crucial discrimination between theoretical models. The present preliminary analysis does not make use of the three recorded components of wave motion at each array element. The wave-number frequency spectral method can, however, be extended to this general case and orbits of the particle motions calculated.

A further use of the array data relates to two hypotheses now often appealed to: (1) that strong-motion accelerograms are largely superpositions of random motions[2] and (2) that coda waves from local earthquakes arise from scattering[3] from randomly-distributed heterogeneities in the crust. From SMART 1 recordings of the January 29 earthquake, both hypotheses appear to be only partly correct. Comparison of seismograms and wave-number frequency spectral plots shows that coherent energy (i.e., physically correlated) is present throughout the 20 sec duration of strong shaking, at least for frequencies $0.5 < f < 2$ Hz. (In this frequency range no problems from either spatial or temporal aliasing should arise.) Further, the major part of this coherent energy corresponds to the expected body and surface waves of seismology. In most time windows, however, at higher frequencies ($f > 6$ Hz), the wave number spectra lose coherence.

The illustration given in Fig. 5.8 is the NS component in window 3; the maximum energy (point A) is weak and represents very slow waves approaching from the southwest. At higher frequencies, the calculated spectra are consistent with the hypothesis of a large proportion of scattered waves arriving from widely-distributed heterogeneities. The actual extent of geological structural variations is not yet known from borehole information in the SMART 1 region. Seismic surveys indicate, however, a surficial layer of recent alluvium with P wave velocities of 500 to 1000 m/sec overlying pleistocene rock with P wave velocities of 1800 to 2000 m/sec.

Another example of the capability of a near-source array like SMART 1 is that spatial correlations of waveform can answer the long-standing question of what is the minimum distance from the seismic source at which surface waves appear. Theoretical calculations are not specific and definite observational field evidence has not been observed. In the example above (Fig. 5.6), Rayleigh waves of period 2 sec are clearly present 30 km from the shallow-focus source. More extensive analyses[4] of all the above questions will be given in later studies using the complete set of earthquakes recorded by SMART 1.

5.5 References

1. Capon, J., "High-Resolution Frequency-Wave Number Spectrum Analysis," Proc. IEEE, 57, 1408-1418 (1969).
2. Housner, G.W. and P.C. Jennings, "Generation of Artificial Earthquakes," J. Eng. Mech. Div., ASCE, 90, 113-150 (1964).
3. Aki, K. and B. Chouet, "Origin of Coda Waves, Source Attenuation and Scattering Effects," J. Geophys. Res., 80, 3322-3342 (1975).
4. Bolt, B.A., Tsai, Y.B, Yeh K. and M. K. Hsu, "Earthquake Strong Motions Recorded by a Large Near-Source Array of Digital Seismographs," Earthquake Eng. Struct. Dyn., 10, 561-573, (1982).

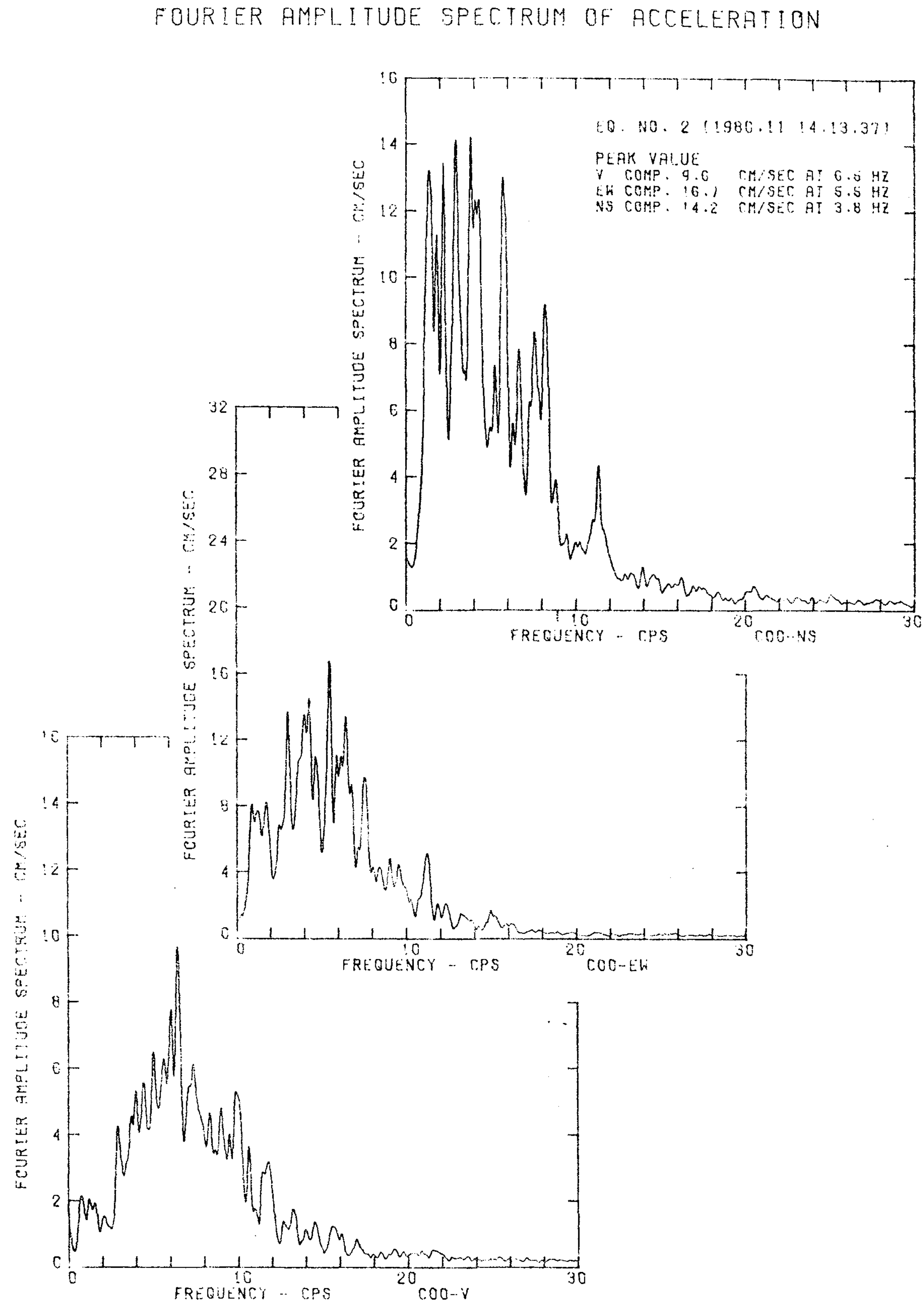

Fig. 5.1 Smoothed Fourier spectra of acceleration waveforms of the vertical, EW and NS components at COO for Event 2

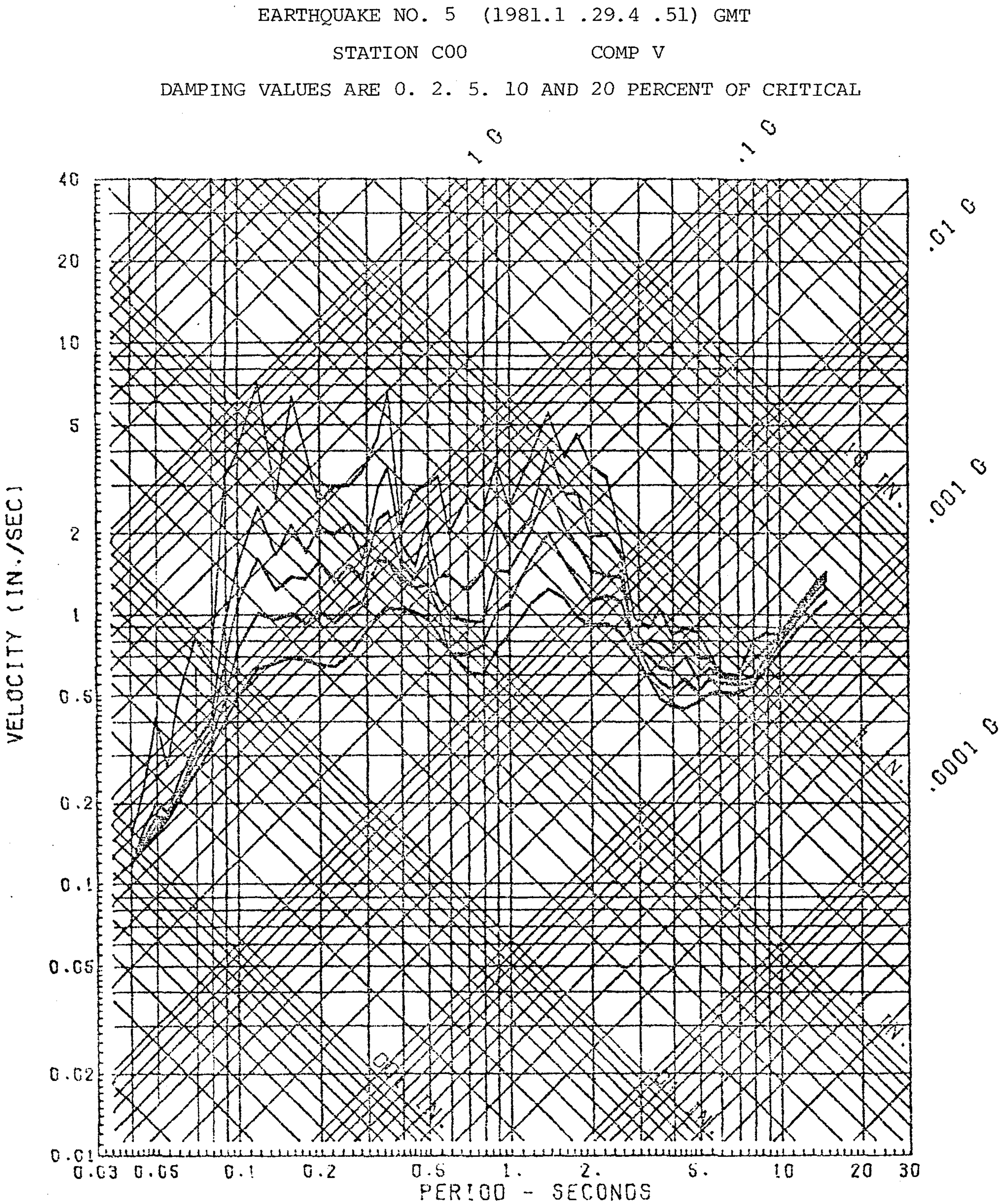

Fig. 5.2a Response spectrum of the vertical component at COO for Event 5

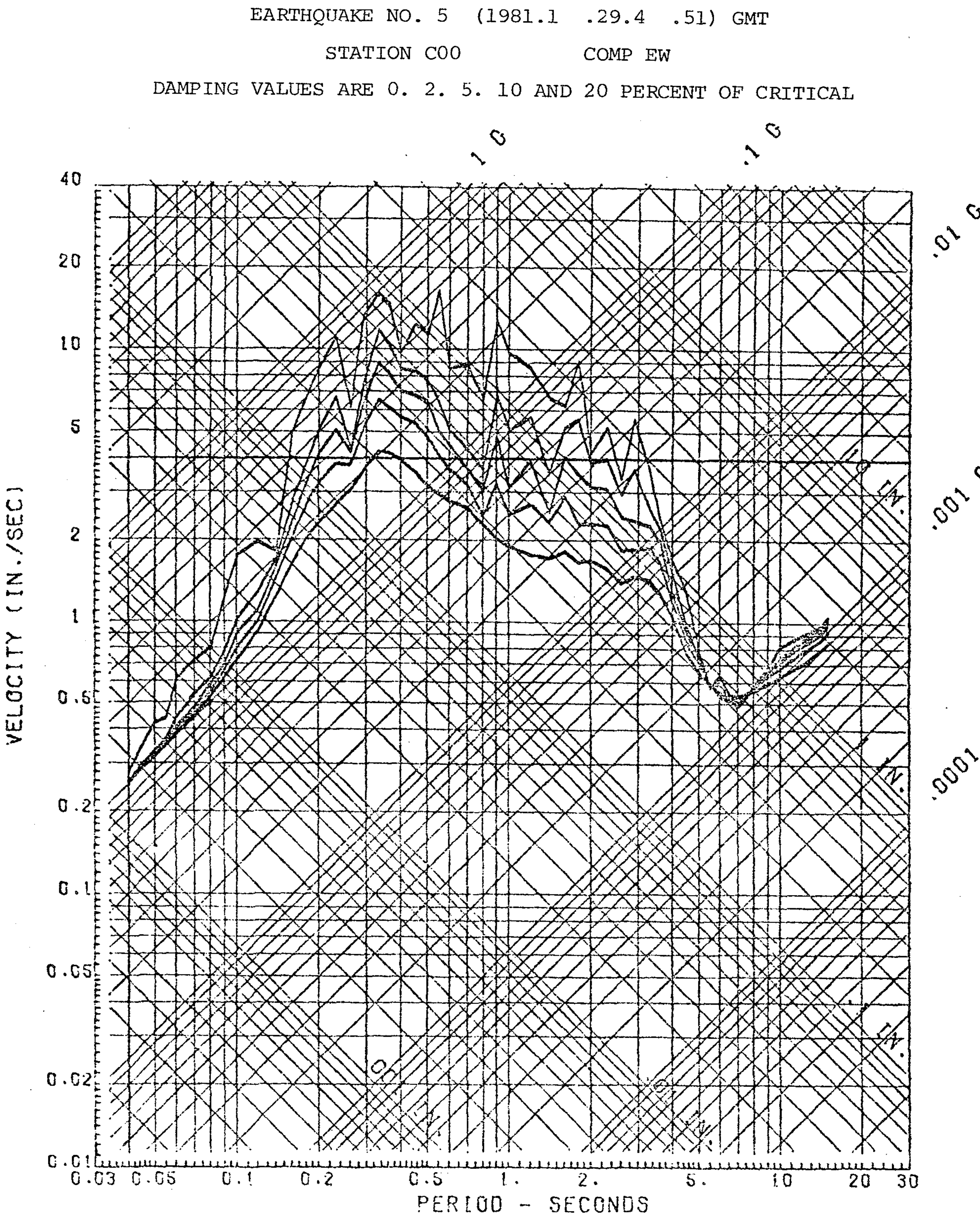

Fig. 5.2b Response spectrum of the EW component at COO for Event 5

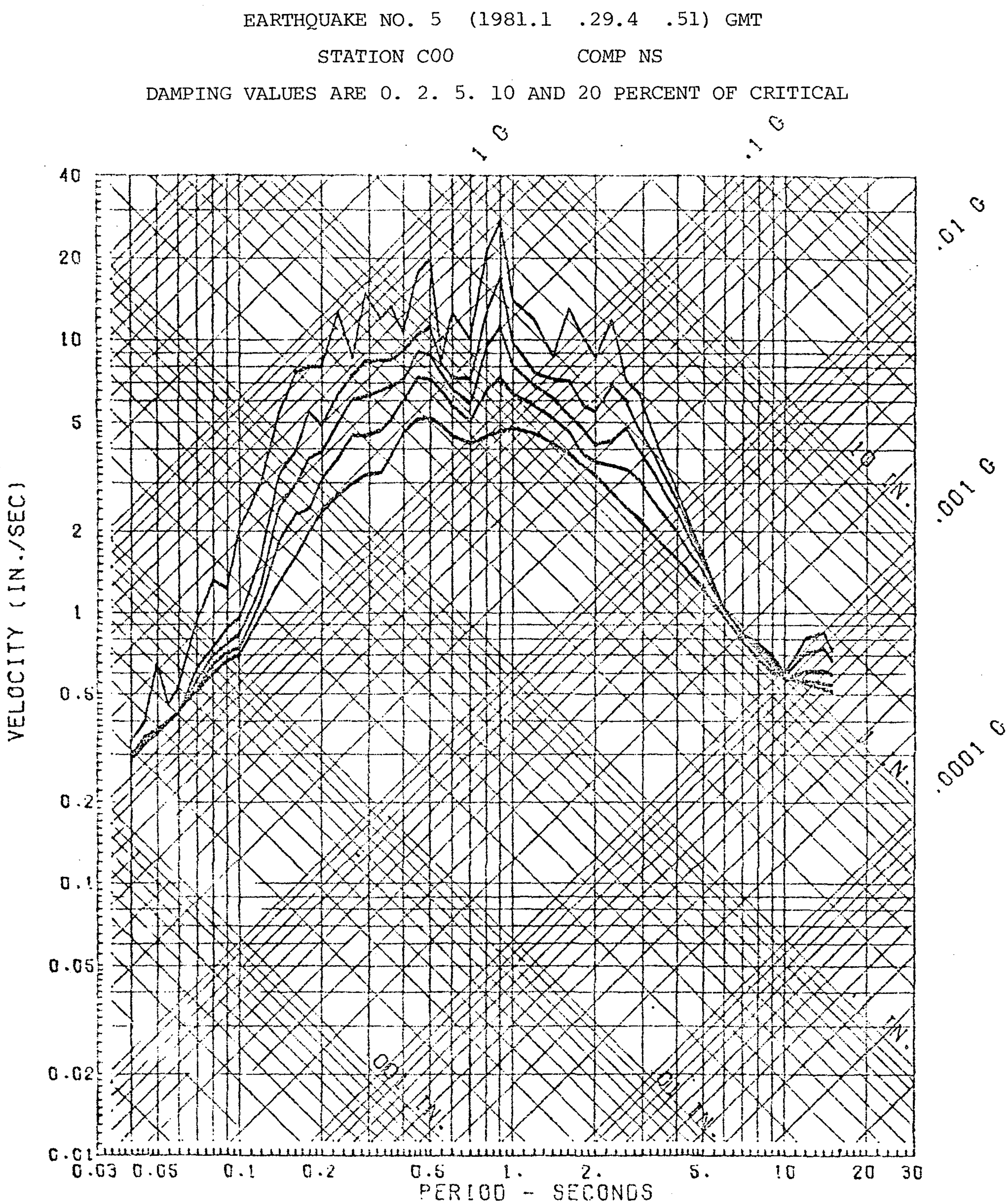

Fig. 5.2c Response spectrum of the NS component at COO for Event 5

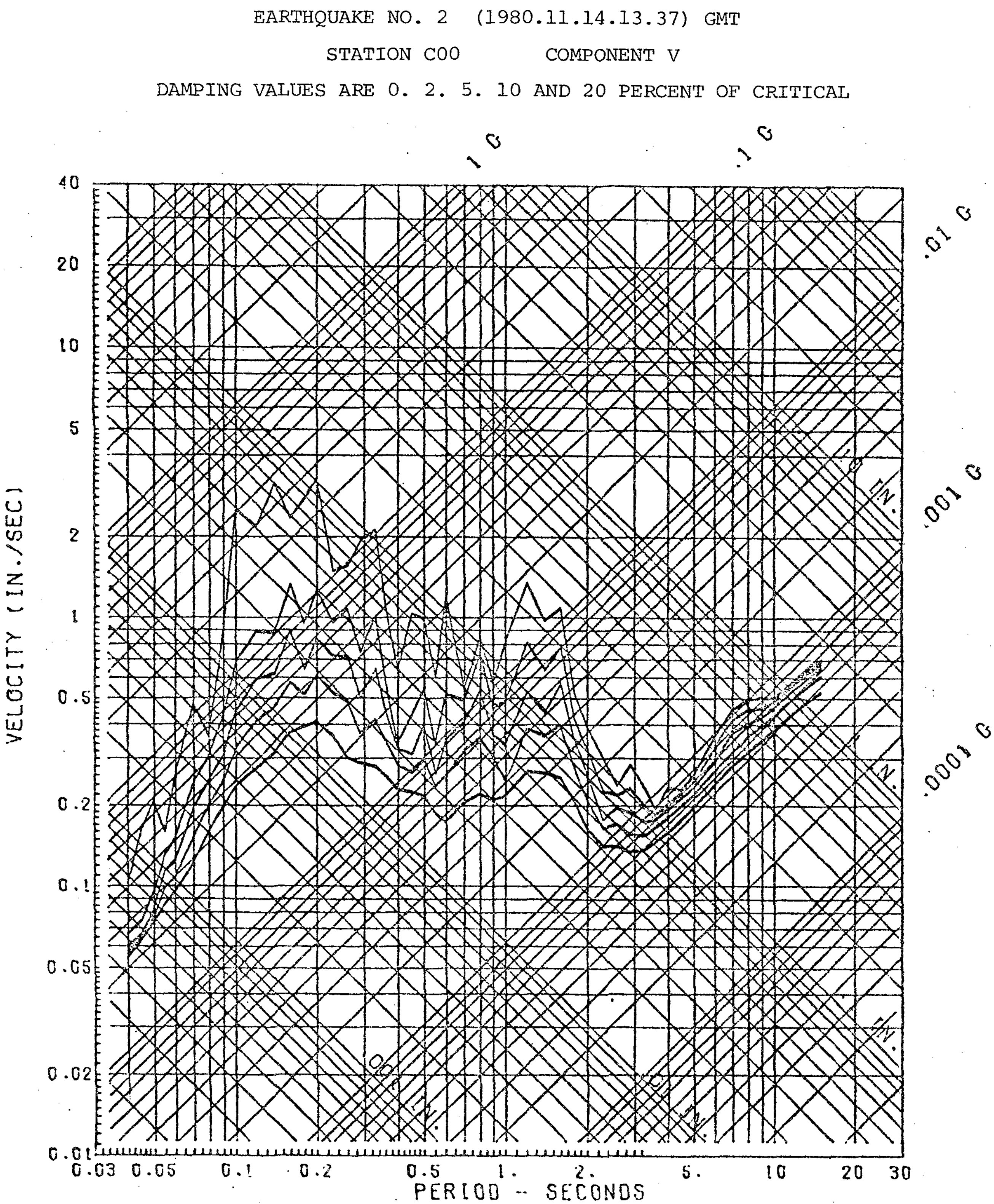

Fig. 5.3a Response spectrum of the vertical component at C00 for Event 2

EARTHQUAKE NO. 2 (1980.11.14.13.37) GMT

STATION C00 COMPONENT EW

DAMPING VALUES ARE 0. 2. 5. 10 AND 20 PERCENT OF CRITICAL

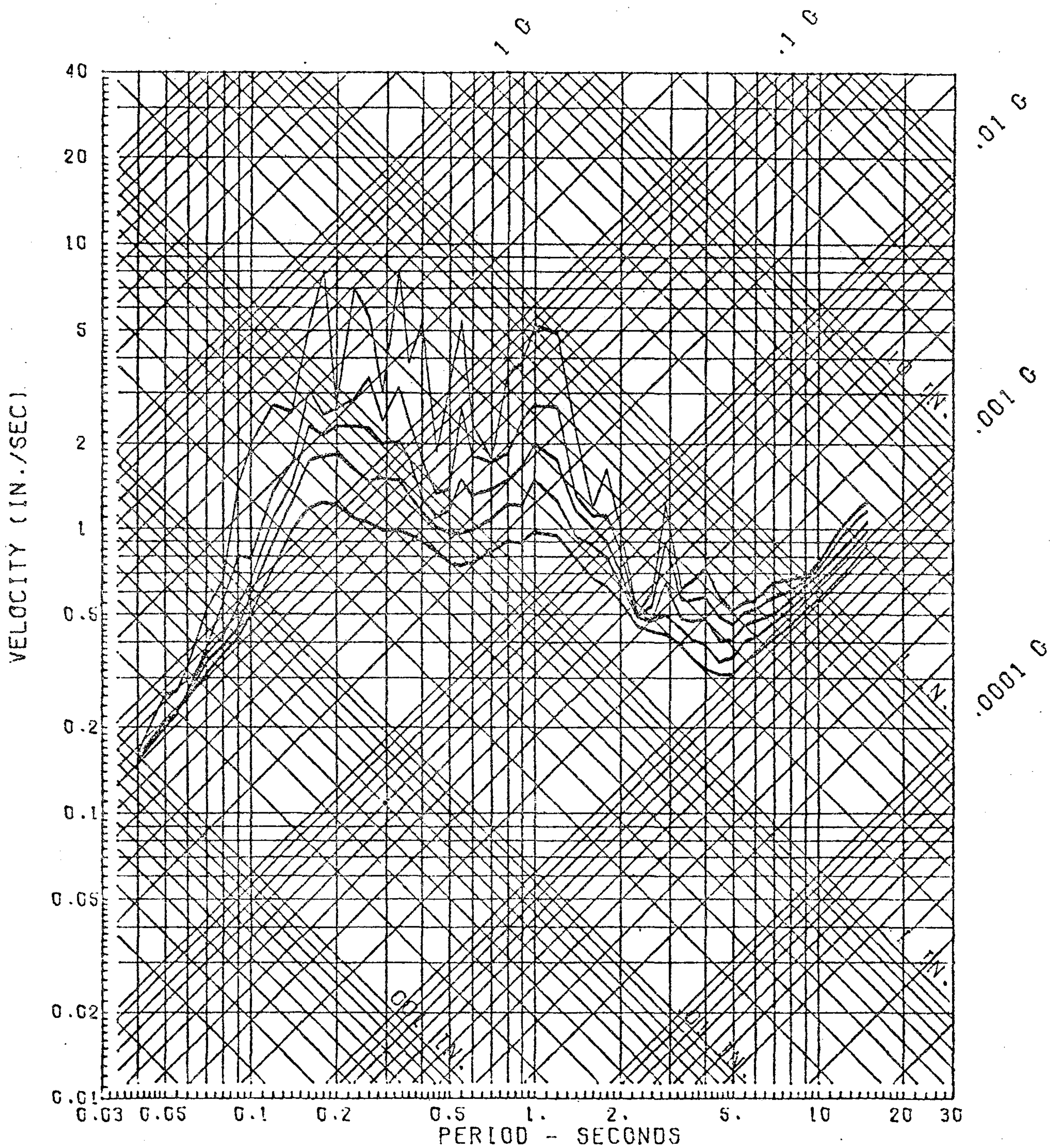

5.3b Response spectrum of the EW component at C00 for Event 2

EARTHQUAKE NO. 2 (1980.11.14.13.37) GMT

STATION COO COMPONENT NS

DAMPING VALUES ARE 0. 2. 5. 10 AND 20 PERCENT OF CRITICAL

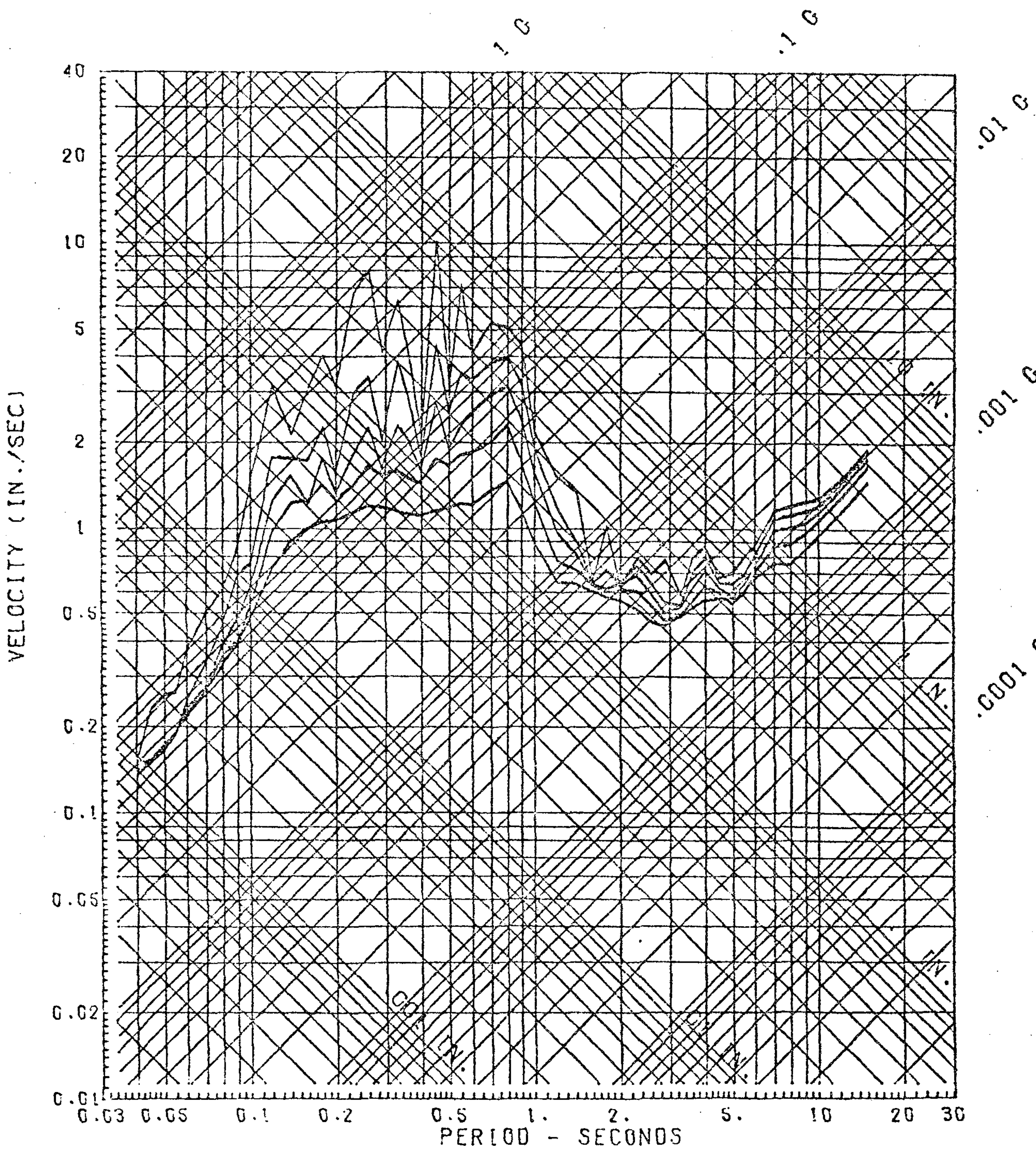

Fig. 5.3c Response spectrum of the NS component at COO for Event 2

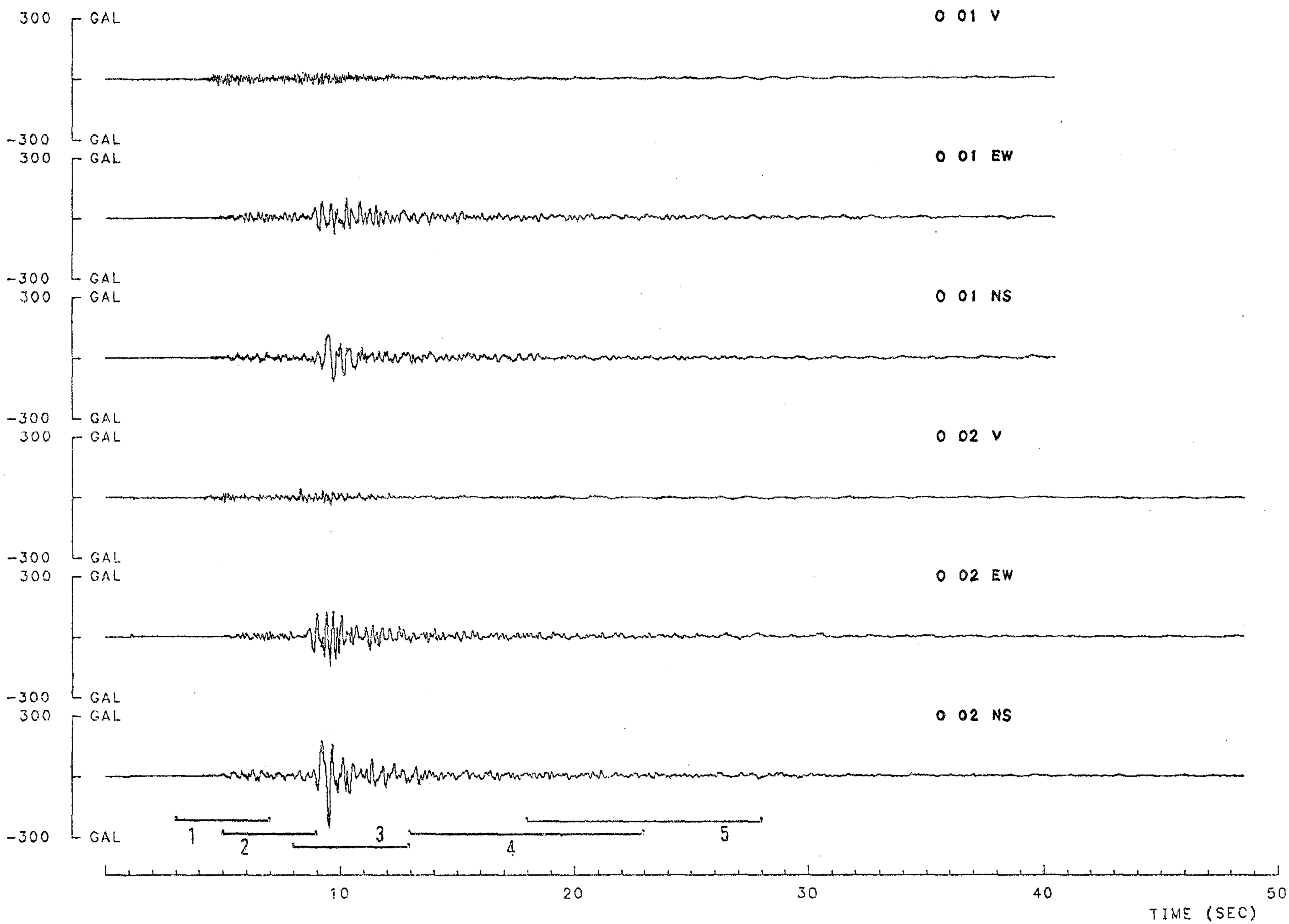

Fig. 5.4 SMART 1 accelerograms at array element 001 and 002 for Event 5 showing time windows 1 to 5 (1 gal = 0.001g)

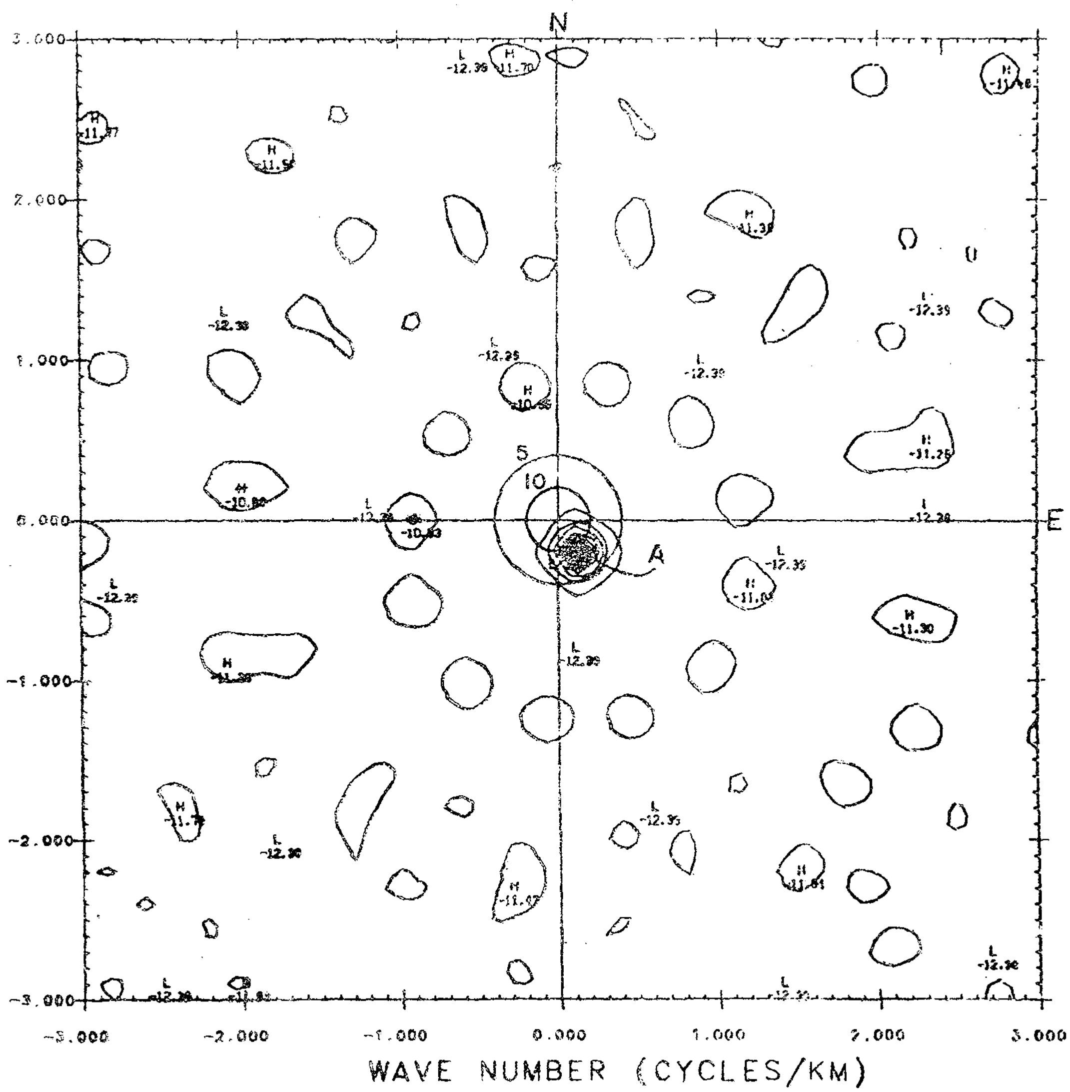

Fig. 5.5 Contours of the summed power at 26 stations of the vertical component of seismic waves in time window 1 (see Fig. 5.4) at a frequency of 2 Hz plotted against wave number in the EW and NS directions. The circles indicate constant velocities of 5 and 10 km/sec. Peak power is at A.

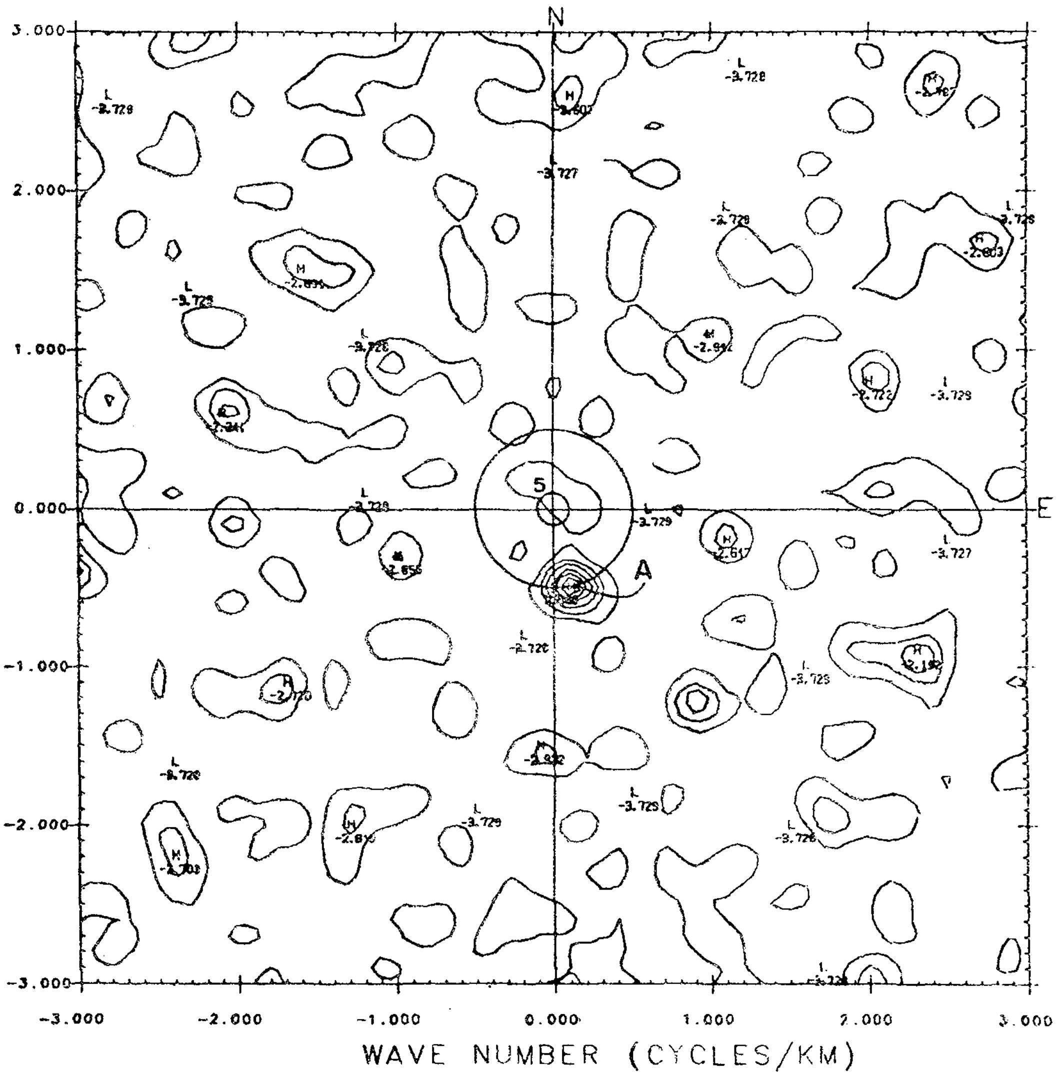

Fig. 5.6 Similar wave number diagram to Fig. 5.5 for time window 4 and a frequency of 0.5 Hz. The clear peak A of high energy corresponds to coherent wave motion of period 2 sec across the array during this time interval with velocity 1 km/sec and azimuth of approach E 75° S.

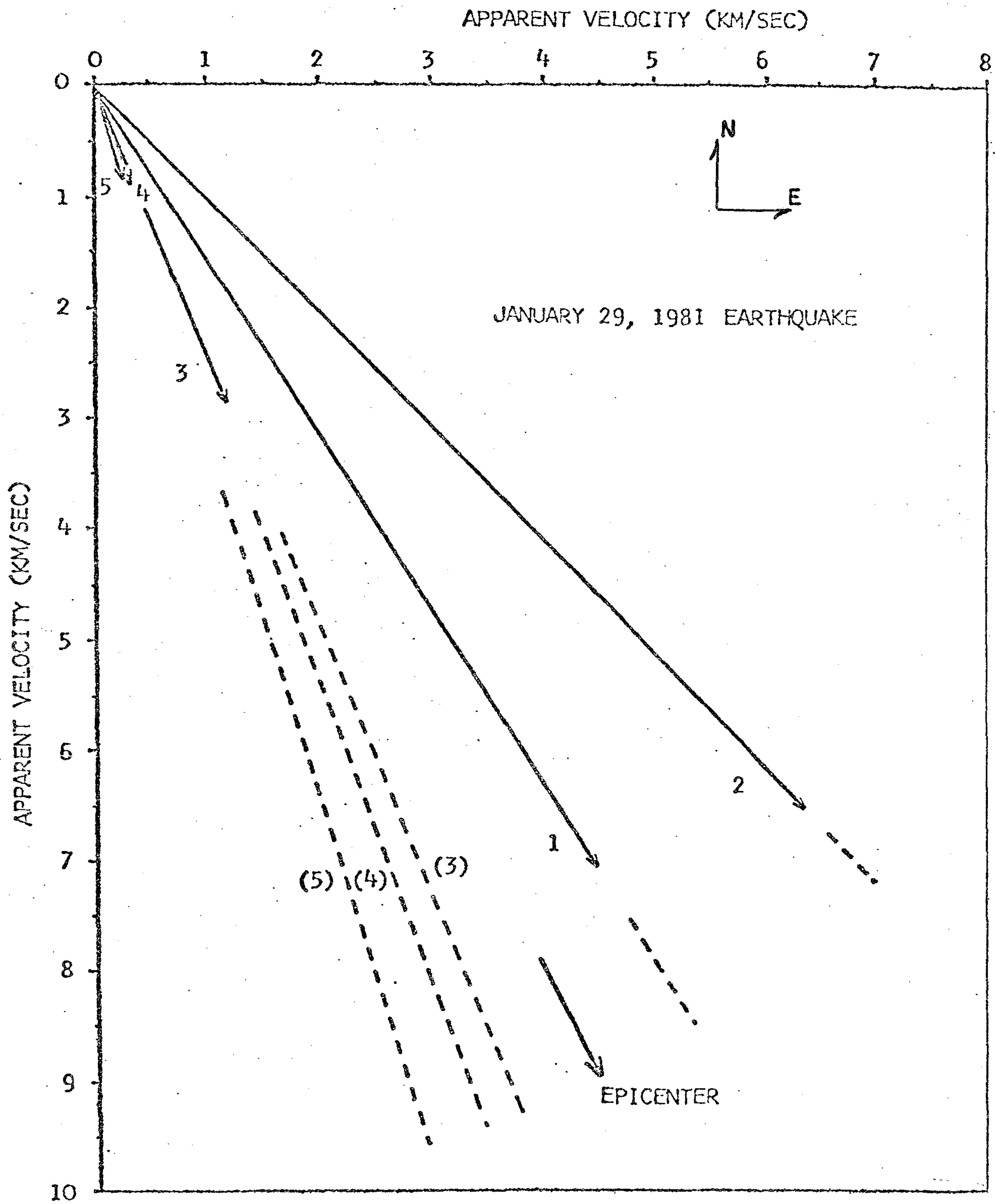

Fig. 5.7 Vectors showing azimuth of approach and apparent velocity of the predominant coherent waves in five time intervals for Event 5. (Epicenter azimuth is relative to array center.)

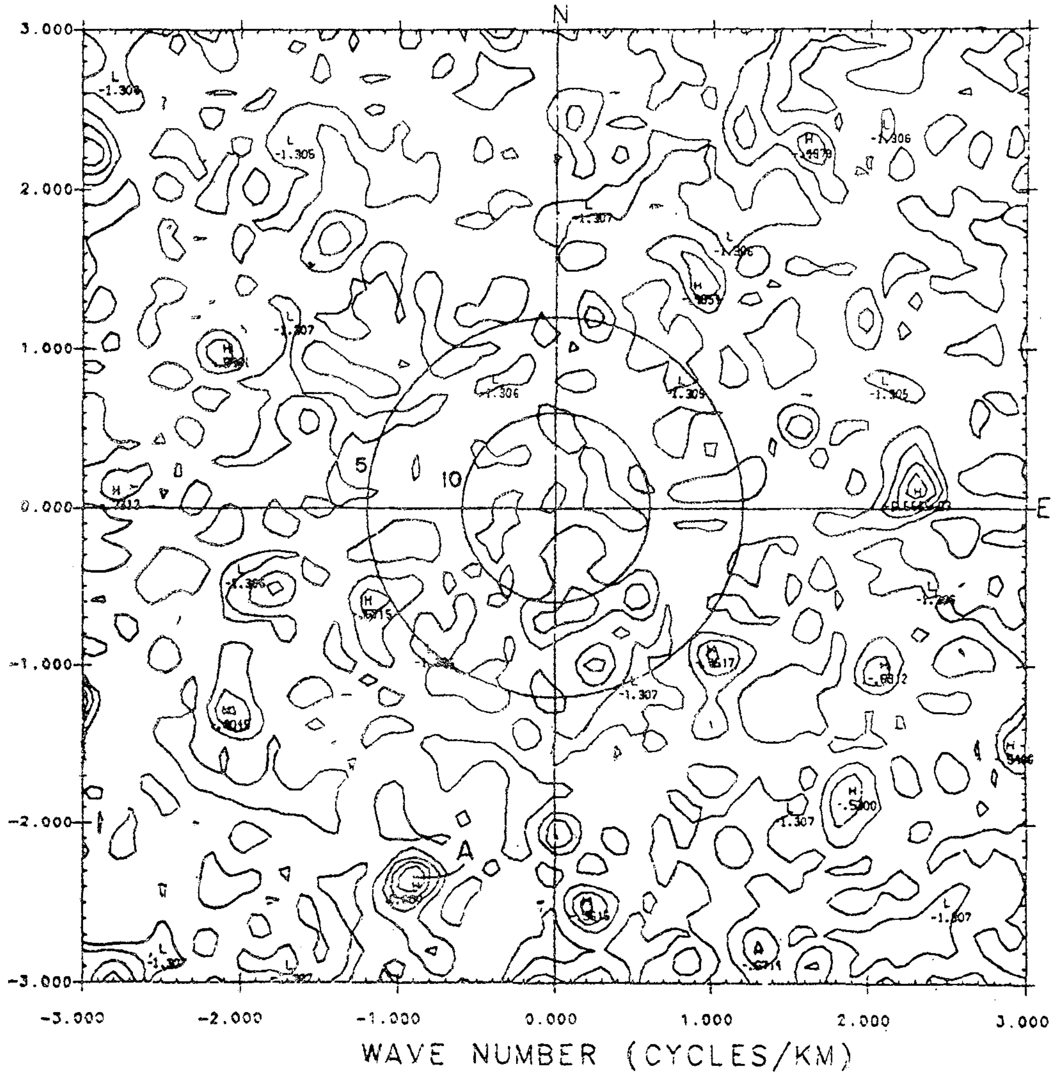

Fig. 5.8 Contours as in Fig. 5.5 of the NS component for time window 3 and a frequency of 6 Hz. The circles indicate constant velocities of 5 and 10 km/sec. The maximum power (point A) is now to be found to the southwest at an apparent velocity of 2.4 km/sec.

6. LOCAL MAGNITUDE VARIATIONS ACROSS ARRAY

6.1 Magnitude Measurements

For all records analyzed, the strong-motion accelerograms from stations of the SMART 1 array were converted to equivalent Wood-Anderson seismograms using a response spectrum written by A. Roca that is similar to that used by Kanamori and Jennings.[1] Richter local magnitude is given as

$$M_L = \log A - \log A_o . \qquad (1)$$

It was determined by two methods based on the peak amplitude A (in millimeters) of the equivalent Wood-Anderson records as follows:

1. For the largest event of January 29, 1981 (see Table 1.2, Event 5), the equivalent Wood-Anderson seismogram appeared normal so that, by definition, the peak amplitude was taken to be the greatest value recorded for the zero-to-peak displacement on the Wood-Anderson record.

2. For the smaller events transformed, recordings (accelerogram or equivalent Wood-Anderson seismogram) showed evidence of incompleteness. Some records appeared to trigger late as distinct phases were not always readily apparent. Further, surface waves seemed disproportionately large, as if they had been used to set the record scale because P and S phases were missing. Long-period perturbations of the Wood-Anderson record were apparent in the records with low signal-to-noise ratio (S/N). The causes for this arise from two sources: (i) when the S/N is low, the least significant bit is unable to sample low signals adequately; (ii) a mid-record shift in the DC level is often apparent in the original accelerogram - a problem occurring in the early stages because of "sticky" pendulums in some of the new instruments.

In the second case, the peak amplitude was taken as one-half of the greatest manually-measured peak-to-peak Wood-Anderson displacement. The log of the peak Wood-Anderson displacement was averaged for the two horizontal components (log A) and added to $-\log A_o$, determined individually for each station by linearly interpolating the $-\log A_o$ table published by Richter.[2]

The adequacy of the second technique for determining log A is not always assured because of subtle changes observed in the computed Wood-Anderson records across the array. The technique, however, was employed for all events, except that of January 29, 1981. Further, an event recorded on March 22, 1981 had such extreme S/N and DC-level shift problems that it was felt that even the second technique of amplitude measurement was not applicable.

It should be noted (Event 2, Table 1.2) that on November 14, 1980, a magnitude 5.9 earthquake (Taiwan magnitude) occurred about 10 km from the array, triggering several of the array instruments. Unfortunately for this study, the hypocenter was at a depth of over 60 km, precluding proper application of the Richter attenuation relation ($-\log A_o$ versus distance), based on shallow southern California earthquakes (depth less than 15 km).

The various measurements and computed magnitudes are listed in Table 6.1. The following summary compares the magnitudes of the earthquakes assigned by the Institute of Earth Sciences and also those determined from SMART 1.

Event	Date	Taiwan M_L	SMART 1 $M_L \pm$ s.e.
1	October 18, 1980	5.8	5.66 ± 0.08
5	January 29, 1981	6.9	6.24 ± 0.08
7	March 2, 1981	6.9	6.51 ± 0.04
8	March 10, 1981	4.4	4.10 ± 0.11

It is interesting to note that all magnitudes determined by SMART 1 are consistently smaller than those given by the Institute. Several explanations may be offered.

1. The magnitude determination for many smaller earthquakes in Taiwan is based on measured durations. The single Wood-Anderson instrument at the Institute provides the calibration of the nationwide network of short period seismometers. Such procedures give rise to unresolved problems from the mechanisms and crustal scattering.

2. The attenuation curve, $-\log A_o$ versus distance, used for the SMART 1 magnitudes, was originally designed for southern California and may not be applicable to Taiwan earthquakes.

3. The final determination of Richter magnitudes assigned to an earthquake is meant to be made as an average of magnitude determinations over a wide azimuthal distribution. The area sampled by SMART 1 would normally be represented by only the Taipei Institute station (if any), and the results here may indicate that, due to local geologic conditions, magnitude estimates are lower for the SMART 1 area than the average over the rest of Taiwan.

6.2 Peak Amplitude Attenuation

The linear regression of the logarithm of peak amplitude onto distance was determined for several components, as listed in Table 6.1. Several of these are also plotted in Figs. 6.1 to 6.5.

We would expect that the slope of the regressed curve would be negative owing to the physics of attenuation. It is seen, however, that for some components the slope is positive, indicating that the peak amplitude is actually increasing with the distance travelled across the array. Though the data are scattered, these positive slopes appear significant. This is particularly true of the log A attenuation plot for January 29, 1981 (Fig. 6.1), which shows minimal scatter of the data points. Linear regression for the two horizontal components individually, log A_{EW} and log A_{NS}, shows distinctly different attenuation curves. (N.B. For every station, A_{NS} was greater than A_{EW}.) As Event 5 occurred SSE of the array, the difference between the two horizontal components indicates that significant SV energy is contributing to the peak horizontal amplitude. Initially, it was supposed that as the seismic energy travelled across the array, there was refraction of the wavefronts due to the wedge-shaped delta structure under the Lotung area, causing a transfer of energy from the EW component into the NS component. On its own, however, this explanation of the transfer of horizontal component energy does not necessarily explain the positive slope in the log A plot. Further, the plot of log A_{HZ} (Fig. 6.2), where A_{HZ} is the peak amplitude of the vector sum of the horizontal components, still shows an increase in peak amplitude with distance across the array. By comparison, the log peak amplitude plot for the vertical component (log A_Z), in Fig. 6.3, shows a definite negative slope. It is possible, therefore, that path effects and mode conversion are enhancing the horizontal components of the waves by some transfer of energy from the vertical component.

The SMART 1 results also indicate that local (Richter) magnitude estimates are subject to significant variation due to local structural changes within a linear dimension of 2 km. Contours illustrating the M_L variation for Event 5 are drawn in Fig. 6.6. The equivalent Richter magnitude for this earthquake ranged between 6.0 and 6.4 across SMART 1 with a mean of 6.24 ± 0.08. The scatter about the mean is not random, however, but as shown in Fig. 6.6, there is a systematic azimuthal trend.

It is important to reiterate that the local magnitude estimate for the January 29, 1981 main shock by the Institute of Earth Sciences in Taipei is

6.9. This value is calculated from a Wood-Anderson seismograph operated in Taipei and follows standard procedures used in Taiwan for many years. A direct comparison between this value and the SMART 1 mean of 6.24 and the "true" Richter magnitude cannot be made because regional attenuation curves are not yet available for Taiwan.

6.3 References

1. Kanamori, H. and P.C. Jennings, "Determination of Local Magnitude, M_L, from Strong-Motion Accelerograms," Bull. Seism. Soc. Am., 68, 471-485 (1978).

2. Richter, C., Elementary Seismology, W.H. Freeman, San Francisco (1958).

TABLE 6.1

Peak Amplitudes and Magnitudes

(see Notes at end)

October 18, 1980

Station	Dist (km)	$-\log A_o$	$\log A_Z$	M_Z	log A	M_L
C-00	45.47	2.509	2.862	5.371	3.243	5.753
I-06	45.27	2.505	2.846	5.352	3.214	5.720
I-09	45.45	2.509	3.000	5.509	3.262	5.771
I-12	45.67	2.513	2.811	5.324	3.173	5.686
M-01	46.37	2.527	2.747	5.275	3.177	5.704
M-02	46.14	2.523	2.661	5.184	3.197	5.720
M-04	45.03	2.500	2.797	5.298	3.116	5.617
M-05	44.70	2.494	2.777	5.271	3.059	5.553
M-06	44.46	2.489	2.881	5.371	3.091	5.580
M-07	44.19	2.484	2.863	5.347	3.138	5.622
M-08	44.90	2.498	2.888	5.386	3.164	5.662
M-10	45.82	2.516	2.827	5.344	3.200	5.716
M-12	46.47	2.529	2.745	5.274	3.179	5.708
O 06	43.46	2.469	2.634	5.103	3.109	5.578
O 09	45.28	2.506	2.638	5.144	2.972	5.478
O 12	47.47	2.549	2.608	5.157	3.204	5.753
				$\overline{M}_Z = 5.29 \pm 0.11$		$\overline{M}_L = 5.66 \pm 0.08$

TABLE 6.1 (continued)

January 29, 1981

Station	Dist (km)	$-\log A_o$	$\log A_Z$	M_Z	log A	M_L
C-00	30.28	2.111	3.540	5.651	4.209	6.320
I-03	30.25	2.110	3.343	5.453	4.198	6.308
I-06	30.09	2.104	3.410	5.514	4.104	6.208
I-12	30.48	2.119	3.523	5.642	4.147	6.266
M-01	31.08	2.143	3.376	5.519	4.106	6.249
M-02	30.75	2.130	3.430	5.560	4.151	6.281
M-03	30.22	2.109	3.376	5.485	4.034	6.143
M-04	29.65	2.086	3.526	5.612	4.147	6.233
M-05	29.41	2.076	3.490	5.566	4.097	6.173
M-06	29.29	2.071	3.952	6.024	4.137	6.208
M-07	28.78	2.051	3.472	5.523	4.137	6.189
M-08	29.91	2.096	3.650	5.746	4.185	6.281
M-09	30.38	2.115	3.383	5.498	4.118	6.233
M-10	30.82	2.133	3.424	5.557	4.137	6.270
M-11	31.22	2.149	3.603	5.751	–	–
M-12	31.27	2.151	3.469	5.620	4.134	6.285
O-01	31.92	2.177	3.352	5.529	4.184	6.361
O-02	31.07	2.143	3.442	5.585	4.202	6.345
O-03	30.03	2.101	3.437	5.538	4.125	6.226
O-04	29.12	2.065	3.367	5.432	4.097	6.162
O-05	28.46	2.038	3.523	5.562	4.008	6.046
O-06	28.29	2.031	3.476	5.508	4.118	6.149
O-07	28.71	2.048	3.624	5.672	4.093	6.141

TABLE 6.1 (continued)

January 29, 1981

Station	Dist (km)	$-\log A_o$	$\log A_Z$	M_Z	log A	M_L
O-09	30.57	2.123	3.492	5.615	4.140	6.263
O-10	31.58	2.163	3.471	5.634	4.161	6.324
O-12	32.26	2.190	3.380	5.570	4.205	6.396
				$\bar{M}_Z = 5.59 \pm 0.12$		$\bar{M}_L = 6.24 \pm 0.08$

TABLE 6.1 (continued)

January 29, 1981

Station	Dist (km)	$-\log A_o$	$\log A_{HZ}$	M_{HZ}
C-00	30.28	2.111	4.572	6.683
I-03	30.25	2.110	4.524	6.634
I-06	30.09	2.104	4.446	6.550
I-12	30.48	2.119	4.625	6.744
M-01	31.08	2.143	4.712	6.855
M-02	30.75	2.130	4.564	6.694
M-03	30.22	2.109	4.514	6.622
M-04	29.65	2.086	4.668	6.755
M-05	29.41	2.076	4.593	6.669
M-06	29.29	2.071	4.424	6.495
M-07	28.78	2.051	4.549	6.600
M-08	29.91	2.096	4.506	6.602
M-09	30.38	2.115	4.471	6.587
M-10	30.82	2.133	4.609	6.742
M-11	31.22	2.149	-	-
M-12	31.27	2.151	4.691	6.842
O-01	31.92	2.177	4.611	6.788
O-02	31.07	2.143	4.818	6.961
O-03	30.03	2.101	4.711	6.812
O-04	29.12	2.065	4.536	6.601
O-05	28.46	2.038	4.442	6.480
O-06	28.29	2.031	4.502	6.534
O-07	28.71	2.048	4.429	6.478
O-09	30.57	2.123	4.551	6.674
O-10	31.58	2.163	4.487	6.650

TABLE 6.1 (continued)

January 29, 1981

Station	Dist (km)	$-\log A_o$	$\log A_{HZ}$	M_{HZ}
O-12	32.26	2.190	4.683	6.874

M_{HZ} = 6.68

± 0.13

TABLE 6.1 (continued)

January 29, 1981

Station	Dist (km)	log A_{EW}	log A_{NS}
C-00	30.28	4.0648	4.3528
I-03	30.25	4.0539	4.3419
I-06	30.09	3.9434	4.2654
I-12	30.48	3.9768	4.3178
M-01	31.08	3.7960	4.4160
M-02	30.75	3.9712	4.3305
M-03	30.22	3.8423	4.2257
M-04	29.65	4.0513	4.2429
M-05	29.41	3.9941	4.2004
M-06	29.29	4.0496	4.2244
M-07	28.78	4.0238	4.2509
M-08	29.91	4.0756	4.2909
M-09	30.38	3.9488	4.2871
M-10	30.82	3.9639	4.3097
M-11	31.22	–	4.3236
M-12	31.27	3.8723	4.3959
O-01	31.92	3.9606	4.4073
O-02	31.07	3.8889	4.5144
O-03	30.03	4.0158	4.2335
O-04	29.12	4.0251	4.1694
O-05	28.46	3.9338	4.0816
O-06	28.29	4.0269	4.2082
O-07	28.71	3.9285	4.2568
O-09	30.57	3.9587	4.3222

TABLE 6.1 (continued)

January 29, 1981

Station	Dist (km)	log A_{EW}	log A_{NS}
O-10	31.58	3.9910	4.3311
O-12	32.26	3.9859	4.4244

March 2, 1981

Station	Dist (km)	-log A_o	log A_Z	M_Z	log A	M_L
M-05	194.28	3.500	2.554	6.054	3.057	6.557
O-02	196.46	3.500	-	-	2.970	6.470
O-06	192.98	3.500	2.436	5.936	3.014	6.514
				$\overline{M}_Z = 6.00 \pm 0.08$		$\overline{M}_L = 6.51 \pm 0.04$

TABLE 6.1 (continued)

March 10, 1981

Station	Dist (km)	$-\log A_o$	$\log A_Z$	M_Z	log A	M_L
C-00	6.99	1.440	2.182	3.622	2.848	4.288
I-03	6.88	1.438	2.000	3.438	2.744	4.182
I-06	7.17	1.443	2.292	3.736	2.613	4.056
I-09	7.11	1.442	2.588	4.030	2.642	4.085
I-12	6.82	1.436	2.241	3.677	2.666	4.103
M-02	6.01	1.420	1.949	3.370	2.688	4.109
M-03	6.48	1.430	2.276	3.706	2.638	4.067
M-04	7.03	1.441	-	-	2.774	4.214
M-05	7.45	1.449	2.152	3.601	2.690	4.139
M-08	7.89	1.458	2.124	3.582	2.611	4.069
M-09	7.65	1.453	2.000	3.453	2.602	4.055
M-10	7.15	1.443	2.021	3.464	2.473	3.916
O-01	4.97	1.400	1.978	3.378	2.658	4.058
O-02	5.29	1.406	2.182	3.588	2.640	4.046
O-03	6.16	1.423	2.262	3.686	2.639	4.062
O-04	7.14	1.443	2.316	3.759	2.952	4.395
O-05	8.05	1.461	-	-	2.517	3.978
O-06	8.76	1.475	-	-	2.509	3.984
O-09	8.33	1.467	1.863	3.330	2.599	4.065
				$\overline{M}_Z = 3.59 \pm 0.18$		$\overline{M}_L = 4.10 \pm 0.11$

TABLE 6.1 (continued)

Notes

1. $-\log A_o$ is linearly interpolated from values given in Richter[2].

2. $\log A = (\log A_{EW} + \log A_{NS})/2$ where A_{EW} and A_{NS} are peak amplitudes (in millimeters) for the Wood-Anderson instrument displacement on the east-west and north-south components, respectively.

3. A_Z is the peak vertical amplitude for an equivalent Wood-Anderson instrument.

4. A_{HZ} is the peak horizontal amplitude measured from a record given by the Pythagorean (vector) sum of the two horizontal components.

TABLE 6.2

Attenuation Across SMART 1

Linear Regression (see Footnotes)

Type of Displacement	a	b	r^2*
October 18, 1980 Δ ∿ 45 km			
A_Z	4.158	-0.0302	0.0726
A	1.632	+0.0336	0.1974
January 29, 1981 Δ ∿ 30 km			
A_Z	4.751	-0.0420	0.1221
A_{EW}	4.622	-0.0215	0.1029
A_{NS}	2.152	+0.0710	0.6615
A_{HZ}	3.025	+0.0512	0.2784
A	3.364	+0.0256	0.2980
March 2, 1981 Δ ∿ 194 km			
A_Z	-15.081	+0.0908	1.0000
A	6.022	-0.0155	0.3907
March 10, 1981 Δ ∿ 7 km			
A_Z	2.201	-0.0072	0.0013
A	2.884	-0.0322	0.0731

* test for fit: $r^2 = 1$ for perfect fit

$$\log A = a + b\Delta$$

A ≡ W-A displacement in millimeters

Δ ≡ epicentral distance in kilometers

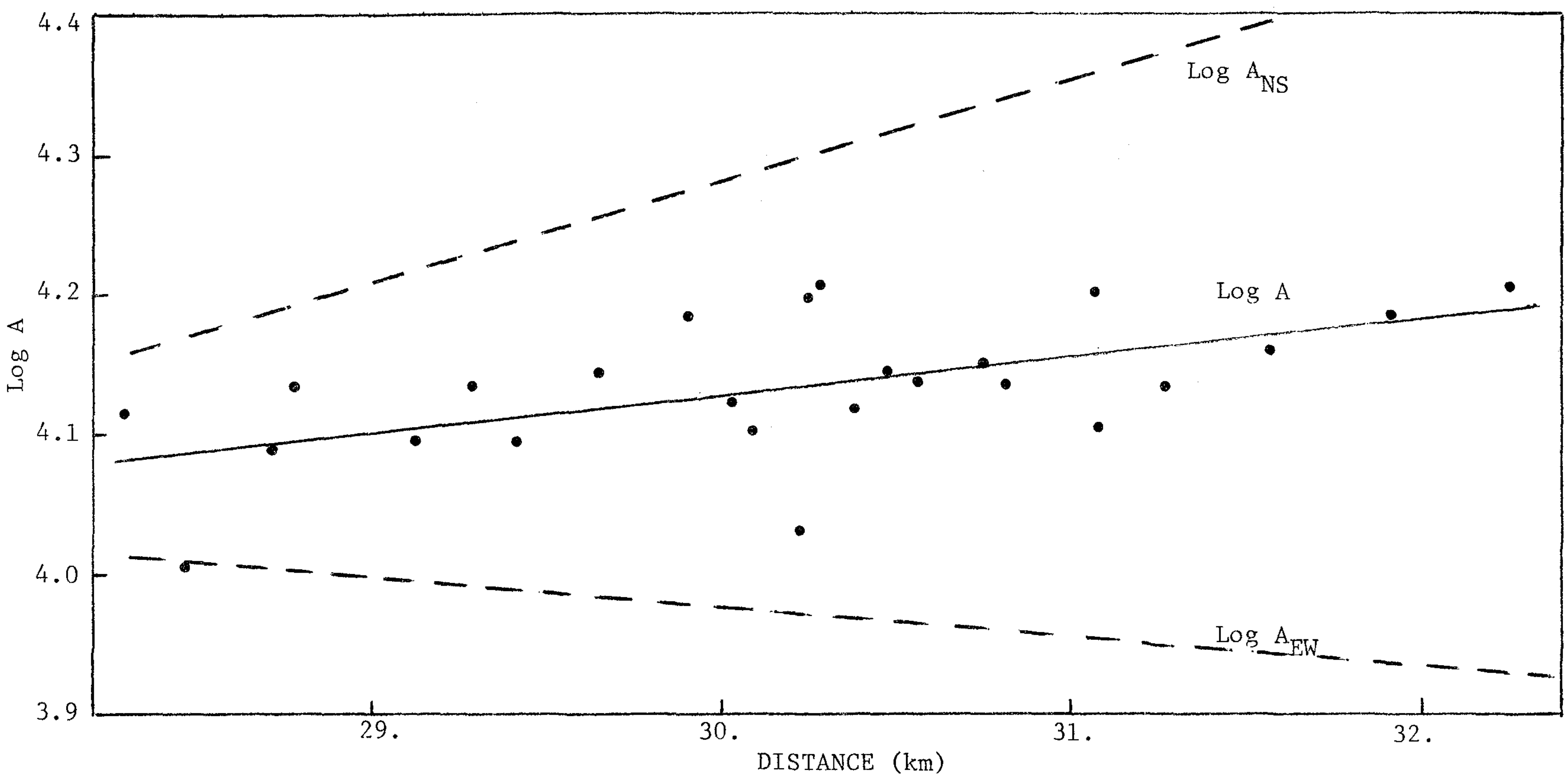

Fig. 6.1 Attenuation curve of log A for Event 5 (January 29, 1981)

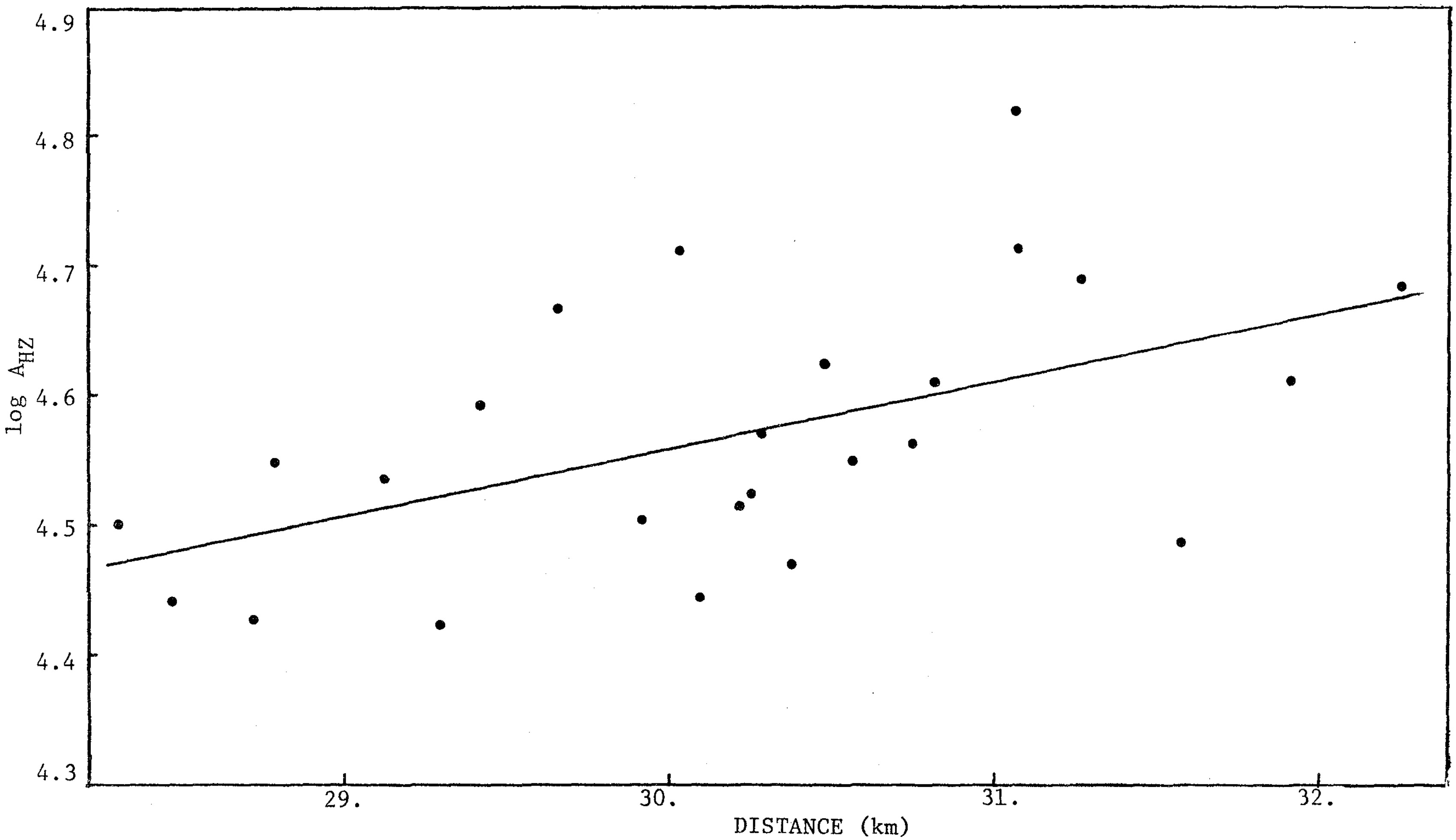

Fig. 6.2 Attenuation curve of log A_{HZ} for Event 5 (January 29, 1981)

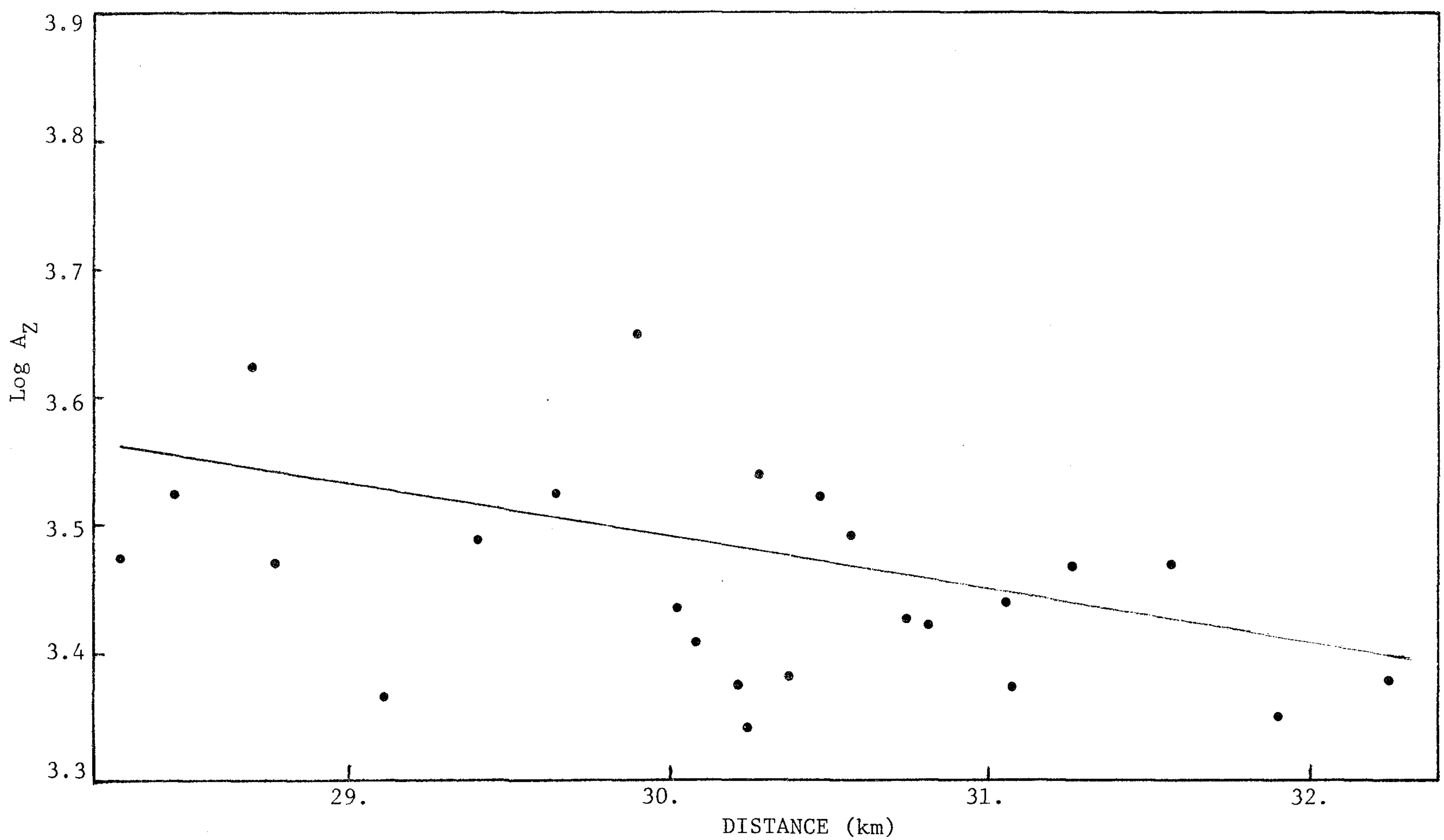

Fig. 6.3 Attenuation curve of log A_Z for Event 5 (January 29, 1981)

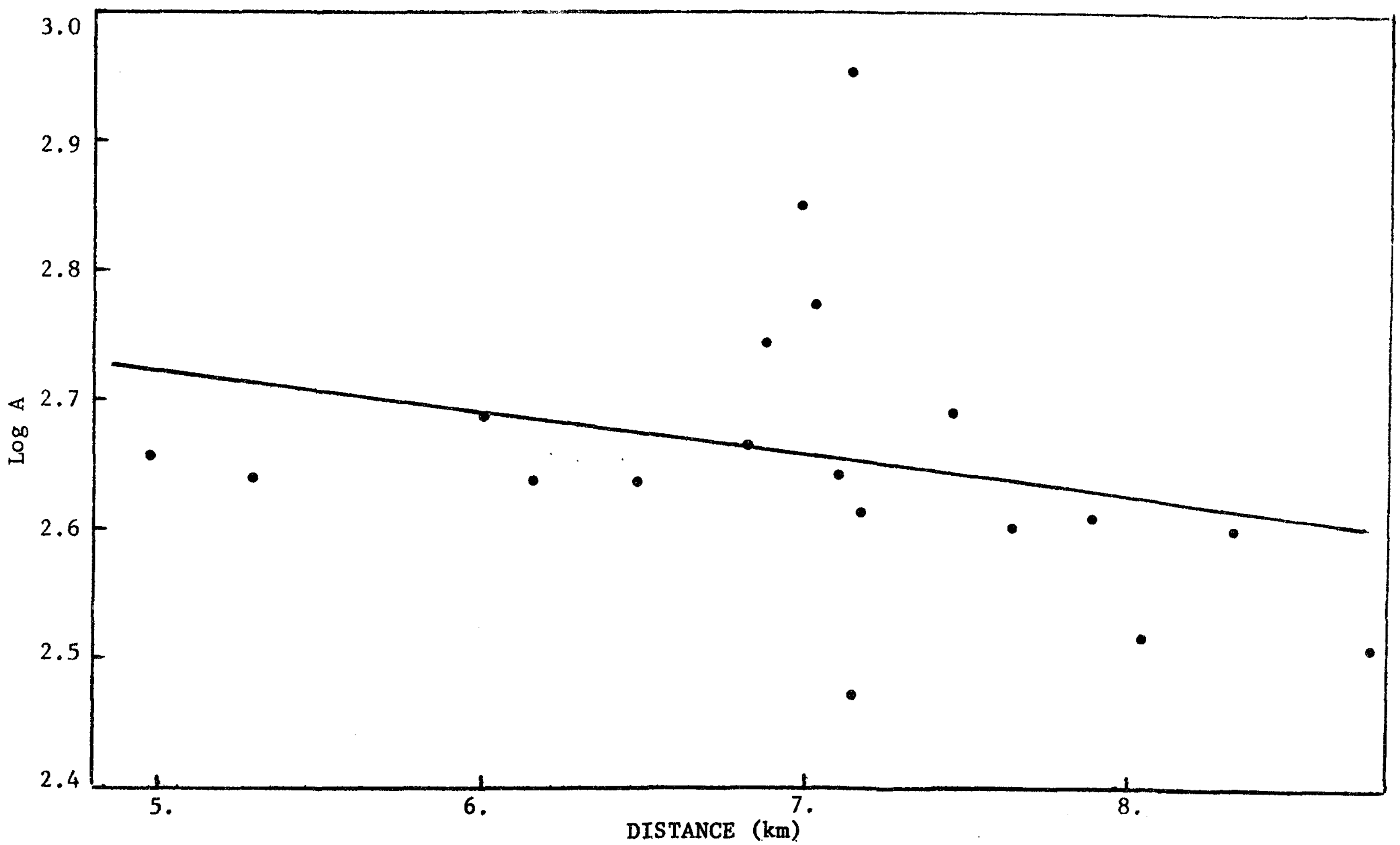

Fig. 6.4 Attenuation curve of log A for Event 8 (March 10, 1981)

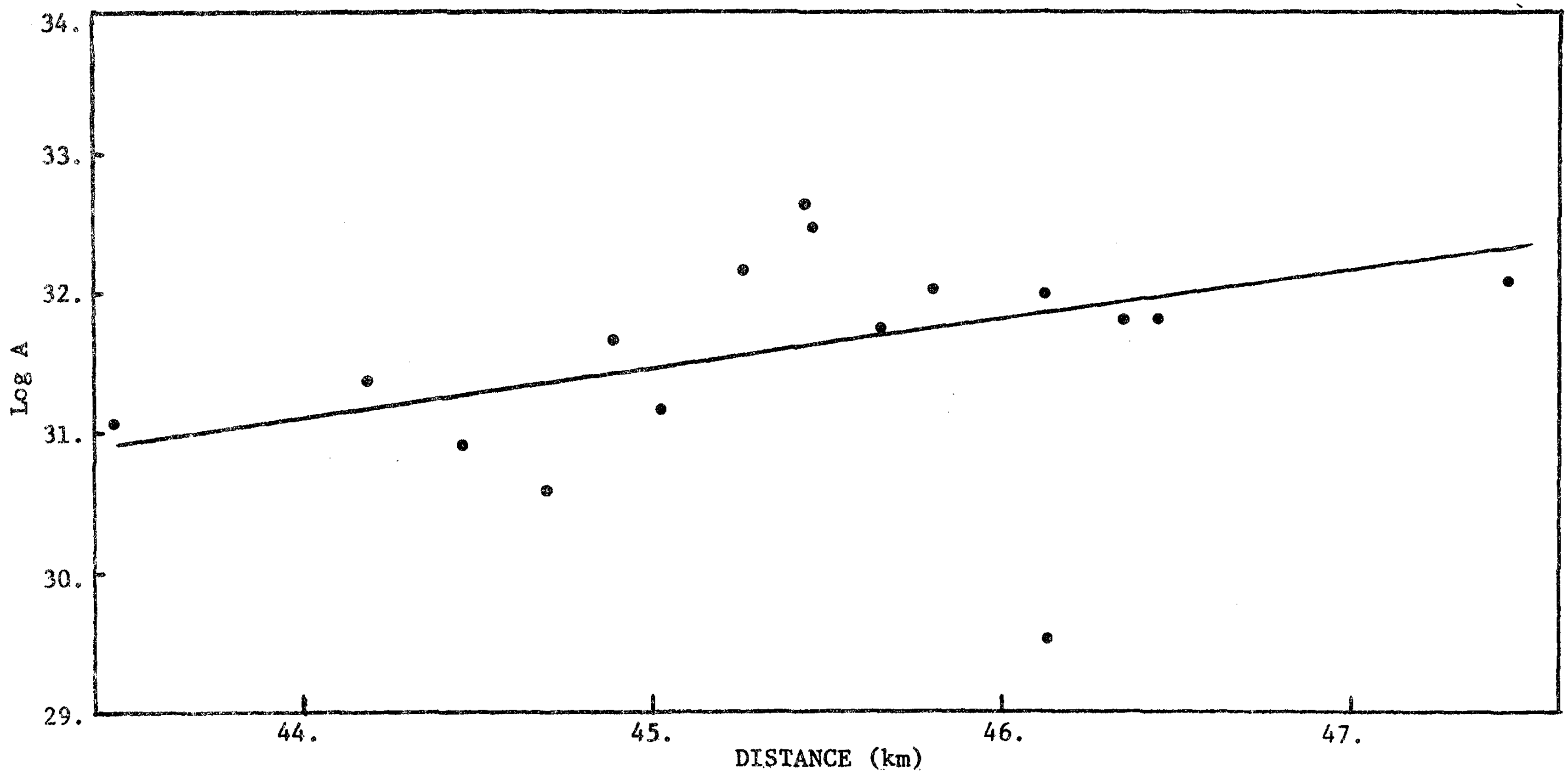

Fig. 6.5 Attenuation curve of log A for Event 1 (October 18, 1980)

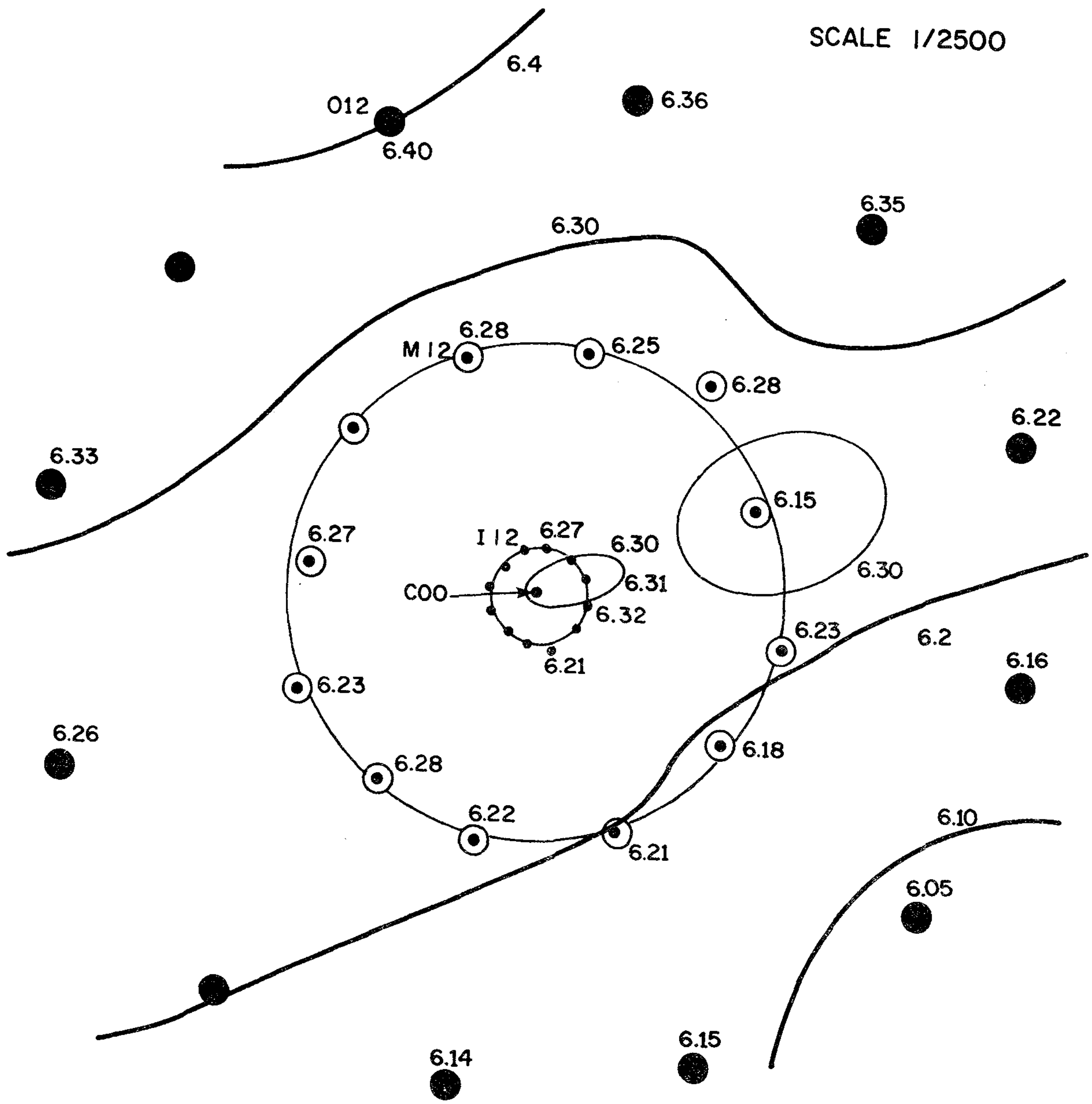

Fig. 6.6 Contours of computed Richter magnitude for Event 5. Values for individual magnitudes are shown at those array elements which recorded this earthquake.

7. IDENTIFICATION OF WAVE TYPES, DIRECTIONS, AND VELOCITIES

7.1 Correlation and Coherence

In an attempt to identify wave types, directions, and velocities produced by the earthquakes of November 14, 1980 (Event 2), and January 29, 1981, (Event 5), let us first examine the cross correlation coefficient given by

$$\rho_{ij}(\tau) \equiv \frac{R_{ij}(\tau)}{\sqrt{R_{ii}(0)\ R_{jj}(0)}} \tag{1}$$

where

$$R_{ij}(\tau) \equiv \int_{t_0-\Delta T/2}^{t_0+\Delta T/2} x_i(t)\ x_j(t+\tau)\ dt \tag{2}$$

and where $x_i(t)$ and $x_j(t)$ are the recorded acceleration time-histories in the x-direction (see Fig. 7.1) at stations i and j, respectively, Δt is a time window centered on time t_0, and τ is a time lag. If the ground motions at these stations were produced primarily by a single travelling wave, then the above cross correlation coefficient, which can range from +1 to -1, would show high correlation for τ equal to the time required for the wave to travel between the two stations. This value of τ would, of course, depend upon the direction of wave propagation as well as wave velocity.

Plots of the cross correlation coefficient given by (1) are shown in Figs. 7.2a to 7.2c for both earthquakes mentioned above using time windows which contain the significant high intensity motions as shown in Fig. 7.3, and for selected station pairs as indicated. The distances given in these figures are true distances (not projected distances) between corresponding station pairs. The maximum absolute values of the cross correlation coefficients are shown in Fig. 7.4 along with an exponential curve fitted by least squares.

It is significant to note that the cross correlation coefficient plots in Figs. 7.2a to 7.2c are not characteristic of motions dominated by a single travelling wave train. Their shapes and low values of correlation suggest the simultaneous presence of multiple waves travelling in different directions with different velocities. The wide scatter of maximum absolute values in Fig. 7.4 also supports this general conclusion. As a consequence resolution of the motions into their frequency components and into their components of principal directions is required before identification of wave types, directions, and velocities is possible.

Following along these lines, let us transform the x and y recorded components of horizontal ground motion at a point into their $\tilde{x}$ and $\tilde{y}$ components in accordance with Fig. 7.1; thus,

$$\begin{aligned} \tilde{x}(t) &= x(t)\cos\phi + y(t)\sin\phi \\ \tilde{y}(t) &= -x(t)\sin\phi + y(t)\cos\phi \quad . \end{aligned} \tag{3}$$

Next, using time and frequency domain windows, the Fourier transforms of these new components are calculated using relations of the type

$$A_{\tilde{x}}(f) \equiv \int_{t_0-\Delta T/2}^{t_0+\Delta T/2} \tilde{x}(t)\exp(-i2\pi ft)\,dt \tag{4}$$

$$\begin{aligned} \tilde{x}(t) \equiv &\int_{-f_0-\Delta f/2}^{-f_0+\Delta f/2} A_{\tilde{x}}(f)\exp(i2\pi ft)\,df \\ &+ \int_{f_0-\Delta f/2}^{f_0+\Delta f/2} A_{\tilde{x}}(f)\exp(i2\pi ft)\,df \end{aligned} \tag{5}$$

where window lengths ΔT and Δf are centered on time t_0 and frequency f_0, respectively. A coherence function for components $\tilde{x}_i$ and $\tilde{x}_j$ (i and j refer to station numbers) can now be defined by

$$\gamma_{\tilde{x}_i\tilde{x}_j}(f) \equiv \frac{\left| S_{\tilde{x}_i\tilde{x}_j}(f) \right|^2}{S_{\tilde{x}_i\tilde{x}_i}(f)\ S_{\tilde{x}_j\tilde{x}_j}(f)} \tag{6}$$

where

$$S_{\tilde{x}_i\tilde{x}_j}(f) \equiv \int_{-\infty}^{\infty} R_{\tilde{x}_i\tilde{x}_j}(\tau)\ \exp(-i2\pi f\tau)\ d\tau \tag{7}$$

$$R_{\tilde{x}_i\tilde{x}_j}(\tau) \equiv \int_{t_0-\Delta T/2}^{t_0+\Delta T/2} \tilde{x}_i(t)\ \tilde{x}_j(t+\tau)\ dt \tag{8}$$

and where $S_{\tilde{x}_i\tilde{x}_i}(f)$ and $R_{\tilde{x}_j\tilde{x}_j}(f)$ are similarly defined. Note that the coherence function (6), which ranges from 0 to 1, provides a measure of the statistical dependence of motion $\tilde{x}_j$ on motion $\tilde{x}_i$.

Coherence functions as defined by (6) are plotted in Figs. 7.5a and 7.5b for components of motion produced by the earthquake of January 29, 1981, in the $\tilde{y}$ and $\tilde{x}$ directions, respectively. In what follows the value $\phi = 64^o$ is adopted so that the $\tilde{x}$ direction corresponds with the direction to the epicenter from station C00. The station pairs represented in these figures are located along the radial line of SMART 1 running from station 006 to 012 which is oriented in approximately the epicentral direction. The distance coordinate shown in these plots represents true distance between stations i and j. Note that while the average coherence with distance is relatively low for most frequencies over the range $0<f<10$ Hz, it is relatively high in the neighborhood of frequencies 3.0 and 4.5 Hz, in Fig. 7.5a and at frequencies about 1.1 and 3.5 Hz in Fig. 7.5b, as indicated by f_1 and f_2, respectively. This observation is encouraging as the corresponding Fourier amplitude spectra for motions $\tilde{x}_i$ and $\tilde{x}_j$ for all station pairs have large peaks in the vicinity of the same frequencies. Thus, the high intensity ground motions which are caused primarily by frequencies in the neighborhood of f_1 and f_2 appear to be caused largely by single wave trains moving across the array. In other frequency ranges, the motions appear to be caused to a much greater degree by multiple waves moving with different apparent velocities.

Let us now examine the influence of direction ϕ on the cross spectral density function defined by (7) for components $\tilde{x}(t)$ and $\tilde{y}(t)$ as given by (3) using measured components $x(t)$ and $y(t)$ for station pairs which are separated by only 0.2 km. This shortest distance between station pairs is selected so that coherences $\gamma_{\tilde{x}_i\tilde{x}_j}$ and $\gamma_{\tilde{y}_i\tilde{y}_j}$ are as large as possible; thus, the variations in $S_{\tilde{x}_i\tilde{x}_j}$ with respect to direction ϕ and frequency f show variations in the intensities of motions $\tilde{x}_i$ and $\tilde{x}_j$. Figures 7.6a and 7.6b show plots of $S_{\tilde{x}_i\tilde{x}_j}$ as a function of frequency f for discrete values of direction ϕ over the entire range $-90^{\circ}<\phi<+90^{\circ}$. Figure 7.6a represents the earthquake of January 29, 1981, using station pair C00-I12 while Fig. 7.6b represents the earthquake of November 14, 1980, using station pair I06-C00. From these figures, it is clear that the high intensity motions tend to be concentrated in the neighborhood of frequencies f_1, f_2, and f_3. For these discrete frequencies, the values of ϕ yielding the greatest values of cross spectral density can be observed. It should be pointed out that functions $S_{\tilde{x}_i\tilde{x}_j}$ need not be generated through the use of (3), (4), (5), (7), and (8) for each value of ϕ since they are more easily obtained from the transformation

$$S_{\tilde{x}_i\tilde{x}_j}(f,\phi) = S_{x_ix_j}(f)\cos^2\phi + S_{y_iy_j}(f)\sin^2\phi + S_{x_iy_j}(f)\cos\phi\sin\phi + S_{y_ix_j}(f)\cos\phi\sin\phi \quad . \tag{9}$$

The cross spectral density function (9) can easily be maximized with respect to ϕ for discrete values of frequency f, to give the direction of maximum intensity. The directions of maximum intensity shown in Fig. 7.7 were obtained by first maximizing the spectral densities for f = 2.9 Hz and then averaging the corresponding two values of ϕ for each set of adjacent station pairs along the array line 006 to 012 during the earthquake of January 29, 1981. There is a definite shift in the direction of maximum intensity at this frequency as one moves across the array from station 006 to station 012.

The direction of maximum intensity as a function of frequency f_0 can also be obtained by maximizing the variance function[3,4,5] (see (8))

$$R_{\tilde{x}_i\tilde{x}_i}(\tau=0,\phi) = R_{x_ix_i}(0)\cos^2\phi + R_{y_iy_i}(0)\ \sin^2\phi + 2R_{x_iy_i}(0)\ \cos\phi\ \sin\phi \quad (10)$$

with respect to ϕ; thus, giving

$$\phi_0(f_0) = \frac{1}{2}\tan^{-1}\frac{2R_{x_iy_i}(0)}{R_{x_ix_i}(0) - R_{y_iy_i}(0)} \ . \quad (11)$$

Angle ϕ_o in (11) denotes the two principal directions which are 90^o apart; one being the major principal direction, the other the minor principal direction. The corresponding principal variances will be denoted by $R_{\tilde{x}_i\tilde{x}_i}(f_0,\phi_0)$ and $R_{\tilde{y}_i\tilde{y}_i}(f_0,\phi_0)$. The angles of maximum intensity obtained by this procedure are quite close to those obtained by the previously described procedure of maximizing the cross spectral density function for station pairs with respect to direction ϕ

7.2 The Principal Variance Ratio

Let us now define a principal variance ratio as given by

$$R(f_0,\phi_0) \equiv \frac{R_{\tilde{y}_i\tilde{y}_i}(f_0,\phi_0)}{R_{\tilde{x}_i\tilde{x}_i}(f_0,\phi_0)} \quad (12)$$

which varies over the range $0<R<1$. If we examine, the motion at station i for discrete values of f_0, consistent with the discrete frequencies of the Fast Fourier Transform method used in evaluating (4) and (5), we find the following results. First, when $R(f_0,\phi_0) = 1$ there are no principal directions because the harmonic motion at frequency f_0 moves along a circular path at constant angular velocity, $2\pi f_0$, as shown in Fig. 7.8; i.e., the motion is equivalent to two resultant harmonics in orthogonal directions having equal amplitudes but being 90^o out-of-phase. When $R(f_0,\phi_0)<1$, principal directions do exist with the motion being along a straight line for $R(f_0,\phi_0) = 0$ and along an ellipse for $0<R(f_0,\phi_0)<1$. In the latter case, the resultant harmonics in the principal directions have different amplitudes as shown in Fig. 7.8 and they are 90^o out-of-phase. Secondly, it is significant to note that only for $R(f_0,\phi_0) = 0$ can a pure single harmonic wave exist. For $R(f_0,\phi_0)>0$ multiple waves moving in different directions are present. Thus, in the interest of identifying wave types, directions, and velocities, attention should be concentrated on those discrete frequencies having low values of $R(f_0,\phi_0)$. Fortunately, in the SMART 1 data analysed here as will be shown subsequently, those frequencies usually represent waves of high energy transmission.

Figures 7.9a and 7.9b show plots of the major principal variance, the principal variance ratio, and dominant (or major principal) direction for the ground motions recorded at stations C00, I03, and I06 during the earthquakes of January 29, 1981, and November 14, 1980, respectively. It is significant to note in Fig. 7.9a that at frequencies, f_1, f_2, f_3, and f_4, representing high intensity motions, the corresponding variance ratios are low indicating relatively pure single wave transmissions at these frequencies. Note that the dominant directions are nearly toward the epicenter for frequencies f_1 and f_2 but are much closer to the normal direction for frequencies f_3 and f_4. This observation suggests that Rayleigh waves are the primary source of energy transmission for frequencies less than about 2.5 Hz and that shear waves (SH waves, perhaps in part Love waves) are the primary source of energy transmission for frequencies from 2.5 Hz to about 6 Hz. Above these frequencies, the directions of propagation are quite variable. In Fig. 7.9b, the variance ratio has fairly low values at frequencies f_1 and f_2 which also correspond to frequencies of relatively high intensity. However the variance ratio is quite high for most frequencies suggesting a mix of waves. Again it is significant to note the change in dominant direction from the epicentral direction (in the range $1.4<f_0<2.0$ Hz to the normal direction (at higher frequencies up to 8 Hz). As mentioned earlier, this change suggests a shift with increasing frequency from dominant Rayleigh wave transmission to SH or Love wave transmission.

Let us now examine in further detail, the ground motion characteristics at frequencies $f_1 = 1.17$ Hz and $f_3 = 2.85$ Hz, as indicated in Fig. 7.9a, for many stations in addition to stations C00, I03, and I06. As suggested above, the dominant ground motions at these frequencies seem to be caused primarily by Rayleigh and shear (SH) waves, respectively. Figures 7.10a and 7.10b show the dominant directions at frequencies 1.17 Hz and 2.85 Hz, respectively, at many stations for the earthquake of January 29, 1981, evaluated using (11). The average dominant direction ϕ_0 over the array is also shown in these figures as computed from frequency-wave number spectral analysis [6]. Note that the average dominant direction in Fig. 7.10a is reasonably close to the epicentral direction while the average dominant direction in Fig. 7.10b is close to the normal direction.

We may now use these two average dominant directions to generate corresponding cross correlation functions defined by (8) for ground motions recorded at station pairs across the array during the earthquake of January 29, 1981. We plot in Fig. 7.11 for each station pair the delay time τ, for maximum cross correlation, against the corresponding relative distance between stations as projected on the average dominant axis. Straight lines fitted by least squares yield wave velocities (inverse values of the line slopes) equal to 2.4 km/sec and 5.3 km/sec for frequencies 1.17 and 2.85 Hz, respectively.

The Rayleigh wave identified above at frequency 1.17 Hz moving in the direction $\phi = 68^{o}$ at velocity 2.4 km/sec is with little doubt the same wave type characterized in Chapter 5 by the wave number spectrum analysis which showed waves at frequencies 1 to 2 Hz moving in the direction $\phi = 68^{o}$ at velocity 3.0 km/sec.

Because a uniform elastic half space transmits Rayleigh waves at a velocity equal to 0.9 times the shear wave velocity, an explanation is needed of the mixture in the same time window of SH waves with local velocity of 5.3 km/sec and Rayleigh waves with velocities of 2.4 km/sec. The usual seismological interpretation of this large difference in local apparent velocities is that the SH waves are associated with longer travel paths from the earthquake source to the array in the vicinity of which the SH wave fronts move steeply upwards through the soil. Thus the apparent shear wave velocity is largely controlled by the more rigid, deeper rocks in the crust. On the other hand, the Rayleigh waves develop near the surface between the source and the array so that their wave velocities are largely controlled by the shallower materials.

According to this explanation the vertical component ground motions in the time windows studied should be significant in the frequency range of the Rayleigh waves but relatively insignificant in the frequency range of the shear (transverse) waves described above. This prediction was tested by computing particle motions from the accelerograms as a function of frequency. Results are shown in Fig. 7.12. The particle orbits agree well with the above prediction with significant vertical displacement in the frequency bands 0.25 to 1.5 Hz and 0.75 to 1.5 Hz, but almost none transverse to the wave direction in the 2.5 to 3.1 Hz frequency band.

7.3 References

1. Jenkis, G. M. and O. G. Watts, Spectral Analysis and Its Applications, San Francisco, Holden-Day Inc., (1969).

2. Bendat, J. S. and A. G. Piersol, Engineering Applications of Correlation and Spectral Analysis, John Wiley and Sons, (1980).

3. Penzien, J. and M. Watabe, "Characteristics of 3-Dimensional Earthquake Ground Motion," Earthquake Eng. Struct. Dynamics, 3, 365-373, (1975).

4. Kubo, T. and J. Penzien, "Analysis of Three-Dimensional Strong Ground Motions along Principal Axes, San Fernando Earthquake," Earthquake Eng. Struct. Dynamics, 7, 265-278, (1979).

5. Kubo, T. and J. Penzien, "Simulation of Three-Dimensional Strong Ground Motions along Principal Axes, San Fernando Earthquake," Earthquake Eng. Struct. Dynamics, 7, 279-294, (1979).

6. Bolt, B. A., Tsai, Y. B., Yeh, K. and M. K. Hsu, "Earthquake Strong Motions Recorded by a Large Near-Source Array of Digital Seismographs," Earthquake Eng. Struct. Dynamics, 10, 561-573, (1982).

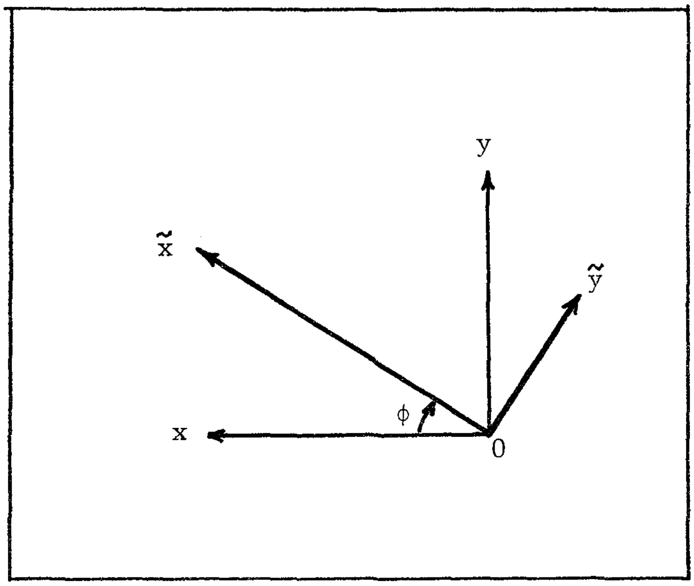

Fig. 7.1 Coordinate transformation of two horizontal components.

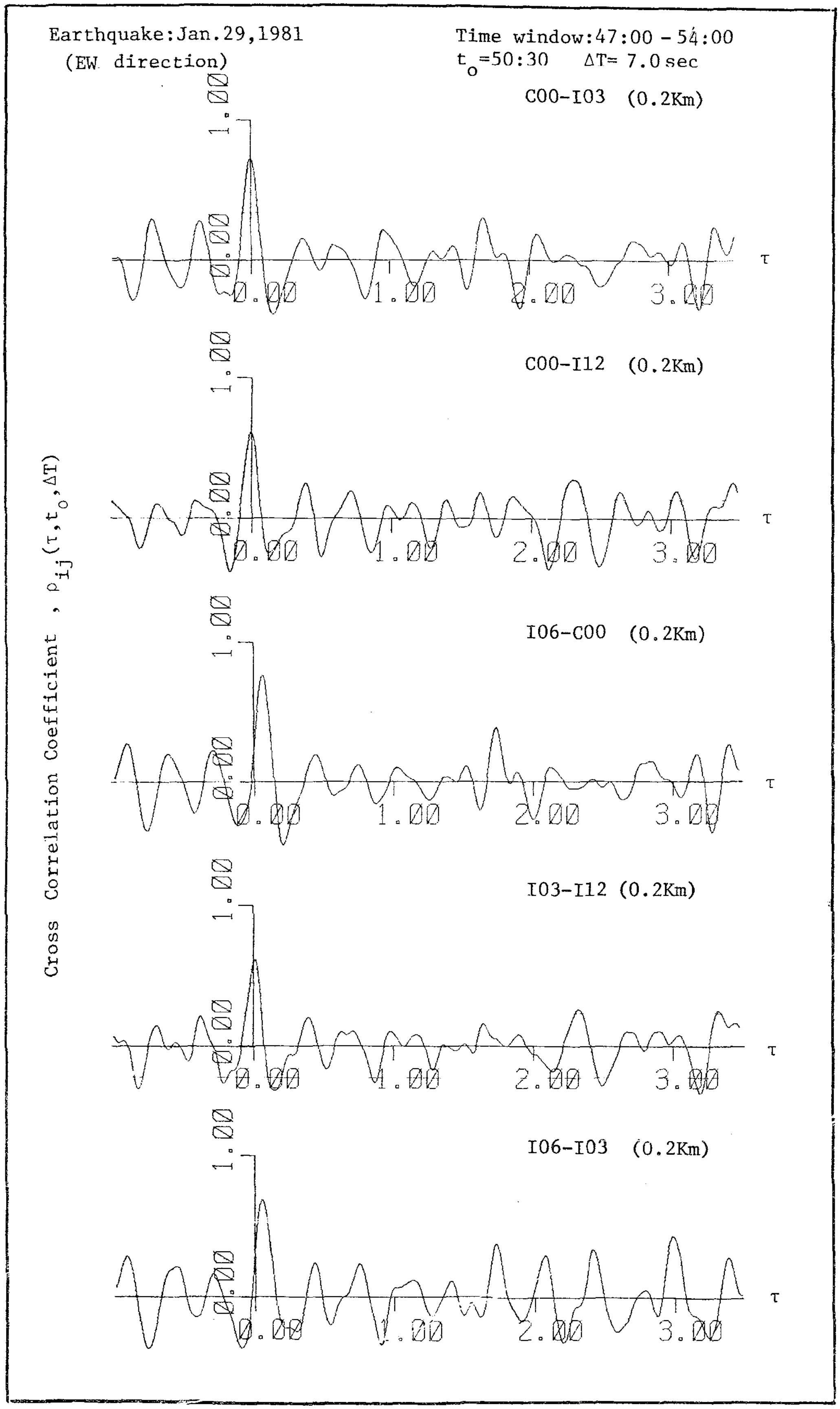

Fig. 7.2a Correlation coefficient for different station pairs: Event 5; EW direction; time window 47:00 - 54:00

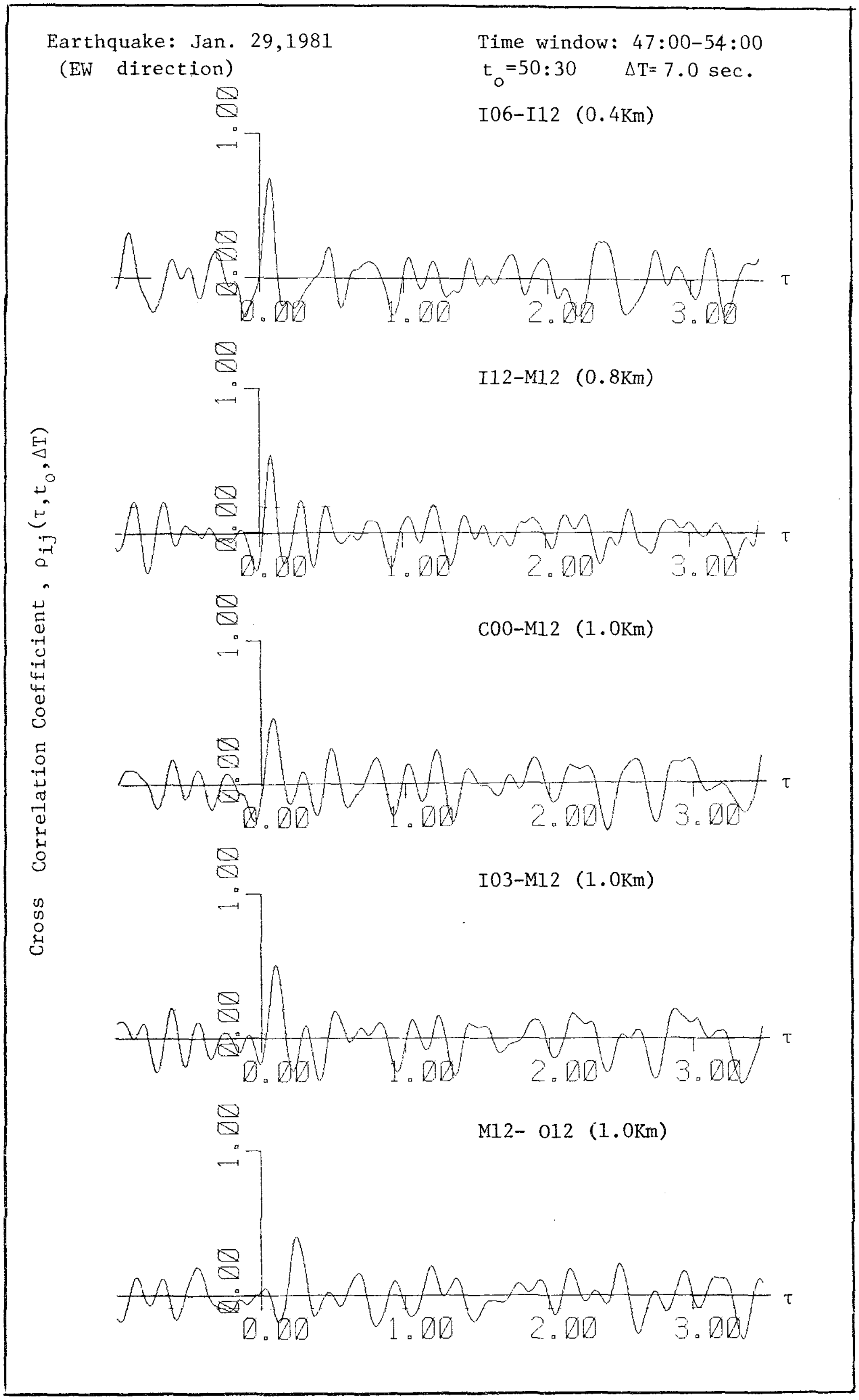

Fig. 7.2a continued

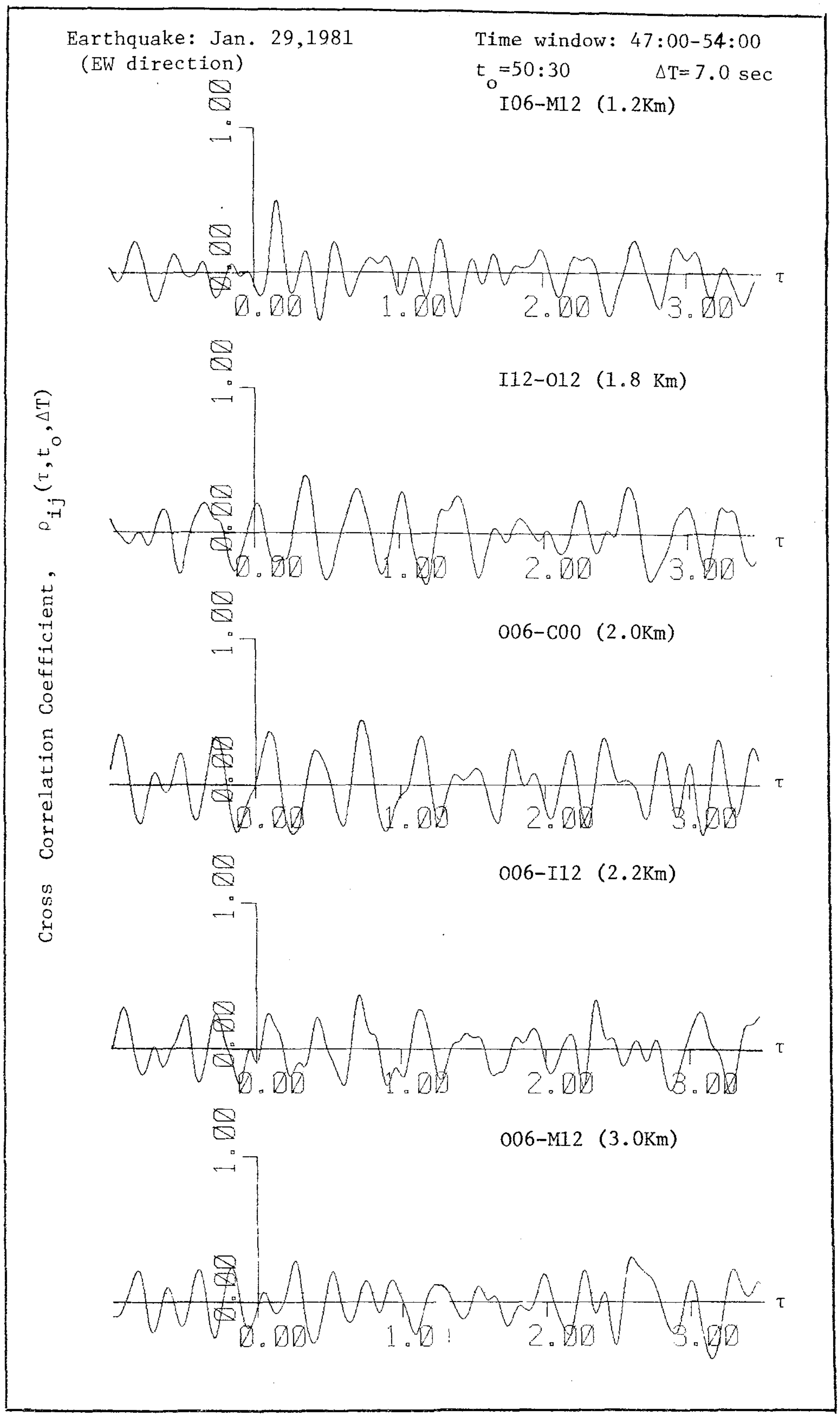

Fig. 7.2a continued

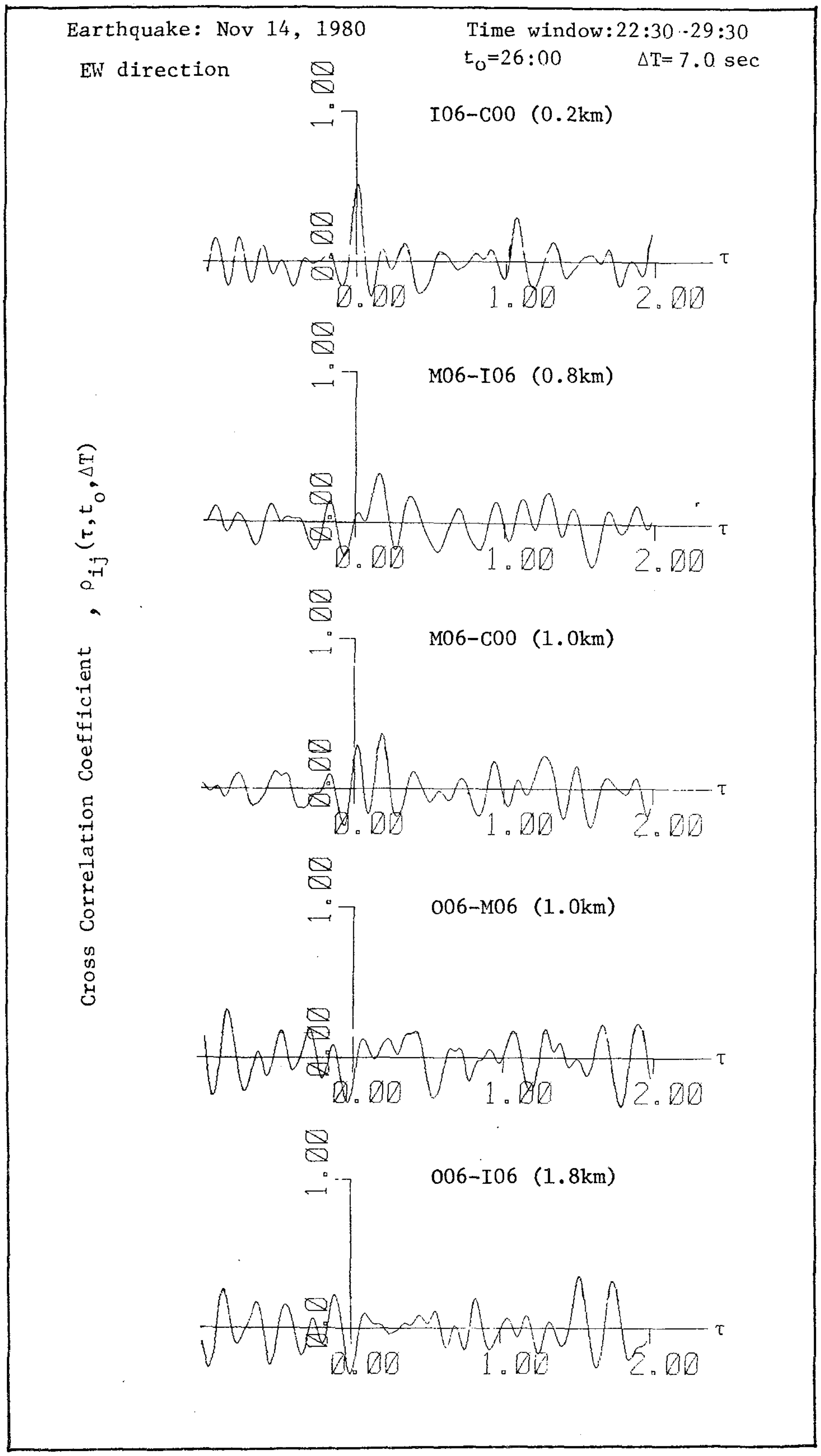

Fig. 7.2b Correlation coefficient for different station pairs: Event 2; EW direction; time window 22:30 - 29:30

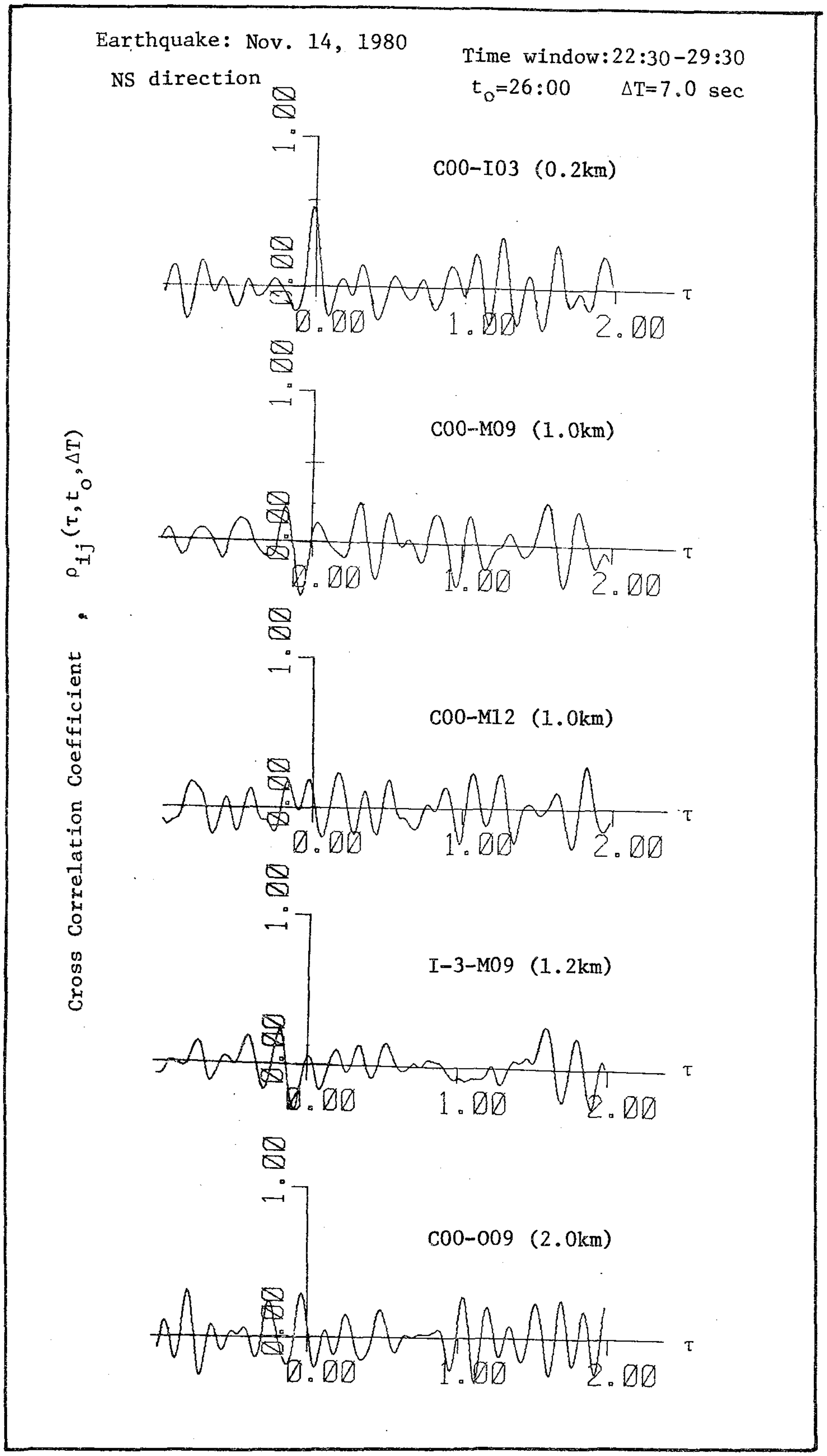

Fig. 7.2c Correlation coefficient for different station pairs: Event 2; NS direction; time window 22:30 - 29:30

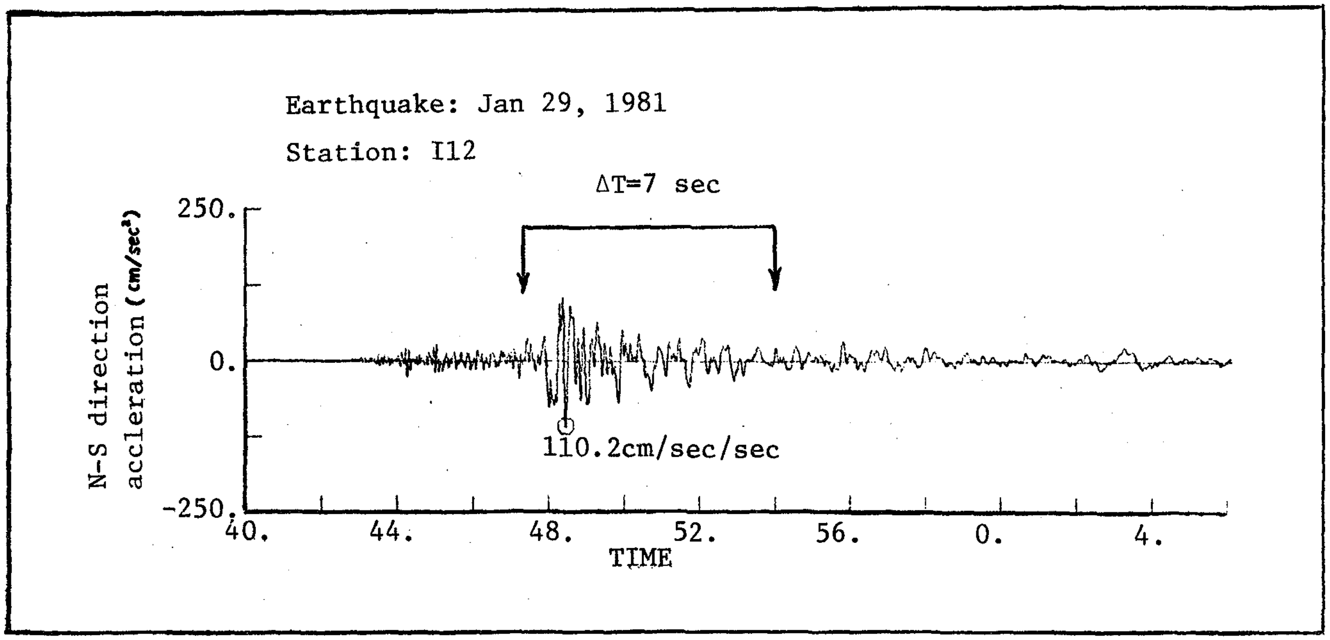

Fig. 7.3 Time window used in the analysis: Event 5

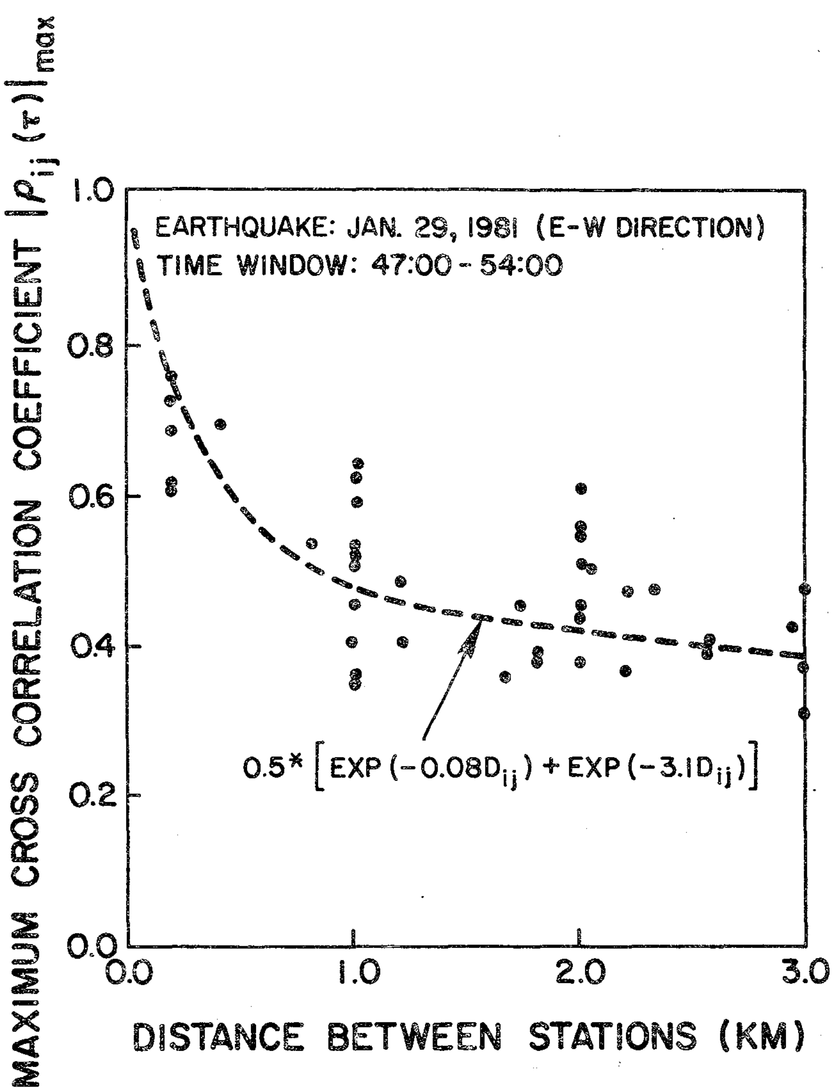

Fig. 7.4 Attenuation of correlation coefficient ρ

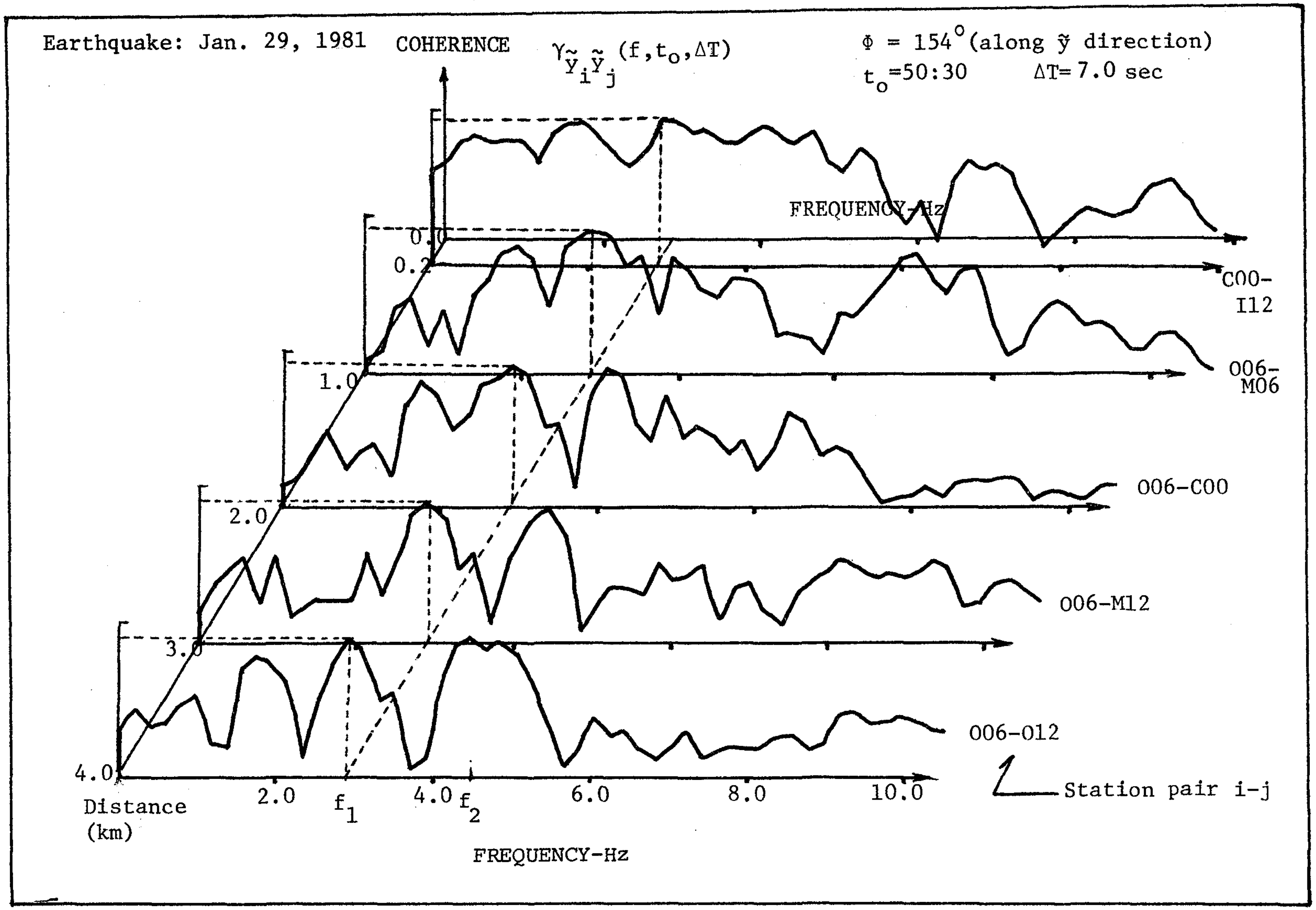

Fig. 7.5a Coherence functions between stations along the profile 006 to 012: Event 5; $\phi = 154^\circ$ ($\tilde{y}$ direction)

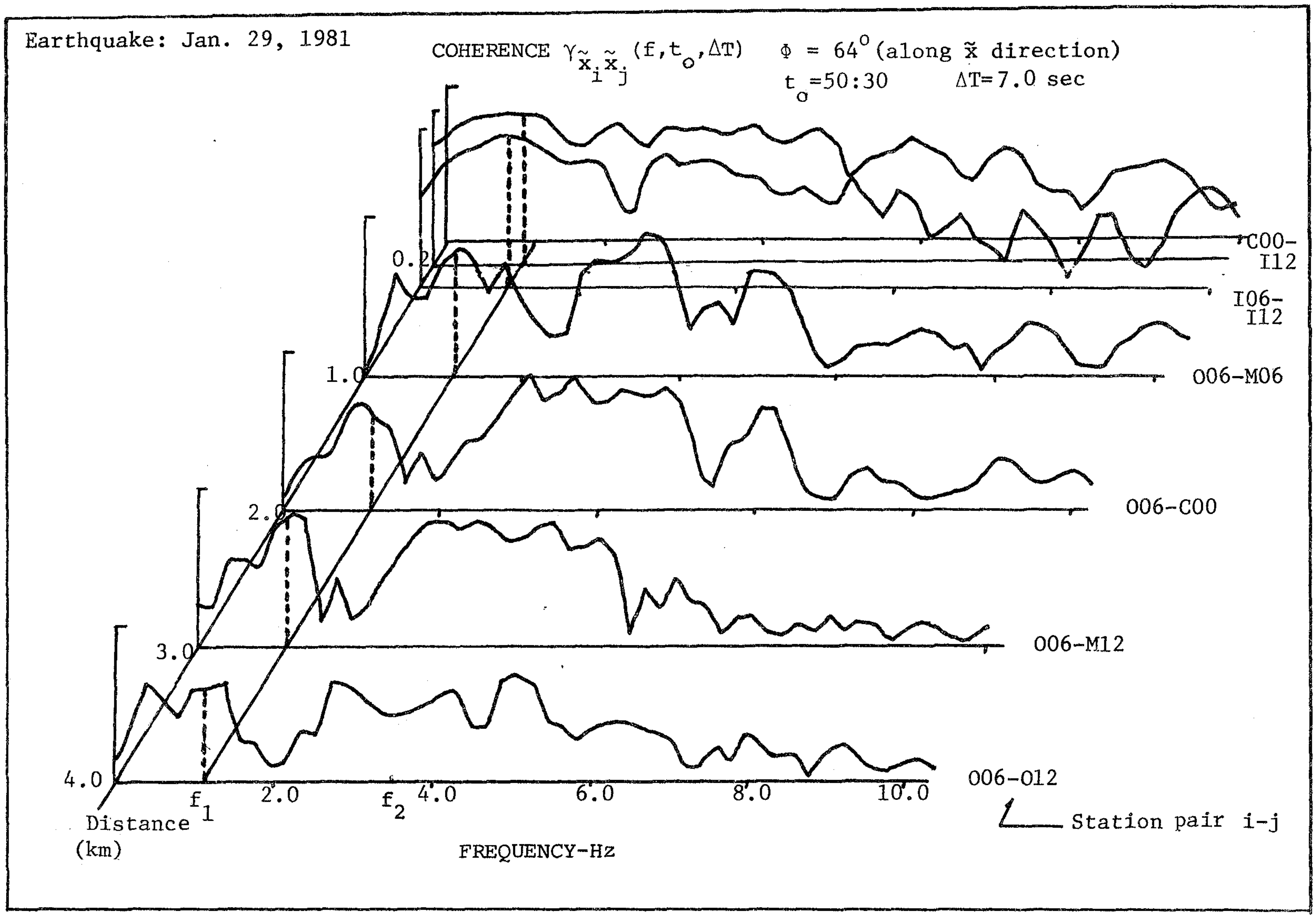

Fig. 7.5b Coherence functions between stations along the profile 006 to 012: Event 5; $\phi = 64°$ ($\tilde{x}$ direction)

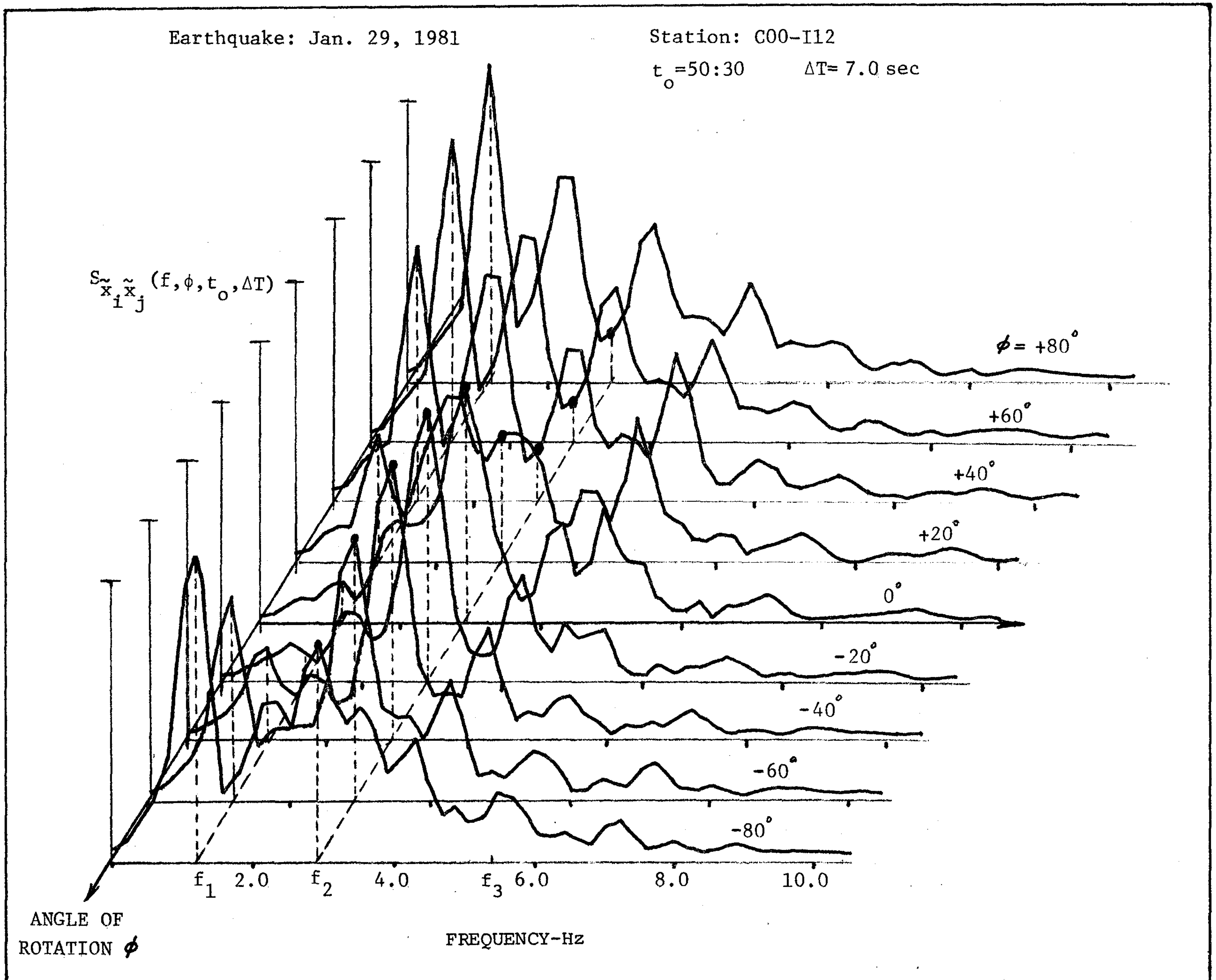

Fig. 7.6a Variation of the cross spectral density function with respect to polarization: Event 5: C00 - I12

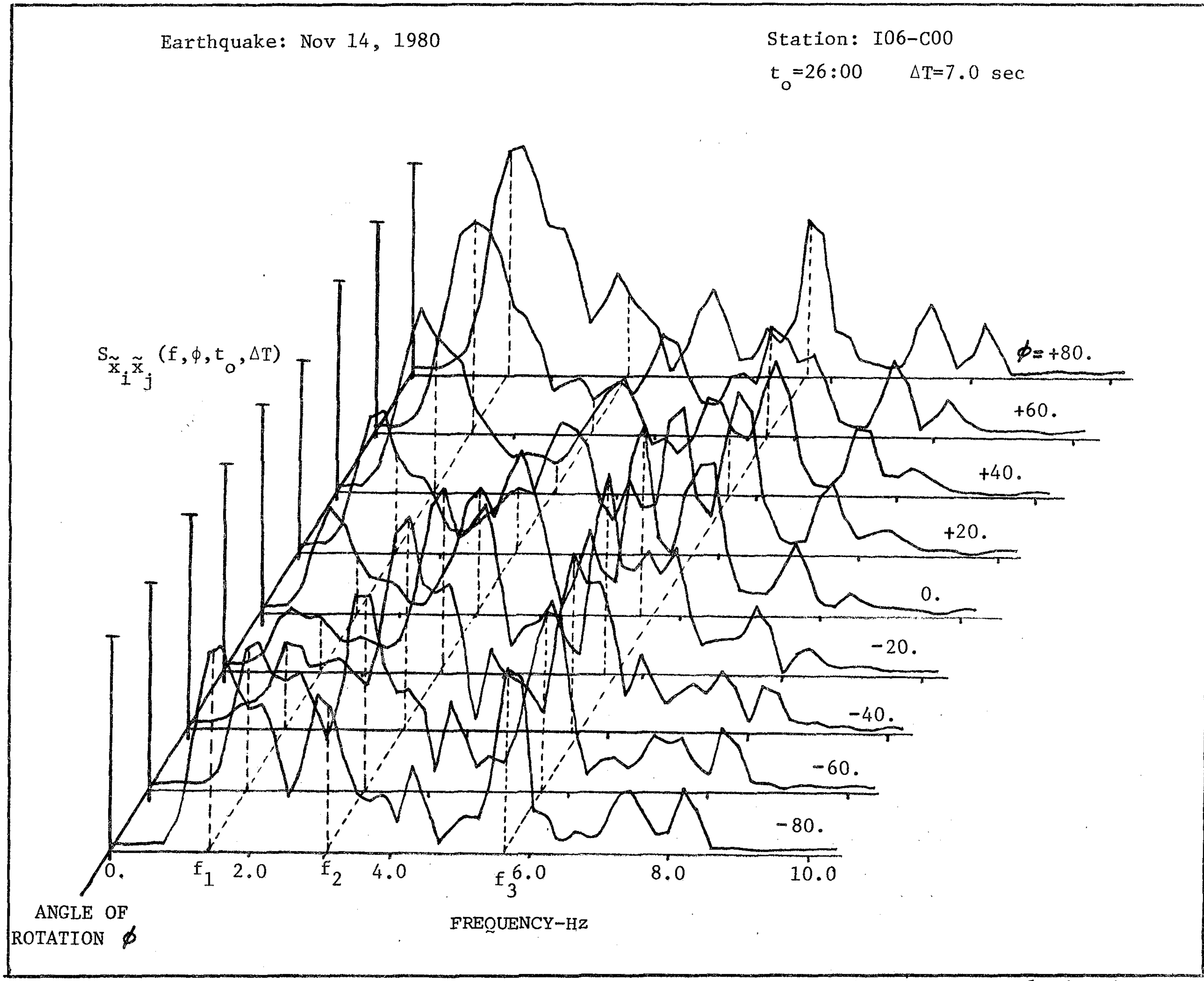

Fig. 7.6b Variation of the cross spectral density function with respect to polarization: Event 2; I06 - C00

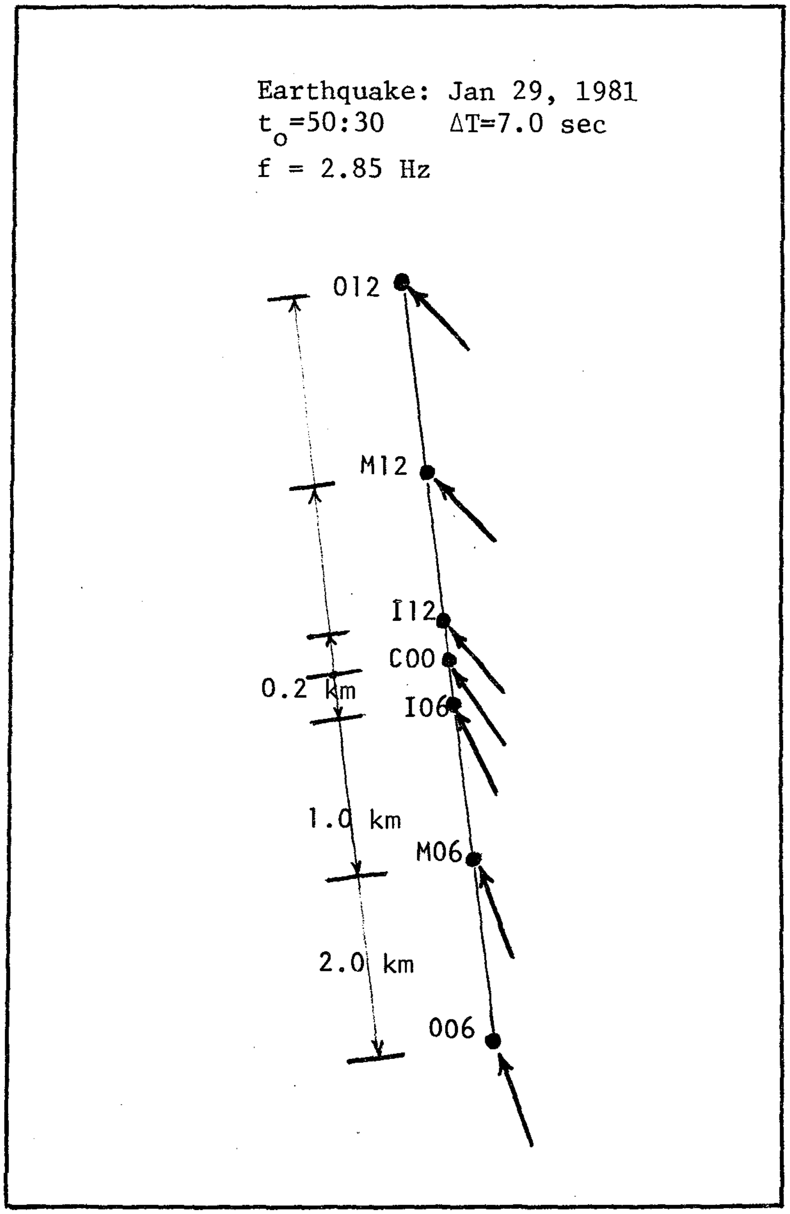

Fig. 7.7 Direction of wave propagation

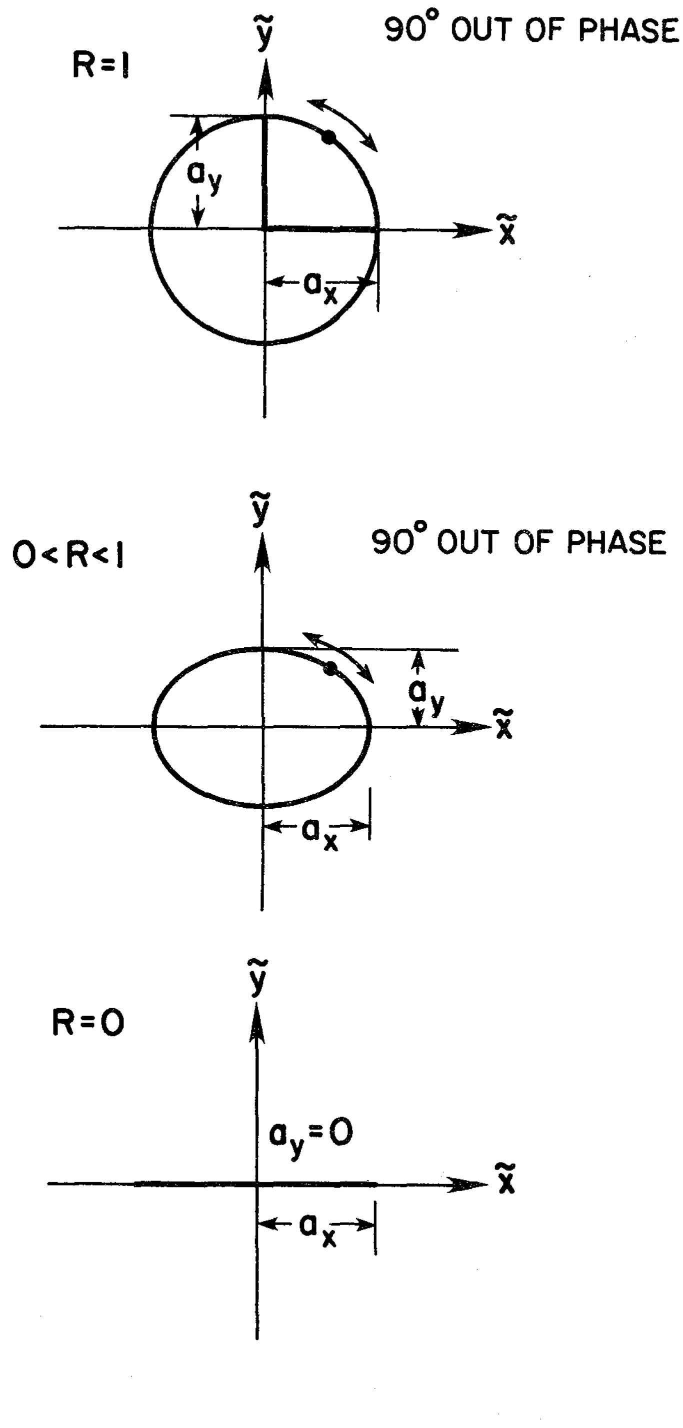

Fig. 7.8 Physical meaning of principal variance ratio

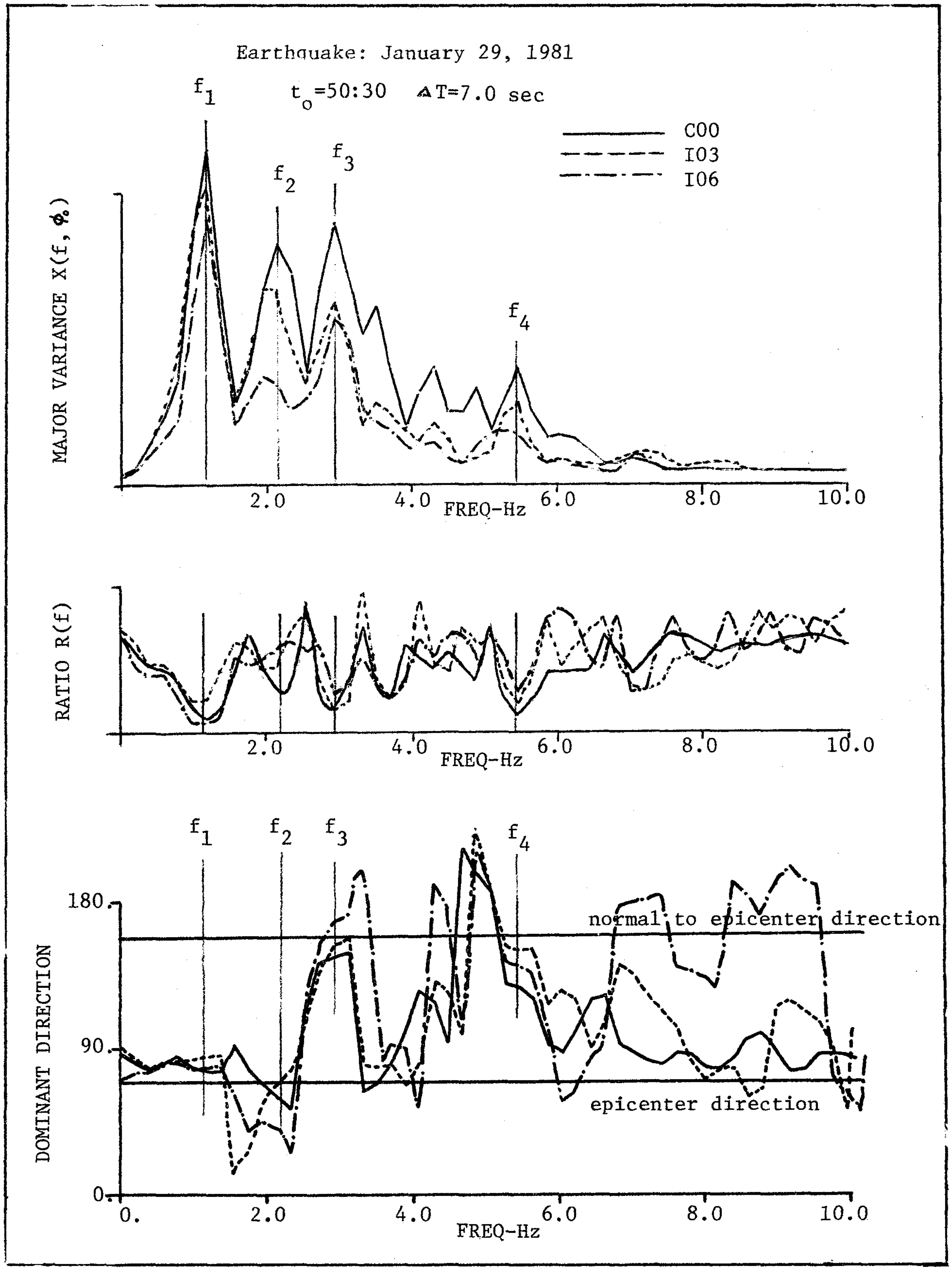

Fig. 7.9a Major principal variance, variance ratio and dominant direction for Event 5

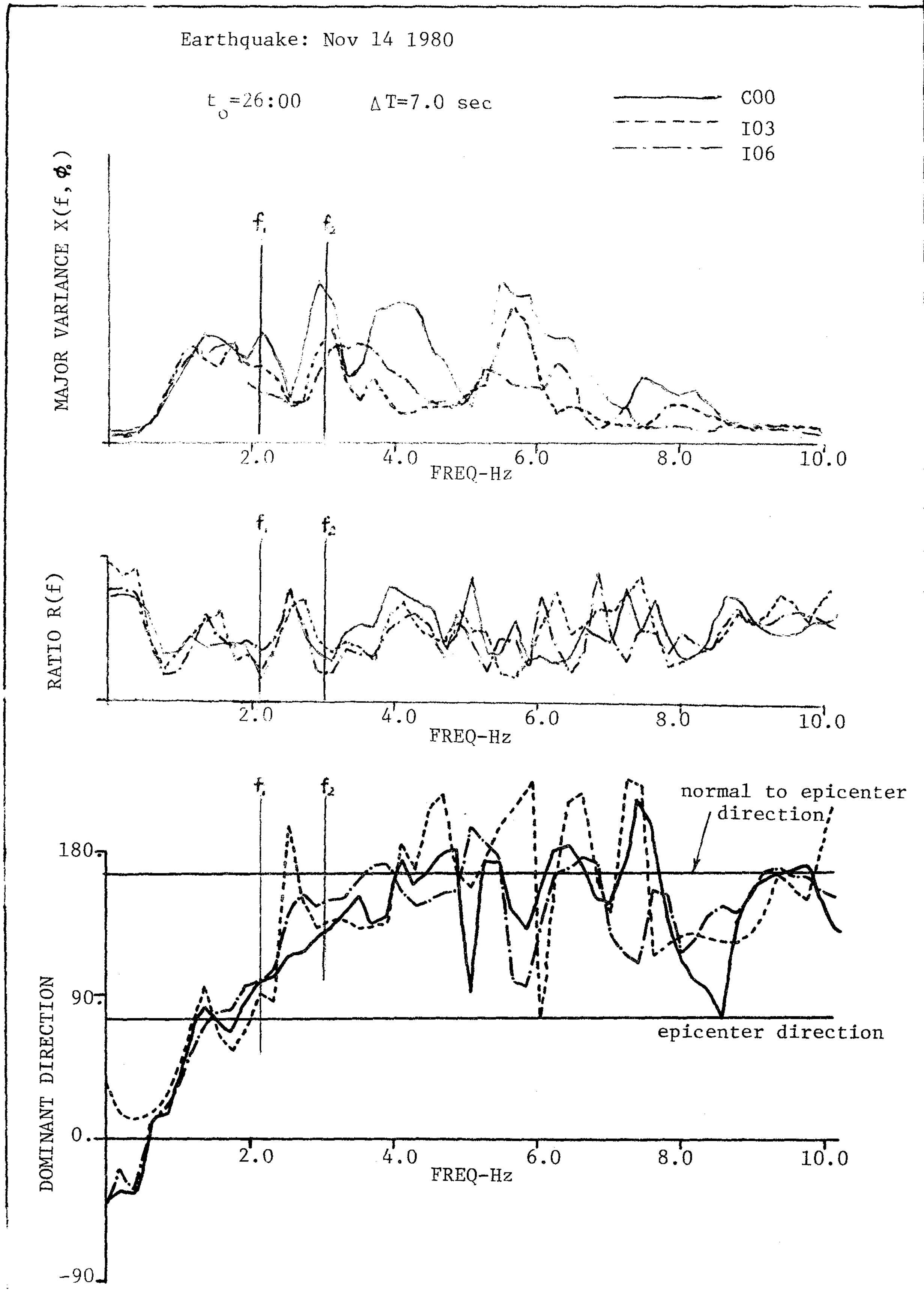

Fig. 7.9b Major principal variance, variance ratio and dominant direction for Event 2

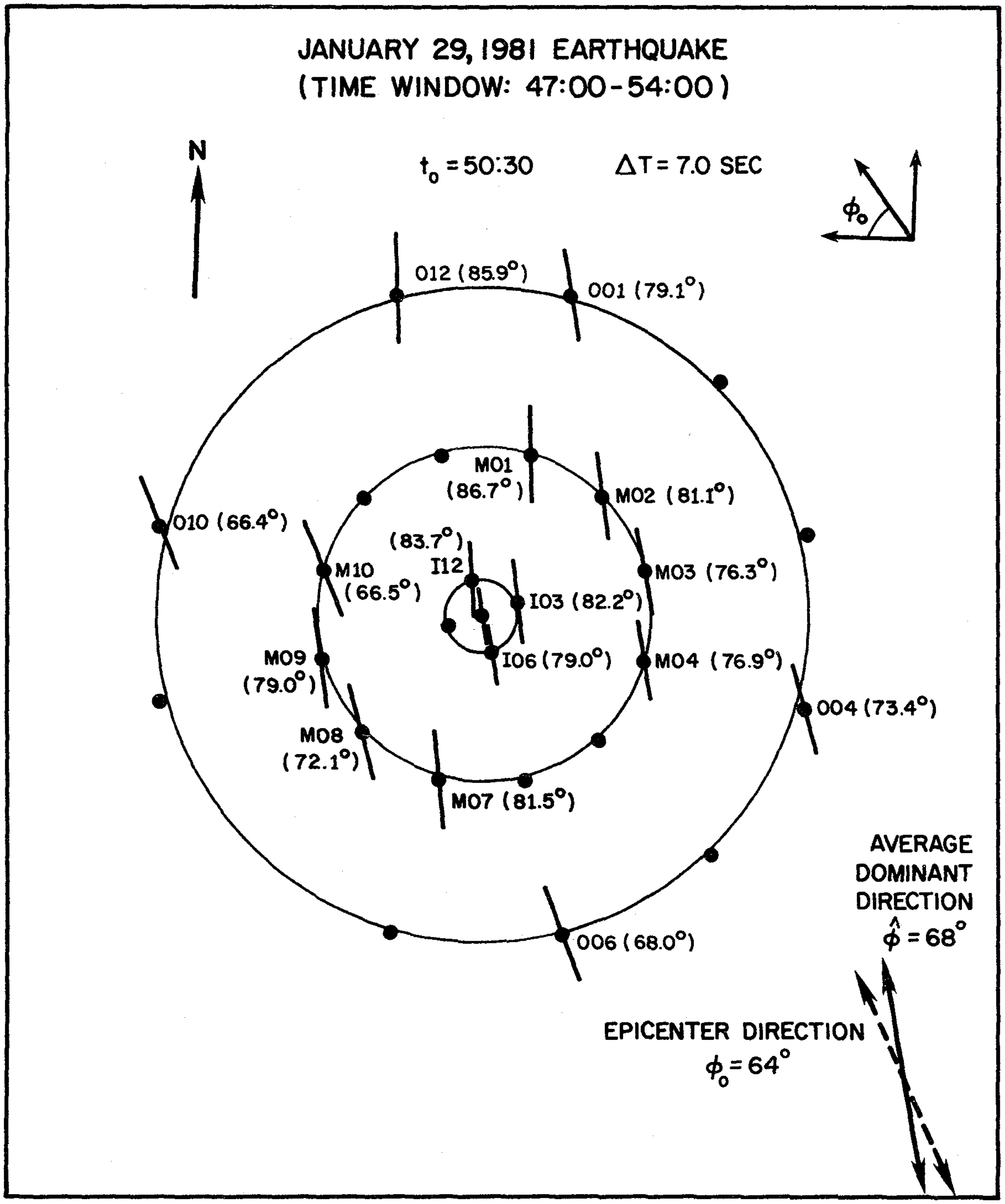

Fig. 7.10a Dominant directions at 1.17 Hz for Event 5

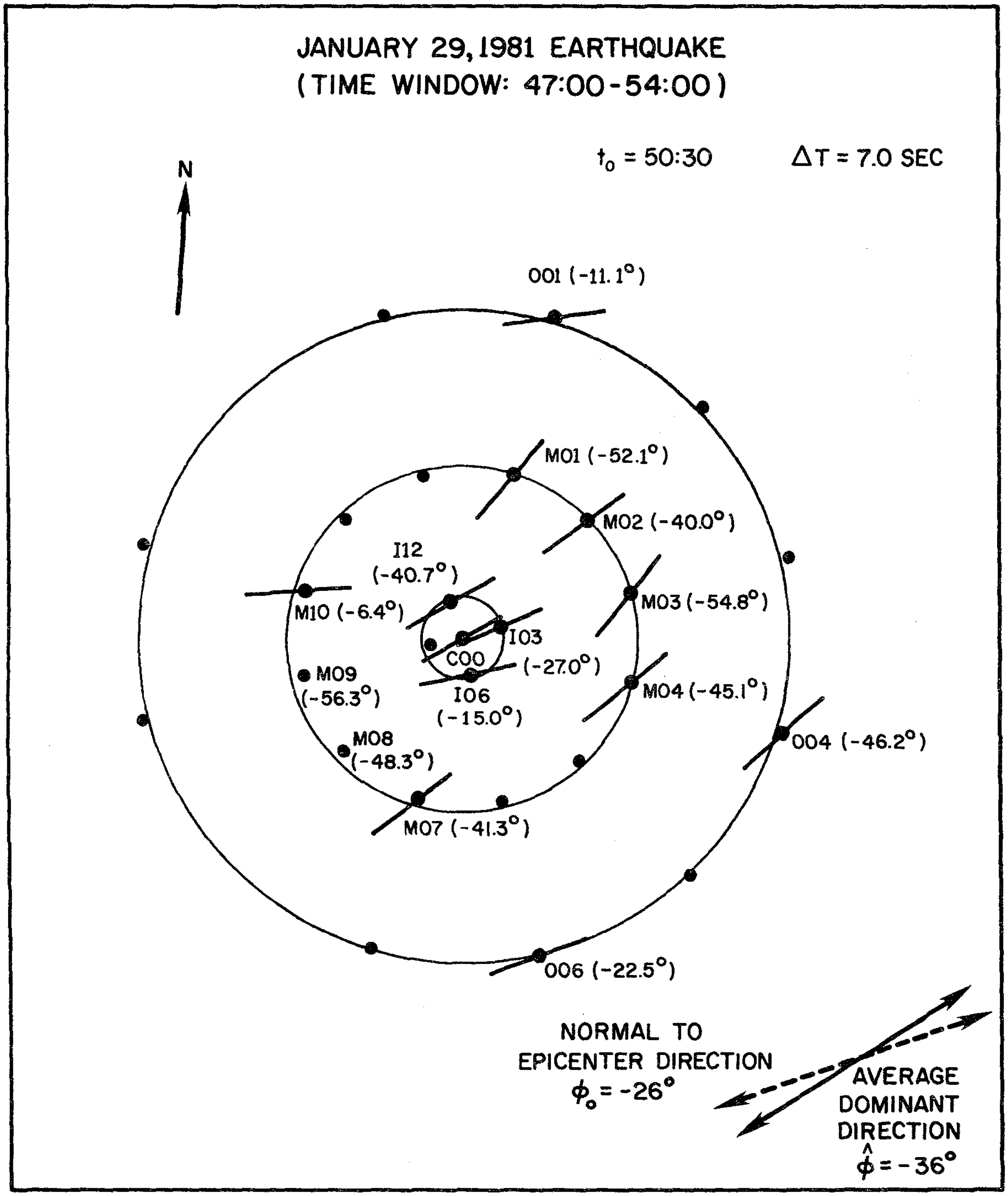

Fig. 7.10b Dominant directions at 2.85 Hz for Event 5

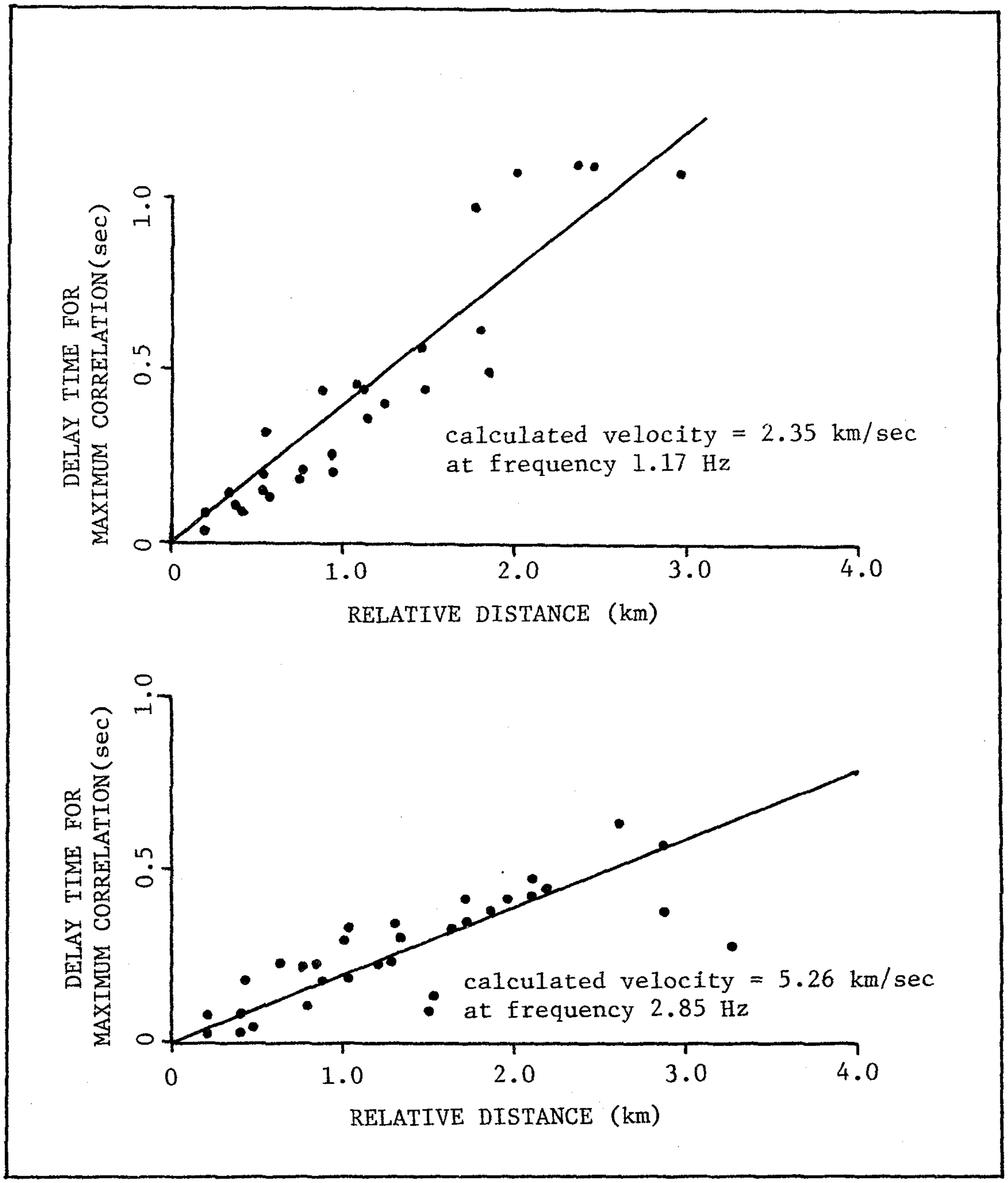

Fig. 7.11 Identification of wave velocity at frequencies 1.17 Hz and 2.85 Hz

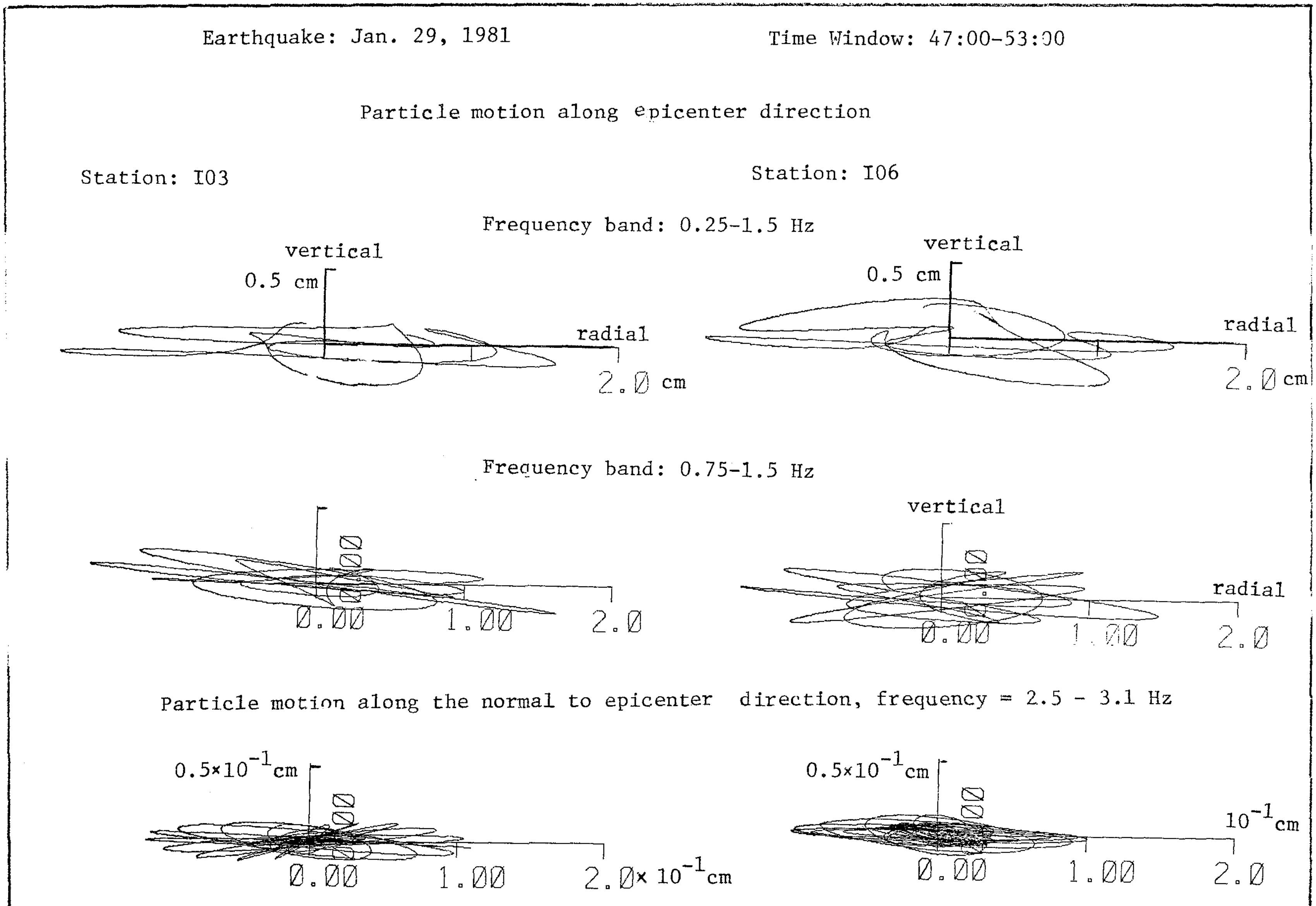

Fig. 7.12 Particle ground motions drawn in two vertical planes for Event 5 and time window 47:00-53:00

8. ENGINEERING ANALYSIS OF SMART 1 ARRAY ACCELEROGRAMS

8.1 Introduction

The engineering studies of the ground motion data from the SMART 1 array concentrate on the influence of spatial variations of ground motions on the dynamic response of large structural systems such as industrial buildings, bridges, and dams. The results presented in this chapter focus on the correlations of multi-support excitations and their influence on the dynamic response of linear structural systems for selected accelerograms recorded during the earthquakes of November 14, 1980 (Event 2) and January 29, 1981 (Event 5).

8.2 Response of Linear Systems to Multi-Support Excitations

A. General System

The equations of motion for a discrete parameter, linear structural system subjected to multi-support excitations can be written in the form

$$\underline{m}\,\ddot{\underline{r}}^t + \underline{c}\,\dot{\underline{r}}^t + \underline{k}\,\underline{r}^t = \underline{p}(t) \tag{1}$$

where $\underline{r}^t$ is the total displacement vector from a fixed reference containing n components, i.e., $n = n_s + n_b$ where n_s is the number of degrees of freedom in the system exclusive of support displacements and n_b is the number of degrees of freedom associated with the support displacements, $\underline{p}(t)$ is the load vector containing non-zero components only for the support interaction forces, and $\underline{m}$, $\underline{c}$, and $\underline{k}$ are the n x n mass, damping, and stiffness matrices, respectively. This equation can be partitioned and written in the form

$$\begin{bmatrix} \underline{m}_{ss} & \underline{m}_{sb} \\ \underline{m}_{bs} & \underline{m}_{bb} \end{bmatrix} \begin{Bmatrix} \ddot{\underline{r}}_s^t \\ \ddot{\underline{r}}_b^t \end{Bmatrix} + \begin{bmatrix} \underline{c}_{ss} & \underline{c}_{sb} \\ \underline{c}_{bs} & \underline{c}_{bb} \end{bmatrix} \begin{Bmatrix} \dot{\underline{r}}_s^t \\ \dot{\underline{r}}_b^t \end{Bmatrix} + \begin{bmatrix} \underline{k}_{ss} & \underline{k}_{sb} \\ \underline{k}_{bs} & \underline{k}_{bb} \end{bmatrix} \begin{Bmatrix} \underline{r}_s^t \\ \underline{r}_b^t \end{Bmatrix} = \begin{Bmatrix} \underline{o} \\ \underline{p}_b \end{Bmatrix} \qquad (2)$$

where $\underline{r}_s^t$ and $\underline{r}_b^t$ represent the n_s and n_b degrees of freedom, respectively.

The total response can be separated into quasi-static and dynamic response of the form

$$\underline{r}^t = \begin{Bmatrix} \underline{r}_s^{qs} \\ \underline{r}_b^{qs} \end{Bmatrix} + \begin{Bmatrix} \underline{r}_s^d \\ \underline{o} \end{Bmatrix} \qquad (3)$$

where components in vector $\underline{r}_b^{qs}$ are identical to the corresponding prescribed support displacements in vector $\underline{r}_b^t$, components in $\underline{r}_s^{qs}$ are the quasi-static displacements in the n_s degrees of freedom caused by the support displacements in $\underline{r}_b^t$, and components in $\underline{r}_s^d$ are dynamic displacements in the n_s degrees of freedom.

The quasi-static response is obtained from the first equation of (2) upon letting $\ddot{\underline{r}}^t$ and $\dot{\underline{r}}^t$ equal zero vectors; thus

$$\underline{r}_s^{qs} = - \underline{k}_{ss}^{-1} \; \underline{k}_{sb} \; \underline{r}_b^t \; . \qquad (4)$$

The dynamic response is obtained from the first equation of (2) upon substitution of (3) and (4); thus

$$\underline{m}_{ss}\ddot{\underline{r}}_s^d + \underline{c}_{ss}\dot{\underline{r}}_s^d + \underline{k}_{ss}\underline{r}_s^d = [\underline{m}_{ss}\underline{k}_{ss}^{-1} \; \underline{k}_{sb} - \underline{m}_{sb}] \; \ddot{\underline{r}}_b^t + [\underline{c}_{ss}\underline{k}_{ss}^{-1}\underline{k}_{sb} - \underline{c}_{sb}] \; \dot{r}_b^t \qquad (5)$$

The second term on the right hand side of (5) equals zero for stiffness proportional damping and is small for other forms of damping when the damping ratios are low, say less than 10 percent of critical; therefore, it can be dropped from the equation without introducing significant error. The dynamic response can then be obtained from the approximate relation

$$\underline{m}_{ss}\ddot{\underline{r}}_s^d + \underline{c}_{ss}\dot{\underline{r}}_s^d + \underline{k}_{ss}\underline{r}_s^d \simeq [\underline{m}_{ss}\underline{k}_{ss}^{-1}\,\underline{k}_{sb} - \underline{m}_{sb}]\,\ddot{\underline{r}}_b^t \quad . \tag{6}$$

Solving for fixed base structural mode shapes and frequencies using

$$\underline{m}_{ss}\ddot{\underline{r}}_s^d + \underline{k}_{ss}\underline{r}_s^d = \underline{o} \quad , \tag{7}$$

the vector $\underline{r}_s^d$ can be expressed in terms of the resulting $n_s \times n_s$ modal matrix $\underline{\Phi}_s$ and the n_s fixed base modal coordinates $\underline{Y}_s$ as given by

$$\underline{r}_s^d = \underline{\Phi}_s\,\underline{Y}_s \quad . \tag{8}$$

Introducing (8) into (6) and using the orthogonality properties of the fixed base modes, uncoupled normal mode equations of motion for the fixed base structure are obtained as given by

$$\underline{M}_s\ddot{\underline{Y}}_s + \underline{C}_s\dot{\underline{Y}}_s + \underline{K}_s\underline{Y}_s = \underline{\Phi}_s^T\,[\underline{m}_{ss}\underline{k}_{ss}^{-1}\,\underline{k}_{sb} - \underline{m}_{sb}]\,\ddot{\underline{r}}_b^t \quad , \tag{9}$$

where $\underline{M}_s$, $\underline{C}_s$, and $\underline{K}_s$ are $n_s \times n_s$ diagonal matrices defined by

$$\begin{aligned} \underline{M}_s &\equiv \underline{\Phi}_s^T\,\underline{m}_{ss}\underline{\Phi}_s \\ \underline{C}_s &\equiv \underline{\Phi}_s^T\,\underline{c}_{ss}\underline{\Phi}_s = 2\,\underline{M}_s\underline{\omega}_s\underline{\xi}_s \\ \text{and} \quad \underline{K}_s &\equiv \underline{\Phi}_s^T\,\underline{k}_{ss}\underline{\Phi}_s = \underline{\omega}_s^2\,\underline{M}_s \end{aligned} \tag{10}$$

where $\underline{\omega}_s$ is a diagonal matrix containing the fixed base normal mode frequencies, and $\underline{\xi}_s$ is a vector containing the n_s normal mode damping ratios. It is assumed here that the damping matrix $\underline{c}_{ss}$ is of the Caughey form so that uncoupled damped normal modes exist.

It should be recognized that generalized shape functions and corresponding amplitudes could also be used in formulating the original discrete parameter equations of motion. Normally, however, the standard finite element approach would be used.

B. Special Case of the General System

Consider a special case of the general system formulated above where $n_s = 1$, $n_b = 2$, and $n = 3$. Let the two prescribed single-component support displacements at supports A and B in this case be denoted by $v_{gA}(t)$ and $v_{gB}(t)$, respectively. Equation (3) can now be written as

$$\underline{r}^t = \begin{Bmatrix} r_1^t(t) \\ v_{gA}(t) \\ v_{gB}(t) \end{Bmatrix} = \begin{Bmatrix} r_1^{qs}(t) \\ v_{gA}(t) \\ v_{gB}(t) \end{Bmatrix} + \begin{Bmatrix} r_1^d(t) \\ o \\ o \end{Bmatrix} . \tag{11}$$

Note that the single degree of freedom in the fixed base system as represented by $r_1^d(t)$ could be any single normal mode of the multi-degree fixed base system or any other single generalized shape function for that system.

The quasi-static solution as given by (4) becomes

$$r_1^{qs} = -\frac{k_{12}}{k_{11}} v_{gA} - \frac{k_{13}}{k_{11}} v_{gB} , \tag{12}$$

and (5), yielding the dynamic response, reduces to

$$\ddot{r}_1^d + 2\xi_1\omega_1\dot{r}_1^d + \omega_1^2 r_1^d = \left(\frac{k_{12}}{k_{11}} - \frac{m_{12}}{m_{11}}\right)\ddot{v}_{gA} + \left(\frac{k_{13}}{k_{11}} - \frac{m_{13}}{m_{11}}\right)\ddot{v}_{gB} \tag{13}$$

where

$$\begin{aligned} \omega_1 &= \sqrt{k_{11}/m_{11}} \\ \xi_1 &= c_{11}/2m_{11}\omega_1 \quad . \end{aligned} \tag{14}$$

For the subsequent development, it is convenient to write (13) in the form

$$\ddot{r}_1^d + 2\xi_1\omega_1\dot{r}_1^d + \omega_1^2 r_1^d = -A\,\ddot{v}_{gA} - B\,\ddot{v}_{gB} \tag{15}$$

where

$$A \equiv -\left(\frac{k_{12}}{k_{11}} - \frac{m_{12}}{m_{11}}\right) \quad ; \quad B \equiv -\left(\frac{k_{13}}{k_{11}} - \frac{m_{13}}{m_{11}}\right) \tag{16}$$

Now compare the maximum absolute value of dynamic response with the two simultaneous inputs as expressed by (15) with the average of the maximum absolute values of response produced by the two inputs applied as rigid base inputs separately, i.e., the averages of the maximum absolute values of response derived from

$$\ddot{r}_1^d + 2\xi_1\omega_1\dot{r}_1^d + \omega_1^2 r_1^d = -(A+B)\,\ddot{v}_{gA} \tag{17}$$

$$\ddot{r}_1^d + 2\xi_1\omega_1\dot{r}_1^d + \omega_1^2 r_1^d = -(A+B)\,\ddot{v}_{gB} \quad . \tag{18}$$

Letting $S_a^{AA}(\xi,T)$ and $S_a^{BB}(\xi,T)$ represent the standard pseudo-acceleration response spectra for ground accelerations $\ddot{v}_{gA}$ and $\ddot{v}_{gB}$, respectively, the maximum absolute values for r_1^d as given by (17) and (18) will be

$\frac{1}{\omega_1^2}(A+B)S_a^{AA}(\xi,T)$ and $\frac{1}{\omega_1^2}(A+B)S_a^{BB}(\xi,T)$, respectively. The average of these two maximum responses will be $\frac{1}{2\omega_1^2}(A+B)[S_a^{AA}(\xi,T) + S_a^{BB}(\xi,T)]$. The quantity T introduced here is the fixed base structural period $2\pi/\omega_1$.

Consider now the maximum absolute value of response resulting from (15). It is convenient to designate inputs $\ddot{v}_{gA}$ and $\ddot{v}_{gB}$ so that $|A| \leq |B|$ and to introduce a participation factor ratio γ defined by

$$\gamma \equiv \frac{A}{B} \quad . \tag{19}$$

Because $|A| \leq |B|$, γ must always be in the range

$$-1 \leq \gamma \leq +1 \tag{20}$$

Using this participation factor ratio, (15) can be written as

$$\ddot{r}_1^d + 2\xi_1\omega_1\dot{r}_1^d + \omega_1^2 r_1^d = -B[\gamma\ddot{v}_{gA} + \ddot{v}_{gB}] \tag{21}$$

Defining $S_a^{AB}(\gamma,\xi,T)$ as the standard pseudo-acceleration response spectrum derived using $1/2[\gamma\ddot{v}_{gA} + \ddot{v}_{gB}]$ as the single input to the single degree of freedom system, the maximum absolute value of response resulting from (21) is $\frac{2B}{\omega_1^2}\ S_a^{AB}(\gamma,\xi,T)$.

A generalized dynamic response ratio $\Phi^d(\gamma,\xi,T)$ is now defined as the ratio of the maximum absolute value of response derived from (21) to the average of the maximum absolute values of response given by (17) and (18); thus

$$\Phi^d(\gamma,\xi,T) \equiv \frac{4}{(\gamma+1)} \frac{S_a^{AB}(\gamma,\xi,T)}{[S_a^{AA}(\xi,T) + S_a^{BB}(\xi,T)]} \tag{22}$$

Note that as $\ddot{v}_{gA}(t)$ and $\ddot{v}_{gb}(t)$ approach full positive correlation with each other, $\Phi^d(1,\xi,T)\rightarrow 1$.

The generalized dynamic response ratio defined by (22) can be used effectively to measure the modified dynamic response resulting from the differences in the two simultaneous inputs $\ddot{v}_{gA}$ and $\ddot{v}_{gB}$. These differences obviously depend upon the distance between supports A and B as well as other factors.

Since $S_a^{AB}(1,\xi,T)$ and $S_a^{AB}(-1,\xi,T)$ are the pseudo-acceleration response spectra for single degree of freedom inputs $1/2[\ddot{v}_{gB} + \ddot{v}_{gA}]$ and $1/2[\ddot{v}_{gB} - \ddot{v}_{gA}]$, i.e., the in-phase and out-of-phase components, respectively, for motions at A and B, the non-dimensional normalized form of (22) given by

$$\frac{(\gamma+1)}{2}\ \Phi^d(\gamma,\xi,T) = \frac{2\ S_a^{AB}(\gamma,\xi,T)}{[S_a^{AA}(\xi,T) + S_a^{BB}(\xi,T)]} \tag{23}$$

can be used for $\gamma = +1$ and $\gamma = -1$ to measure the intensity of in-phase motions and out-of-phase motions, respectively.

Example No. 1 of the Special Case - Consider the simple system shown in Fig. 8.1 with support inputs at A and B as indicated. For this system,

(4) and (6) become

$$r_1^{qs} = \frac{1}{2}\,[v_{gA} + v_{gB}] \tag{24}$$

and

$$\ddot{r}_1^d + 2\xi_1\omega_1\dot{r}_1^d + \omega_1^2 r_1^d = -\frac{1}{2}\,[\ddot{v}_{gA} + \ddot{v}_{gB}] \tag{25}$$

where $\omega_1 = \sqrt{k/m}$, and ξ_1 is the fixed base damping ratio. Constants A and B as defined by (16) are both equal to 1/2; thus $\gamma = +1$. The dynamic response ratio reduces to the form

$$\Phi^d(1,\xi,T) = \frac{2S_a^{AB}(\gamma,\xi,T)}{[S_a^{AA}(\xi,T) + S_a^{BB}(\xi,T)]} \tag{26}$$

and the shear forces are given by

$$V_A(t) = \frac{k}{2}\left[r_1^d + \left(\frac{v_{gB}-v_{gA}}{2}\right)\right] \quad ; \quad V_B(t) = \frac{k}{2}\left[r_1^d - \left(\frac{v_{gB}-v_{gA}}{2}\right)\right] . \tag{27}$$

Let us now define two new acceleration spectra $S_A(\xi,T)$ and $S_B(\xi,T)$ by the relations

$$\begin{aligned} S_A(\xi,T) &\equiv \omega_1^2\left|r_1^d + \left(\frac{v_{gB}-v_{gA}}{2}\right)\right|_{max} ; \\ S_B(\xi,T) &\equiv \omega_1^2\left|r_1^d - \left(\frac{v_{gB}-v_{gA}}{2}\right)\right|_{max} . \end{aligned} \tag{28}$$

Note that when $\ddot{v}_B = \ddot{v}_A$,

$$S_B(\xi,T) = S_A(\xi,T) = S_a^{AA}(\xi,T)$$

and when $\ddot{v}_A = \ddot{v}_B$,

$$S_B(\xi,T) = S_A(\xi,T) = S_a^{BB}(\xi,T) .$$

If a new generalized dynamic response ratio $\Phi^t(\xi,T)$ is defined as the ratio of the average of the maximum absolute values of $V_A(t)$ and $V_B(t)$ produced by the multiple inputs as represented by (24) and (25) to the average of maximum absolute shears as produced by separate rigid base (single input) inputs $\ddot{v}_{gA}$ and $\ddot{v}_{gB}$, then

$$\Phi^{t}(\xi,T) = \frac{S_A(\xi,T) + S_B(\xi,T)}{S_a^{AA}(\xi,T) + S_a^{BB}(\xi,T)} \quad . \tag{29}$$

Note that for systems of the above type which are statically indeterminant through their supports, the forces produced by the quasi-static responses are proportional to the out-of-phase ground displacement $(v_{gB}-v_{gA})/2$.

Example No. 2 of the Special Case - Consider the simple system shown in Fig. 8.2 with support inputs at A and B as indicated. It is of interest to consider the absolute maximum response of a single mode of vibration for simultaneous inputs $\ddot{v}_A(t)$ and $\ddot{v}_B(t)$ and to compare this maximum response with the average of the corresponding absolute maximum responses produced by rigid base inputs $\ddot{v}_A(t)$ and $\ddot{v}_B(t)$.

Considering the first mode, its dynamic response is given by

$$v^{d}(x,t) = r_1^{d}(t) \sin\frac{\pi x}{2} \quad , \tag{30}$$

and its quasi-static response is given by

$$v^{qs}(x,t) = v_{gA}(t) + \left(\frac{v_{gB}(t) - v_{gA}(t)}{L}\right) x \quad . \tag{31}$$

Adding (30) and (31), the total response is given by

$$v^{t}(x,t) = r_1^{d}(t)\ \Phi_1(x) + v_{gA}\Phi_2(x) + v_{gB}\Phi_3(x) \tag{32}$$

where

$$\begin{aligned} \Phi_1(x) &= \sin\frac{\pi x}{L} \\ \Phi_2(x) &= 1 - \frac{x}{L} \\ \Phi_3(x) &= \frac{x}{L} \quad . \end{aligned} \tag{33}$$

The principle of virtual work and standard finite element methods give

$$m_{11} = \frac{\bar{m}L}{2} \quad ; \quad m_{12} = m_{13} = \frac{\bar{m}L}{2}$$

$$k_{11} = \frac{\pi^4 \overline{EI}}{2L^3} \quad ; \quad k_{12} = k_{13} = 0 \tag{34}$$

from which

$$\omega_1^2 = k_{11}/m_{11} = \frac{\pi^4 \overline{EI}}{\bar{m}L^4} \quad ; \quad T_1 = 2\pi/\omega_1 \quad . \tag{35}$$

Substituting (34) into (16) gives $A = B = 2/\pi$; therefore, γ as defined by (19) equals 1. Because this structure is statically determinant through its supports, the quasi-static response produces no internal forces in the system. This is consistent with (4) with $r_1^{qs} = o$. It is quite clear now that the generalized dynamic response ratio given by (26) for $\xi=\xi_1$ and $T=T_1$ is a direct measure of the modified total force (or stress) response caused by the differences in the two inputs $\ddot{v}_A(t)$ and $\ddot{v}_B(t)$.

For the second mode response, (32) and (33) still apply except that

$$\phi_1(x) = \sin \frac{2\pi x}{L} \quad . \tag{36}$$

This mode shape leads to

$$m_{11} = \frac{\bar{m}L}{2} \quad ; \quad m_{12} = \frac{\bar{m}L}{2\pi} \quad ; \quad m_{13} = -\frac{\bar{m}L}{2\pi}$$

$$k_{11} = \frac{8\pi^4 \overline{EI}}{L^3} \quad ; \quad k_{12} = k_{13} = o \quad . \tag{37}$$

Thus,

$$\omega_1^2 = \frac{k_{11}}{m_{11}} = \frac{16\pi^4 \overline{EI}}{\bar{m}L^4} \quad \text{(second mode freq.)} \quad . \tag{38}$$

Substituting (37) into (16) gives $A = 1/\pi$ and $B = -1/\pi$; therefore, γ as defined by (19) equals -1. From (26), it is seen that $\Phi^d(-1,\xi,T)$ becomes infinite. The reason for this is that the second mode is excited only by the out-of-phase motion $(\ddot{v}_{gB}-\ddot{v}_{gA})/2$. In other words, the rigid base (in-phase) inputs produce no second mode response.

8.3 Correlations of Multi-Support Excitations

A. Multiple Components at One Support

Consider input accelerations $a_{rx}(t)$, $a_{ry}(t)$, and $a_{rz}(t)$ at support r in directions x, y, and z, respectively. These motions can easily be transformed to any other orthogonal set of axes, say $\bar{x}$, $\bar{y}$, and $\bar{z}$, through a transformation matrix $\underline{a}$ which satisfies the condition $\underline{a}^T\underline{a} = \underline{I}$, where I is the identity matrix. Then

$$\begin{Bmatrix} a_{r\bar{x}}(t) \\ a_{r\bar{y}}(t) \\ a_{r\bar{z}}(t) \end{Bmatrix} = \begin{bmatrix} a_{11} & a_{12} & a_{13} \\ a_{21} & a_{22} & a_{23} \\ a_{31} & a_{32} & a_{33} \end{bmatrix} \begin{Bmatrix} a_{rx}(t) \\ a_{ry}(t) \\ a_{rz}(t) \end{Bmatrix} . \tag{39}$$

The transformation giving the principal axes, i.e., the directions for which no cross-correlations exist among the three transformed components of acceleration[1] can easily be found. For small structures, the directions of the principal axes for all inputs would be approximately the same; however, for large structures significant differences could exist, particularly when the site conditions are complex .

B. Uni-Directional Components at Two Supports

Let $a_{ri}(t)$ and $a_{si}(t)$ be the recorded ground accelerations at stations r and s, respectively, in the i th coordinate direction (i = x,y,z) at time t. These motions can be separated into their in-phase and out-of-phase components as shown by

$$a_{ri}(t) = \left[\frac{a_{ri}(t) + a_{si}(t)}{2}\right] + \left[\frac{a_{ri}(t) - a_{si}(t)}{2}\right]$$
$$a_{si}(t) = \left[\frac{a_{ri}(t) + a_{si}(t)}{2}\right] - \left[\frac{a_{ri}(t) - a_{si}(t)}{2}\right] \qquad (40)$$

The first term on the right-hand side of (40) represents the in-phase component while the second term represents the out-of-phase component. It is very informative to compare these two components directly for different pairs of stations and for different directions when studying the correlations of $a_{ri}(t)$ and $a_{si}(t)$. As pointed out previously, (23) can also be used for this same purpose by letting $\gamma = +1$ and $\gamma = -1$ and comparing the two results obtained.

Correlation studies of $a_{ri}(t)$ and $a_{si}(t)$ can also be carried out using the so called "moving window" technique. To develop this method, the Fast Fourier Transform algorithm can be used to generate

$$a_{ri}(i\bar{\omega},t) \equiv \int_{t-\frac{\Delta t}{2}}^{t+\frac{\Delta t}{2}} a_{ri}(\alpha)\; e^{-i\bar{\omega}\alpha} d\alpha \qquad (41)$$

$$b_{ri}(\bar{\omega},t,\alpha) \equiv \frac{1}{2\pi} \int_{\bar{\omega}-\frac{\Delta\bar{\omega}}{2}}^{\bar{\omega}+\frac{\Delta\bar{\omega}}{2}} a_{ri}(i\bar{\beta},t)\; e^{+i\bar{\beta}\alpha} d\bar{\beta} \qquad (42)$$

where α is a dummy variable for time t, Δt is the window width in the time domain, $\Delta\bar{\omega}$ is the window width in the frequency domain, and $\bar{\beta}$ is a dummy variable for circular frequency $\bar{\omega}$. Time t in (41) can be varied continuously for a fixed value of Δt resulting in a moving window in the time domain. Likewise, frequency $\bar{\omega}$ in (42) can be varied continuously for a fixed value of $\Delta\bar{\omega}$ resulting in a moving window in the frequency domain. Equation (41) is actually the Fourier Transform of $a_{ri}(t)$, but considering only its values over the time range Δt centered on t, while (42) is the inverse Fourier Transform of $a_{ri}(i\bar{\omega},t)$ but considering only its values over the frequency range $\Delta\bar{\omega}$ centered on $\bar{\omega}$. In some cases, $a_{ri}(i\bar{\omega},t)$ and $b_{ri}(i\bar{\omega},t,\alpha)$ are calculated for Δt infinite and $\Delta\bar{\omega}$ equal a finite value, respectively; while in other cases, they are calculated for Δt equal a finite value and $\Delta\bar{\omega}$ infinite, respectively. In certain special cases, finite values are used for both Δt and $\Delta\bar{\omega}$.

To continue with this moving window approach, generate the cross-correlation coefficients (or functions) as defined by

$$\rho_{ri,si}(\bar{\omega},t,\tau) \equiv \frac{\int_{-\infty}^{\infty} b_{ri}(\bar{\omega},t,\alpha)\; b_{si}(\bar{\omega},t,\alpha+\tau)\; d\alpha}{\sqrt{\int_{-\infty}^{\infty} b_{ri}(\bar{\omega},t,\alpha)^2\; \alpha} \;\; \sqrt{\int_{-\infty}^{\infty} b_{si}(\bar{\omega},t,\alpha+\tau)^2 d\alpha}} \tag{43}$$

where τ is a time difference. By this definition, the cross correlation coefficients fall in the range

$$-1 \leq \rho_{ri,si}(\bar{\omega},t,\tau) \leq +1 \quad . \tag{44}$$

The use of (43) to study the cross correlation of motions $a_{ri}(t)$ and $a_{si}(t)$ is described in the next section.

8.4 Numerical Results of Analyses

A. Directions of Principal Axes

Directions of principal axes were determined for the ground accelerations produced at stations M02, M05, and M12 during the earthquake of November 14, 1980 (Event 2), and at stations C00, I06, and 009 during the earthquake of January 29, 1981 (Event 5). The directions of these axes when projected on a horizontal plane are shown in Figs. 8.3 and 8.4 for eight different overlapping time segments of 4 sec. each. The crosses and dots indicate that the major and minor axes, respectively, are approximately vertical while the short and long solid lines indicate directions of the intermediate and major axes, respectively. The most significant of these results are those for time segments in the range $0<t<8$ sec. which covers the high intensity periods of the motions.

During this high intensity time range, the major principal axis for Event 2 points downward towards the hypocenter located approximately 10 km S16°E of the center station of the array and at a depth of 62 km. This observation is consistent with high P-wave contributions to the ground motions. During the time range $6<t<18$ sec., the 4-sec. segments show the major principal axis to be approximately horizontal and usually pointing in the general direction of the epicenter.

For Event 5, the major principal axis is approximately vertical only during the first 4-sec. segment at stations C00 and I06. For all other time segments, it is approximately horizontal. During the high intensity time range and considerably beyond, the directions of the major principal axis correlate reasonably well with direction to the epicenter located 30 km S26°E of the array's center station. The hypocenter depth for this earthquake was approximately 11 km. These observations are consistent with high S-wave contributions to the high intensity motions.

B. In-Phase and Out-Of-Phase Components of Uni-Directional Motions

In-phase and out-of-phase components of uni-directional motion at selected pairs of stations were calculated using the definition of (40). Figs. 8.5 to 8.9 show Fourier amplitude spectra for each of these components as recorded during Event 2 and Event 5, respectively, for the station pair C00 and I03. The in-phase component for the earthquake of November 14, 1980, is much stronger than the out-of-phase component except for frequencies in the approximate range 5 to 6 Hz. The large percentage of in-phase motion is consistent with wave fronts of the P-wave type moving in an approximately vertical direction as indicated by the vertically oriented major principal axis previously described. The in-phase and out-of-phase components for Event 5 are approximately equal in intensity if averaged over the entire frequency band $0<t<7$ Hz; however, there is a definite shifting of the intensity from one component to the other as a function of frequency. To illustrate this observation, notice the high percentage of out-of-phase motion for frequencies in the neighborhood of 1, 3, and 5 Hz and the low percentage for frequencies in the neighborhood of 2, 4, and 6 Hz. While some effort has been made to rationalize the cause of this phenomenon, no explanation will be set forth at this time. Obviously, further study of these and other results is needed.

C. Non-Dimensional Normalized Dynamic Response Ratio

The generalized dynamic response ratio $\Phi^d(\gamma,\xi,T)$ defined by (22) can be used to correlate the in-phase and out-of-phase components of uni-directional motions at station pairs when placed in its non-dimensional normalized form shown by (23) and when evaluated for $\gamma = +1$ and $\gamma = -1$. Plots of this non-dimensional normalized ratio against structural period T are shown in Figs. 8.9 to 8.13 for $\xi = 0.05$.

Figures 8.9 and 8.10 show plots of this ratio for station pairs C00 and I03 and C00 and I06, respectively, using $\gamma = +1$ which emphasizes the in-phase component of motion. Notice that the percentage of in-phase motion for Event 2 is very high compared with the corresponding percentage for Event 5, particularly as shown by the longer structural periods. This observation is quite similar for station pairs C00 and I03 and C00 and I06. Clearly, the results of Figs. 8.9 and 8.10 are consistent with mainly propagating SV-waves for Event 2 and predominant S-waves propagating horizontally for Event 5.

The non-dimensional normalized response ratio for $\gamma = +1$, $\xi = 0.05$, and for station pair C00 and I03 is again plotted against structural period T in Figs. 8.11 and 8.12. Also plotted in these figures is the same response ratio for $\gamma = -1$ which emphasizes the out-of-phase component of motion. Again notice the very high percentage of in-phase motion ($\gamma = +1$) for Event 2, as compared with Event 5. Comparison of curves in these same figures for $\gamma = -1$ shows a high higher percentage of out-of-phase motion for Event 5 as compared with Event 2. The plots in Fig. 8.13 correspond to those in Fig. 8.12 except they represent station pair C00 and I06 instead of station pair C00 and I03. The results for both station pairs are quite similar.

The observation previously mentioned of an oscillatory shifting of the intensities of in-phase and out-of-phase motions with frequency for Event 5 is again apparent in Figs. 8.12 and 8.13.

D. Shear Ratio

The generalized response ratio $\Phi^t(\xi,T)$ defined by (29) (called the shear ratio here) is plotted in Figs. 8.14 and 8.15 for Event 2 and Event 5, respectively, using the recorded EW motions for station pair C00 and I03. The plot in Fig. 8.14 showing the shear ratio to be nearly equal to 1 over the entire structural period range indicates a very large percentage of in-phase motion, in fact, so large a percentage that the rigid base input assumption usually made in engineering practice would be reasonably valid for this case. This observation is quite significant considering the fact that stations C00 and I03 are separated by 200 m.

The shear ratio plot in Fig. 8.15 for Event 5 is quite different from that in Fig. 8.14. It shows a shear ratio considerably less than 1 over most of the structural period range which indicates the double-support input produces response considerably less than the average of the separate rigid base inputs. The out-of-phase components are obviously strong for this case causing a large reduction in structural response.

By definition, the shear ratio must approach infinity as the structural period approaches zero because the quasi-static shear forces approach infinity while the dynamic shear forces remain finite. This fact explains why the shear ratio is larger than 1 for the shorter structural periods. The quasi-static response also increases the shear ratio above unity in the longer structural period range for the case of Event 2 because of the large percentage of in-phase motion. One should note that the shear ratio is exactly unity when the motions at stations C00 and I03 are identically equal. This ratio can exceed unity only as a result of the quasi-static response caused by the out-of-phase motion.

E. Cross-Correlation Coefficients

The cross correlation coefficient defined by (43) can be used to study the correlation of motions $a_{ri}(t)$ and $a_{si}(t)$ measured at stations r and s, respectively, in the i th direction. Letting Δt and $\Delta\bar{\omega}$ in (41) and (42), respectively, become infinite, the cross correlation coefficient is a function of time difference τ only. Figure 8.16 shows plots of this coefficient for the EW components of motion at two station pairs, namely C00 and I06, and I06 and M08, as recorded during Event 2. The maximum cross correlations for these two station pairs were found to be +0.476 and -0.291, respectively, while the corresponding cross correlations for zero time difference were found to be +0.204 and +0.167. These correlations are relatively low as their numerical values are dominated by the higher frequencies in the ground motions. The values of time difference τ associated with maximum values of correlation are now being used to assist in studies of wave transmission characteristics (wave type, velocity, and direction). The results of these studies will be reported later.

Because of the dominance of higher frequencies on the cross correlation coefficient and the differences in correlation which exist among frequencies, a moving window in the frequency domain was used to obtain cross correlation as a function of frequency $\bar{\omega}$ and time difference τ. In this case Δt was set equal to infinity.

Figures 8.17 to 8.20 show this correlation plotted against ground motion period ($2\pi/\bar{\omega}$) for $\tau=0$ and for $\Delta f=\Delta\bar{\omega}/2\pi=0.488$ Hz. East-west components of motion for stations C00, I03, I06, and 012 recorded during Event 2 and Event 5 were used as indicated. Figures 8.17 and 8.18 show the cross correlations to be very high for the longer periods of motion recorded during Event 2, and they show a relatively fast drop in correlation with decreasing periods below 1 sec. In contrast, the cross correlations are relatively low over the entire period range for the motions recorded during Event 5, as shown in Figs. 8.19 and 8.20, except in the near neighborhood of certain discrete periods. The significance of the oscillatory character of these cross correlation functions is now under investigation with no definitive conclusion having yet been reached.

Cross correlation coefficients have been generated for components of motion using both time and frequency moving windows. For example, they were generated for the major principal components of motion at stations M02 and M05 as recorded during the earthquake of November 14, 1980, within the time period 9 to 14 sec. and within the frequency band 2.6 to 3.0 Hz; see Fig. 8.21. The resulting cross correlation is plotted against time difference τ in Fig. 8.22. Because of the narrow band character of the components of motion and the phase angles involved, this function has the appearance of a slowly varying harmonic with a 3.3 sec. period which peaks at about $\tau = 5$ sec. where $\rho = 0.8$. The significance of this shape is now being correlated with other information to shed light on the wave transmission characteristics to be reported later.

F. Pseudo-Acceleration Response Spectra

Standard normalized pseudo-acceleration response spectra were generated using 5 percent of critical damping for the components of motion recorded during Event 2 and Event 5. The averages of these spectra are shown plotted against structural period in Figs. 8.23 to 8.26 where they can be compared with previously published average spectra representing 4 different soil types[2]. The average spectra for these two earthquakes have shapes which correlate best with the previously published averages for hard site conditions. This observation is not consistent with the relatively soft site conditions of the SMART 1 array, and this suggests dominant influences from the source mechanism.

8.5 References

1. Penzien, J. and M. Watabe, "Characteristics of 3-Dimensional Earthquake Ground Motions," Earthquake Engineering and Structural Dynamics, Vol. 3, No. 4, April-June, 1975.

2. Seed, H.B., C. Ugas, and J. Lysmer, "Site-Dependent Spectra for Earthquake-Resistant Design," Report No. EERC-74-12, Earthquake Engineering Research Center, University of California, Berkeley, November, 1974.

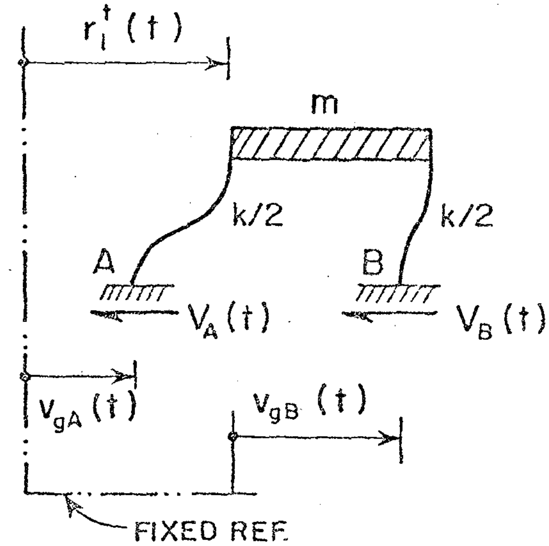

Fig. 8.1 Simple shear frame with multi-support excitations.

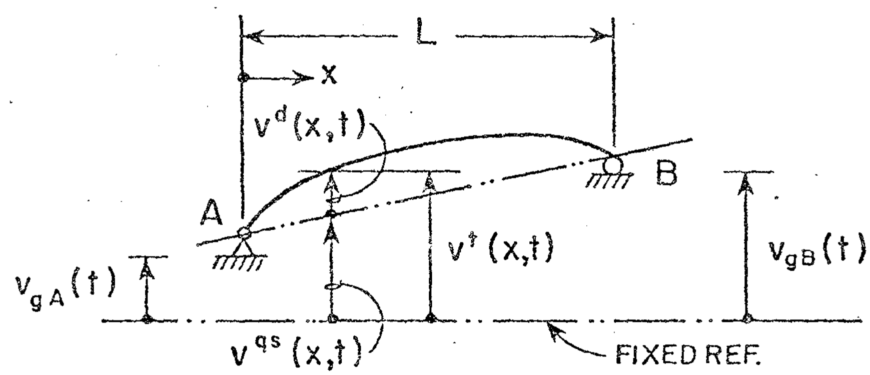

Fig. 8.2 Simple beam with multi-support excitations.

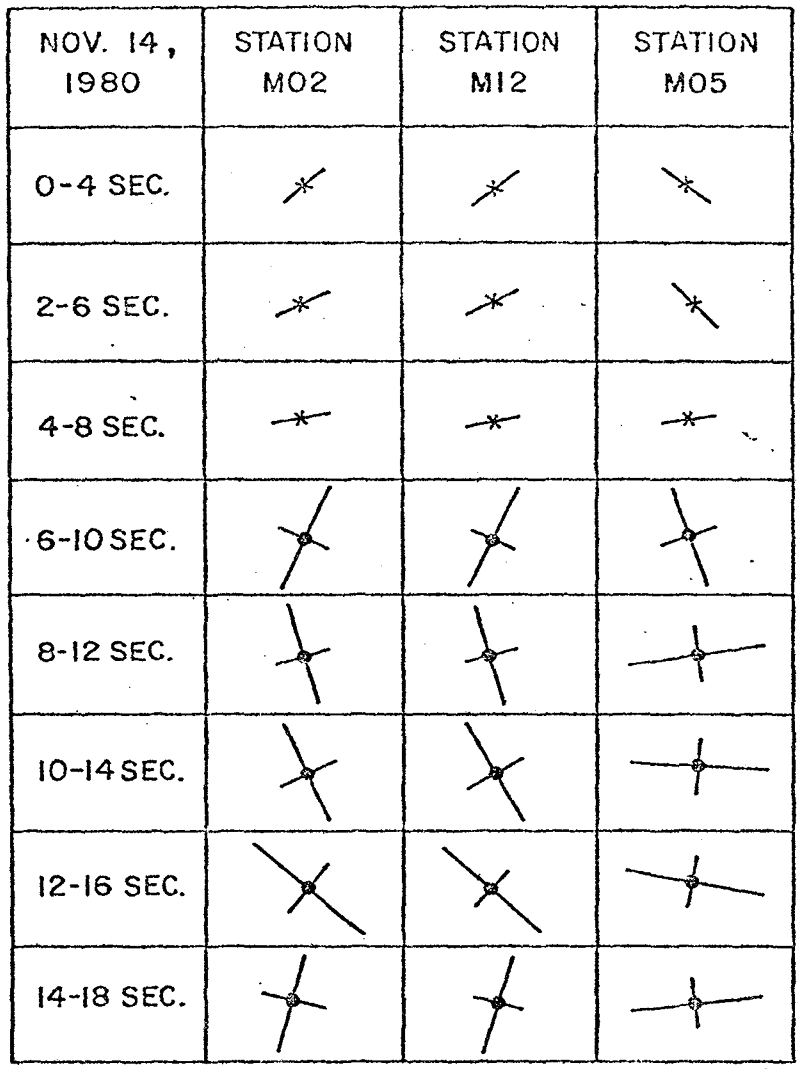

Fig. 8.3 Directions of principal axes for ground motions produced by the earthquake of November 14, 1980.

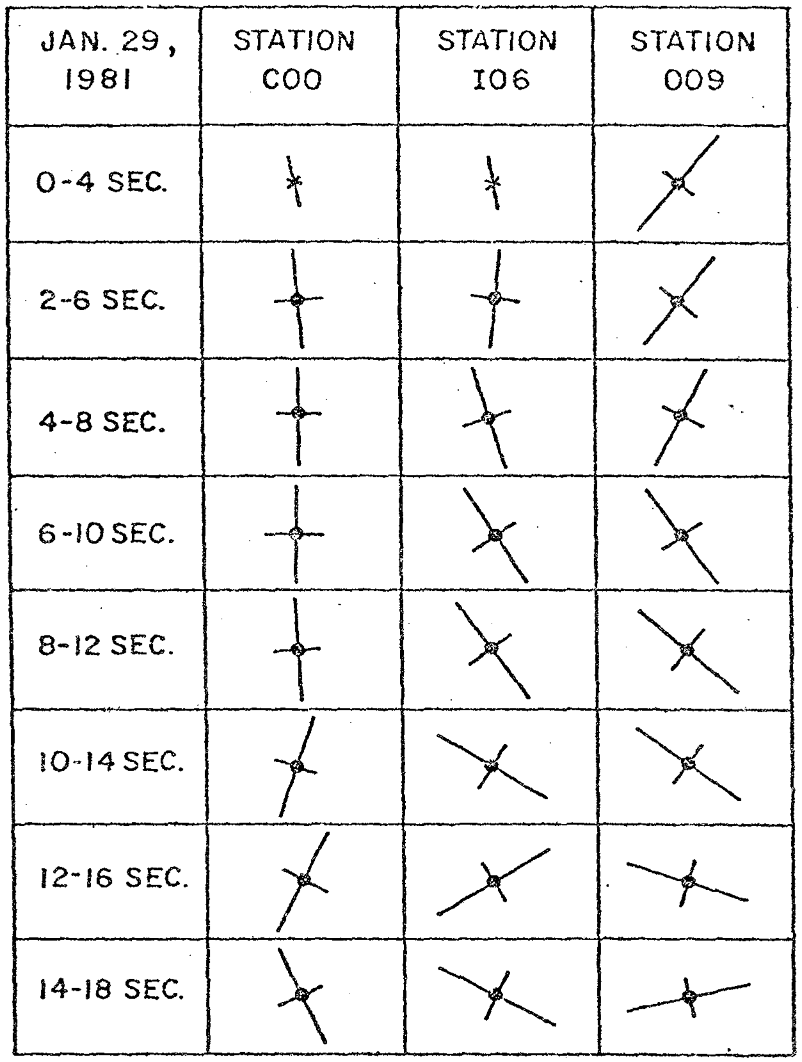

Fig. 8.4 Directions of principal axes for ground motions produced by the earthquake of January 29, 1981.

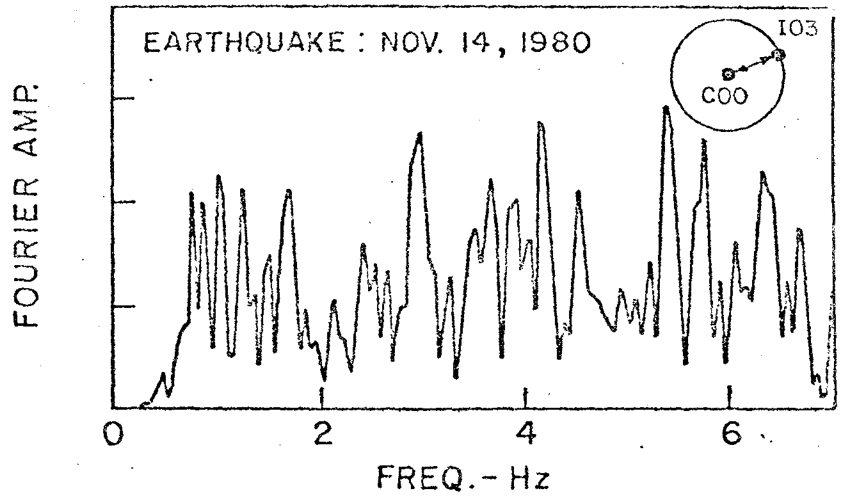

Fig. 8.5 Fourier amplitude spectrum of the EW in-phase component of motion for the station pair C00 and I03: Event 2

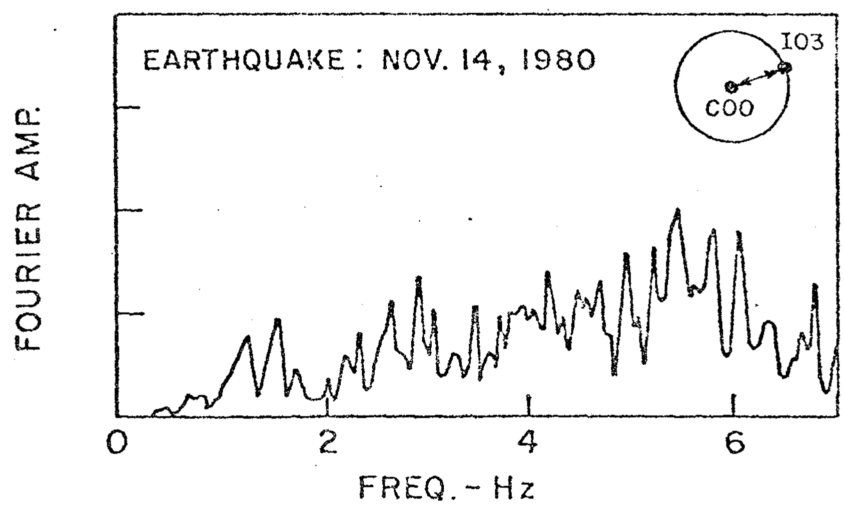

Fig. 8.6 Fourier amplitude spectrum of the EW out-of-phase component of motion for the station pair C00 and I03: Event 2

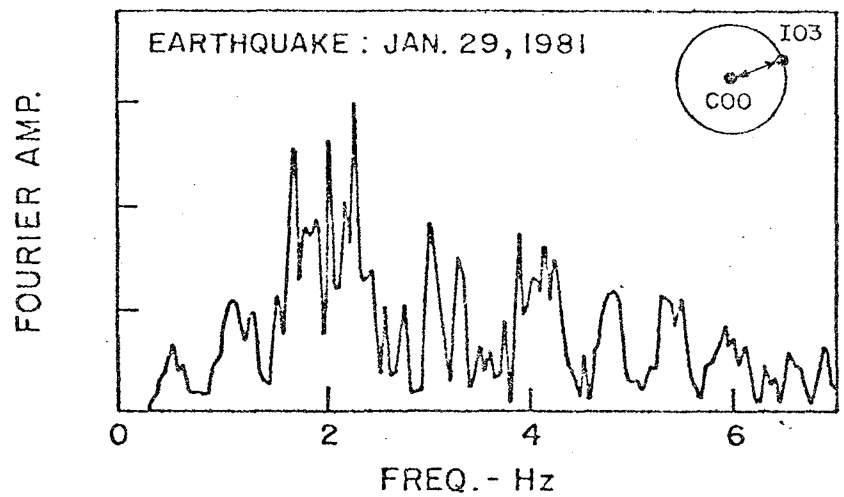

Fig. 8.7 Fourier amplitude spectrum of the E-W in-phase component of motion for the station pair COO and I03: Event 5

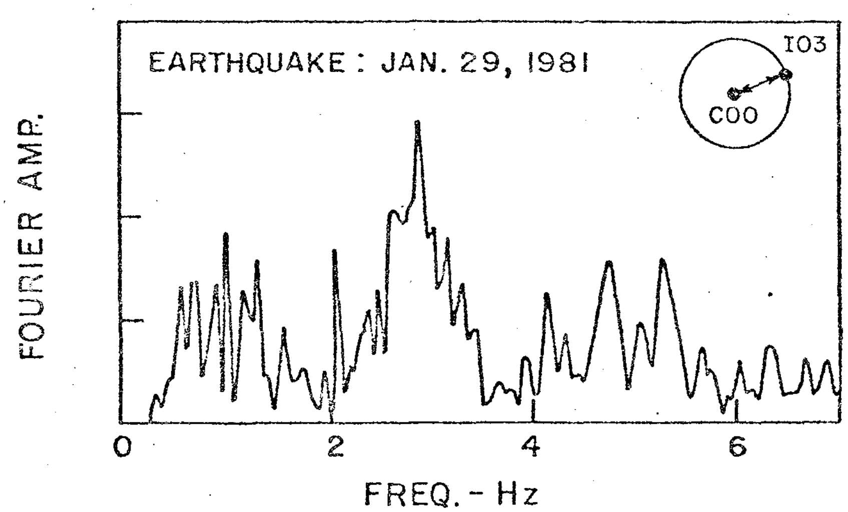

Fig. 8.8 Fourier amplitude spectrum of the EW out-of-phase component of motion for the station pair COO and I03: Event 5

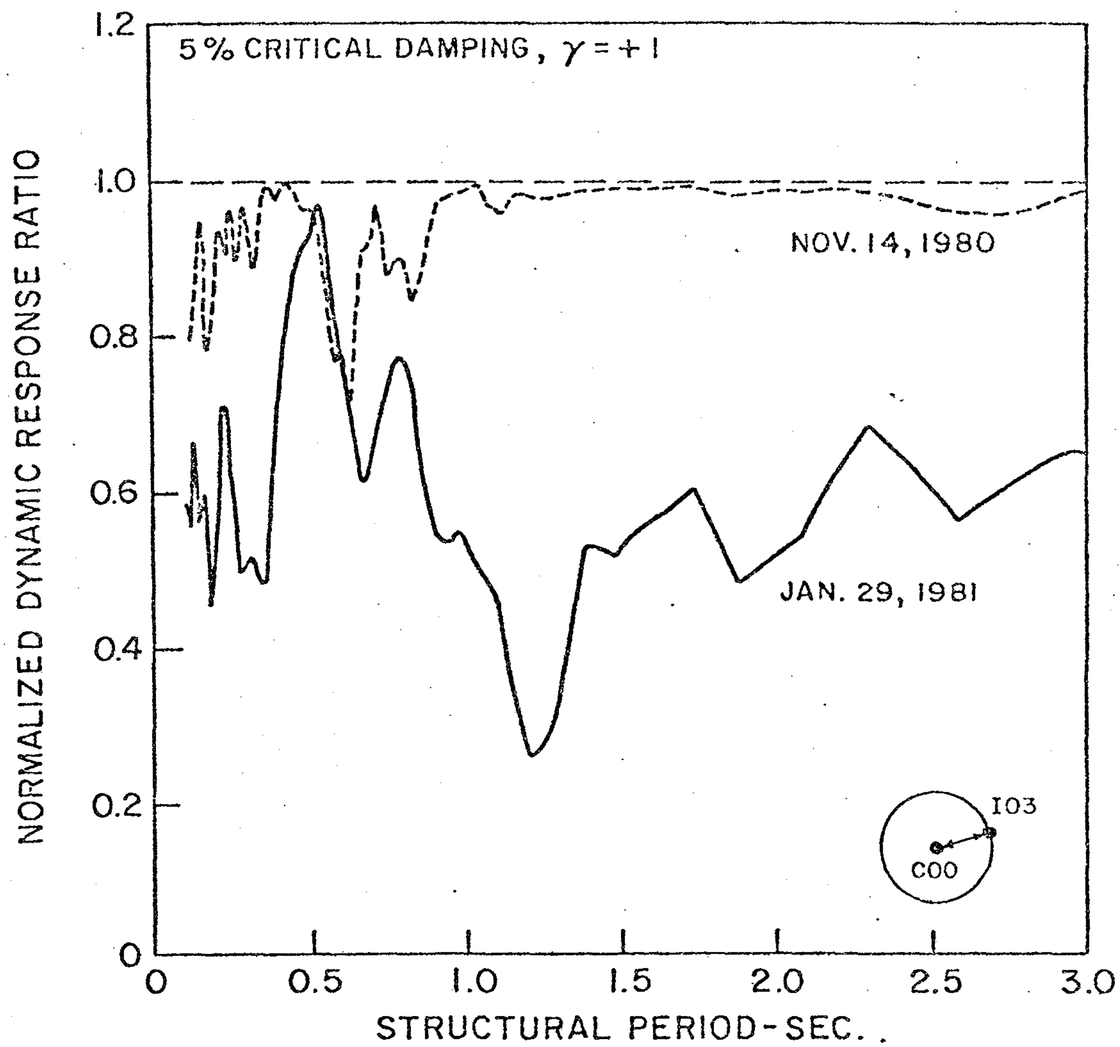

Fig. 8.9 Normalized dynamic response ratio of EW components of motion at stations C00 and I03: $\gamma = +1$

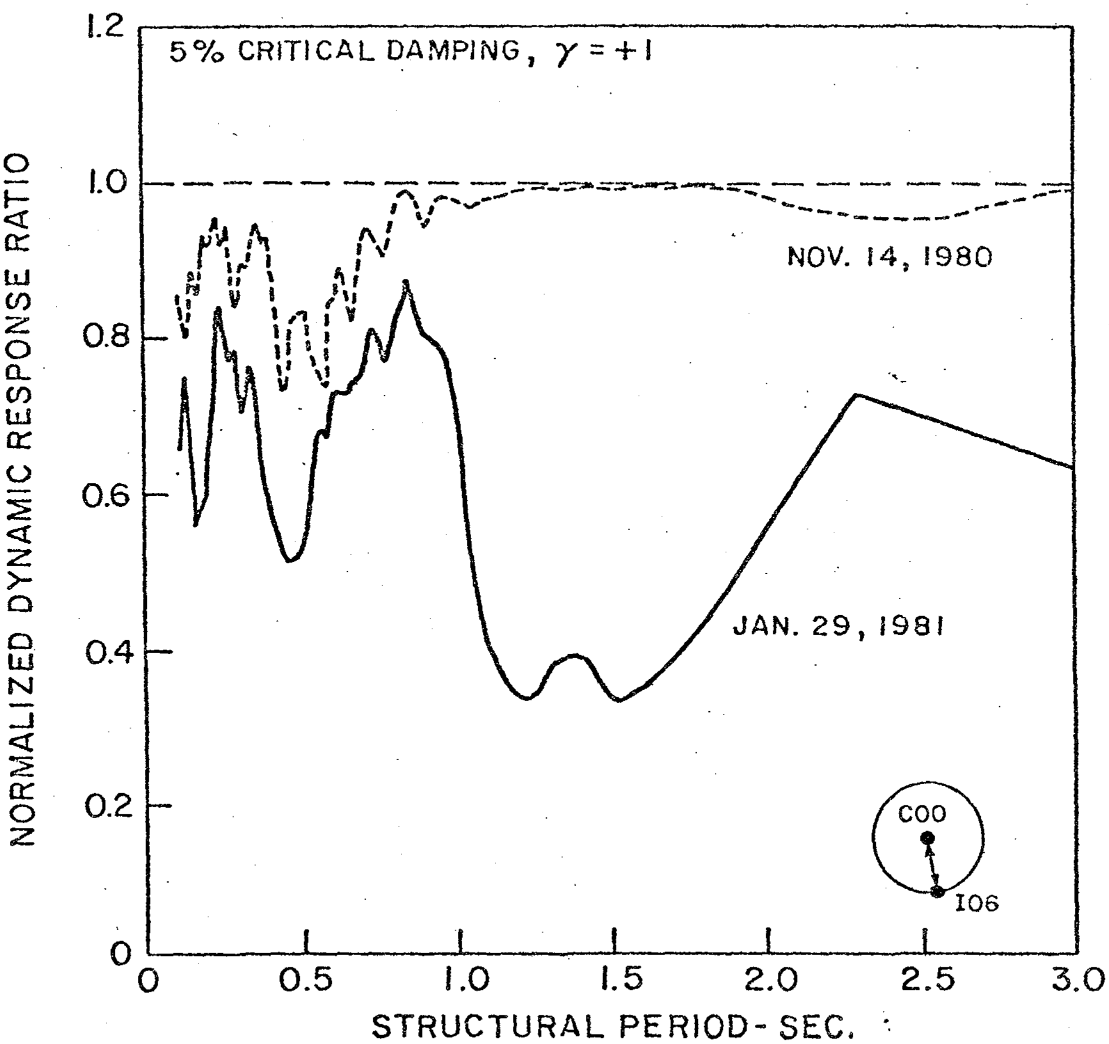

Fig. 8.10 Normalized dynamic response ratio of EW components of motion at stations C00 and I06: $\gamma = +1$

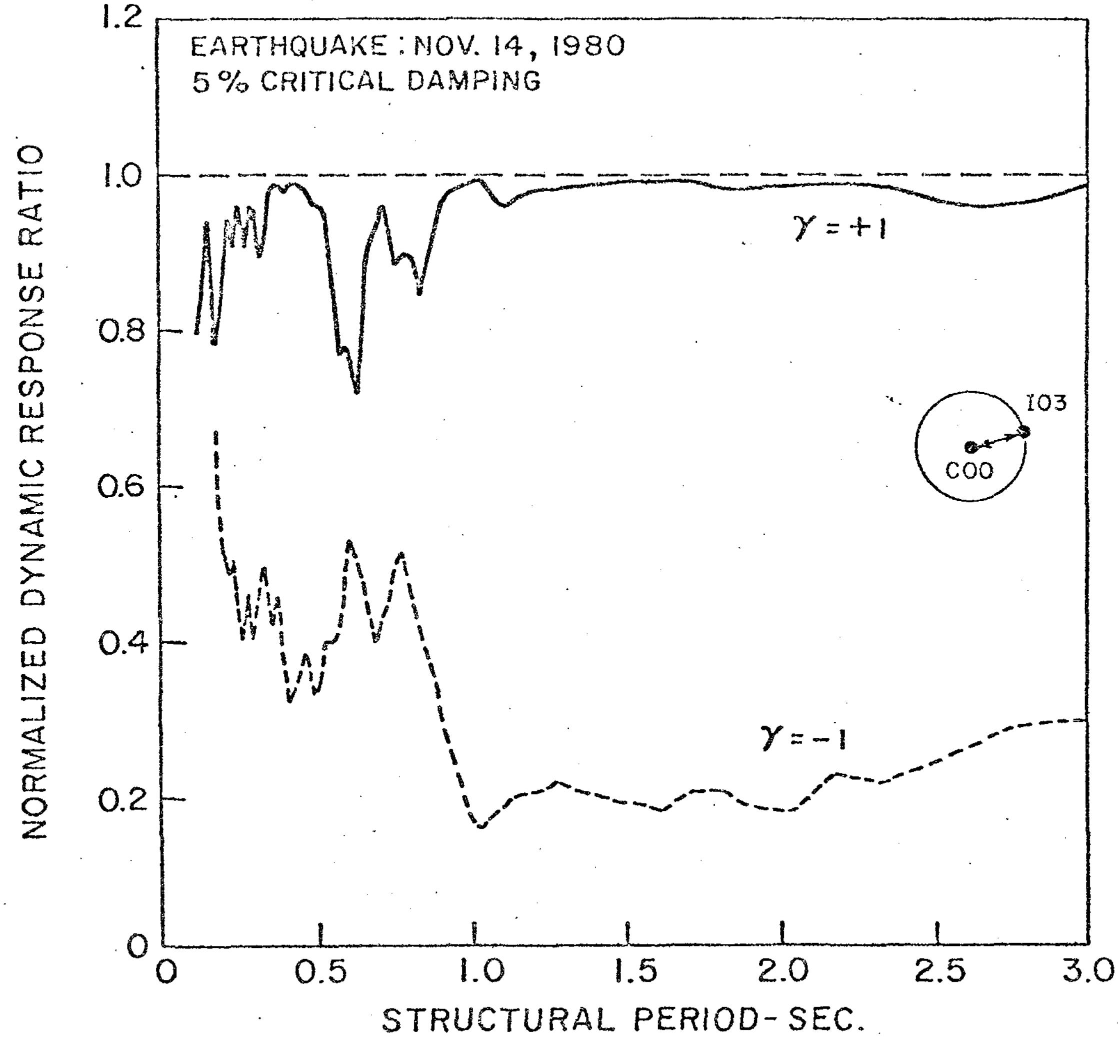

Fig. 8.11 Normalized dynamic response ratio of EW components of motion at stations C00 and I03: Event 2; $\gamma = +1$, $\gamma = -1$

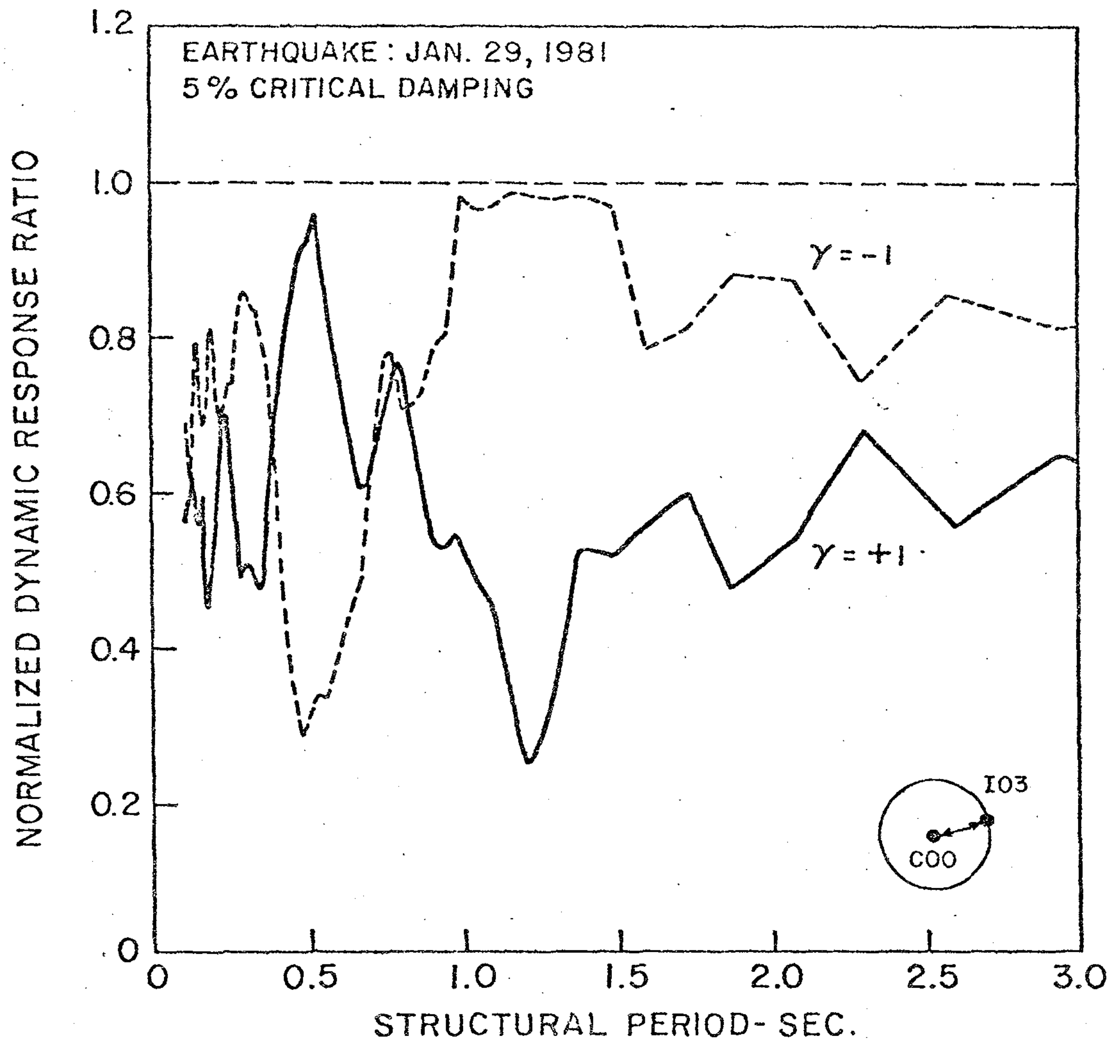

Fig. 8.12 Normalized dynamic response ratio of EW components of motion at stations C00 and I03: Event 5; $\gamma = +1$, $\gamma = -1$

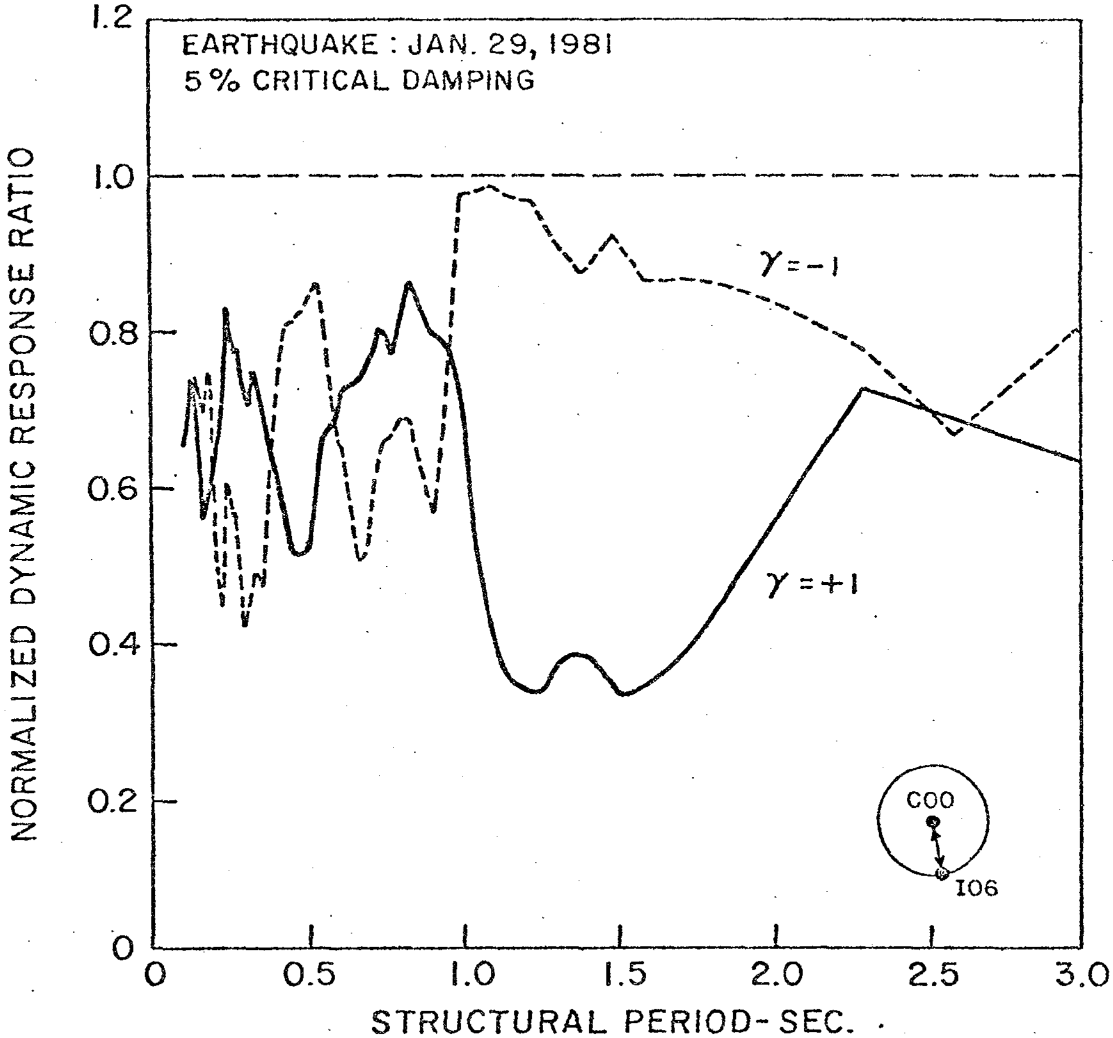

Fig. 8.13 Normalized dynamic response ratio of EW components of motion at stations C00 and I06: Event 5; γ = =1, γ = -1

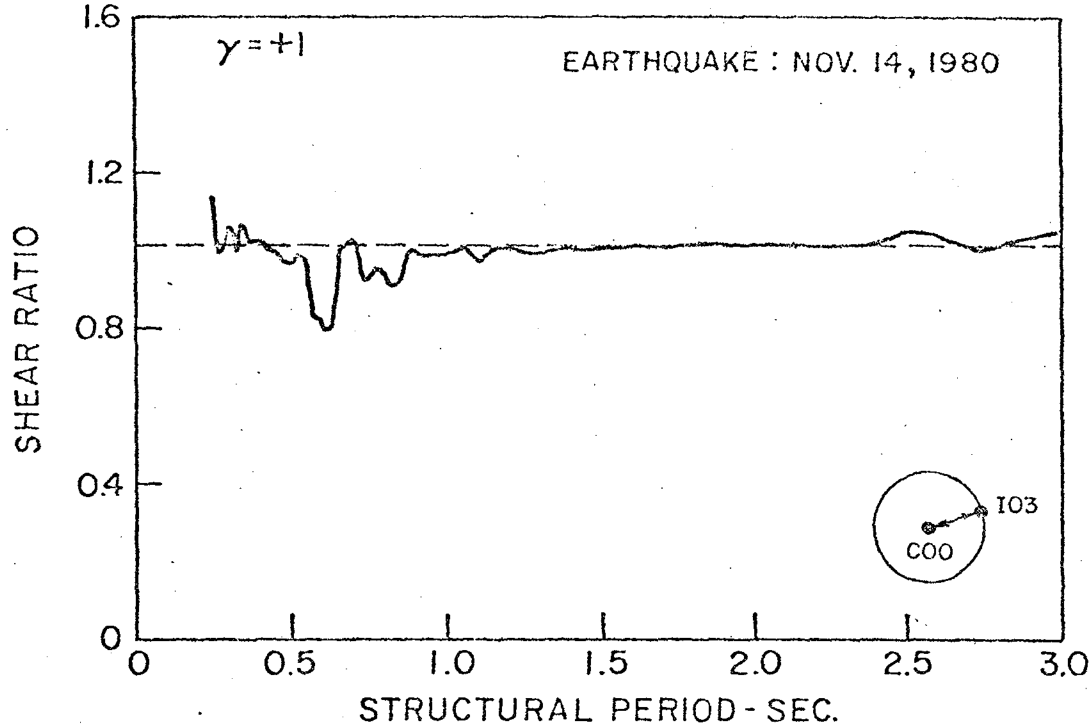

Fig. 8.14 Shear ratio of EW components of motion at stations C00 and I03: Event 2

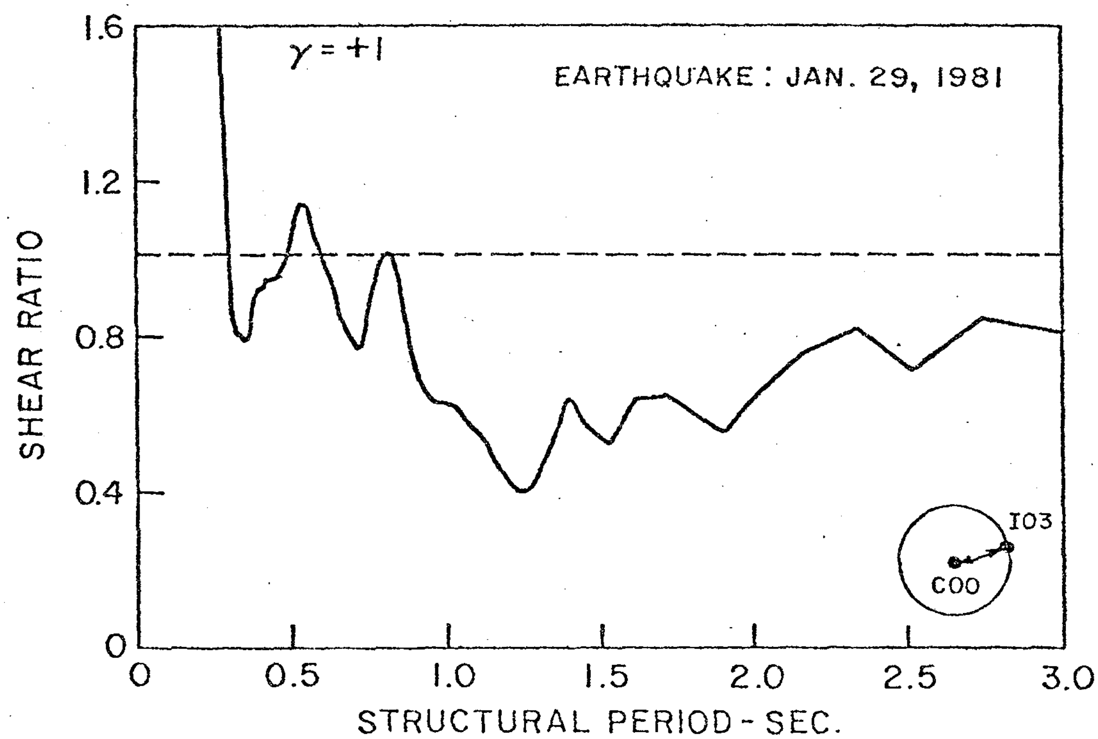

Fig. 8.15 Shear ratio of EW components of motion at stations C00 and I03: Event 5

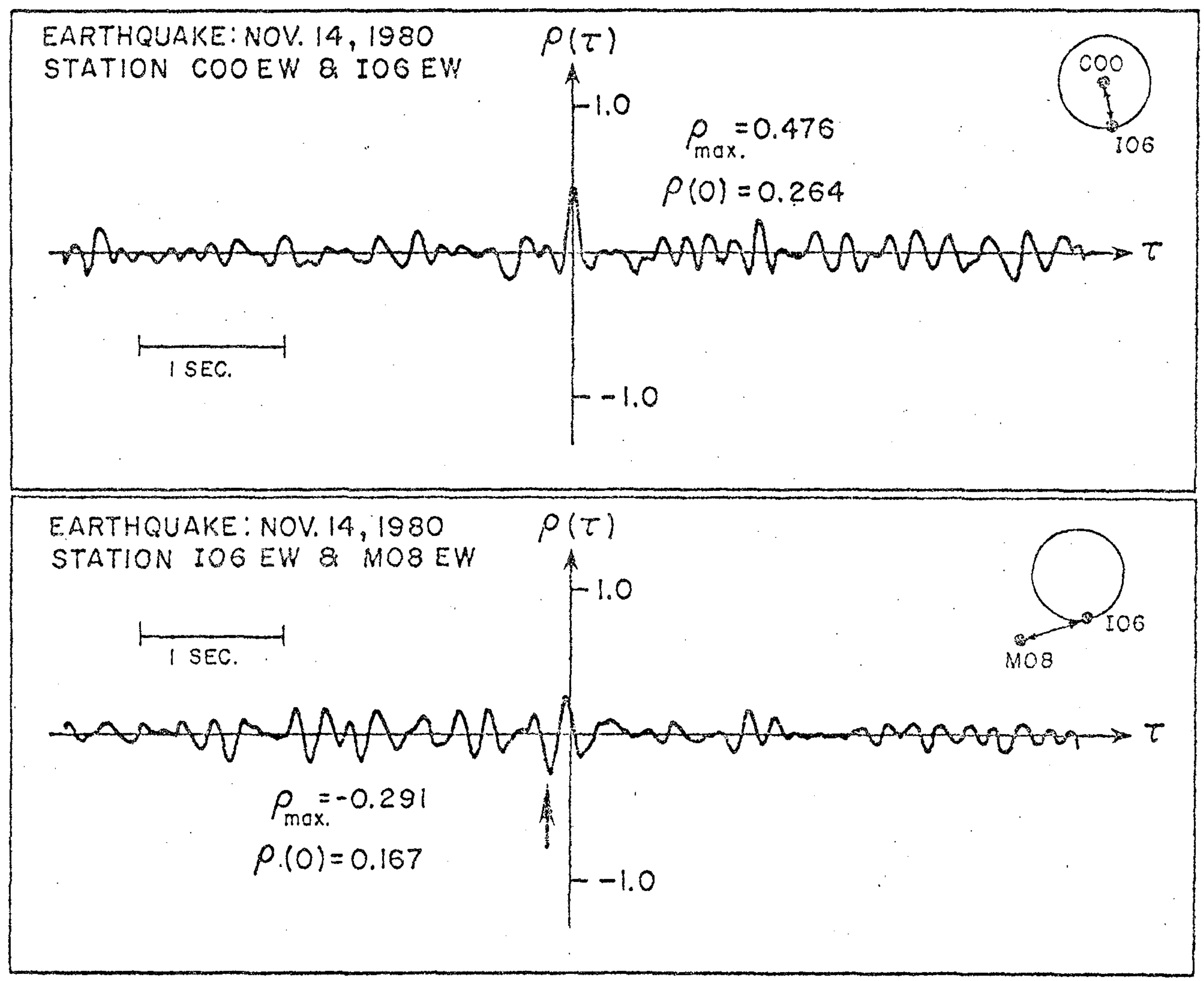

Fig. 8.16 Cross correlation coefficient of EW components of motion for the station pair C00 and I06, and for I06 and M08.

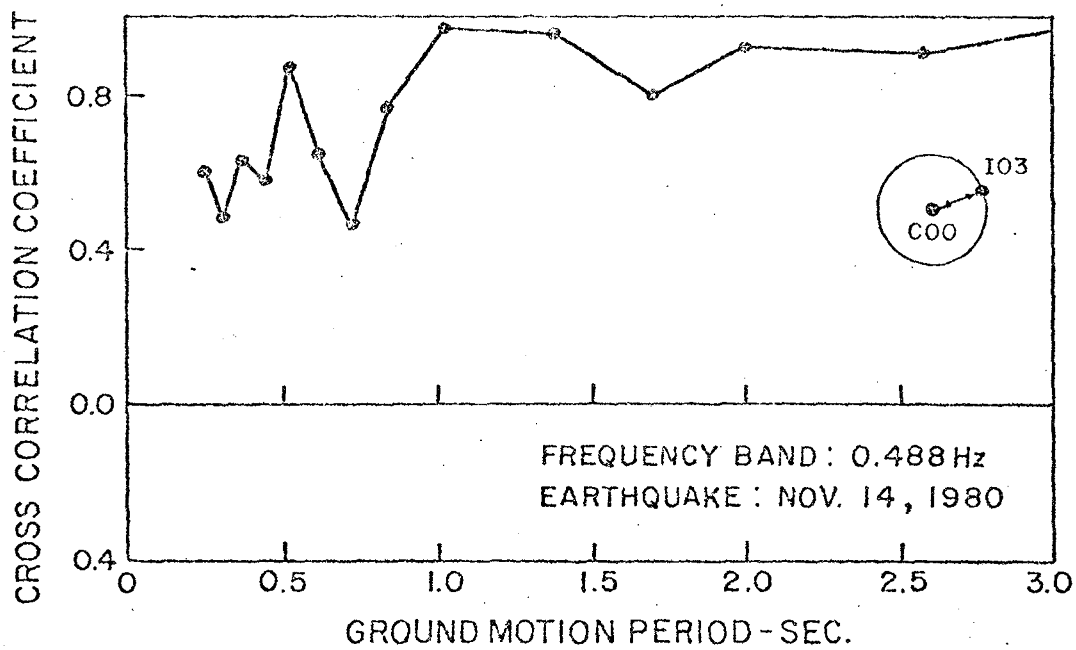

Fig. 8.17 Cross correlation coefficient of EW components of motion for the station pair C00 and I03 using a frequency domain moving window: Event 2

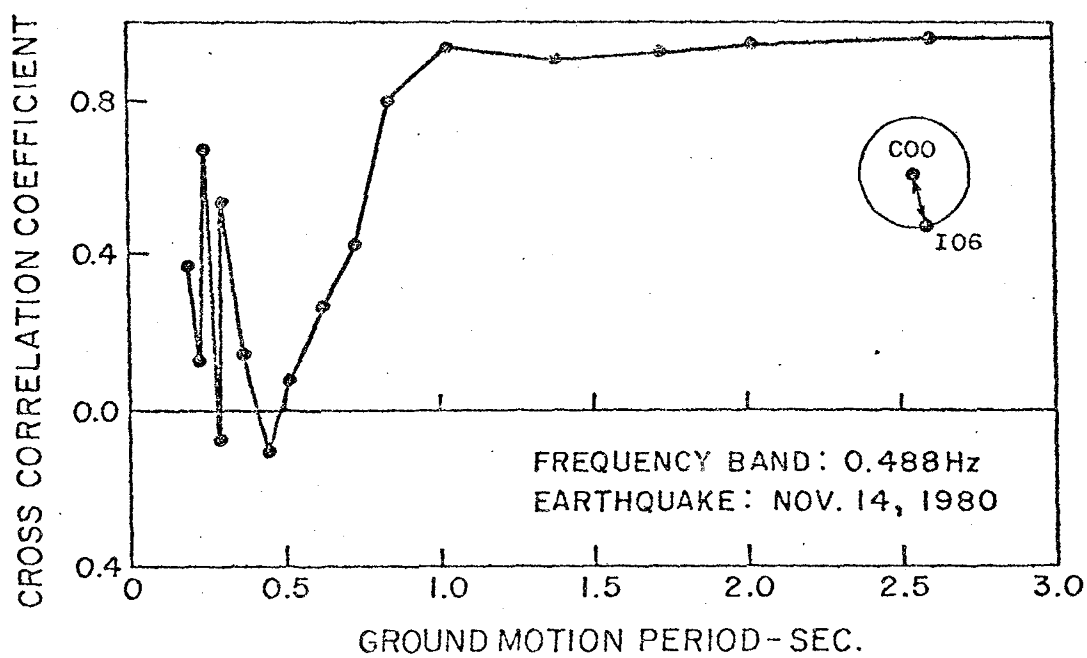

Fig. 8.18 Cross correlation coefficient of EW components of motion for the station pair C00 and I06 using a frequency domain moving window: Event 2

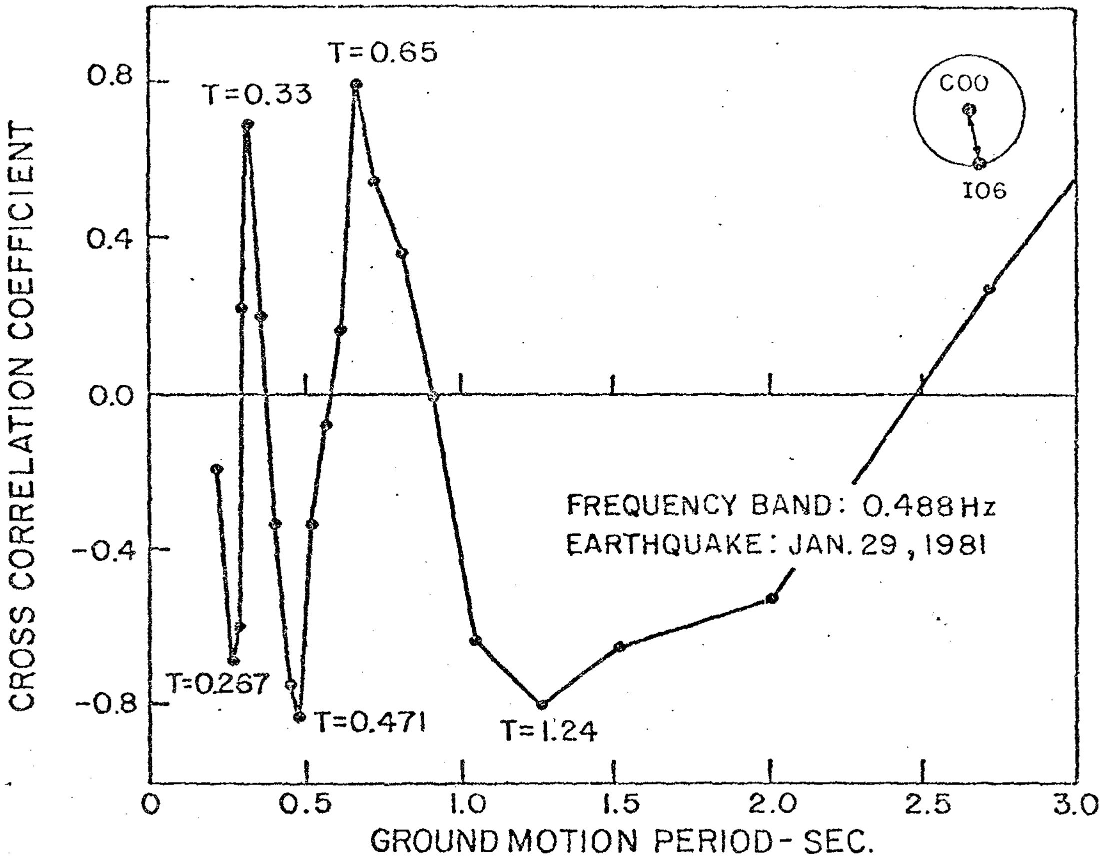

Fig. 8.19 Cross correlation coefficient of EW components of motion for the station pair C00 and I06 using a frequency domain moving window: Event 5

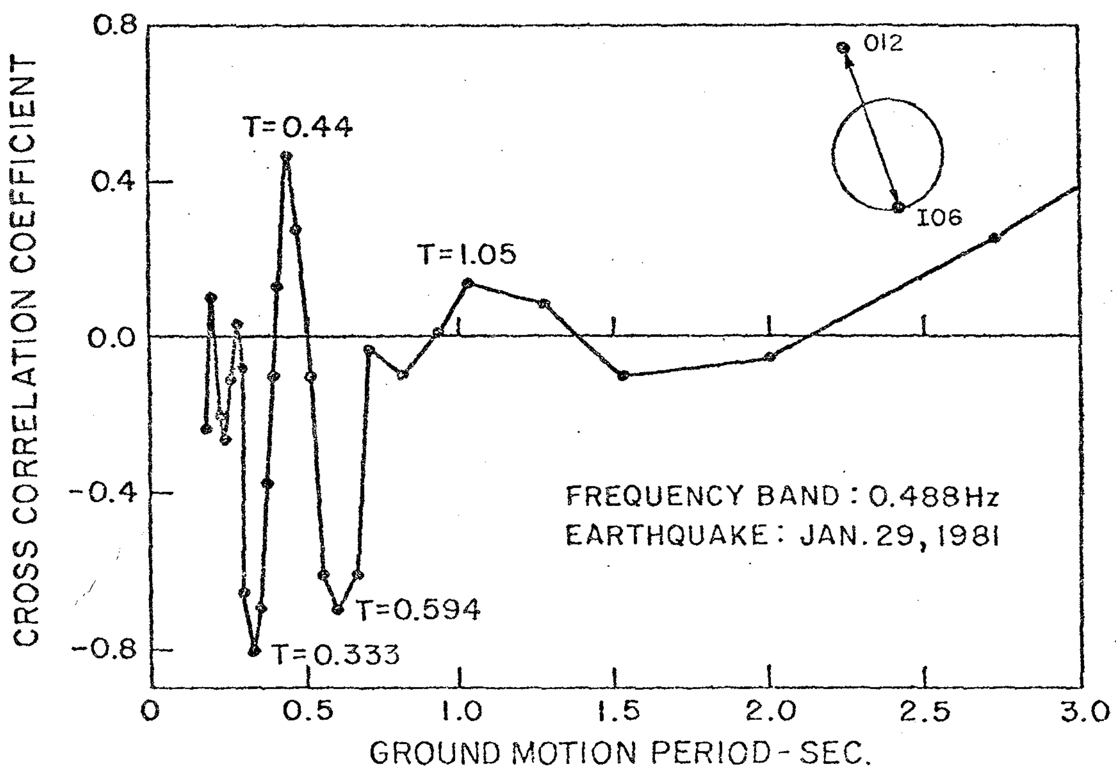

Fig. 8.20 Cross correlation coefficient of EW components of motion for the station pair I06 and 012 using a frequency domain moving window: Event 5

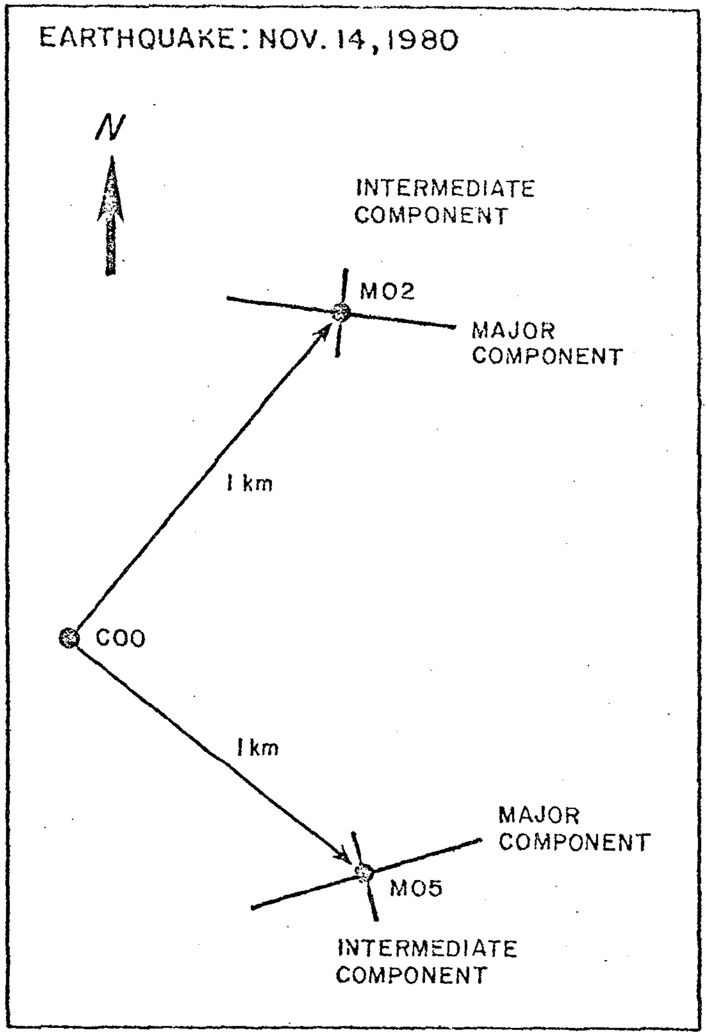

Fig. 8.21 Direction of principal axes at stations M02 and M05 using both frequency and time domain moving windows: Event 2

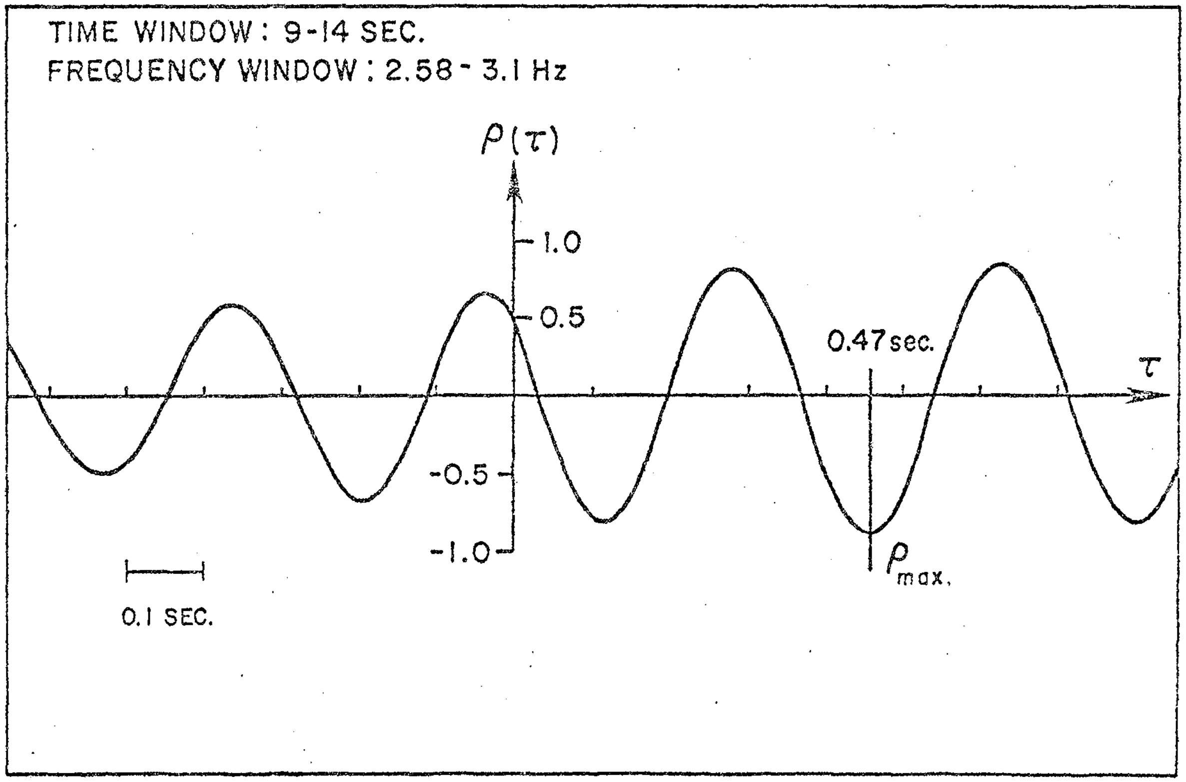

Fig. 8.22 Cross correlation coefficient of major principal components of motion at stations M02 and M05: Event 2

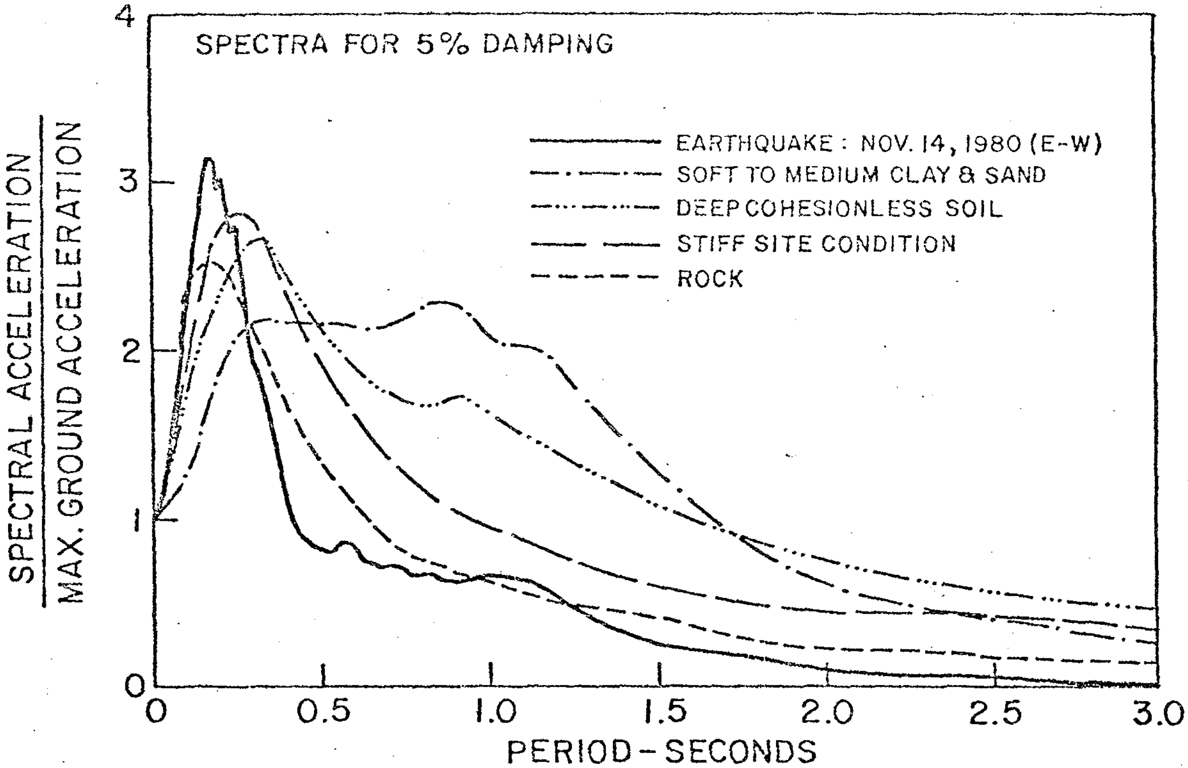

Fig. 8.23 Normalized pseudo-acceleration response spectra: EW component; Event 2

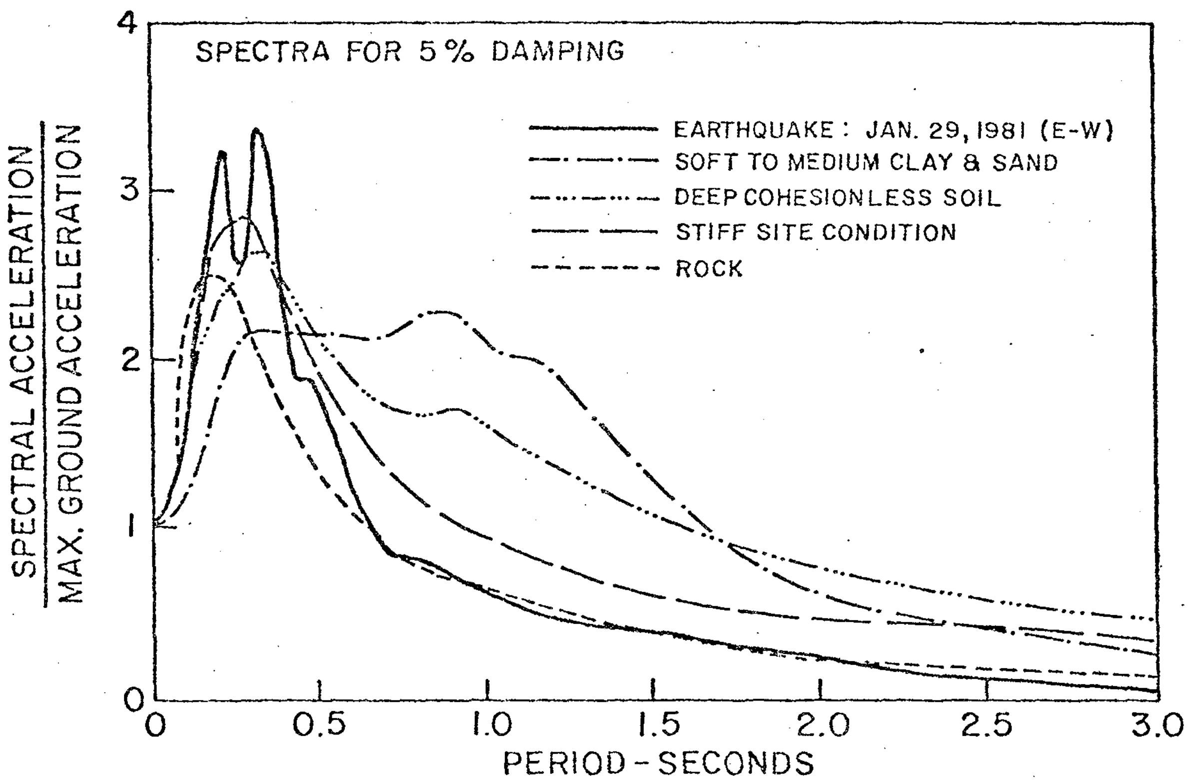

Fig. 8.24 Normalized pseudo-acceleration response spectra: EW component; Event 5

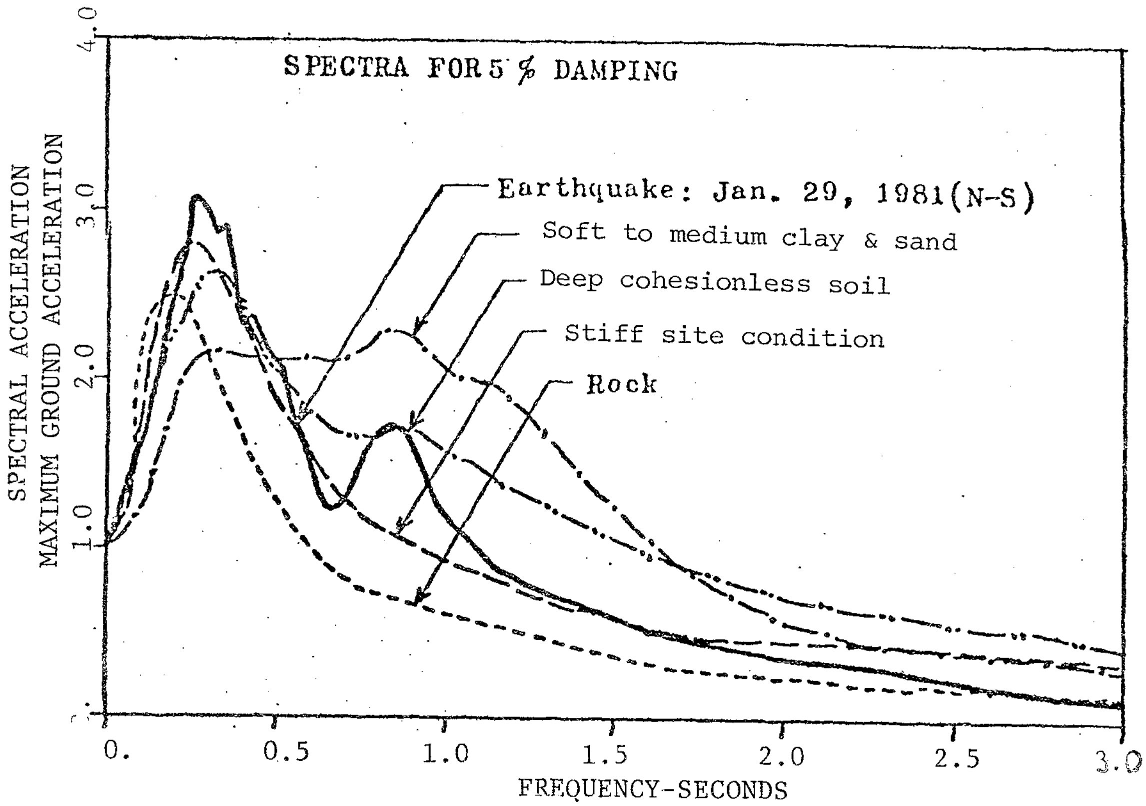

Fig. 8.25 Normalized pseudo-acceleration response spectra: NS component; Event 5

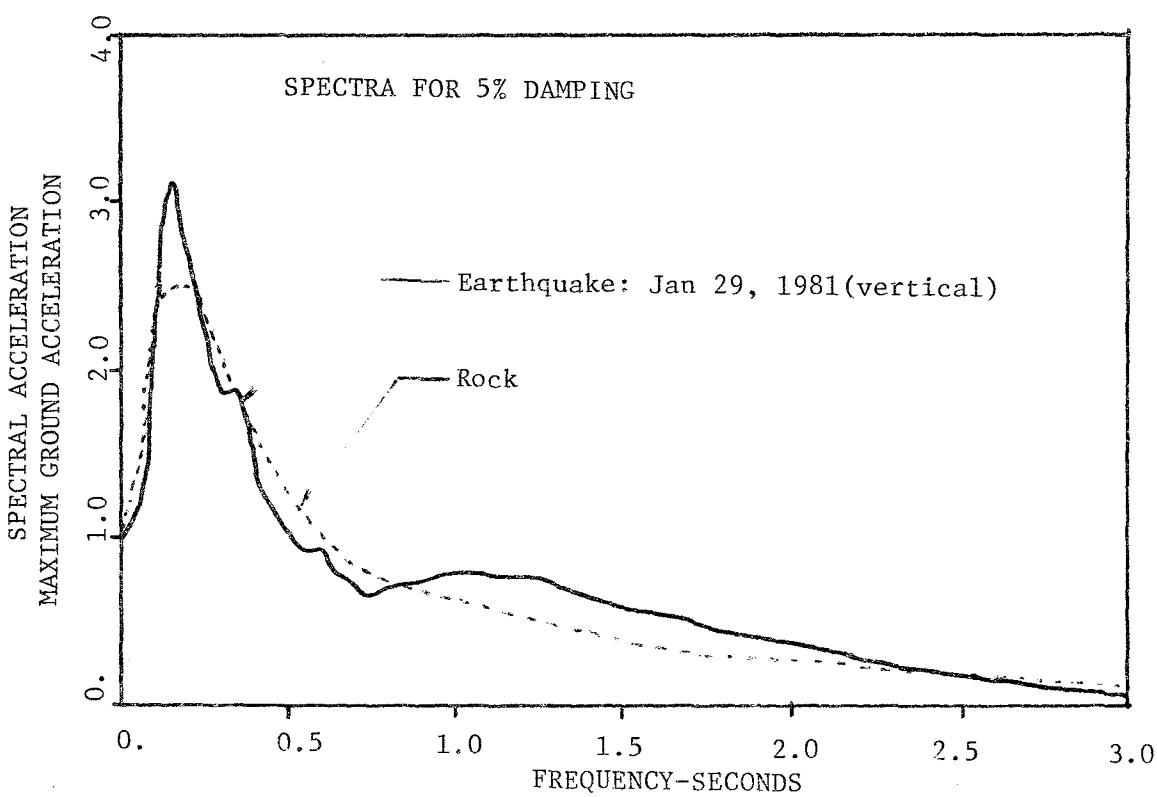

Fig. 8.26 Normalized pseudo-acceleration response spectra: vertical component; Event 5

9. CONCLUSIONS AND RECOMMENDATIONS

9.1 Conclusions

This report summarizes the design, installation, operational and analysis aspects of the development of the SMART 1 array, particularly up to about the end of its first year of operation (September 1980 - September 1981). The array represents a substantial investment in research funds and technical effort by the National Science Foundation and the National Science Council and by seismologists, engineers, and technicians at the Institute of Earth Sciences and the University of California, Berkeley. As the report demonstrates, the enterprise has exceeded the initial expectations with a valuable file of strong-motion data already available. Because the instrument selection, array installation and operation of this digital array involve novel features, it was thought valuable to set out in more detail than usual the more important experiences encountered in practice. Such practical matters should be helpful in the design and operation of other large-scale digital arrays.

The seismological and engineering research based on the measurements of strong motion of earthquakes obtained since September 1980 using SMART 1 is, of course, only in its beginning stages. Nevertheless, we have incorporated in this report some preliminary studies of the recorded ground motions to indicate the type of research that is now feasible and to give an idea of the probable applications. The complete results will eventually be published elsewhere.

This summary report also provides an opportunity to evaluate strengths and weaknesses of the various aspects of the concept of large digital arrays, although perhaps a decade is needed for a balanced and complete critique. An assumption at the International Workshop on Strong Motion in Hawaii (reference 1, Section 1.3) was "There is an adequate understanding of the nature of earthquake ground motion to be able to design useful strong-motion arrays which will provide answers to some of the important unresolved questions facing the designers of structures and other facilities in the earthquake-prone regions of the world." Based on the first year of operation of SMART 1, this expectation is substantially correct, but it must be stressed that siting and local technical competence were relatively favorable in this case.

As described in the first chapter of the report, the site of the SMART 1 array on the Lanyang plain is located at the northeast part of Taiwan, only a few hours by car or train from the Institute of Earth Sciences in Taipei. Electricity and telephone services are excellent and the local road system is superior. Cooperation from local authorities and land owners was uniformly favorable. The region was selected also because it has the highest seismic activity in Taiwan, with both shallow and intermediate focus earthquakes of sufficient strength to trigger array elements. The expectation of earthquake recordings in the short term has proved correct. A seismic reflection survey had been done in 1976 across the Lanyang plain which showed a flat surficial alluvial layer with 800 to 1000 m/sec P wave propagation velocity, underlain by dipping alluvial layers with 1800-2000 m/sec P wave propagation velocity. It is clear, however, that a full understanding of the recorded wave patterns will require more detailed mapping of the soil layers and geological structure; further geophysical surveys supplemented by boreholes will be required. The region is undergoing economic development with some multi-story buildings, substantial bridges and harbor facilities now appearing and planned. Some structures have already been instrumented with regular three-component accelerometers so that valuable engineering comparisons between structural response and array recordings will be possible.

The selection of a concentric circular array has proved beneficial. From the seismological point of view, this configuration helps in the determination of wave velocity, wave number, and the structure under this array, given various source locations. In other locations, where sources are restricted to specific faults, an omni-directional configuration may not be optimal. From the engineering point of view, the 2 km radius of the outer ring, containing 12 instruments, yields an inter-element distance that is larger than needed in practice. For most spatial variation of ground motion of engineering interest, a more densely spaced array is required. The inter-element spacing of the inner ring (about 100 m) is, however, directly applicable, even though the relative distance between stations in some smaller-scale arrays is much less. (The spacing is about 20 m in the 1979 El Centro, California, differential array[2].)

The instruments selected for SMART 1 have proved to be relatively trouble-free and to have a number of useful characteristics. In particular, the crystal oscillator is precise and the anti-aliasing filter adequate. A trigger level setting of 0.05g has proved satisfactory. Because each instrument is checked every 2 to 3 days, no conclusion can be reached about reliability of such digital devices when servicing is long-term. Initial experience with the special digital processing equipment designed for SMART 1 is favorable. The data playback and correction, including removal of time marks, glitches and the DC shift are remarkably fast. Generally, it takes less than fifteen minutes to scan and correct a single acceleration record. So far only the digital records of two major earthquakes, November 14, 1980 (Event 2) and January 29, 1981 (Event 5) have been analyzed to any extent

from 9-track tape copies. The experience with these tapes and records on the Mod Comp mini-computer system at the U.C. Seismographic Station has been quite satisfactory. A number of tape copies have been made available for analysis at other research centers but a survey of their performance is premature.

It should be pointed out that some of the smaller ground motions that have triggered array elements at the 0.05g threshold setting provide only limited digital samples. This leads to accelerograms that appear stepwise discontinuous when played back visually.. The difficulty can be overcome if necessary by decreasing the trigger level and increasing the gain.

In response to a crucial need in engineering design, research with array records has concentrated on what can be learned about in-phase and out-of-phase components of horizontal seismic ground motion. It has been found that, in the frequency range 1.0 to 10 Hz, cross-correlation coefficients are dominated by higher frequencies. Cross-correlations as a function of frequency for different pairs of stations have shown that high Fourier amplitudes of in-phase or out-of-phase waves may produce a high dynamic response of linear systems. The model indicates the influence on the structure of the out-of-phase input.

Another aspect of the phase problem, related to foundation-structure interaction, is the frequency dependence of the dominant direction of incident wave propagation. It has been demonstrated with SMART 1 records that the variance ratio R(f) can be used to infer the dominant directions of the harmonic wave components. For high values of R(f), there is no dominant direction at this frequency f. Also, different types of seismic waves (P. SH, Rayleigh, Love, etc.) can be identified by the use of the ratio of the principal variances and the maximum power spectral density function.

The principal variance calculation also provides a way to identify inter-element wave propagation characteristics for comparison with the average values obtained from frequency-wave number analysis for the whole array. Most probabilistic analyses of structural response assume that the ground motion inputs are uncorrelated, i.e., the cross-spectral density function of the excitation is assumed zero. Because of the special configuration of the SMART 1 array, there is no difficulty in calculating the coherence between different station pairs and thus establishing a cross-spectral model. Studies of the phase change and distance attenuation of the amplitude of the cross-spectra show promise, even though the parameters of the cross-spectral density function depend on the focal depth and magnitude of the earthquake.

In the measurement of coherency of Rayleigh waves of frequency about 1 Hz propagating across the array, a loss of correlation was found to be significant for the largest earthquake recorded. This effect may be due to the scattering of waves for larger station separation. McLaughlin et al.[3] have also discussed wave attenuation and random scattering in a study of waves across a sparser array from underground explosions in Nevada.

A few other papers on strong motion recorded by other arrays have recently appeared, allowing limited comparison with SMART 1. Smith et al.[1] have analyzed digital accelerograms from a small-scale linear El Centro differential array for the 1979 Imperial Valley earthquake. Because absolute time was not available at each element, they use an aftershock record to align the arrival of P waves and establish the time reference. In their subsequent correlation study, they define the covariance of two records in the usual way (see Chapter 7), as

$$r_{x_i x_j}(k) = \frac{\sigma^2_{x_i x_j}(k)}{\sigma_{x_i x_i}\,\sigma_{x_j x_j}} \quad .$$

It is important to study the covariance not only for k=0, but also for different values of k, and this analysis is being done with the SMART 1 data.

Besides the establishment of a cross-spectrum model of ground motion, spatial averaging of array data also provides important information on the effect of rigid non-embedded foundations on the seismic waves (the "tau" effect). We have defined a ground motion spectral ratio RTAU as the ratio of the spectrum of the array-average time history to the array-average spectrum of each individual time history, i.e.,

$$\text{RTAU} = \frac{F\{\ddot{v}_{g1} + \ddot{v}_{g2} + \ . \ . \ . + \ddot{v}_{gm}\}}{F\{\ddot{v}_{g1}\} + F\{\ddot{v}_{g2}\} + \ . \ . \ . \ F\{\ddot{v}_{gm}\}}$$

where F{ } is the Fourier transform of the time signal. The average of the free-field ground motions at each instant in time over the array provides an estimate of the translational motion that a rigid foundation, secured to the ground over the array dimension, will undergo as a result of the seismic excitation. Calculations using ground motion measurements over the inner ring yield a spectral ratio RTAU that approaches 1 from 1 Hz up to 4 Hz, and then decays to zero above 4 Hz (see Figs. 9.1 to 9.3). Further, it has been found that the foundation averaging "tau" depends on the phase difference of the input signals.

Another promising line of research using inter-element array motions concerned the ground strains developed. The seismic behavior of oil or gas pipelines is predominantly controlled by the ground strain/displacement characteristics. Free field motion on the surface of the ground is sufficient to represent ground motion input for such systems because, even for buried pipelines, depth in general is shallow relative to the surface soil layer. By transforming coordinates to the longitudinal direction and the transverse direction, the normal ground strain ε_{ij} along the epicentral direction between stations 006 to 012 (see Fig. 1.2) was expressed as

$$\varepsilon_{ij} = \frac{U_x^i - U_x^j}{L_{ij}} ,$$

where ε_{ij} represents the average strain between stations i and j, and U_x^i and U_x^j are ground displacements in the x direction at the two stations, respectively; L_{ij} is the distance between i and j. Based on this procedure, the strain time histories for the SMART 1 site are as shown in Fig. 9.4. The maximum strains at the site are given in Table 9.1.

Finally, as noted in the work of N. Newmark, measurements of torsional components of strong ground motion are of engineering importance. The close element spacing and circular geometry of SMART 1 allow estimation of rotational motions (i.e., the components of curl $\underset{\sim}{u}$). Some promising calculations have begun on this parameter and details will be published elsewhere.

9.2 Recommendations

A special seminar on Strong-Motion Seismic Instrument Arrays was held in Taipei and Lotung on September 7 - 10, 1981, with about thirty seismologists and earthquake engineers participating. It was agreed that the SMART 1 project is one of the most productive undertaken under the present Cooperative Science Program. The meeting participants (listed at end of Section 9.3) strongly endorsed the following recommendations:

1. Support should continue by both the NSF and the NSC for the operation of the SMART 1 array with provision of the necessary funds for the

vital analysis and interpretation of data already obtained and likely to be obtained in the future.

2. The efficiency of data analysis at the Institute of Earth Sciences, Academia Sinica, which handles the data processing for the SMART 1 array, needs improvement by acquisition of additional computer CPU capacity and peripheral hardware and software support.

3. A seismic profile should be conducted to allow critical delineation of the subsurface structure of the Lanyang sedimentary basin near the array site and at least one borehole to basement rock should be drilled and logged within the array.

4. The present SMART 1 array should be augmented by the addition of a string of downhole sensors and one or more extended surface radial arms to an appropriate distance for the study of attenuation of strong ground motion on various foundation materials.

5. Strong motion instruments should be installed in high-rise buildings and other suitable structures in the vicinity of the SMART 1 array site particularly for structural response studies and soil-structure interaction studies.

6. Timely distribution of the raw data and analysis results to the general scientific and engineering communities is essential. The principal investigators of the SMART 1 project are urged to take proper measures to ensure that scientific data and information are expeditiously distributed for general use and application.

9.3 References

1. Smith, S.W., J.E. Ehrenberg, and E.N. Hernandez, "Analysis of the El Centro Differential Array for the 1979 Imperial Valley Earthquake," Bull. Seism. Soc. Am., 72, 237-258 (1982).

2. King, J.L. and B.E. Tucker, "Analysis of Differential Array Data from El Centro, U.S.A. and GARM, U.S.S.R.," Proceedings of 3rd International Conference on Microzonation, (1982).

3. McLaughlin, K.L., D. Vasco, and T.V. McEvilly, "On the Importance of Being Coherent, or How Random Scattering and Three-Dimensional Velocity Structure May Make Seismology Interesting," Abstract, Seism. Soc. Am. Annual Meeting, April, (1982).

List of Participants

U.S.A.

A.H.-S. Ang
Department of Civil Engineering
University of Illinois
Urbana, Illinois 61801

B.A. Bolt
Seismographic Station
University of California
Berkeley, California 94720

D.M. Boore
Office of Earthquake Studies
U.S. Geological Survey
Menlo Park, California 94025

D.E. Hudson
Department of Civil Engineering
University of Southern California
Los Angeles, California 90007

W.D. Iwan
Division of Engineering and Applied Science
California Institute of Technology
Pasadena, California 91125

S.C. Liu
National Science Foundation
Washington, D.C. 20550

J. Penzien
Department of Structural Engineering
University of California
Berkeley, California 94720

T.L. Teng
Department of Geological Sciences
University of Southern California
Los Angeles, California 90007

T.M. Wooton
California Division of Mines and Geology
Sacramento, California 95816

F.T. Wu
Department of Geological Sciences
State University of New York
Binghamton, New York 13901

R.O.C.

C.C. Chen
Department of Civil Engineering
National Taiwan University
Taipei 107

S.T. Chen
Department of Construction Engineering and Technology
National Taiwan Institute of Technology
Taipei 107

R.Y. Cheng
Sinotech Engineering Consultants, Inc.
Taipei 105

M.K. Hsu
Institute of Earth Sciences, Preparatory Office
Academia Sinica
Taipei 107

S.P. Lai
Department of Construction Engineering and Technology
National Taiwan Institute of Technology
Taipei 107

P.H. Lee
Geophysics Department
Central Weather Bureau
Taipei 100

C.C. Liu
Institute of Earth Sciences, Preparatory Office
Academia Sinica
Taipei 107

C.H. Loh
Department of Civil Engineering
National Taiwan University
Taipei 107

S.T. Mau
Department of Civil Engineering
National Taiwan University
Taipei 107

Y.S. Pan
Office of Chief Geologist
Chinese Petroleum Company
Taipei 100

C.T. Shyu
Institute of Oceanography
National Taiwan University
Taipei 107

Y.B. Tsai
Institute of Earth Sciences, Preparatory Office
Academia Sinica
Taipei 107

C.S. Wang
Institute of Earth Sciences, Preparatory Office
Academia Sinica
Taipei 107

T.H. Yao
Division of Natural and Mathematical Sciences
National Science Council
Taipei 107

C.H. Yeh
Department of Civil Engineering
National Taiwan University
Taipei 107

Y.T. Yeh
Institute of Earth Sciences, Preparatory Office
Academia Sinica
Taipei 107

G.K. Yu
Department of Geophysics
National Central University
Chungli 320

TABLE 9.1

Maximum ground strain [x 10^{-5}] along the profile from site 006 to 012 of SMART 1.

Segment	Strain ε_{ij}
006-M06	-3.3
M06-I06	-3.1
I06-C00	-3.1
C00-I12	4.6
I12-M12	2.4
M12-012	-2.5

Earthquake: Jan. 29, 1981

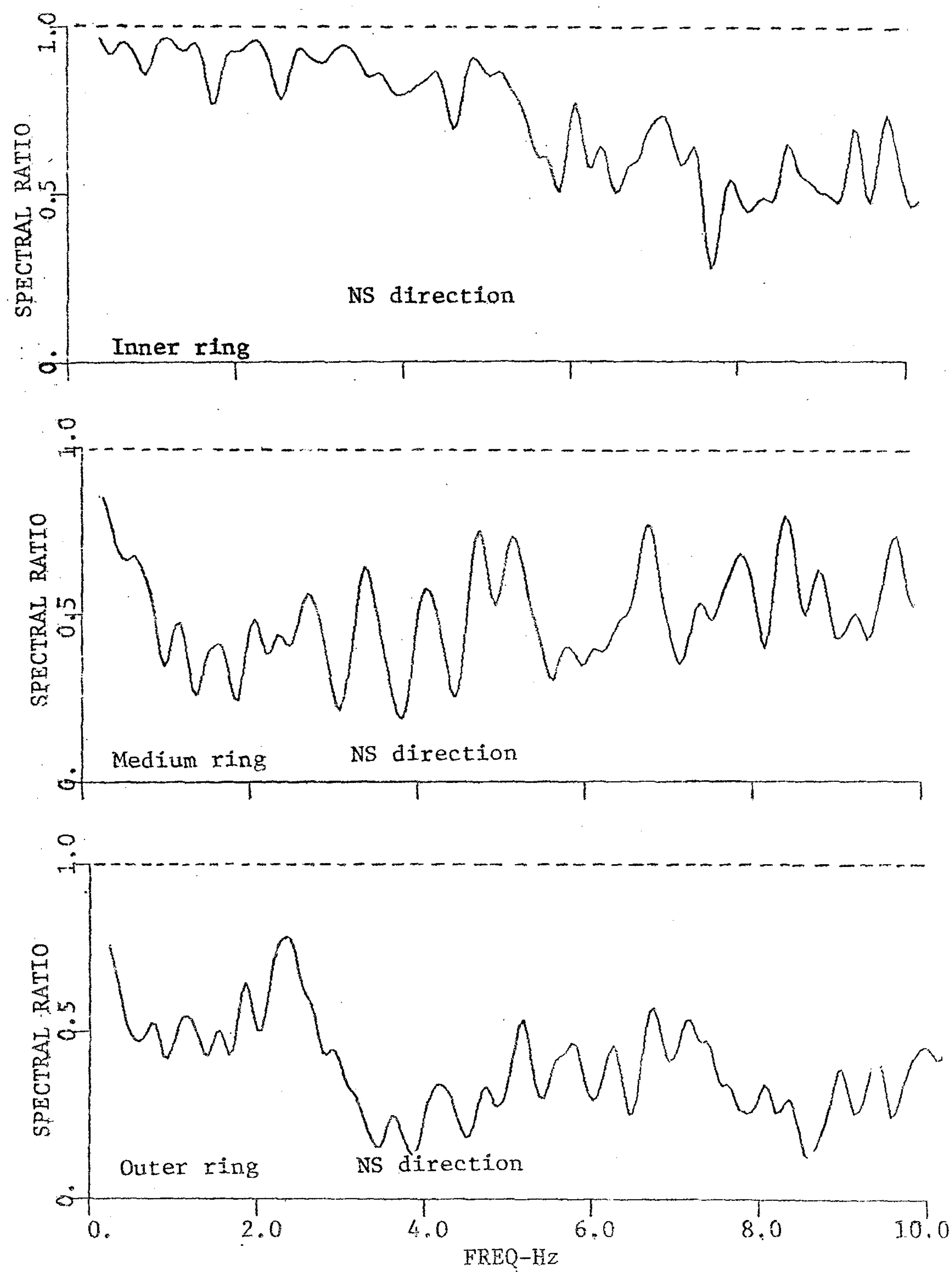

Fig. 9.1 Spectral ratio RTAU in the NS direction: Event 5

Earthquake: Jan. 29, 1981

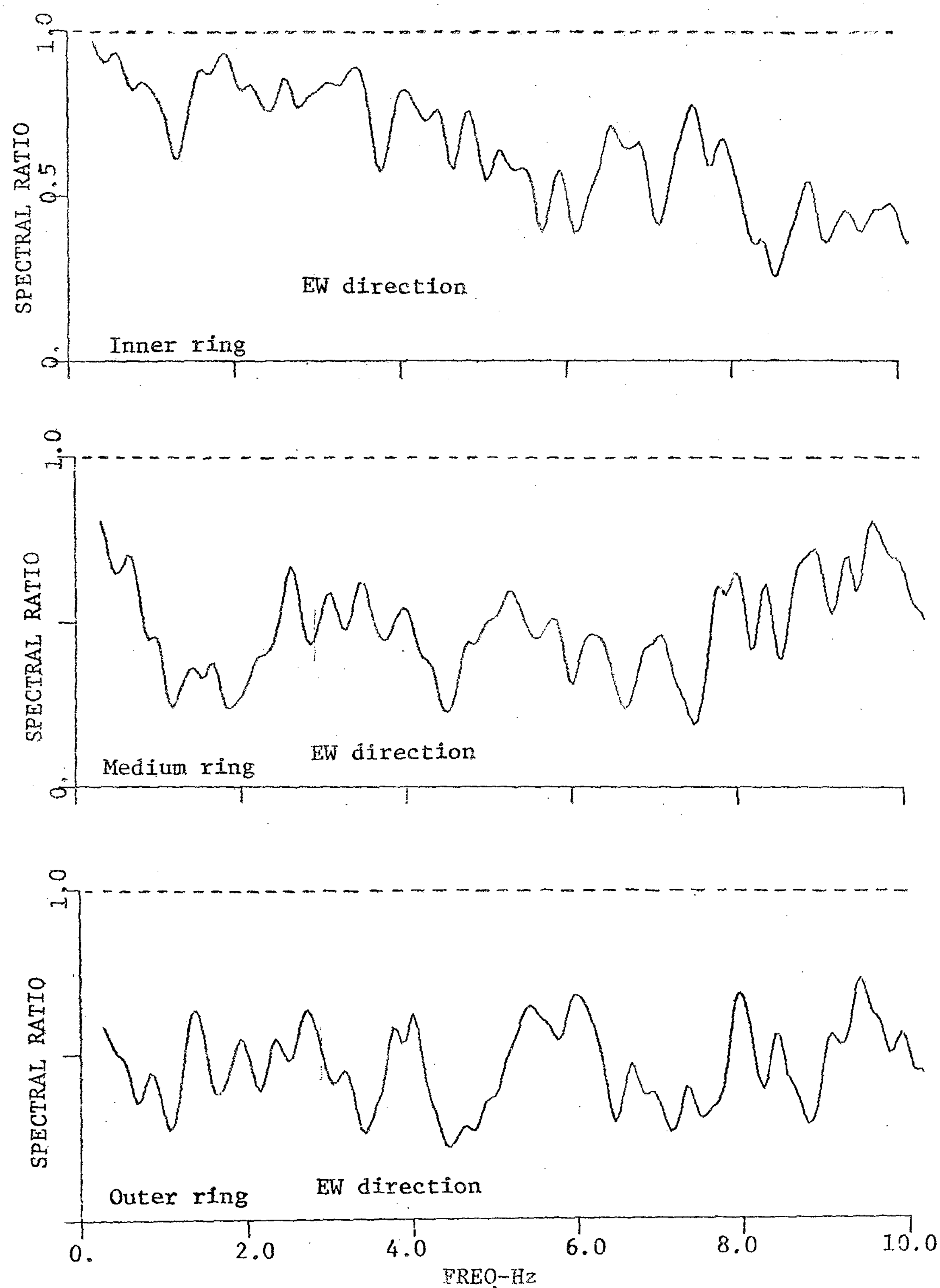

Fig. 9.2 Spectral ratio RTAU in the EW direction: Event 5

Earthquake: Nov. 14, 1980

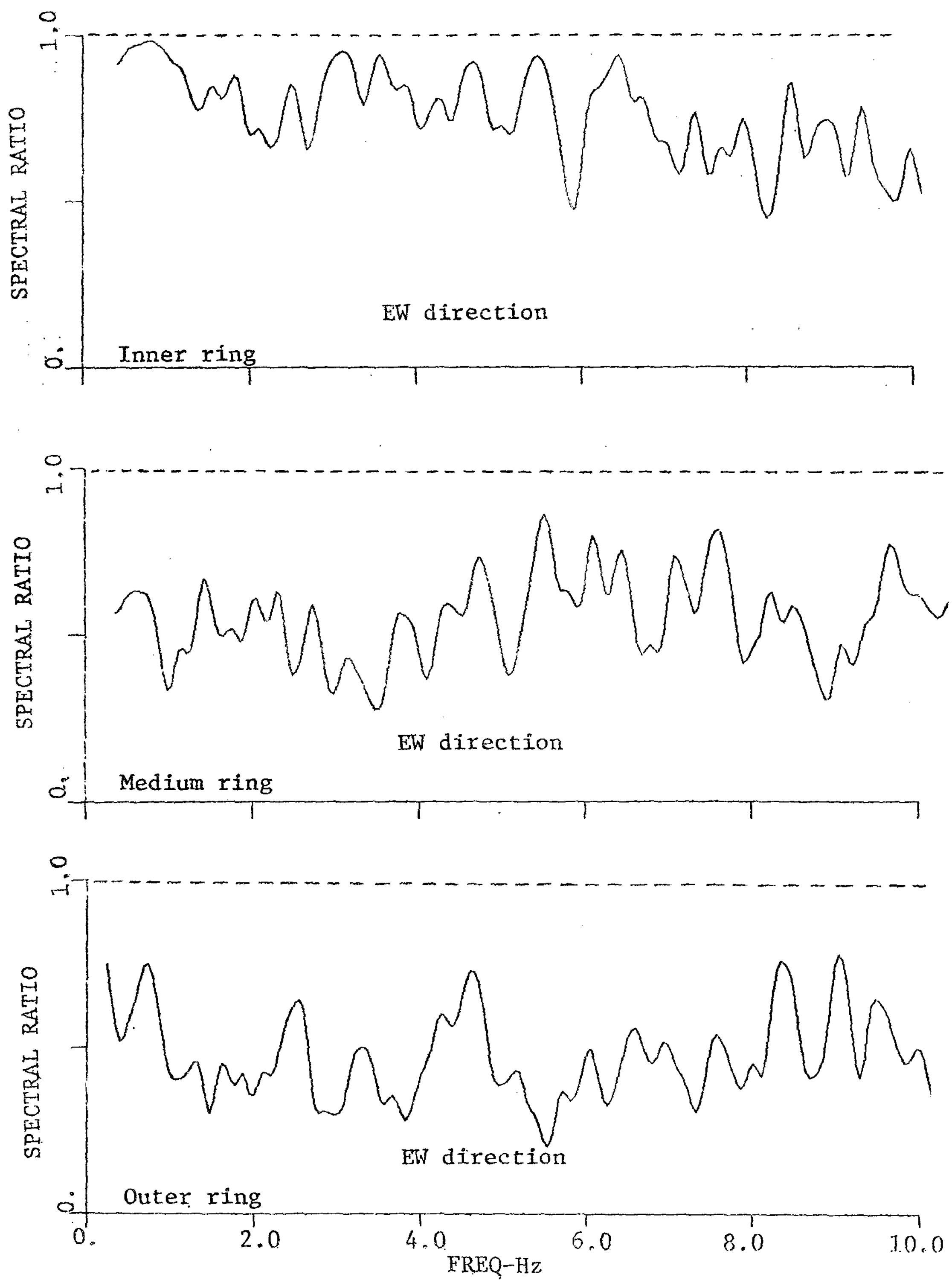

Fig. 9.3 Spectral ratio RTAU in the EW direction: Event 2

Earthquake: Jan. 29, 1981
(radial direction)

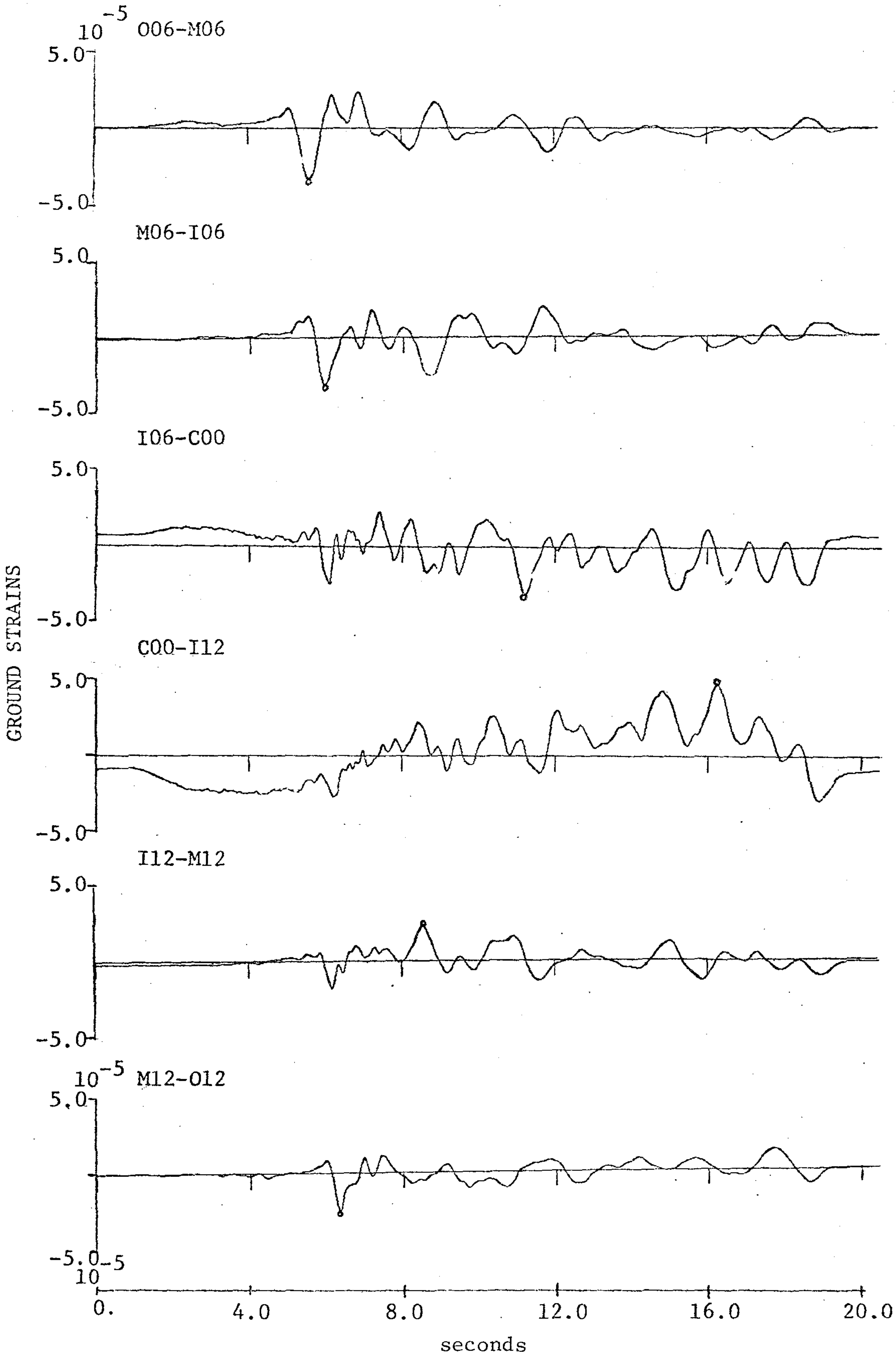

Fig. 9.4 Ground strains between selected pairs of elements: Event 5

APPENDIX A

3-Component Data Listing of Station I03 of Earthquake of January 29, 1981 (Event 5)

TAIWAN EARTHQUAKE(SMART 1) JAN 29,1981

STATION NO. I03 COMPONENT: EAST-WEST

INSTRUMENT AND BASELINE CORRECTED DATA IN MM/SEC/SEC, AT EQUAL-SPACED INTERVAL OF 0.01 sec.

0	0	0	0	0	0	0	0	0	0	0	0	0	0	0	0	0	0	0	0
0	0	0	0	0	0	0	0	0	0	0	0	0	0	0	0	0	0	0	0
0	0	0	0	0	0	0	0	0	0	0	0	0	0	0	0	0	0	0	0
0	0	0	0	0	0	0	0	0	0	0	0	0	0	0	-1	-1	-1	-1	-1
-1	-1	-1	-1	-1	-1	-1	-1	-1	-1	-1	-1	-1	-1	-1	-1	-1	-1	-1	-1
-11	-1	-1	-1	-1	-1	8	-1	-1	-1	-1	-11	-1	-1	-1	-1	-1	-1	-1	-1
-1	-1	-1	-1	-1	-1	-11	-11	-1	-1	8	8	-1	-1	-1	-11	-11	-1	-1	8
-1	-1	-11	-21	-21	-11	-11	-1	18	38	28	8	-1	-21	-21	-11	-1	-1	-1	8
8	18	8	-1	-1	-1	8	8	-1	-11	-31	-21	-1	-1	8	-1	-1	-1	-1	-1
-1	-1	-1	-1	-1	-1	-1	-1	-1	-1	-1	8	8	8	-1	-1	-1	-1	-1	8
28	48	58	38	-1	-31	-71	-101	-111	-81	-31	-1	28	18	-11	-51	-81	-81	-51	-21
-11	-1	-1	-1	-21	-41	-41	-21	-1	8	28	48	48	38	-1	-21	-51	-51	-41	-1
18	38	28	38	48	58	48	28	18	-1	-21	-41	-31	-31	-51	-71	-31	8	68	78
38	-1	-11	-11	-1	8	28	28	8	-1	-1	8	28	68	68	38	-1	-31	-11	-1
-1	8	58	98	88	38	-1	-21	-51	-91	-111	-91	-31	-1	38	38	8	-11	-51	-81
-121	-161	-191	-181	-131	-81	-31	-11	-1	18	68	128	188	198	148	68	-1	-51	-71	-61
-21	28	108	158	168	149	109	79	59	39	0	-40	-90	-110	-130	-150	-160	-120	-60	0
39	49	29	0	-10	-30	-40	-60	-70	-50	-30	0	0	0	19	49	59	49	9	-30
-70	-60	0	89	149	129	79	29	0	0	-10	-40	-90	-100	-70	-10	39	79	79	29
-20	-80	-100	-70	-20	0	0	-20	-20	0	9	19	19	39	69	89	79	69	29	0
-20	-50	-50	-30	9	79	139	159	129	59	-10	-90	-130	-120	-70	-30	-10	-10	-10	-20
-20	-20	0	0	0	0	0	29	49	39	0	-30	-60	-50	0	39	69	59	9	-20
-59	-99	-129	-119	-89	-69	-49	-29	-19	0	20	50	50	20	0	0	20	50	90	120
140	120	80	30	0	-39	-79	-99	-79	-49	-19	-19	-29	-59	-59	-19	30	60	100	40
-19	-79	-99	-69	-29	0	20	40	90	130	150	110	20	-59	-129	-159	-139	-99	-59	-39
-39	-49	-49	-39	-19	0	10	20	30	20	10	0	-19	-29	-9	30	110	160	170	120
60	0	-49	-89	-89	-49	0	60	80	50	10	-9	-9	0	20	50	80	110	150	160
180	200	240	280	310	330	330	320	300	260	220	150	50	-19	-99	-159	-239	-369	-479	-569
-589	-579	-539	-479	-399	-269	-158	-88	-48	-8	51	151	251	341	371	361	331	291	291	301
281	231	191	151	131	111	121	171	231	281	281	251	191	131	91	51	11	-18	-88	-178
-258	-348	-408	-438	-438	-418	-278	-18	291	501	501	361	151	-8	-138	-228	-348	-478	-598	-678
-718	-718	-708	-728	-748	-758	-688	-468	-158	41	61	1	-48	-18	81	251	411	501	521	501
501	521	561	561	511	431	361	311	291	251	211	111	-8	-188	-368	-468	-478	-448	-448	-498
-568	-608	-598	-508	-348	-158	-8	61	91	81	61	41	1	-48	-138	-158	-68	91	271	421
521	611	661	671	671	651	571	441	271	151	51	1	-68	-158	-238	-338	-418	-458	-468	-418
-318	-198	-58	31	81	81	61	41	31	31	51	71	91	111	121	111	91	51	1	-28
-68	-118	-158	-178	-188	-178	-148	-118	-78	-78	-88	-118	-138	-138	-98	-28	21	81	91	81
51	51	91	151	211	241	251	231	221	191	171	151	151	181	231	291	331	341	351	351
331	281	171	11	-108	-198	-228	-228	-218	-198	-208	-218	-248	-268	-268	-258	-218	-138	-38	41
101	111	51	-8	-88	-138	-168	-208	-248	-298	-318	-298	-238	-178	-148	-118	-68	1	91	161
171	121	11	-68	-118	-88	-8	61	141	191	231	281	331	361	381	391	401	370	280	110
-139	-369	-459	-439	-349	-229	-139	-79	-59	-29	10	80	120	120	70	10	0	0	30	70
90	80	90	110	150	160	140	80	0	-69	-149	-199	-209	-189	-179	-189	-199	-229	-259	-289
-299	-279	-219	-139	-29	70	180	250	290	320	300	250	190	120	100	170	240	290	350	360
350	350	350	370	400	410	370	300	210	120	50	0	-49	-119	-189	-239	-289	-309	-289	-229
-149	-59	0	20	10	-19	-59	-79	-79	-79	-79	-89	-119	-169	-219	-279	-299	-279	-229	-179
-119	-59	-19	0	30	60	70	70	30	0	-39	-59	-59	-39	-19	-9	0	10	40	70
100	120	110	60	0	-99	-179	-239	-269	-269	-259	-229	-189	-119	-39	0	20	0	-19	-59
-79	-49	0	20	30	20	0	-9	0	0	40	90	130	170	200	220	220	220	220	190
150	110	80	70	40	0	-39	-129	-199	-249	-279	-299	-309	-289	-249	-179	-89	0	10	10

-9	-39	-79	-120	-170	-210	-220	-190	-110	-30	0	19	29	39	49	49	49	9	-20	-80
-110	-100	-60	-10	39	89	119	119	89	39	0	0	0	0	9	9	19	29	49	89
139	199	239	269	269	239	219	219	219	249	269	289	289	289	269	249	219	179	119	79
29	0	-50	-90	-130	-150	-170	-200	-220	-220	-210	-180	-140	-100	-90	-100	-130	-140	-140	-130
-130	-140	-160	-160	-160	-140	-100	-90	-80	-80	-70	-30	0	49	99	119	109	79	49	0
-10	-40	-60	-80	-110	-130	-130	-110	-60	0	69	129	169	179	169	159	149	129	99	69
29	19	19	39	69	99	129	139	149	149	139	129	129	119	109	99	79	79	79	89
99	119	119	119	129	129	99	59	9	-20	-40	-40	-20	0	0	0	-20	-40	-60	-50
-30	0	0	19	19	0	-20	-60	-100	-120	-130	-130	-150	-180	-220	-250	-270	-270	-230	-200
-140	-80	-60	-40	-20	0	39	79	109	129	129	129	99	59	9	0	-20	-40	-50	-80
-110	-140	-150	-160	-150	-140	-129	-119	-99	-69	-39	-19	0	0	0	-19	-39	-59	-79	-69
-49	-19	0	40	70	90	110	110	100	70	40	10	0	-19	-29	-29	-29	-29	-29	-29
-39	-39	-29	-19	0	10	30	60	80	100	110	120	130	140	150	160	150	120	110	100
100	90	80	50	10	-19	-79	-139	-189	-219	-219	-219	-209	-169	-119	-69	-29	-19	-19	-19
-19	-9	-9	0	0	0	0	-9	0	0	10	20	20	20	20	20	20	30	50	70
80	70	70	70	80	100	120	130	120	120	110	110	100	90	70	60	50	30	10	0
-29	-59	-79	-99	-109	-119	-109	-89	-39	0	10	30	30	30	30	30	30	30	30	20
10	0	0	0	10	20	10	0	-49	-99	-129	-129	-119	-99	-79	-69	-59	-59	-69	-89
-99	-119	-119	-119	-99	-69	-39	-8	11	51	101	141	181	201	201	181	151	111	81	71
71	71	71	81	71	61	41	21	11	1	1	1	-8	-8	-18	-28	-48	-68	-78	-88
-78	-78	-88	-98	-108	-118	-118	-118	-108	-98	-88	-78	-78	-58	-48	-28	-8	1	31	51
61	71	71	81	91	91	101	101	111	111	111	111	101	81	71	51	21	1	-18	-28
-38	-38	-38	-48	-58	-68	-78	-88	-98	-98	-98	-98	-88	-68	-48	-18	1	21	41	51
51	51	31	31	31	31	31	31	41	51	51	51	41	41	31	11	1	-18	-18	-8
1	51	81	101	101	91	71	61	61	51	41	21	1	1	-18	-28	-38	-48	-58	-58
-48	-48	-38	-28	-28	-18	1	1	31	51	71	91	101	111	111	111	101	101	101	91
61	41	11	1	1	1	-8	-18	-18	-28	-28	-8	1	21	41	41	31	1	-8	-28
-48	-48	-48	-38	-48	-68	-98	-138	-148	-168	-168	-178	-178	-178	-168	-148	-108	-58	-28	-8
-18	-28	-28	-18	-8	1	1	1	11	11	11	1	-8	-48	-78	-108	-118	-128	-138	-148
-168	-168	-168	-168	-148	-128	-118	-108	-88	-78	-68	-68	-68	-68	-58	-48	-18	1	11	51
91	111	131	141	131	131	141	141	151	161	171	171	171	171	171	171	171	161	141	121
111	91	71	51	31	11	1	1	1	1	1	1	1	1	1	11	11	21	31	31
41	51	51	61	71	81	101	111	111	121	121	131	141	161	171	171	171	161	151	131
111	81	51	11	1	-18	-18	-18	-18	-18	-28	-38	-68	-78	-88	-98	-88	-88	-88	-108
-128	-148	-159	-169	-169	-159	-159	-169	-179	-179	-179	-159	-139	-109	-89	-79	-79	-89	-89	-89
-99	-109	-109	-129	-149	-169	-169	-169	-149	-129	-89	-49	-9	10	30	40	50	50	50	40
20	0	0	0	20	50	90	120	160	170	190	200	180	160	140	120	100	100	100	90
80	60	40	20	0	0	0	0	0	-9	-19	-29	-29	-19	0	0	0	10	10	20
30	39	39	39	49	59	69	79	89	79	69	59	39	19	9	9	0	0	0	0
0	0	9	19	9	9	0	0	-20	-20	-20	-10	0	0	9	9	0	0	0	-10
-20	-30	-40	-50	-40	-20	0	0	9	9	0	-20	-40	-50	-70	-80	-80	-80	-80	-80
-90	-91	-91	-91	-91	-91	-81	-81	-71	-61	-51	-21	-1	-1	18	28	28	28	38	48
58	68	78	88	88	98	98	98	98	108	108	108	98	98	98	98	98	88	78	58
38	18	-1	-11	-31	-51	-81	-101	-121	-141	-151	-161	-171	-161	-161	-151	-152	-142	-142	-132
-112	-82	-52	-22	-12	-2	-2	-2	-2	7	7	17	7	7	-2	-2	-2	-2	-2	-2
-2	-2	-2	-2	-2	-2	-2	-2	-2	-2	-2	-2	-2	-2	-2	-2	-2	-2	-2	7
-2	-2	-2	-2	17	47	77	107	137	156	166	156	146	126	106	76	56	26	-3	-3
-13	-23	-13	-3	-3	6	26	46	56	56	46	36	26	6	-3	-23	-33	-63	-83	-103
-123	-153	-163	-183	-193	-203	-203	-203	-193	-183	-173	-153	-133	-123	-103	-83	-73	-63	-43	-43
-23	-23	-23	-23	-24	-24	-34	-34	-34	-24	-14	-4	-4	-4	-4	5	25	45	65	75
85	95	95	95	105	105	105	95	85	75	75	75	75	85	85	95	115	125	135	145
145	145	135	125	125	115	115	105	115	115	115	115	115	95	85	55	45	15	-4	-4
-24	-34	-34	-34	-44	-54	-54	-65												

TAIWAN EARTHQUAKE(SMART 1) JAN 29, 1981

STATION NO. I03 COMPONENT: NORTH-SOUTH

INSTRUMENT AND BASELINE CORRECTED DATA IN MM/SEC/SEC. AT EQUAL-SPACED INTERVAL OF 0.01 SEC.

1	1	1	1	1	1	1	1	1	1	1	1	1	1	1	1	1	1	1	1
1	1	1	1	1	1	1	1	1	1	1	1	1	1	1	1	1	1	1	1
1	1	1	1	1	1	1	1	1	1	1	1	1	1	1	1	1	1	1	1
1	1	1	1	1	1	1	1	1	1	1	1	1	1	1	1	2	2	2	2
2	2	2	2	2	2	2	2	2	2	2	2	2	2	2	2	2	2	2	2
2	2	2	2	-7	2	2	2	2	2	2	2	2	2	2	2	2	2	2	2
2	2	2	2	2	2	2	2	2	2	2	2	2	2	12	12	2	2	-7	-7
-7	2	2	2	2	2	2	-17	-27	-17	-7	2	22	22	2	-7	-17	-17	-7	2
2	2	-7	-7	2	2	12	12	22	32	22	2	2	-7	-7	2	2	42	62	32
12	2	2	2	2	2	-7	-17	-17	2	-7	-17	-27	-7	2	2	2	-17	-37	-57
-67	-57	-37	-7	2	2	2	12	2	-7	-27	-37	-27	-7	22	52	52	22	2	-7
2	2	2	42	82	72	22	2	-17	-37	-47	-57	-27	-17	2	2	12	22	32	32
12	2	-27	-67	-77	-57	-17	2	52	92	102	52	2	2	22	12	-27	-67	-47	2
32	42	52	72	82	42	2	-37	-67	-87	-97	-97	-77	-37	2	2	-17	-57	-67	-57
-47	-67	-77	-57	-7	22	32	2	-17	-17	-7	-7	-7	2	2	12	2	2	2	23
13	3	13	73	133	173	163	133	93	53	3	-26	-46	-26	-6	-6	-16	-16	-6	23
43	33	3	-16	-36	-66	-106	-146	-156	-136	-86	-16	33	93	73	3	-36	-56	-56	-56
-56	-36	-6	33	53	43	53	53	53	43	13	-6	-36	-56	-36	3	33	73	83	73
43	13	3	-6	-16	-6	3	33	63	83	63	13	-16	-36	-56	-66	-66	-36	3	43
63	53	23	3	3	53	113	133	123	113	83	23	-26	-86	-126	-146	-146	-126	-66	-6
13	24	24	14	4	-45	-95	-145	-165	-145	-65	14	94	114	104	84	64	54	44	44
44	34	24	34	44	44	44	54	74	84	74	44	4	-55	-95	-95	-75	-85	-105	-95
-65	-45	-35	-45	-45	-25	-15	-5	4	4	4	44	94	114	84	34	4	-5	-15	-55
-85	-115	-105	-94	-64	-44	-24	-14	5	25	55	25	-14	-34	-14	5	5	-4	-24	-24
-24	-24	-34	-34	-34	-44	-34	-4	25	75	75	45	15	5	-14	-34	-34	-34	-34	-34
-34	-24	-4	5	25	35	45	85	155	215	225	176	116	56	6	-23	-63	-63	-23	6
36	46	46	16	-13	-83	-163	-233	-293	-323	-313	-283	-243	-203	-163	-153	-163	-183	-213	-223
-233	-233	-213	-153	-53	6	66	126	206	286	336	336	316	287	237	157	67	17	7	7
47	117	147	127	77	7	-62	-152	-252	-362	-432	-492	-522	-532	-492	-432	-342	-212	-62	77
207	307	417	517	607	657	657	617	557	497	467	478	508	558	608	658	678	688	718	748
788	808	808	808	828	858	858	788	588	278	-1	-211	-371	-511	-631	-701	-741	-761	-761	-731
-721	-751	-791	-791	-751	-651	-460	-200	69	239	319	369	399	369	279	179	99	19	-60	-150
-210	-230	-250	-300	-370	-430	-470	-520	-590	-650	-700	-740	-750	-680	-480	-190	59	199	219	169
109	10	-99	-219	-309	-319	-249	-129	0	80	150	170	110	10	-39	-39	10	60	120	120
80	30	0	-19	-9	30	170	300	410	490	580	650	680	670	640	591	501	391	251	131
41	11	-18	-38	-58	-78	-108	-158	-208	-258	-318	-368	-398	-418	-418	-428	-428	-428	-428	-428
-438	-468	-498	-528	-548	-538	-488	-408	-308	-218	-157	-117	-117	-157	-187	-197	-157	-97	-7	62
142	192	222	222	232	242	272	322	362	402	442	452	462	422	282	112	-27	-97	-97	-57
-7	32	112	172	202	212	233	283	323	323	303	273	233	183	133	63	13	-36	-66	-86
-86	-56	-26	13	43	73	93	123	163	183	153	103	23	-36	-116	-186	-236	-286	-326	-336
-336	-316	-286	-226	-176	-125	-105	-95	-115	-125	-155	-165	-185	-205	-235	-285	-325	-365	-405	-415
-345	-205	-115	-115	-175	-215	-225	-205	-155	-65	14	124	214	254	264	254	234	234	244	264
254	244	234	194	154	104	54	14	-5	14	74	175	265	335	385	425	435	425	415	415
425	445	455	465	455	395	295	195	95	15	-24	-84	-134	-164	-164	-154	-144	-124	-104	-84
-94	-94	-94	-94	-64	-4	55	125	165	185	165	125	65	15	-14	-54	-94	-144	-174	-204
-204	-184	-104	5	95	155	165	125	45	-23	-103	-163	-183	-173	-123	-73	-23	6	6	-13
-23	-63	-123	-183	-213	-243	-243	-243	-233	-223	-213	-213	-223	-223	-203	-183	-123	-53	6	46
86	96	96	86	86	116	156	206	236	236	236	236	236	236	236	226	216	196	166	106
56	16	6	-23	-33	-53	-63	-73	-83	-103	-123	-143	-163	-183	-173	-163	-163	-173	-183	-203
-223	-233	-233	-233	-213	-183	-123	-63	-3	36	76	126	166	186	186	136	46	-33	-113	-133

-113	-63	-3	36	86	116	106	76	16	-33	-113	-173	-213	-243	-263	-253	-223	-173	-103	-43
-3	-3	-3	-3	-23	-43	-53	-33	-13	6	16	56	106	176	236	266	286	286	266	236
196	156	126	106	76	46	16	16	-3	-13	-33	-43	-53	-63	-63	-63	-43	-33	-33	-33
-43	-53	-73	-93	-103	-113	-93	-73	-63	-43	-13	16	56	106	136	136	126	106	76	36
6	-13	-33	-43	-53	-43	-33	-3	16	16	36	56	66	56	46	46	36	26	26	16
16	26	46	76	96	126	136	146	156	156	146	136	136	146	146	136	126	96	76	46
36	26	16	16	16	16	26	36	46	46	26	6	-33	-73	-93	-93	-103	-83	-73	-53
-63	-83	-113	-133	-153	-163	-163	-153	-133	-103	-83	-83	-93	-103	-103	-103	-103	-84	-54	-14
15	15	35	35	25	15	5	-14	-44	-54	-44	-24	-14	-24	-24	-34	-44	-64	-94	-134
-184	-214	-234	-234	-234	-214	-194	-164	-134	-114	-104	-104	-84	-64	-34	-4	-4	5	-4	-24
-34	-14	5	35	85	145	195	235	265	285	295	285	265	235	205	185	195	215	245	275
295	295	275	235	195	155	115	85	55	45	45	45	55	65	54	44	14	4	-35	-65
-105	-145	-175	-205	-235	-255	-265	-245	-215	-195	-165	-135	-125	-105	-95	-85	-75	-55	-25	14
54	114	164	194	204	204	204	204	194	184	174	154	124	84	24	-15	-75	-115	-115	-125
-105	-85	-65	-55	-55	-65	-75	-75	-65	-55	-45	-35	-35	-45	-75	-95	-115	-125	-115	-75
-45	-15	-5	4	-5	-15	-55	-86	-116	-126	-136	-136	-146	-146	-126	-116	-86	-56	-36	-16
-6	3	13	13	13	13	13	-6	-36	-76	-106	-126	-116	-86	-26	13	73	113	133	133
133	133	143	143	153	163	163	153	123	93	63	53	53	63	83	113	143	173	193	203
213	223	223	223	203	163	123	83	43	13	-16	-66	-96	-116	-126	-116	-86	-56	-16	-6
-6	-16	-36	-66	-96	-126	-156	-176	-196	-196	-196	-166	-146	-126	-126	-126	-116	-106	-86	-66
-46	-26	-16	-16	-16	-6	12	22	52	92	132	152	162	162	152	122	82	52	32	12
12	12	12	12	12	12	2	-7	-27	-37	-37	-37	-37	-47	-57	-57	-47	-27	-7	12
22	32	22	12	-7	-27	-27	-7	2	12	12	-7	-17	-37	-47	-57	-57	-57	-47	-37
-17	12	22	32	22	12	-17	-37	-67	-87	-87	-87	-87	-77	-77	-57	-47	-37	-37	-37
-37	-47	-57	-77	-97	-107	-107	-87	-67	-27	2	12	42	52	42	42	42	52	52	62
62	62	72	72	72	72	62	52	42	32	12	12	2	-7	-7	-7	2	12	12	12
12	12	12	12	22	52	92	132	152	142	132	112	82	52	12	2	-17	-27	-46	-46
-36	-26	-6	13	13	13	13	13	13	13	13	13	13	13	13	13	13	13	3	3
-6	-6	-6	-6	13	13	13	23	23	13	13	13	13	23	43	53	43	33	13	13
3	-6	-6	-6	-6	-16	-26	-46	-56	-66	-76	-86	-96	-96	-116	-126	-136	-136	-146	-146
-146	-146	-136	-126	-106	-96	-86	-86	-76	-76	-76	-76	-76	-76	-66	-76	-76	-76	-66	-56
-26	3	13	43	53	53	43	24	14	4	-5	-5	-5	14	14	44	84	114	154	184
214	234	244	244	244	234	224	204	184	164	154	144	134	114	84	64	44	24	24	34
44	64	74	74	64	44	14	4	-15	-35	-45	-45	-35	-35	-25	-35	-35	-45	-55	-65
-85	-95	-105	-115	-104	-84	-54	-24	-4	15	15	15	25	25	25	25	15	15	-4	-24
-54	-64	-84	-104	-124	-144	-154	-164	-164	-174	-164	-164	-144	-134	-124	-124	-134	-124	-114	-104
-84	-64	-44	-24	-4	-4	5	5	5	5	5	15	15	16	16	16	16	16	16	16
26	46	56	66	66	56	36	26	16	16	16	16	16	16	16	16	6	6	-3	-3
6	16	16	36	56	76	86	86	86	86	76	66	56	46	36	26	16	16	17	17
17	-2	-22	-42	-62	-62	-52	-32	-2	17	17	17	17	17	-2	-22	-52	-72	-92	-92
-92	-72	-62	-42	-32	-22	-12	-12	-12	-12	-2	-2	-2	-2	-2	-12	-12	-12	-12	-2
7	17	17	28	38	28	28	28	18	18	18	18	28	48	78	98	128	148	158	168
168	168	158	138	128	118	118	118	128	128	128	128	138	158	168	178	188	188	178	168
158	148	138	118	108	98	88	78	58	39	19	19	0	-20	-30	-40	-40	-40	-20	-20
-10	-10	-30	-50	-70	-90	-110	-120	-140	-150	-160	-170	-170	-180	-180	-180	-180	-180	-170	-170
-180	-180	-190	-190	-190	-180	-170	-160	-140	-110	-90	-90	-90	-90	-100	-120	-130	-140	-140	-139
-129	-119	-119	-99	-89	-79	-69	-69	-59	-49	-49	-39	-19	0	10	20	20	20	20	20
20	20	20	20	20	20	10	0	0	10	10	20	20	40	60	80	100	100	100	100
100	100	100	120	140	160	180	200	220	230	230	230	220	200	170	160	150	160	171	181
181	181	171	151	131	101	71	51	31	21	11	1	-18	-18	-28	-28	-38	-58	-78	-98
-118	-128	-138	-148	-148	-148	-148	-138	-128	-118	-108	-98	-88	-88	-88	-88	-78	-68	-58	-48
-38	-38	-38	-38	-38	-38	-38	-38	-38	-58	-68	-68	-78	-78	-68	-58	-38	-18	-8	11
11	1	1	-8	-8	-8	-8	1												

TAIWAN EARTHQUAKE(SMART 1) JAN 29, 1981

STATION NO: I03 COMPONENT: VERTICAL

INSTRUMENT AND BASELINE CORRECTED DATA IN MM/SEC/SEC. AT EQUAL-SPACED INTERVAL OF 0.01 SEC.

-2	-2	-2	-2	-2	-2	-2	-2	-2	-2	-2	-2	-2	-2	-2	-2	-2	-2	-2	-2
-2	-2	-2	-2	-2	-2	-2	-2	-2	-2	-2	-2	-2	-2	-2	-2	-2	-2	-2	-2
-2	-2	-2	-2	-2	-2	-2	-2	-2	-2	-2	-2	-2	-2	-2	-2	-2	-2	-2	-2
-2	-2	-12	-2	-2	-2	-2	-2	-2	-2	-2	-2	-2	-2	-2	-2	-2	-2	-2	7
17	7	-2	-12	-42	-32	-2	17	37	37	17	-2	-12	-32	-52	-62	-42	-2	7	17
7	-2	-2	-12	-32	-42	-52	-62	-42	-2	37	57	67	77	97	97	67	17	-2	-22
-12	-2	37	67	67	47	17	7	-2	7	57	107	137	127	67	-2	-72	-122	-142	-112
-12	67	107	87	37	-2	-2	-12	-22	-42	-72	-82	-62	-22	-2	-2	37	77	117	137
97	-2	-92	-92	-62	-62	-72	-82	-92	-82	-92	-82	-32	-2	-2	-12	-2	37	37	-2
-62	-32	37	107	117	77	-2	-112	-202	-222	-222	-202	-102	37	207	297	307	257	147	-12
-152	-162	-52	67	167	207	207	127	7	-52	-72	-52	-22	-2	27	77	57	-2	-62	-62
-72	-142	-142	-2	157	207	127	67	47	7	-92	-232	-322	-352	-322	-242	-152	-12	127	247
307	297	257	237	157	-22	-232	-322	-282	-192	-112	-112	-102	-2	97	117	57	37	97	157
117	37	17	87	137	97	7	-42	-52	-32	-42	-102	-122	-62	47	177	217	257	267	257
167	-32	-302	-442	-432	-302	-132	47	227	347	357	247	77	-72	-202	-262	-272	-242	-202	-152
-102	-62	-2	77	187	217	157	17	-32	-22	-32	-82	-82	-22	17	17	-12	-52	-42	-12
17	77	107	107	107	97	47	-2	-62	-72	-52	-42	-72	-132	-152	-102	-2	77	107	77
27	-2	-22	-42	-72	-102	-52	17	97	137	127	47	-22	-52	-12	27	57	7	-12	-32
-12	-22	-82	-152	-142	-62	17	97	147	157	117	77	47	47	17	-12	-82	-112	-122	-122
-62	7	77	117	127	127	107	67	27	-2	-22	-62	-72	-82	-92	-112	-112	-52	37	137
197	207	177	97	-12	-112	-142	-132	-92	-32	7	17	-2	-2	7	57	87	77	77	107
127	77	-2	-52	-102	-122	-132	-102	-62	-22	-2	27	27	7	17	47	37	-12	-72	-72
-52	-32	-2	37	107	157	157	117	27	-52	-122	-102	-22	17	37	57	117	167	147	57
-2	-62	-92	-92	-92	-92	-92	-51	28	148	168	38	-111	-201	-201	-181	-141	-61	8	98
218	298	318	228	78	-41	-151	-221	-281	-281	-231	-161	-101	-41	8	78	128	118	88	48
38	18	-51	-161	-191	-151	-71	48	198	308	328	298	278	248	148	-1	-151	-161	-121	-111
-121	-91	-11	38	68	88	108	108	88	78	58	8	-21	-81	-151	-221	-261	-241	-161	-21
68	78	28	-1	8	-1	-31	-31	18	108	138	118	128	148	88	-31	-121	-121	-121	-151
-151	-91	-11	18	68	138	178	118	8	-31	-71	-131	-231	-271	-241	-191	-91	38	218	328
308	228	138	38	-21	-51	-71	-121	-221	-251	-191	-121	-111	-101	-51	-1	58	118	188	208
148	-1	-131	-111	-1	88	48	-1	-1	78	158	208	188	78	-1	-21	-1	48	98	109
49	-40	-110	-100	-30	29	49	19	0	0	9	9	-30	-120	-190	-220	-220	-220	-180	-90
0	9	-30	-100	-90	-10	39	39	9	0	9	0	-40	-120	-150	-120	-50	-20	-10	0
9	9	9	29	79	109	99	79	79	129	189	169	99	69	69	79	79	69	59	19
0	-60	-110	-150	-150	-110	-50	-20	9	89	159	169	79	-20	-80	-70	-40	0	49	139
189	159	49	-30	-60	-50	-50	-50	0	39	89	109	89	49	9	-10	-40	-30	-20	-10
-20	-30	-60	-90	-110	-100	-50	0	49	109	119	89	39	0	-10	-10	-30	-70	-100	-100
-80	-40	0	-10	-50	-120	-180	-190	-180	-160	-140	-90	-30	9	49	69	49	0	-20	-30
-10	19	79	129	150	150	140	120	70	20	0	-39	-79	-89	-69	-29	0	20	60	80
50	10	-9	-29	-49	-69	-59	-19	10	30	40	70	120	170	190	180	120	20	-39	-139
-209	-219	-169	-79	-9	20	60	100	130	120	80	30	0	-39	-69	-69	-59	-39	-29	-39
-59	-79	-99	-129	-129	-89	-39	-19	0	40	110	170	170	130	70	20	-9	-59	-89	-99
-69	-9	40	100	110	80	40	20	40	40	30	0	-39	-89	-129	-129	-109	-79	-59	-29
0	60	110	120	110	80	30	-9	-69	-109	-109	-89	-39	0	20	20	10	10	20	10
20	30	30	20	10	10	10	10	10	10	40	80	120	130	100	60	10	0	0	0
-19	-39	-29	0	30	50	30	0	-39	-89	-129	-149	-149	-139	-109	-69	-9	10	10	0
0	0	0	10	20	30	20	20	20	20	40	70	80	60	30	40	50	40	30	40
50	60	70	70	70	60	40	10	0	-39	-59	-59	-29	0	20	40	50	60	60	50
50	40	10	-19	-29	-9	0	0	0	0	0	0	0	10	20	40	40	50	60	70
50	20	0	0	0	0	0	0	0	0	0	-9	-39	-69	-79	-89	-89	-69	-39	-19

-29	-59	-69	-49	-29	-49	-69	-79	-79	-69	-49	-9	20	60	70	60	10	-19	-79	-99
-99	-89	-79	-79	-69	-39	-19	-9	0	0	0	10	0	0	0	0	0	-9	-9	0
0	20	30	10	0	-9	0	0	0	0	10	10	0	-9	-29	-29	0	10	29	39
69	79	69	49	19	0	-10	-40	-50	-40	-20	0	9	19	19	29	29	39	29	19
0	-30	-30	-30	-30	-10	0	19	39	49	59	69	69	49	19	0	-10	-30	-30	-30
-20	0	0	29	69	79	79	59	39	9	0	0	0	-10	-30	-40	-50	-50	-40	-30
-10	0	9	29	49	39	9	-10	-30	-20	-10	0	0	0	9	19	19	9	9	9
9	9	29	49	49	39	39	39	39	19	9	0	-30	-50	-70	-80	-80	-70	-50	-30
0	0	-10	-30	-60	-70	-70	-70	-60	-40	-20	0	0	9	19	29	39	29	9	9
0	0	0	-10	-30	-40	-40	-20	-10	0	9	29	59	79	89	79	59	49	29	19
9	0	0	-20	-30	-20	0	9	19	29	28	28	38	48	48	28	18	8	-1	-11
-11	-1	8	28	38	48	48	38	28	18	-1	-1	-1	-1	8	18	18	18	18	18
8	8	8	-1	8	8	8	-1	-11	-51	-61	-61	-61	-71	-71	-61	-41	-11	-1	8
-1	-1	-21	-31	-31	-41	-51	-61	-71	-61	-41	-21	-21	-11	-1	-1	18	38	38	48
28	8	-1	-1	-1	-11	-21	-21	-21	-11	-11	-1	-1	-21	-31	-41	-51	-51	-41	-31
-31	-21	-11	-11	-1	-1	-1	-1	-1	-1	-1	-1	-11	-31	-41	-51	-51	-51	-31	-1
8	18	38	48	38	38	28	18	8	-1	-1	8	18	28	38	58	78	98	88	58
18	-1	-1	-1	-1	8	8	18	38	38	38	18	-1	-1	-11	-11	-1	8	8	8
18	48	68	68	48	38	18	8	8	8	8	8	8	18	28	28	28	18	8	8
8	8	-1	-1	-1	-1	-1	-1	8	8	-1	-11	-31	-41	-51	-51	-31	-21	-11	-11
-1	-1	-1	-1	-1	-1	-11	-21	-41	-51	-61	-71	-61	-61	-61	-51	-41	-31	-21	-11
-1	-1	-1	-1	-11	-11	-11	-11	-21	-21	-11	-1	-1	-11	-21	-31	-31	-21	-11	-1
-1	-11	-11	-1	-1	8	8	8	18	28	38	48	38	28	18	8	-1	-1	-1	-1
18	28	48	48	38	28	18	8	-1	-1	-1	-1	-1	-1	8	18	28	18	18	18
8	18	18	18	8	-1	-1	-1	-11	-11	-11	-11	-1	-1	-1	8	18	28	38	38
28	8	-1	-1	-11	-21	-21	-21	-21	-1	-1	8	8	8	8	-1	-1	-1	-21	-41
-41	-31	-21	-11	-11	-11	-1	-1	-1	-21	-41	-61	-61	-61	-51	-41	-31	-31	-21	-21
-21	-11	-1	-11	-21	-21	-21	-11	-1	-1	8	8	8	8	18	18	18	18	28	48
68	78	78	58	38	18	8	8	8	18	28	38	48	58	58	48	38	8	-1	-1
-1	-1	-1	8	28	38	48	48	38	28	28	28	28	28	18	8	-1	-1	-21	-31
-41	-41	-31	-31	-20	-10	0	-10	-10	-10	-20	-20	-20	-20	-20	-20	-30	-30	-30	-20
-10	0	0	0	0	-10	-30	-50	-60	-60	-50	-40	-20	-20	-10	0	-10	-20	-20	-30
-30	-30	-20	-10	0	0	9	9	19	9	9	9	9	0	-10	-30	-30	-30	-20	0
0	19	29	19	9	9	0	0	0	0	0	9	0	0	0	9	9	19	19	19
29	9	9	19	29	29	29	29	29	19	19	19	29	29	19	9	9	9	9	0
0	0	0	9	9	9	9	9	9	9	9	9	9	20	20	10	10	0	0	-9
-19	-29	-29	-19	-19	-9	0	0	10	20	30	20	10	0	-9	-29	-39	-39	-39	-49
-49	-39	-29	-19	-9	-9	-9	-19	-29	-29	-29	-29	-29	-39	-39	-29	-19	0	0	0
10	20	20	10	0	0	-9	-9	-19	-9	-9	0	0	10	10	0	0	0	0	0
0	0	0	0	0	0	0	10	20	30	40	40	40	30	20	10	0	0	0	0
10	10	20	40	50	60	70	80	70	60	40	40	30	30	30	21	21	11	11	11
1	1	1	1	-8	-18	-18	-8	-18	-28	-38	-38	-48	-58	-58	-58	-48	-38	-38	-28
-28	-28	-28	-28	-38	-38	-38	-38	-18	-18	-18	-28	-28	-28	-18	-8	1	1	1	1
1	11	11	11	11	1	11	11	1	1	1	1	11	11	11	11	11	11	11	11
1	1	1	1	-8	1	1	1	1	11	11	11	21	21	21	21	11	11	21	21
21	21	21	21	21	21	21	31	31	31	31	21	11	1	1	1	1	11	11	11
11	11	11	1	1	1	11	11	11	11	1	1	1	1	1	1	1	1	1	11
1	1	1	1	1	1	1	1	-8	-8	-8	1	1	2	12	12	12	12	12	12
22	22	22	22	22	22	12	12	12	22	22	22	12	12	2	2	2	2	2	2
2	2	-7	-7	-7	-17	-17	-7	2	2	-7	-17	-27	-27	-27	-27	-17	-17	-7	-7
2	2	2	2	2	-7	-17	-27	-37	-37	-47	-47	-47	-37	-37	-27	-27	-27	-37	-47
-47	-57	-57	-47	-47	-37	-27	-17	-7	2	2	2	2	2	2	2	-7	-7	-17	-7
-7	2	2	2	2	2	2	2												

APPENDIX B

Time History of Station I03

(see opposite page)

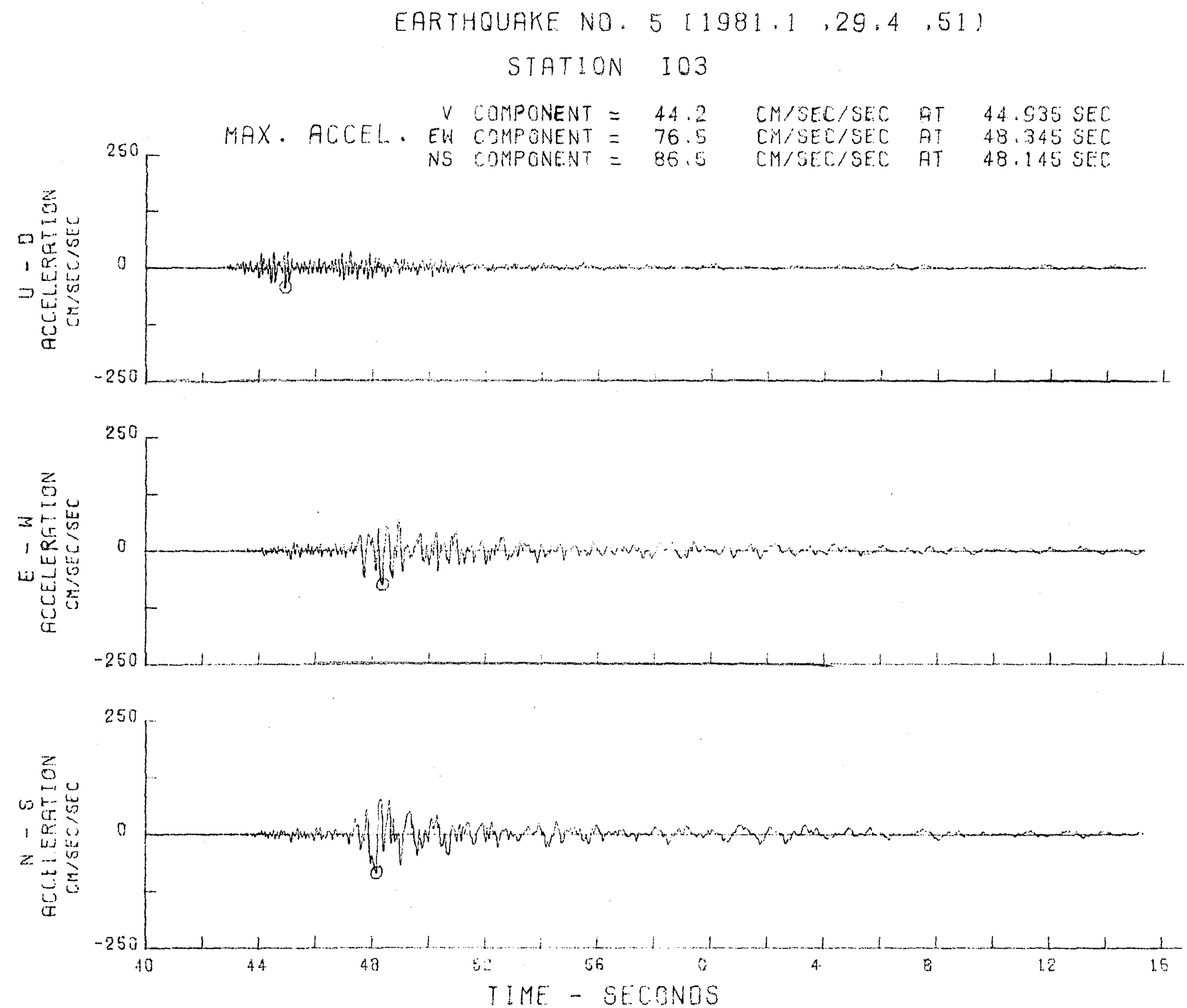

EARTHQUAKE NO. 5 (1981.1 ,29.4 ,51)
STATION I03
MAX. ACCEL. V COMPONENT = 44.2 CM/SEC/SEC AT 44.935 SEC
EW COMPONENT = 76.5 CM/SEC/SEC AT 48.345 SEC
NS COMPONENT = 86.5 CM/SEC/SEC AT 48.145 SEC
U - D ACCELERATION CM/SEC/SEC
E - W ACCELERATION CM/SEC/SEC
N - S ACCELERATION CM/SEC/SEC
250
0
-250
40
44
48
52
56
0
4
8
12
16
TIME - SECONDS

APPENDIX C

Calculated Velocity and Displacement of NS Component of Station I03

(see opposite page)

TAIWAN EARTHQUAKE 1/29/81

STATION I03
COMPONENT NS

MAXIMUM ACCELERATION	85.4	CM/SEC/SEC	AT	8.15	SECONDS
MAXIMUM VELOCITY	13.7	CM/SEC	AT	8.20	SECONDS
MAXIMUM DISPLACEMENT	-2.05	CM	AT	8.00	SECONDS

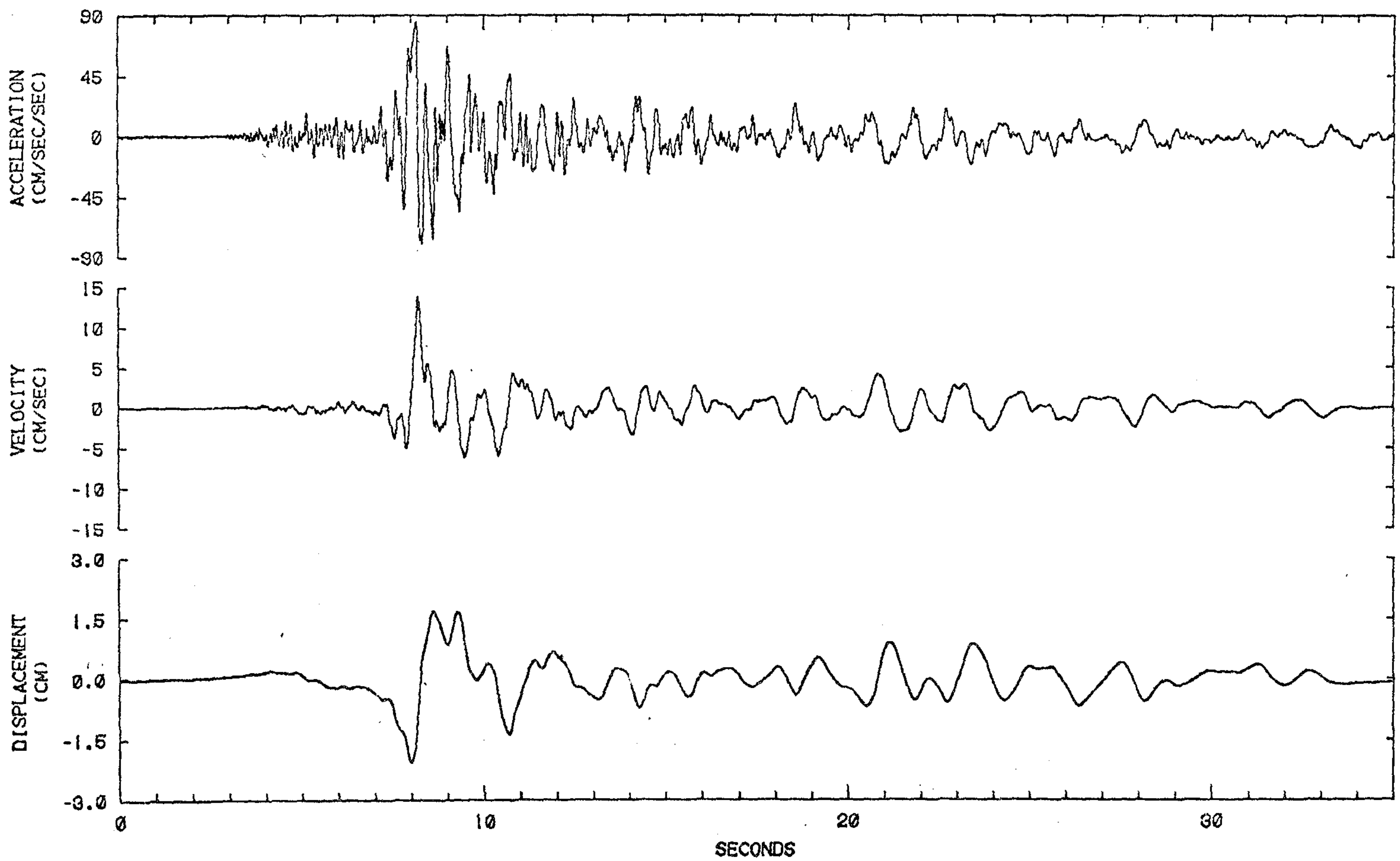

APPENDIX D

Fourier Amplitude Spectrum of Acceleration of Station I03

(see opposite page)

FOURIER AMPLITUDE SPECTRUM OF ACCELERATION

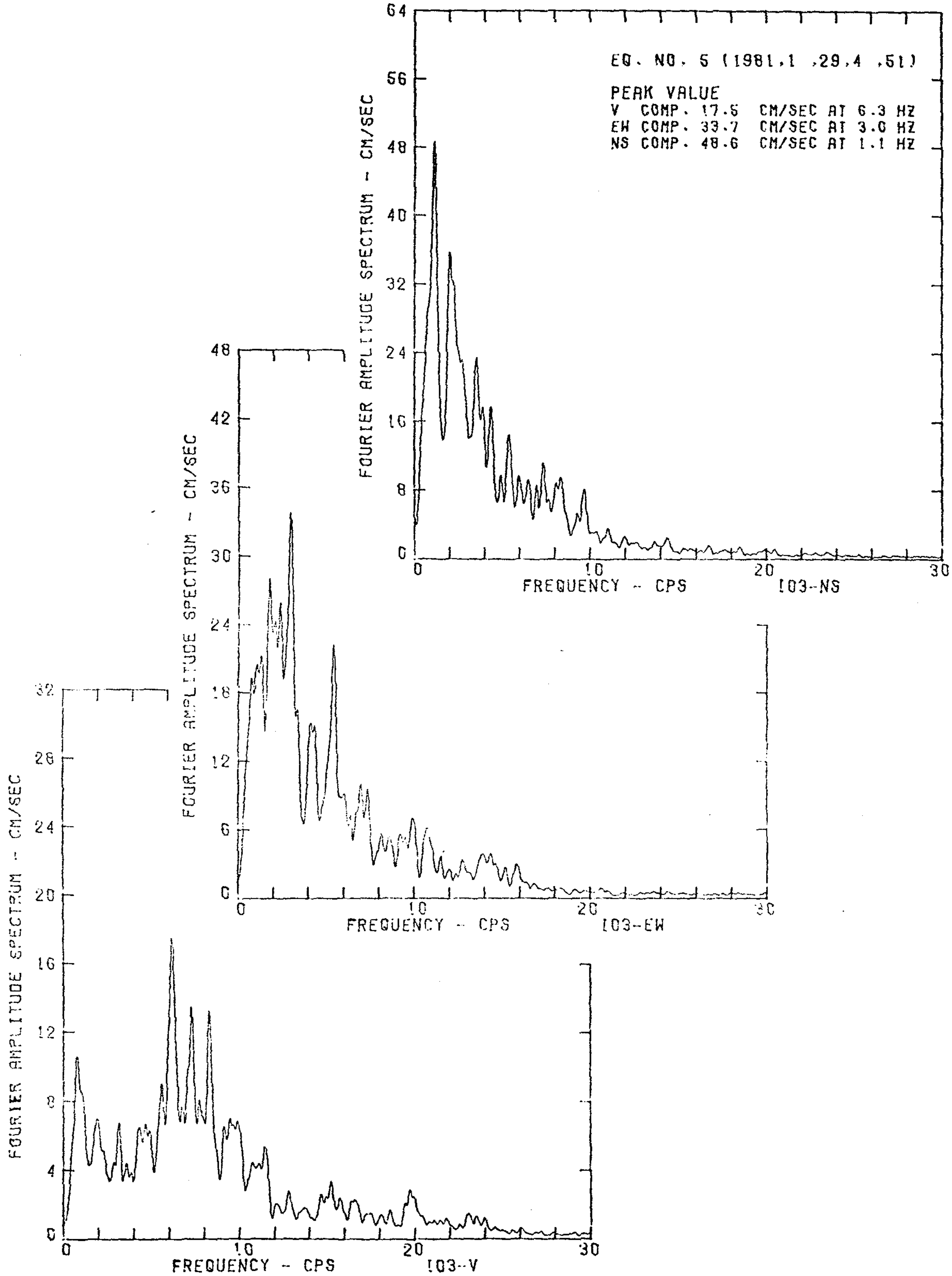

APPENDIX E

Frequency-Wave Number Spectral Formula

The formula for the high resolution method for frequency-wave number analysis can be represented in the following way.

For station j, the spectrum is

$$f_j(\omega) = \int_{t_o}^{t_o+\Delta T} a_j(t)e^{-i\omega t}\,dt \quad .$$

Define the cross-spectrum as

$$S_{j\ell}(\omega) = f_j(\omega)\, f_\ell^*(\omega)$$

and compute

$$P(\omega, \underline{k}) = \{\sum_{j,\ell} Q_{j\ell}(\omega)e^{-i\underline{k}\cdot(\underline{r}_j - \underline{r}_\ell)}\}^{-1} \quad ,$$

where

$$\{Q_{j\ell}(\omega)\} = \{S_{j\ell}(\omega)\}^{-1} \quad .$$

Then normalize the maximum $P(\omega,\underline{k})$ to 0 db. Finally, $P(\omega,\underline{k})$ is contoured. The contoured diagram can be analyzed for average horizontal phase velocity and direction of wave propagation (see Figs. 5.5 and 5.6).

EARTHQUAKE ENGINEERING RESEARCH CENTER REPORTS

NOTE: Numbers in parentheses are Accession Numbers assigned by the National Technical Information Service; these are followed by a price code. Copies of the reports may be ordered from the National Technical Information Service, 5285 Port Royal Road, Springfield, Virginia, 22161. Accession Numbers should be quoted on orders for reports (PB --- ---) and remittance must accompany each order. Reports without this information were not available at time of printing. The complete list of EERC reports (from EERC 67-1) is available upon request from the Earthquake Engineering Research Center, University of California, Berkeley, 47th Street and Hoffman Boulevard, Richmond, California 94804.

UCB/EERC-77/01 "PLUSH - A Computer Program for Probabilistic Finite Element Analysis of Seismic Soil-Structure Interaction," by M.P. Romo Organista, J. Lysmer and H.B. Seed - 1977 (PB81 177 651)A05

UCB/EERC-77/02 "Soil-Structure Interaction Effects at the Humboldt Bay Power Plant in the Ferndale Earthquake of June 7, 1975," by J.E. Valera, H.B. Seed, C.F. Tsai and J. Lysmer - 1977 (PB 265 795)A04

UCB/EERC-77/03 "Influence of Sample Disturbance on Sand Response to Cyclic Loading," by K. Mori, H.B. Seed and C.K. Chan - 1977 (PB 267 352)A04

UCB/EERC-77/04 "Seismological Studies of Strong Motion Records," by J. Shoja-Taheri - 1977 (PB 269 655)A10

UCB/EERC-77/05 Unassigned

UCB/EERC-77/06 "Developing Methodologies for Evaluating the Earthquake Safety of Existing Buildings," by No. 1 - B. Bresler; No. 2 - B. Bresler, T. Okada and D. Zisling; No. 3 - T. Okada and B. Bresler; No. 4 - V.V. Bertero and B. Bresler - 1977 (PB 267 354)A08

UCB/EERC-77/07 "A Literature Survey - Transverse Strength of Masonry Walls," by Y. Omote, R.L. Mayes, S.W. Chen and R.W. Clough - 1977 (PB 277 933)A07

UCB/EERC-77/08 "DRAIN-TABS: A Computer Program for Inelastic Earthquake Response of Three Dimensional Buildings," by R. Guendelman-Israel and G.H. Powell - 1977 (PB 270 693)A07

UCB/EERC-77/09 "SUBWALL: A Special Purpose Finite Element Computer Program for Practical Elastic Analysis and Design of Structural Walls with Substructure Option," by D.Q. Le, H. Peterson and E.P. Popov - 1977 (PB 270 567)A05

UCB/EERC-77/10 "Experimental Evaluation of Seismic Design Methods for Broad Cylindrical Tanks," by D.P. Clough (PB 272 280)A13

UCB/EERC-77/11 "Earthquake Engineering Research at Berkeley - 1976," - 1977 (PB 273 507)A09

UCB/EERC-77/12 "Automated Design of Earthquake Resistant Multistory Steel Building Frames," by N.D. Walker, Jr. - 1977 (PB 276 526)A09

UCB/EERC-77/13 "Concrete Confined by Rectangular Hoops Subjected to Axial Loads," by J. Vallenas, V.V. Bertero and E.P. Popov - 1977 (PB 275 165)A06

UCB/EERC-77/14 "Seismic Strain Induced in the Ground During Earthquakes," by Y. Sugimura - 1977 (PB 284 201)A04

UCB/EERC-77/15 Unassigned

UCB/EERC-77/16 "Computer Aided Optimum Design of Ductile Reinforced Concrete Moment Resisting Frames," by S.W. Zagajeski and V.V. Bertero - 1977 (PB 280 137)A07

UCB/EERC-77/17 "Earthquake Simulation Testing of a Stepping Frame with Energy-Absorbing Devices," by J.M. Kelly and D.F. Tsztoo - 1977 (PB 273 506)A04

UCB/EERC-77/18 "Inelastic Behavior of Eccentrically Braced Steel Frames under Cyclic Loadings," by C.W. Roeder and E.P. Popov - 1977 (PB 275 526)A15

UCB/EERC-77/19 "A Simplified Procedure for Estimating Earthquake-Induced Deformations in Dams and Embankments," by F.I. Makdisi and H.B. Seed - 1977 (PB 276 820)A04

UCB/EERC-77/20 "The Performance of Earth Dams during Earthquakes," by H.B. Seed, F.I. Makdisi and P. de Alba - 1977 (PB 276 821)A04

UCB/EERC-77/21 "Dynamic Plastic Analysis Using Stress Resultant Finite Element Formulation," by P. Lukkunapvasit and J.M. Kelly - 1977 (PB 275 453)A04

UCB/EERC-77/22 "Preliminary Experimental Study of Seismic Uplift of a Steel Frame," by R.W. Clough and A.A. Huckelbridge 1977 (PB 278 769)A08

UCB/EERC-77/23 "Earthquake Simulator Tests of a Nine-Story Steel Frame with Columns Allowed to Uplift," by A.A. Huckelbridge - 1977 (PB 277 944)A09

UCB/EERC-77/24 "Nonlinear Soil-Structure Interaction of Skew Highway Bridges," by M.-C. Chen and J. Penzien - 1977 (PB 276 176)A07

UCB/EERC-77/25 "Seismic Analysis of an Offshore Structure Supported on Pile Foundations," by D.D.-N. Liou and J. Penzien 1977 (PB 283 180)A06

UCB/EERC-77/26 "Dynamic Stiffness Matrices for Homogeneous Viscoelastic Half-Planes," by G. Dasgupta and A.K. Chopra - 1977 (PB 279 654)A06

UCB/EERC-77/27 "A Practical Soft Story Earthquake Isolation System," by J.M. Kelly, J.M. Eidinger and C.J. Derham - 1977 (PB 276 814)A07

UCB/EERC-77/28 "Seismic Safety of Existing Buildings and Incentives for Hazard Mitigation in San Francisco: An Exploratory Study," by A.J. Meltsner - 1977 (PB 281 970)A05

UCB/EERC-77/29 "Dynamic Analysis of Electrohydraulic Shaking Tables," by D. Rea, S. Abedi-Hayati and Y. Takahashi 1977 (PB 282 569)A04

UCB/EERC-77/30 "An Approach for Improving Seismic - Resistant Behavior of Reinforced Concrete Interior Joints," by B. Galunic, V.V. Bertero and E.P. Popov - 1977 (PB 290 870)A06

UCB/EERC-78/01 "The Development of Energy-Absorbing Devices for Aseismic Base Isolation Systems," by J.M. Kelly and D.F. Tsztoo - 1978 (PB 284 978)A04

UCB/EERC-78/02 "Effect of Tensile Prestrain on the Cyclic Response of Structural Steel Connections, by J.G. Bouwkamp and A. Mukhopadhyay - 1978

UCB/EERC-78/03 "Experimental Results of an Earthquake Isolation System using Natural Rubber Bearings," by J.M. Eidinger and J.M. Kelly - 1978 (PB 281 686)A04

UCB/EERC-78/04 "Seismic Behavior of Tall Liquid Storage Tanks," by A. Niwa - 1978 (PB 284 017)A14

UCB/EERC-78/05 "Hysteretic Behavior of Reinforced Concrete Columns Subjected to High Axial and Cyclic Shear Forces," by S.W. Zagajeski, V.V. Bertero and J.G. Bouwkamp - 1978 (PB 283 858)A13

UCB/EERC-78/06 "Three Dimensional Inelastic Frame Elements for the ANSR-I Program," by A. Riahi, D.G. Row and G.H. Powell - 1978 (PB 295 755)A04

UCB/EERC-78/07 "Studies of Structural Response to Earthquake Ground Motion," by O.A. Lopez and A.K. Chopra - 1978 (PB 282 790)A05

UCB/EERC-78/08 "A Laboratory Study of the Fluid-Structure Interaction of Submerged Tanks and Caissons in Earthquakes," by R.C. Byrd - 1978 (PB 284 957)A08

UCB/EERC-78/09 Unassigned

UCB/EERC-78/10 "Seismic Performance of Nonstructural and Secondary Structural Elements," by I. Sakamoto - 1978 (PB81 154 593)A05

UCB/EERC-78/11 "Mathematical Modelling of Hysteresis Loops for Reinforced Concrete Columns," by S. Nakata, T. Sproul and J. Penzien - 1978 (PB 298 274)A05

UCB/EERC-78/12 "Damageability in Existing Buildings," by T. Blejwas and B. Bresler - 1978 (PB 80 166 978)A05

UCB/EERC-78/13 "Dynamic Behavior of a Pedestal Base Multistory Building," by R.M. Stephen, E.L. Wilson, J.G. Bouwkamp and M. Button - 1978 (PB 286 650)A08

UCB/EERC-78/14 "Seismic Response of Bridges - Case Studies," by R.A. Imbsen, V. Nutt and J. Penzien - 1978 (PB 286 503)A10

UCB/EERC-78/15 "A Substructure Technique for Nonlinear Static and Dynamic Analysis," by D.G. Row and G.H. Powell - 1978 (PB 288 077)A10

UCB/EERC-78/16 "Seismic Risk Studies for San Francisco and for the Greater San Francisco Bay Area," by C.S. Oliveira - 1978 (PB 81 120 115)A07

UCB/EERC-78/17 "Strength of Timber Roof Connections Subjected to Cyclic Loads," by P. Gülkan, R.L. Mayes and R.W. Clough - 1978 (HUD-000 1491)A07

UCB/EERC-78/18 "Response of K-Braced Steel Frame Models to Lateral Loads," by J.G. Bouwkamp, R.M. Stephen and E.P. Popov - 1978

UCB/EERC-78/19 "Rational Design Methods for Light Equipment in Structures Subjected to Ground Motion," by J.L. Sackman and J.M. Kelly - 1978 (PB 292 357)A04

UCB/EERC-78/20 "Testing of a Wind Restraint for Aseismic Base Isolation," by J.M. Kelly and D.E. Chitty - 1978 (PB 292 833)A03

UCB/EERC-78/21 "APOLLO - A Computer Program for the Analysis of Pore Pressure Generation and Dissipation in Horizontal Sand Layers During Cyclic or Earthquake Loading," by P.P. Martin and H.B. Seed - 1978 (PB 292 835)A04

UCB/EERC-78/22 "Optimal Design of an Earthquake Isolation System," by M.A. Bhatti, K.S. Pister and E. Polak - 1978 (PB 294 735)A06

UCB/EERC-78/23 "MASH - A Computer Program for the Non-Linear Analysis of Vertically Propagating Shear Waves in Horizontally Layered Deposits," by P.P. Martin and H.B. Seed - 1978 (PB 293 101)A05

UCB/EERC-78/24 "Investigation of the Elastic Characteristics of a Three Story Steel Frame Using System Identification," by I. Kaya and H.D. McNiven - 1978 (PB 296 225)A06

UCB/EERC-78/25 "Investigation of the Nonlinear Characteristics of a Three-Story Steel Frame Using System Identification," by I. Kaya and H.D. McNiven - 1978 (PB 301 363)A05

UCB/EERC-78/26 "Studies of Strong Ground Motion in Taiwan," by Y.M. Hsiung, B.A. Bolt and J. Penzien - 1978 (PB 298 436)A06

UCB/EERC-78/27 "Cyclic Loading Tests of Masonry Single Piers: Volume 1 - Height to Width Ratio of 2," by P.A. Hidalgo, R.L. Mayes, H.D. McNiven and R.W. Clough - 1978 (PB 296 211)A07

UCB/EERC-78/28 "Cyclic Loading Tests of Masonry Single Piers: Volume 2 - Height to Width Ratio of 1," by S.-W.J. Chen, P.A. Hidalgo, R.L. Mayes, R.W. Clough and H.D. McNiven - 1978 (PB 296 212)A09

UCB/EERC-78/29 "Analytical Procedures in Soil Dynamics," by J. Lysmer - 1978 (PB 298 445)A06

UCB/EERC-79/01 "Hysteretic Behavior of Lightweight Reinforced Concrete Beam-Column Subassemblages," by B. Forzani, E.P. Popov and V.V. Bertero - April 1979(PB 298 267)A06

UCB/EERC-79/02 "The Development of a Mathematical Model to Predict the Flexural Response of Reinforced Concrete Beams to Cyclic Loads, Using System Identification," by J. Stanton & H. McNiven - Jan. 1979(PB 295 875)A10

UCB/EERC-79/03 "Linear and Nonlinear Earthquake Response of Simple Torsionally Coupled Systems," by C.L. Kan and A.K. Chopra - Feb. 1979(PB 298 262)A06

UCB/EERC-79/04 "A Mathematical Model of Masonry for Predicting its Linear Seismic Response Characteristics," by Y. Mengi and H.D. McNiven - Feb. 1979(PB 298 266)A06

UCB/EERC-79/05 "Mechanical Behavior of Lightweight Concrete Confined by Different Types of Lateral Reinforcement," by M.A. Manrique, V.V. Bertero and E.P. Popov - May 1979(PB 301 114)A06

UCB/EERC-79/06 "Static Tilt Tests of a Tall Cylindrical Liquid Storage Tank," by R.W. Clough and A. Niwa - Feb. 1979 (PB 301 167)A06

UCB/EERC-79/07 "The Design of Steel Energy Absorbing Restrainers and Their Incorporation into Nuclear Power Plants for Enhanced Safety: Volume 1 - Summary Report," by P.N. Spencer, V.F. Zackay, and E.R. Parker - Feb. 1979(UCB/EERC-79/07)A09

UCB/EERC-79/08 "The Design of Steel Energy Absorbing Restrainers and Their Incorporation into Nuclear Power Plants for Enhanced Safety: Volume 2 - The Development of Analyses for Reactor System Piping,""Simple Systems" by M.C. Lee, J. Penzien, A.K. Chopra and K, Suzuki "Complex Systems" by G.H. Powell, E.L. Wilson, R.W. Clough and D.G. Row - Feb. 1979(UCB/EERC-79/08)A10

UCB/EERC-79/09 "The Design of Steel Energy Absorbing Restrainers and Their Incorporation into Nuclear Power Plants for Enhanced Safety: Volume 3 - Evaluation of Commercial Steels," by W.S. Owen, R.M.N. Pelloux, R.O. Ritchie, M. Faral, T. Ohhashi, J. Toplosky, S.J. Hartman, V.F. Zackay and E.R. Parker - Feb. 1979(UCB/EERC-79/09)A04

UCB/EERC-79/10 "The Design of Steel Energy Absorbing Restrainers and Their Incorporation into Nuclear Power Plants for Enhanced Safety: Volume 4 - A Review of Energy-Absorbing Devices," by J.M. Kelly and M.S. Skinner - Feb. 1979(UCB/EERC-79/10)A04

UCB/EERC-79/11 "Conservatism In Summation Rules for Closely Spaced Modes," by J.M. Kelly and J.L. Sackman - May 1979(PB 301 328)A03

UCB/EERC-79/12 "Cyclic Loading Tests of Masonry Single Piers; Volume 3 - Height to Width Ratio of 0.5," by P.A. Hidalgo, R.L. Mayes, H.D. McNiven and R.W. Clough - May 1979(PB 301 321)A08

UCB/EERC-79/13 "Cyclic Behavior of Dense Course-Grained Materials in Relation to the Seismic Stability of Dams," by N.G. Banerjee, H.B. Seed and C.K. Chan - June 1979(PB 301 373)A13

UCB/EERC-79/14 "Seismic Behavior of Reinforced Concrete Interior Beam-Column Subassemblages," by S. Viwathanatepa, E.P. Popov and V.V. Bertero - June 1979(PB 301 326)A10

UCB/EERC-79/15 "Optimal Design of Localized Nonlinear Systems with Dual Performance Criteria Under Earthquake Excitations," by M.A. Bhatti - July 1979(PB 80 167 109)A06

UCB/EERC-79/16 "OPTDYN - A General Purpose Optimization Program for Problems with or without Dynamic Constraints," by M.A. Bhatti, E. Polak and K.S. Pister - July 1979(PB 80 167 091)A05

UCB/EERC-79/17 "ANSR-II, Analysis of Nonlinear Structural Response, Users Manual," by D.P. Mondkar and G.H. Powell July 1979(PB 80 113 301)A05

UCB/EERC-79/18 "Soil Structure Interaction in Different Seismic Environments," A. Gomez-Masso, J. Lysmer, J.-C. Chen and H.B. Seed - August 1979(PB 80 101 520)A04

UCB/EERC-79/19 "ARMA Models for Earthquake Ground Motions," by M.K. Chang, J.W. Kwiatkowski, R.F. Nau, R.M. Oliver and K.S. Pister - July 1979(PB 301 166)A05

UCB/EERC-79/20 "Hysteretic Behavior of Reinforced Concrete Structural Walls," by J.M. Vallenas, V.V. Bertero and E.P. Popov - August 1979(PB 80 165 905)A12

UCB/EERC-79/21 "Studies on High-Frequency Vibrations of Buildings - 1: The Column Effect," by J. Lubliner - August 1979 (PB 80 158 553)A03

UCB/EERC-79/22 "Effects of Generalized Loadings on Bond Reinforcing Bars Embedded in Confined Concrete Blocks," by S. Viwathanatepa, E.P. Popov and V.V. Bertero - August 1979(PB 81 124 018)A14

UCB/EERC-79/23 "Shaking Table Study of Single-Story Masonry Houses, Volume 1: Test Structures 1 and 2," by P. Gülkan, R.L. Mayes and R.W. Clough - Sept. 1979 (HUD-000 1763)A12

UCB/EERC-79/24 "Shaking Table Study of Single-Story Masonry Houses, Volume 2: Test Structures 3 and 4," by P. Gülkan, R.L. Mayes and R.W. Clough - Sept. 1979 (HUD-000 1836)A12

UCB/EERC-79/25 "Shaking Table Study of Single-Story Masonry Houses, Volume 3: Summary, Conclusions and Recommendations," by R.W. Clough, R.L. Mayes and P. Gülkan - Sept. 1979 (HUD-000 1837)A06

UCB/EERC-79/26 "Recommendations for a U.S.-Japan Cooperative Research Program Utilizing Large-Scale Testing Facilities," by U.S.-Japan Planning Group - Sept. 1979(PB 301 407)A06

UCB/EERC-79/27 "Earthquake-Induced Liquefaction Near Lake Amatitlan, Guatemala," by H.B. Seed, I. Arango, C.K. Chan, A. Gomez-Masso and R. Grant de Ascoli - Sept. 1979(NUREG-CR1341)A03

UCB/EERC-79/28 "Infill Panels: Their Influence on Seismic Response of Buildings," by J.W. Axley and V.V. Bertero Sept. 1979(PB 80 163 371)A10

UCB/EERC-79/29 "3D Truss Bar Element (Type 1) for the ANSR-II Program," by D.P. Mondkar and G.H. Powell - Nov. 1979 (PB 80 169 709)A02

UCB/EERC-79/30 "2D Beam-Column Element (Type 5 - Parallel Element Theory) for the ANSR-II Program," by D.G. Row, G.H. Powell and D.P. Mondkar - Dec. 1979(PB 80 167 224)A03

UCB/EERC-79/31 "3D Beam-Column Element (Type 2 - Parallel Element Theory) for the ANSR-II Program," by A. Riahi, G.H. Powell and D.P. Mondkar - Dec. 1979(PB 80 167 216)A03

UCB/EERC-79/32 "On Response of Structures to Stationary Excitation," by A. Der Kiureghian - Dec. 1979(PB 80166 929)A03

UCB/EERC-79/33 "Undisturbed Sampling and Cyclic Load Testing of Sands," by S. Singh, H.B. Seed and C.K. Chan Dec. 1979(ADA 087 298)A07

UCB/EERC-79/34 "Interaction Effects of Simultaneous Torsional and Compressional Cyclic Loading of Sand," by P.M. Griffin and W.N. Houston - Dec. 1979(ADA 092 352)A15

UCB/EERC-80/01 "Earthquake Response of Concrete Gravity Dams Including Hydrodynamic and Foundation Interaction Effects," by A.K. Chopra, P. Chakrabarti and S. Gupta - Jan. 1980(AD-A087297)A10

UCB/EERC-80/02 "Rocking Response of Rigid Blocks to Earthquakes," by C.S. Yim, A.K. Chopra and J. Penzien - Jan. 1980 (PB80 166 002)A04

UCB/EERC-80/03 "Optimum Inelastic Design of Seismic-Resistant Reinforced Concrete Frame Structures," by S.W. Zagajeski and V.V. Bertero - Jan. 1980(PB80 164 635)A06

UCB/EERC-80/04 "Effects of Amount and Arrangement of Wall-Panel Reinforcement on Hysteretic Behavior of Reinforced Concrete Walls," by R. Iliya and V.V. Bertero - Feb. 1980(PB81 122 525)A09

UCB/EERC-80/05 "Shaking Table Research on Concrete Dam Models," by A. Niwa and R.W. Clough - Sept. 1980(PB81 122 368)A06

UCB/EERC-80/06 "The Design of Steel Energy-Absorbing Restrainers and their Incorporation into Nuclear Power Plants for Enhanced Safety (Vol 1A): Piping with Energy Absorbing Restrainers: Parameter Study on Small Systems," by G.H. Powell, C. Oughourlian and J. Simons - June 1980

UCB/EERC-80/07 "Inelastic Torsional Response of Structures Subjected to Earthquake Ground Motions," by Y. Yamazaki April 1980(PB81 122 327)A08

UCB/EERC-80/08 "Study of X-Braced Steel Frame Structures Under Earthquake Simulation," by Y. Ghanaat - April 1980 (PB81 122 335)A11

UCB/EERC-80/09 "Hybrid Modelling of Soil-Structure Interaction," by S. Gupta, T.W. Lin, J. Penzien and C.S. Yeh May 1980(PB81 122 319)A07

UCB/EERC-80/10 "General Applicability of a Nonlinear Model of a One Story Steel Frame," by B.I. Sveinsson and H.D. McNiven - May 1980(PB81 124 877)A06

UCB/EERC-80/11 "A Green-Function Method for Wave Interaction with a Submerged Body," by W. Kioka - April 1980 (PB81 122 269)A07

UCB/EERC-80/12 "Hydrodynamic Pressure and Added Mass for Axisymmetric Bodies," by F. Nilrat - May 1980(PB81 122 343)A08

UCB/EERC-80/13 "Treatment of Non-Linear Drag Forces Acting on Offshore Platforms," by B.V. Dao and J. Penzien May 1980(PB81 153 413)A07

UCB/EERC-80/14 "2D Plane/Axisymmetric Solid Element (Type 3 - Elastic or Elastic-Perfectly Plastic) for the ANSR-II Program," by D.P. Mondkar and G.H. Powell - July 1980(PB81 122 350)A03

UCB/EERC-80/15 "A Response Spectrum Method for Random Vibrations," by A. Der Kiureghian - June 1980(PB81 122 301)A03

UCB/EERC-80/16 "Cyclic Inelastic Buckling of Tubular Steel Braces," by V.A. Zayas, E.P. Popov and S.A. Mahin June 1980(PB81 124 885)A10

UCB/EERC-80/17 "Dynamic Response of Simple Arch Dams Including Hydrodynamic Interaction," by C.S. Porter and A.K. Chopra - July 1980(PB81 124 000)A13

UCB/EERC-80/18 "Experimental Testing of a Friction Damped Aseismic Base Isolation System with Fail-Safe Characteristics," by J.M. Kelly, K.E. Beucke and M.S. Skinner - July 1980(PB81 148 595)A04

UCB/EERC-80/19 "The Design of Steel Energy-Absorbing Restrainers and their Incorporation into Nuclear Power Plants for Enhanced Safety (Vol 1B): Stochastic Seismic Analyses of Nuclear Power Plant Structures and Piping Systems Subjected to Multiple Support Excitations," by M.C. Lee and J. Penzien - June 1980

UCB/EERC-80/20 "The Design of Steel Energy-Absorbing Restrainers and their Incorporation into Nuclear Power Plants for Enhanced Safety (Vol 1C): Numerical Method for Dynamic Substructure Analysis," by J.M. Dickens and E.L. Wilson - June 1980

UCB/EERC-80/21 "The Design of Steel Energy-Absorbing Restrainers and their Incorporation into Nuclear Power Plants for Enhanced Safety (Vol 2): Development and Testing of Restraints for Nuclear Piping Systems," by J.M. Kelly and M.S. Skinner - June 1980

UCB/EERC-80/22 "3D Solid Element (Type 4-Elastic or Elastic-Perfectly-Plastic) for the ANSR-II Program," by D.P. Mondkar and G.H. Powell - July 1980(PB81 123 242)A03

UCB/EERC-80/23 "Gap-Friction Element (Type 5) for the ANSR-II Program," by D.P. Mondkar and G.H. Powell - July 1980 (PB81 122 285)A03

UCB/EERC-80/24 "U-Bar Restraint Element (Type 11) for the ANSR-II Program," by C. Cughourlian and G.H. Powell July 1980(PB81 122 293)A03

UCB/EERC-80/25 "Testing of a Natural Rubber Base Isolation System by an Explosively Simulated Earthquake," by J.M. Kelly - August 1980(PB81 201 360)A04

UCB/EERC-80/26 "Input Identification from Structural Vibrational Response," by Y. Hu - August 1980(PB81 152 308)A05

UCB/EERC-80/27 "Cyclic Inelastic Behavior of Steel Offshore Structures," by V.A. Zayas, S.A. Mahin and E.P. Popov August 1980(PB81 196 180)A15

UCB/EERC-80/28 "Shaking Table Testing of a Reinforced Concrete Frame with Biaxial Response," by M.G. Oliva October 1980(PB81 154 304)A10

UCB/EERC-80/29 "Dynamic Properties of a Twelve-Story Prefabricated Panel Building," by J.G. Bouwkamp, J.P. Kollegger and R.M. Stephen - October 1980(PB82 117 128)A06

UCB/EERC-80/30 "Dynamic Properties of an Eight-Story Prefabricated Panel Building," by J.G. Bouwkamp, J.P. Kollegger and R.M. Stephen - October 1980(PB81 200 313)A05

UCB/EERC-80/31 "Predictive Dynamic Response of Panel Type Structures Under Earthquakes," by J.P. Kollegger and J.G. Bouwkamp - October 1980(PB81 152 316)A04

UCB/EERC-80/32 "The Design of Steel Energy-Absorbing Restrainers and their Incorporation into Nuclear Power Plants for Enhanced Safety (Vol 3): Testing of Commercial Steels in Low-Cycle Torsional Fatigue," by P. Spencer, E.R. Parker, E. Jongewaard and M. Drory

UCB/EERC-80/33 "The Design of Steel Energy-Absorbing Restrainers and their Incorporation into Nuclear Power Plants for Enhanced Safety (Vol 4): Shaking Table Tests of Piping Systems with Energy-Absorbing Restrainers," by S.F. Stiemer and W.G. Godden - Sept. 1980

UCB/EERC-80/34 "The Design of Steel Energy-Absorbing Restrainers and their Incorporation into Nuclear Power Plants for Enhanced Safety (Vol 5): Summary Report," by P. Spencer

UCB/EERC-80/35 "Experimental Testing of an Energy-Absorbing Base Isolation System," by J.M. Kelly, M.S. Skinner and K.E. Beucke - October 1980(PB81 154 072)A04

UCB/EERC-80/36 "Simulating and Analyzing Artificial Non-Stationary Earthquake Ground Motions," by R.F. Nau, R.M. Oliver and K.S. Pister - October 1980(PB81 153 397)A04

UCB/EERC-80/37 "Earthquake Engineering at Berkeley - 1980," - Sept. 1980(PB81 205 874)A09

UCB/EERC-80/38 "Inelastic Seismic Analysis of Large Panel Buildings," by V. Schricker and G.H. Powell - Sept. 1980 (PB81 154 338)A13

UCB/EERC-80/39 "Dynamic Response of Embankment, Concrete-Gravity and Arch Dams Including Hydrodynamic Interaction," by J.F. Hall and A.K. Chopra - October 1980(PB81 152 324)A11

UCB/EERC-80/40 "Inelastic Buckling of Steel Struts Under Cyclic Load Reversal," by R.G. Black, W.A. Wenger and E.P. Popov - October 1980(PB81 154 312)A08

UCB/EERC-80/41 "Influence of Site Characteristics on Building Damage During the October 3, 1974 Lima Earthquake," by P. Repetto, I. Arango and H.B. Seed - Sept. 1980(PB81 161 739)A05

UCB/EERC-80/42 "Evaluation of a Shaking Table Test Program on Response Behavior of a Two Story Reinforced Concrete Frame," by J.M. Blondet, R.W. Clough and S.A. Mahin

UCB/EERC-80/43 "Modelling of Soil-Structure Interaction by Finite and Infinite Elements," by F. Medina - December 1980(PB81 229 270)A04

UCB/EERC-81/01 "Control of Seismic Response of Piping Systems and Other Structures by Base Isolation," edited by J.M. Kelly - January 1981 (PB81 200 735)A05

UCB/EERC-81/02 "OPTNSR - An Interactive Software System for Optimal Design of Statically and Dynamically Loaded Structures with Nonlinear Response," by M.A. Bhatti, V. Ciampi and K.S. Pister - January 1981 (PB81 218 851)A09

UCB/EERC-81/03 "Analysis of Local Variations in Free Field Seismic Ground Motions," by J.-C. Chen, J. Lysmer and H.B. Seed - January 1981 (AD-A099508)A13

UCB/EERC-81/04 "Inelastic Structural Modeling of Braced Offshore Platforms for Seismic Loading," by V.A. Zayas, P.-S.B. Shing, S.A. Mahin and E.P. Popov - January 1981(PB82 138 777)A07

UCB/EERC-81/05 "Dynamic Response of Light Equipment in Structures," by A. Der Kiureghian, J.L. Sackman and B. Nour-Omid - April 1981 (PB81 218 497)A04

UCB/EERC-81/06 "Preliminary Experimental Investigation of a Broad Base Liquid Storage Tank," by J.G. Bouwkamp, J.P. Kollegger and R.M. Stephen - May 1981(PB82 140 385)A03

UCB/EERC-81/07 "The Seismic Resistant Design of Reinforced Concrete Coupled Structural Walls," by A.E. Aktan and V.V. Bertero - June 1981(PB82 113 358)A11

UCB/EERC-81/08 "The Undrained Shearing Resistance of Cohesive Soils at Large Deformations," by M.R. Pyles and H.B. Seed - August 1981

UCB/EERC-81/09 "Experimental Behavior of a Spatial Piping System with Steel Energy Absorbers Subjected to a Simulated Differential Seismic Input," by S.F. Stiemer, W.G. Godden and J.M. Kelly - July 1981

UCB/EERC-81/10 "Evaluation of Seismic Design Provisions for Masonry in the United States," by B.I. Sveinsson, R.L. Mayes and H.D. McNiven - August 1981

UCB/EERC-81/11 "Two-Dimensional Hybrid Modelling of Soil-Structure Interaction," by T.-J. Tzong, S. Gupta and J. Penzien - August 1981(PB82 142 118)A04

UCB/EERC-81/12 "Studies on Effects of Infills in Seismic Resistant R/C Construction," by S. Brokken and V.V. Bertero - September 1981

UCB/EERC-81/13 "Linear Models to Predict the Nonlinear Seismic Behavior of a One-Story Steel Frame," by H. Valdimarsson, A.H. Shah and H.D. McNiven - September 1981(PB82 138 793)A07

UCB/EERC-81/14 "TLUSH: A Computer Program for the Three-Dimensional Dynamic Analysis of Earth Dams," by T. Kagawa, L.H. Mejia, H.B. Seed and J. Lysmer - September 1981(PB82 139 940)A06

UCB/EERC-81/15 "Three Dimensional Dynamic Response Analysis of Earth Dams," by L.H. Mejia and H.B. Seed - September 1981 (PB82 137 274)A12

UCB/EERC-81/16 "Experimental Study of Lead and Elastomeric Dampers for Base Isolation Systems," by J.M. Kelly and S.B. Hodder - October 1981

UCB/EERC-81/17 "The Influence of Base Isolation on the Seismic Response of Light Secondary Equipment," by J.M. Kelly - April 1981

UCB/EERC-81/18 "Studies on Evaluation of Shaking Table Response Analysis Procedures," by J. Marcial Blondet - November 1981

UCB/EERC-81/19 "DELIGHT.STRUCT: A Computer-Aided Design Environment for Structural Engineering," by R.J. Balling, K.S. Pister and E. Polak - December 1981

UCB/EERC-81/20 "Optimal Design of Seismic-Resistant Planar Steel Frames," by R.J. Balling, V. Ciampi, K.S. Pister and E. Polak - December 1981

UCB/EERC-82/01 "Dynamic Behavior of Ground for Seismic Analysis of Lifeline Systems," by T. Sato and A. Der Kiureghian - January 1982 (PB82 218 926)A05

UCB/EERC-82/02 "Shaking Table Tests of a Tubular Steel Frame Model," by Y. Ghanaat and R. W. Clough - January 1982 (PB82 220 161)A07

UCB/EERC-82/03 "Experimental Behavior of a Spatial Piping System with Shock Arrestors and Energy Absorbers under Seismic Excitation," by S. Schneider, H.-M. Lee and G. W. Godden - May 1982

UCB/EERC-82/04 "New Approaches for the Dynamic Analysis of Large Structural Systems," by E. L. Wilson - June 1982

UCB/EERC-82/05 "Model Study of Effects of Damage on the Vibration Properties of Steel Offshore Platforms," by F. Shahrivar and J. G. Bouwkamp - June 1982

UCB/EERC-82/06 "States of the Art and Practice in the Optimum Seismic Design and Analytical Response Prediction of R/C Frame-Wall Structures," by A. E. Aktan and V. V. Bertero - July 1982

UCB/EERC-82/07 "Further Study of the Earthquake Response of a Broad Cylindrical Liquid-Storage Tank Model," by G. C. Manos and R. W. Clough - July 1982

UCB/EERC-82/08 "An Evaluation of the Design and Analytical Seismic Response of a Seven Story Reinforced Concrete Frame - Wall Structure," by A. C. Finley and V. V. Bertero - July 1982

UCB/EERC-82/09 "Fluid-Structure Interactions: Added Mass Computations for Incompressible Fluid," by J. S.-H. Kuo - August 1982

UCB/EERC-82/10 "Joint-Opening Nonlinear Mechanism: Interface Smeared Crack Model," by J. S.-H. Kuo - August 1982

UCB/EERC-82/11 "Dynamic Response Analysis of Techi Dam," by R. W. Clough, R. M. Stephen and J. S.-H. Kuo - August 1982

UCB/EERC-82/12 "Prediction of the Seismic Responses of R/C Frame-Coupled Wall Structures," by A. E. Aktan, V. V. Bertero and M. Piazza - August 1982

UCB/EERC-82/13 "Preliminary Report on the SMART 1 Strong Motion Array in Taiwan," by B. A. Bolt, C. H. Loh, J. Penzien, Y. B. Tsai and Y. T. Yeh - August 1982